

PETROLOGY OF EOCENE VOLCANISM IN CENTRAL ANATOLIA:
IMPLICATIONS FOR THE EARLY TERTIARY EVOLUTION OF THE
CENTRAL ANATOLIAN CRYSTALLINE COMPLEX

A THESIS SUBMITTED TO
THE GRADUATE SCHOOL OF NATURAL AND APPLIED SCIENCES
OF
MIDDLE EAST TECHNICAL UNIVERSITY

BY

FATMA GENELİ

IN PARTIAL FULFILLMENT OF THE REQUIREMENTS
FOR
THE DEGREE OF DOCTOR OF PHILOSOPHY
IN
GEOLOGICAL ENGINEERING

FEBRUARY 2011

Approval of the thesis

**PETROLOGY OF EOCENE VOLCANISM IN CENTRAL ANATOLIA:
IMPLICATION FOR THE EARLY TERTIARY EVOLUTION OF THE
CENTRAL ANATOLIAN CRYSTALLINE COMPLEX**

submitted by **FATMA GENELİ** in partial fulfillment of the requirements for
the degree of **Doctor of Philosophy in Geological Engineering Department,**
Middle East Technical University by,

Prof. Dr. Canan Özgen
Dean, Graduate School of Natural and Applied Sciences _____

Prof. Dr. M. Zeki Çamur
Head of Department, **Geological Engineering** _____

Prof. Dr. M. Cemal Göncüoğlu
Supervisor, **Geological Engineering Dept., METU** _____

Assoc. Prof. Dr. Gonca Kuşcu
Co- Supervisor, **Geological Engineering Dept.,
Muğla University** _____

Examining Committee Members:

Prof. Dr. Asuman Türkmenoğlu
Geological Engineering Dept., METU _____

Prof. Dr. Cemal Göncüoğlu
Geological Engineering Dept., METU _____

Prof. Dr. Mehmet Arslan
Geological Engineering Dept., Karadeniz Teknik Üniv. _____

Assoc. Prof. Dr. Sönmez Sayılı
Geological Engineering Dept., Ankara University _____

Assist. Prof. Dr. Fatma Toksoy Köksal
Geological Engineering Dept., METU _____

Date: February 11, 2011

I hereby declare that all information in this document has been obtained and presented in accordance with academic rules and ethical conduct. I also declare that, as required by these rules and conduct, I have fully cited and referenced all material and results that are not original to this work.

Name, Last name: Fatma Geneli

Signature:

ABSTRACT

PETROLOGY OF THE EOCENE VOLCANISM IN THE CENTRAL ANATAOLIA: IMPLICATION FOR THE EARLY TERTIARY EVOLUTION OF THE CENTRAL ANATOLIAN CRYSTALLINE COMPLEX

Geneli, Fatma

Ph.D., Department of Geological Engineering

Supervisor : Prof. Dr. M. Cemal Göncüoğlu

Co-supervisor: Assoc. Prof. Dr. Gonca Kuşcu

February 2011, 227 pages

In the Central Anatolian Crystalline Complex (CACC) the Late Cretaceous post-collisional granitic magmatism is followed by Eocene extension, resulting in formation of roughly E-W trending transtensional basins. Formation of these basins was accompanied by calc-alkaline- mildly alkaline volcanism. The volcanic rocks, mainly subaqueous lava flows and subaerial domes are concentrated along these basins and associated with Middle Eocene (Bartonian) Mucur Formation. They are basic to intermediate and are classified as basalt, basaltic andesite and rarely alkali basalt and trachy-andesite. All studied samples are strongly and variably LREE enriched relative to chondrite with the $(La/Sm)_N$ ratio of 2.26- to 6.17. They have negative Nb-Ta and Ti anomalies in the primitive mantle normalized diagram, and are characterized by low Nb/La (0.21 to 0.62), Ce/Pb (3.70-34.90) and Nb/U ratios (1.11-30), which may indicate an interaction with the Late Cretaceous granitic host rocks in the course of their ascent.

The volcanic rocks display similar but variable ranges of Sr, Nd and Pb isotope values. Relatively high values of ϵNd (0.53 to 4.33) indicate an isotopically

depleted mantle source. Combined trace element and isotope compositions of the Eocene samples suggest that they were derived from a heterogeneous lithospheric mantle source that had been metasomatized by subduction related agents such as fluids and/or melts during a previous geodynamic event.

Geochemistry and geotectonic setting point out that lithospheric delamination was the most likely mechanism to generate these calc-alkaline to mildly alkaline volcanic rocks in the CACC.

Keywords: Extension, Eocene, volcanism, calc- alkaline, lithospheric delamination.

ÖZ

ORTA ANADOLU'DA EOSEN VOLKANİZMASININ PETROLOJİSİ: ORTA ANADOLU KRİSTALEN KOMPLEKSİNİN ERKEN TERSİYER EVRİMİNDEKİ ÖNEMİ

Geneli, Fatma

Doktora, Jeoloji Mühendisliği Bölümü

Tez Yöneticisi : Prof. Dr. M. Cemal Göncüoğlu

Ortak Tez Yöneticisi : Doç. Dr. Gonca Kuşcu

Şubat 2011, 227 sayfa

Orta Anadolu'da Üst Kretase granitik magmatizması, kabaca doğu- batı yönünde uzanan transtensional sedimanter basenlerin oluşumu ile sonuçlanan Eosen gerilmeli rejimi ile devam eder. Bu basenlerin oluşumu, kalk-alkali-hafif alkali volkanizma ile eş zamanlıdır. Genellikle denizaltı lavları ve yüzeydeki domlar olarak gözlenen volkanik kayalar Orta Eosen (Bartoniye) yaşlı Mucur Formasyonu içinde yüzeylenmektedir. Volkanik kayalar mafik ve ortaç karakterli olup bazalt, bazaltik andezit, andezit ve nadiren alkali bazalt olarak sınıflandırılırlar. Örneklerin hepsi, kondrite göre LREE zenginleşmesi göstermektedir ve $(La/Sm)_N$ değerleri 2.26- 6.17 arasındadır. Volkanik kayalar, ilksel mantoya göre normalize edilmiş diyagramlarda Nb, Ta and Ti negatif anomalisi gösterirler. Düşük Nb/La (0.21- 0.62), Ce/Pb (3.70-34.90) ve Nb/U (1.11-30) oranları, bu kayaların yüzeye çıkması sırasında Üst Kretase granitik kayaları ile etkileşimini gösterebilir.

Volkanik kayalar, benzer Sr, Nd and Pb izotop oranları sunmaktadırlar. Göreli olarak yüksek ϵNd (0.53- 4.33) değerleri izotopik olarak tüketilmiş bir mantoya işaret eder. İz element ve izotop bileşimleri, bu kayaların dalma

batma ile ilişkili akışkan ve eriyikler ile zenginleşmiş heterojen bir mantodan türediğini göstermektedir.

Jeokimyasal ve tektonik ortam değerlendirmeleri, litosferik deliminasyonun kalkalkaliden hafif alkaliye değişen kayaçların oluşumunda önemli bir etken olduğunu göstermektedir.

Anahtar Kelimeler: Gerilme, Eosen, volkanizma, kalkalkali, litosferik deliminasyon.

To the one who deserves the dedication most...

ACKNOWLEDGMENTS

Many people have contributed to this thesis. But among them, there is someone, first and foremost I would like to express my deepest sincere gratitude; Prof. Dr. Cemal Göncüoğlu, my supervisor. I would like to acknowledge his academic guidance, suggestions, and comments during the whole stage of this study. This thesis would have not been possible without his support and encourage. Thank you Professor, I am really proud of being your student.

I would like to thank my co-supervisor Assoc. Prof. Dr. Gonca Kuşcu who is the one encouraging me to study at METU. Without her inspiration I would barely think to join the METU group. I am also thankful to her because of her kindly attitude, help, suggestions, and comments not only related to this thesis but also whenever I need throughout my life. She was always friendly and helpful. Thank you for your never ending encouragement, motivation and support.

I would like to thank Assist. Dr. Fatma Toksoy Köksal for her support and motivation during this study. I am also thankful to her for keeping the TUBITAK project alive. The other member of the Köksal Family, Dr Serhat Köksal, is also thanked for isotope analyses performed in the Central Laboratory, METU. Thank you Köksal couple for your friendly attitude.

I am thankful to Assoc. Dr. John Lassiter for providing me the opportunity to conduct my isotope analyses in his laboratory in the University of Texas at Austin and for his guidance, financial support, suggestions, comments and encouragement not only during my stay in Austin but also every stage of the thesis. You are such a great supervisor that every PhD student could want to have.

Speaking of Austin, I have some other people there to thank. First of all, Dr. Larry Mack for his endless patience, help and comments during my laboratory works. Thank you, Larry. Secondly, Ayşen and Roger, you made my stay in Austin enjoyable. When I was depressed, Ayşen was the only one cheering me up and Roger, I'll never forget your "one thin waffle". Thank you guys, again.

Assoc. Prof. Dr. Sönmez Sayılı, the member of the PhD examining committee, is gratefully acknowledged for his critical and constructive comments that helped the progress of the thesis. I am grateful to Şükrü Acar (MTA) for determining the Eocene micro fossils. Orhan Karaman is also thanked for his help during the field work.

I also would like to thank my friends, Şule Gürboğa, Ayşe Özdemir, Özgür Aktürk, Ayşe Bayrakçeken and Erbir Eker for always being with me, their encouragement, and friendship.

Last but definitely not the least; I am very grateful to my family for their supports and prayers. In this regard, special thanks go to Hülya, my younger sister, for her unlimited patience, supports and encouragement throughout my life. I know you were tired of my funny, sometimes tragicomic PhD stories but you should know that you always made me laugh by "I see dead people" and "fate dude" phrases no matter what happened. Thank you, girl.

The Scientific and Research Council of Turkey (TUBİTAK) is kindly acknowledged for the project 106Y065 and TUBİTAK 2214 International Research Fellowship Programme grant. I am also thankful to the METU for financial support by METU Research Fund Project (BAP-2005-03-09-01).

TABLE OF CONTENTS

ABSTRACT	iv
ÖZ.....	vi
ACKNOWLEDGMENTS	ix
TABLE OF CONTENTS	xi
LIST OF TABLES	xiv
LIST OF FIGURES.....	xv
LIST OF ABBREVIATIONS	xxv
CHAPTERS	
1. INTRODUCTION.....	1
1.1 Purpose and Scope.....	3
1.2 Methods of Study	4
1.2.1 Field work.....	4
1.2.2 Laboratory work	4
1.3. Previous Studies	6
2. GEOLOGY OF THE STUDY AREA.....	12
2.1 Regional Geology.....	12
2.2 Geological Features of the Eocene Units in the Studied Areas.....	18
2.2.1 Geology of the Eocene units in the Çiçekdağ area.....	19
2.2.2 Geology of the Eocene units in Yozgat area	26
3. PETROGRAPHY	34
3.1 Introduction	34
3.2 Petrographical and Textural Properties of the Volcanic Rocks	34
3.2.1 Basalts	35
3.2.2 Andesites	42
3.3 Disequilibrium Textures and Their Petrologic Significance.....	47
3.3.1 Sieve texture on plagioclases and their coexistence with the normal ones.....	47
3.3.2 Pyroxene reaction rims around quartz xenocrysts.....	48

3.3.3 Reaction rim around mafic minerals	50
3.3.4 Embayed quartz crystals.....	50
3.3.5 Mineral zoning	51
3.4 Discussion	51
4. GEOCHEMISTRY and PETROGENESIS.....	54
4.1 Introduction	54
4.2 Analytical Methods	54
4.3 Alteration Effect.....	55
4.4 Classification of the Studied Rocks.....	56
4.4.1 Normative mineralogy.....	56
4.5 Major Oxide and Trace Element Variations.....	58
4.6 Trace and Rare Earth Element (REE) Geochemistry	65
4.7 Isotope Geochemistry	68
4.8 Differentiation Processes.....	69
4.8.1 Fractional crystallization	71
4.8.2 Crustal contamination.....	73
4.8.3 Magma mixing/mingling.....	78
4.9 Source Region and Petrogenesis	79
4.9.1 Melting conditions and partial melting process	79
4.9.2 Source characteristics	84
4.9.2.1 Crustal contamination.....	87
4.9.2.2 Asthenosphere or plume component contaminated by lithospheric mantle	88
4.9.2.3 Lithospheric mantle source	91
4.10 Trace Element Enrichment.....	94
4.10.1 Low degree partial melting.....	94
4.10.2 Mantle metasomatism.....	95
4.10.2.1 Silicate and carbonate metasomatism.....	95
4.10.2.2 Subduction derived components	97
4.10.2.2.1 Melt related enrichment.....	97
4.10.2.2.2 Sediment addition.....	98
4.10.2.2.3 Slab derived fluids.....	99

4.10.3 Timing of metasomatism.....	102
4.11 Review on Geochemistry of Late Cretaceous Magmatism.....	103
5. GEODYNAMIC IMPLICATIONS	109
5.1 Orogenic vs Anorogenic volcanism	109
5.2 The Mechanism That Triggered Eocene Volcanism.....	111
6. DISCUSSION	125
6.1 Evolution of the Sedimentary Basins	125
6.2 Structural Control on Volcanism.....	133
6.3 Discussion on Petrology of Eocene Volcanism	137
6.4 Tectonic Discrimination Diagrams for the Studied Rocks.....	148
6.5 Comparison with Other Post Collision- Extension Related Rocks	151
7. CONCLUSIONS	157
REFERENCES	159
APPENDICES	197
A. Major oxides and trace element compositions of the studied rocks	197
B. Sr, Nd and Pb isotope compositions of Eocene volcanic rocks.....	210
C. Normative compositions of Eocene volcanic rocks.....	212
D. Trace element ratios used in the text	215
E. Major and trace element compositions of Late Cretaceous granitic rocks	222
F. Sr, Nd and Pb isotope compositions of Late Cretaceous granitic rocks	224
CURRICULUM VITAE	225

LIST OF TABLES

Table 3. 1 General petrographical properties of the Eocene volcanic rocks.	36
Table 4. 1 Calculation of partial melting degrees and source compositions used in partial melting modeling.	83
Table 6. 1 Incompatible trace element ratios in Eocene samples and major mantle reservoirs (PM: Primordial Mantle, N MORB: Normal Mid Ocean Ridge Basalt, CC: Continental Crust, GLOSS: Global Subducted Sediments, OIB: Ocean Island Basalt, HIMU, EM I and EM II are isotopically defined OIB end members. PM, N MORB, OIB and OIB end members are taken from Weaver 1991, GLOSS composition is from Plank and Langmuir 1998, “Eocene” represents the average values of the studied rocks).	149

LIST OF FIGURES

Figure 1. 1 Location map of the studied area (CACC: Central Anatolian Crystalline Complex).	5
Figure 2. 1 Generalized geological map of the Central Anatolian Crystalline Complex (CACC) (simplified from Göncüoğlu et al., 1994).....	13
Figure 2. 2 Simplified geological map of the CACC and the sedimentary basins surrounding it (from Göncüoğlu et al., 1994).	14
Figure 2. 3 Generalized columnar section of the basement rocks (Göncüoğlu et al., 1994, modified from Toksoy, 1998).....	17
Figure 2. 4 Generalized columnar section of the sedimentary cover of the CACC (taken from Göncüoğlu et al., 1994).	18
Figure 2. 5 General distribution of the Eocene volcanics in the Central Anatolia (simplified from 1/500.000 scale geological map of MTA and Göncüoğlu et al 1994).....	19
Figure 2. 6 Geological map of Çiçekdağ area (simplified from 1/100.000 geological map of the MTA, Dönmez et al 2005).....	20
Figure 2. 7 Exposure of the Boğazköy Formation around Kaletepe area. The formation contains alternation of sandstones and limestones. Fossil findings from upper part of the limestone level indicates Middle Eocene age.	22
Figure 2. 8 Cross section displaying the contact relationship of the Boğazköy formation with Eocene volcanic rocks around Alimpınar area.	23
Figure 2. 9 In Alimpınar area Eocene lavas are intercalated with sandstone and marl of Boğazköy Formation.	24
Figure 2. 10 The studied rocks are observed as pillow lavas along Çiçekdağ-Kırşehir road.....	24

Figure 2. 11 The investigated rocks show weakly developed columnar jointing towards the northern part of the Alimpınar area.	25
Figure 2. 12 The studied rocks are aphyric and contain vesicles most of which filled with secondary minerals such as quartz.....	25
Figure 2. 13 Geological map of Yozgat area (simplified from Göncüoğlu et al., 1994).....	27
Figure 2. 14 Alternation of conglomerate, sandstone, shale and marl within Mucur formation around north of Yozgat.	28
Figure 2. 15 Sandstones of Mucur Formation contain abundant plant remnants...	29
Figure 2. 16 Fossiliferous limestones within Mucur formation around Sarıhacılı.....	29
Figure 2. 17 Cross section showing contact relation of Eocene lavas with sedimentary rocks. The area between Paşaköy and Karabıyık lava flows lie above the fossiliferous limestone and sandstone.....	30
Figure 2. 18 In general Eocene volcanic rocks are observed as massive lava flows in Yozgat region. Around Paşaköy studied rocks are intercalated with fossiliferous sandstone.	30
Figure 2. 19 Dykes are not common structures of the Eocene volcanic rocks. However, wherever they are observed, there is a chilled margin at the contact zone.	31
Figure 2. 20 The investigated rocks are also observed as pillow lavas around Kürkçü village located south of Yozgat.	32
Figure 2. 21 Columnar jointing is the most common feature of the Eocene lava flows. The picture is taken from south of Yozgat around Gelingüllü area.	32
Figure 2. 22 Flow banding is one of the most diagnostic features of the studied lava flows exposed around Yerköy in Yozgat area.	33
Figure 3. 1 Basalts are characterized by sub parallel to parallel alignment of the tabular plagioclases (10X, XPL).	37

Figure 3. 2 A glomeroporphyritic cluster which contains plagioclases and clinopyroxenes in basalts(10X, XPL, cpx: clinopyroxene; plag: plagioclase).....	37
Figure 3. 3 Vesicular texture is a common feature of the basalts and these cavities are filled with zeolites, quartz and calcite. In this microphotograph zeolites are seen (10X, XPL).....	38
Figure 3. 4 Photomicrograph showing perlitic cracks and plagioclase microlites in the groundmass of basalt (10X, PPL).....	38
Figure 3. 5 Plagioclase phenocryst shows zonation. Alteration is so intense that plagioclase almost turned into clay (10X, PPL).....	39
Figure 3. 6 Photomicrograph displaying altered olivine phenocryst. Olivine is replaced by serpentine (10X, XPL).....	40
Figure 3. 7 Almost euhedral olivine crystal. It is completely replaced by calcite and also contains opaque inclusions (10X, XPL).....	41
Figure 3. 8 Photomicrograph of glomeroporphyritic clinopyroxene and orthopyroxene. Orthopyroxene is distinguished from clinopyroxene by its low interference color (10X, XPL, opx: orthopyroxene, cpx: clinopyroxene).	42
Figure 3. 9 Fluidal texture, represented by almost parallel alignment of the plagioclases, is commonly observed in Eocene rocks (10X, XPL).....	43
Figure 3. 10 Clinopyroxene minerals are common constituent of the glomeroporphyritic clusters (10X, XPL).....	44
Figure 3. 11 Photomicrograph showing an almost euhedral hornblende phenocryst with reaction rim (10X, PPL).	45
Figure 3. 12 Photomicrograph displaying olivine and xenocryst of quartz coexistence in basaltic rocks. Olivine is entirely replaced by serpentine. Quartz, on the other hand, is surrounded by thick clinopyroxene reaction rim (10X, XPL, Q: quartz, Ol: olivine, Cpx: clinopyroxene).	46

Figure 3. 13 Photomicrograph displaying coexistence of sieve textured and normal (clear) type plagioclases in andesites having glassy groundmass (10X, PPL, S: sieve textured plagioclase, N: normal plagioclase).....	48
Figure 3. 14 Photomicrograph showing plagioclase phenocryst with pyroxene inclusions (10X, PPL, Px: pyroxene, plag: plagioclase).	49
Figure 3. 15 Photomicrograph displaying a quartz xenocrystal which is corroded and rounded and also have augite rims indicating a reaction with surrounding groundmass (10X, XPL, Q: quartz, cpx: clinopyroxene).....	50
Figure 3. 16 Photomicrograph illustrating embayed quartz crystals. Mineral contains glass or fluid inclusions but do not have pyroxene rim (10X, XPL, Q: quartz).....	51
Figure 4. 1 Classification of Eocene volcanic rocks a) on total alkali vs silica (TAS) diagram (Irvine and Baragar, 1971) b) Y vs Zr diagram (McLean and Barret, 1993) c) after Winchester and Floyd, (1977), (Pearce, 1996).....	57
Figure 4. 2 Nb vs Zr diagram for Eocene volcanic rocks (symbols are the same as in Fig. 4.1).....	59
Figure 4. 3 Y vs Zr diagram for the studied rocks.	59
Figure 4. 4 Major oxides variation plots for the studied rocks. Green triangles represent Yozgat samples falling into the Group 1 in Nb-Y vs Zr diagram.	61
Figure 4. 5 SiO ₂ vs Mg number plot for Eocene samples. Rocks from group 2 are characterized by high Mg #s (Symbols are the same in Figure 4.4).	62
Figure 4. 6 Trace element variation plots for Eocene samples (Symbols are the same as in Figure 4.4).....	63
Figure 4. 7 Chondrite normalized REE patterns of investigated rocks a) for Group 2, b) for Group 1 and Çiçekdağ samples (Normalizing values are taken from McDonough and Sun, 1995).....	66

Figure 4. 8 Primitive mantle normalized multi element patterns of the studied rocks a) for Group 2, b) for Group 1 and Çiçekdağ samples (primitive mantle normalized values are from McDonough and Sun, 1995).....	67
Figure 4. 9 $^{87}\text{Sr}/^{86}\text{Sr}$ vs $^{143}\text{Nd}/^{144}\text{Nd}$ plot of the studied samples. Most of the rocks placed on BSE (BSE; bulk silicate earth, EMI and EMII; enriched mantle I and II, DM; depleted mantle, HIMU; mantle having high U/Pb ratio). Different mantle reservoirs are from Zindler and Hart, (1986).....	70
Figure 4. 10 $\Delta 7/4$ vs $^{206}\text{Pb}/^{204}\text{Pb}$ plot for Eocene samples. Data sources; DMM, HIMU, EM I, EM II are from Zindler and Hart (1986) and Hofmann (1997). Northern Hemisphere Reference Line (NHRL) from Hart, (1984). (Symbols are the same as in the Figure 4.4).	70
Figure 4. 11 Sc vs Rb bivariate plot displaying Rayleigh fractionating vectors. Phase combinations are given in inset. Abbreviations: plag; plagioclase, cpx; clinopyroxene, ol: olivine, opx; orthopyroxene, amp; amphibole.	72
Figure 4. 12 a) $^{207}\text{Pb}/^{206}\text{Pb}$ vs $^{206}\text{Pb}/^{204}\text{Pb}$ plot for the studied rocks b) Ba/Nb vs $^{206}\text{Pb}/^{204}\text{Pb}$ c) Ba/Nb vs $^{143}\text{Nd}/^{144}\text{Nd}$ d) Ba/Nb vs $^{87}\text{Sr}/^{86}\text{Sr}$ ratios. (Symbols are the same as in Figure 4.4).....	76
Figure 4. 13 Initial $^{87}\text{Sr}/^{86}\text{Sr}$ vs Rb/Sr plot for assessing crustal assimilation process. The composition of the contaminant (MCG119) and the parental (Pk1) are ($^{87}\text{Sr}/^{86}\text{Sr}$: 0.70869, Rb: 207 ppm; Sr: 1009 ppm and 0.70477; 23.9; 552.4 respectively). The tick marks and numbers on the curve show the percentage of the melt (F) remained in the system.	77
Figure 4. 14 $^{206}\text{Pb}/^{204}\text{Pb}$ vs Pb plot for evaluating the effect of crustal assimilation. The compositions of the end members are (MCG23-21 $^{206}\text{Pb}/^{204}\text{Pb}$ 18.95 and Pb 91 ppm; F26 $^{206}\text{Pb}/^{204}\text{Pb}$ 18.31 and Pb 2.5 ppm).....	78
Figure 4. 15 La/Yb vs La plot for the investigated rocks (Symbols are the same as in Figure 4.4).....	80
Figure 4. 16 Calculated partial melting curves assuming batch melting of garnet facies and phlogopite bearing spinel facies sources. Source compositions	

(Dy=0.674 ppm, Yb= 0.441 ppm) are from McDonough and Sun, (1995). Partition Coefficient (Kd) values are from McKenzie and O’Nion, (1991 and 1995) and GERM (Geochemical Earth Reference Model), home page <http://earthref.org/databases/KDD/>. 82

Figure 4. 17 C1 Chondrite (McDonough and Sun, 1995) normalized REE patterns for the Eocene volcanic samples. For comparison purposes, Upper crust, average arc lavas, ocean island basalts and mid ocean ridge basalts were also plotted (Upper crust value from Rudnick and Gao, 2004; OIB and MORB from Sun and McDonough, 1989 and average arc lavas composition represents Aegean arc (<http://georoc.mpch-mainz.gwdg.de/georoc/Start.asp>)). 85

Figure 4. 18 Primitive mantle (McDonough and Sun, 1995) normalized multi element patterns for the Eocene volcanics (Data set and reference values are the same as in Figure 4.17). 85

Figure 4. 19 Zr/Y vs Zr diagram (Pearce and Norry, 1979) for Eocene volcanics. All samples fall into field A representing within plate setting (Symbols are the same as in Figure 4.4). 86

Figure 4. 20 ϵNd vs $^{87}\text{Sr}/^{86}\text{Sr}$ plot for Eocene volcanic samples. Asthenospheric and lithospheric melt fields are taken from Davies and Van Blanckenburg, (1995). (Symbols are the same as in Figure 4.4). 90

Figure 4. 21 Zr/Y vs Nb/La plot for Eocene volcanic rocks. All samples are characterized by relatively low Nb/La and variable Zr/Y ratios. 92

Figure 4. 22 Nb vs Zr plot for Eocene volcanic rocks in comparison with data for Normal Mid Ocean Ridge Basalts (N MORB), Ocean Island Basalts (OIB), West Siberian Basin (Reichow et al., 2005), Ferrar low Ti basalts (Hergt et al., 1991), Parana (Peate and Hawkesworth, 1996) Apuseni Mt (Rosu et al., 2004). (Symbols are the same as in Figure 4.4). 93

Figure 4. 23 $(\text{La}/\text{Yb})_{\text{N}}$ vs Ti/Eu diagram (Su et al., 2010) for Eocene volcanics. The studied rocks are characterized by relatively high Ti/Eu and low $(\text{La}/\text{Yb})_{\text{N}}$ ratios.(Symbols are the same as in Figure 4.4). 96

Figure 4. 24 La/Yb vs Yb and Sr/Y vs Y diagram for Eocene volcanic samples. The studied rocks are characterized by higher Yb content and lower La/Yb ratios than those of adakitic rocks. Adakite fields are taken from Defant and Drummond (1990).	98
Figure 4. 25 $^{207}\text{Pb}/^{204}\text{Pb}$ vs $^{206}\text{Pb}/^{204}\text{Pb}$ plot for Eocene volcanic samples. Field for Central Indian MORB is from Mahoney et al. (1989) and Hofmann (1997). Field for Atlantic and Pacific MORB is from White et al., (1987) and Hofmann, (1997). The field of GLOSS (global subducted sediment composition, which is based on large number of comprehensive dataset (Plank and Langmuir, 1998). The NHRL (Northern Hemisphere Reference Line; Hart, 1984), EM1 and EM2 (enriched mantle end-members; Zindler and Hart, 1986; Hofmann, 1997; Zou et al., 2000) are plotted for reference (Symbols are the same as in Figure 4.4).	100
Figure 4. 26 Ba/La vs Nb/Zr plot for the studied Eocene rocks. High Ba/La ratios of the Eocene samples can be attributed to fluid related metasomatism. (N- MORB and OIB data are from Sun and McDonough, 1989).	101
Figure 4. 27 $^{87}\text{Sr}/^{86}\text{Sr}$ vs Ba/TiO ₂ and Ba/La plots for Eocene volcanic rocks (Symbols are the same as in Figure 4.4).	101
Figure 4. 28 $^{87}\text{Sr}/^{86}\text{Sr}$ vs Rb/Sr and $^{143}\text{Nd}/^{144}\text{Nd}$ vs Sm/Nd plots for the studied rocks. $^{143}\text{Nd}/^{144}\text{Nd}$ ratios increase with increasing Sm/Nd ratios; however, there is not such trend in the Sr isotope.	103
Figure 4. 29 Total alkalis vs silica diagram for Late Cretaceous granitic rocks. Eocene volcanic rocks are plotted for comparison (Dividing line from Irvine and Baragar, (1971) and symbols are the same as in Figure 4.4).	104
Figure 4. 30 Shand index for the analyzed Central Anatolian granites.	105
Figure 4. 31 C1 Chondrite (Sun and McDonough, 1995) normalized REE plot for the Late Cretaceous granites. Shaded area represents Eocene volcanic rocks.	105

Figure 4. 32 Primitive mantle normalized (Sun and McDonough, 1995) multi element patterns for Late Cretaceous granitic rocks.	106
Figure 4. 33 Th/Yb vs Ta/Yb (Pearce, 1983) diagram for the Late Cretaceous granites and the Eocene volcanic rocks.....	107
Figure 4. 34 ϵNd vs $^{87}\text{Sr}/^{86}\text{Sr}$ plot for Eocene volcanic rocks and Late Cretaceous granitic rocks. Data source for granites are taken from İlbeyli et al., (2004), Boztuğ et al., (2007), Köksal and Göncüoğlu, (2008) and this study.....	107
Figure 5. 1 (A to E) Schematic tectonic diagram displaying evolution of the Tauride platform (from Dilek and Kadıoğlu 2009). AFC; assimilation and fractional crystallization; AHO; Alihoca ophiolite; CACC; central Anatolian Crystalline Complex, EF; Ecemis Fault, HG; Horoz Granitoid, ITO; Inner Tauride Ophiolite, ITSZ; Inner Tauride Suture Zone, Kiziltepe Blue Schist, MO; Mersin Ophiolite, SMM; Subduction Metasomatized Mantle, SSZ; Supra-subduction Zone, TO; Tauride Ophiolite, UB; Ulukışla Basin, UG; Uckapılı Granite.	115
Figure 5. 2 (A to H) Block diagram showing geodynamic evolution of the northern part of the CACC during the period of Late Cretaceous- Early Miocene (from Keskin et al., 2008).	118
Figure 5. 3 Schematic cross section displaying proposed geodynamic evolution of the CACC during Late Cretaceous and Eocene time (CACC: Central Anatolian Crystalline Complex, SC: Sakarya Continent, CKB: Central Kızılırmak Basin).	122
Figure 6. 1 Schematic cross section displaying evolution of the Tertiary basins within the CACC (from Göncüoğlu et al., 1994). As a whole, all basins show comparable features. They were formed within the northern part of the Tauride- Anatolide platform which has experienced significant amount of the crustal thickening during the final closure of the IAEO which in turn resulted in extensional tectonic regime accompanied by calc- alkaline volcanism exposed within these basins.	132

Figure 6. 2 Sr- Nd- Pb isotopes vs silica- $1/Sr*1000$ diagram for Eocene samples (AFC: assimilation and fractional crystallization; FC: fractional crystallization).....	139
Figure 6. 3 Nb/La, Ba/La vs isotope diagrams for the studied rocks. Note that trace element ratios show good correlation only with Pb isotopes (Symbols are the same as in Figure 4.4).....	141
Figure 6. 4 Ba/Rb vs Rb/Sr diagram for Eocene volcanic samples. All samples are shifted towards phlogopite bearing source.	142
Figure 6. 5 Nb/La vs Ba/La plot for the studied rocks (E MORB, MORB and orogenic andesite reference fields are taken from Sun and McDonough, 1989 and Gill, 1981 respectively). Data from other extensional area are also plotted. Ulukışla calc- alkaline and ultrapotassic rocks, Alpaslan et al., 2004; 2006 respectively; Rhodope volcanics Marchev et al., 2004; Armutlu volcanics Kürkcüoğlu et al., 2008; Basin and Range Province Hawkesworth et al., 1995, Rogers et al., 1995; Çorum volcanics Keskin et al., 2008; Apuseni Mt Rosu et al., 2004.	144
Figure 6. 6 ϵNd vs Sm/Nd plot. Linear trend that Eocene volcanic samples show suggests derivation from single source.	145
Figure 6. 7 $(Hf/Sm)_N$ vs $(Ta/La)_N$ plot for the studied rocks. Most of the Eocene samples fall into the subduction related fluid metasomatism area which is consistent with overall geochemical signature of the rocks. Fields are from Wang et al., (2004).	147
Figure 6. 8 $Nb*2-Zr/4-Y$ diagram (Meschede, 1986) for the studied Eocene basaltic rocks.	150
Figure 6. 9 $Y/15- La/10-Nb/8$ plot (Cabaniş and Lecolle, 1986) for Eocene basaltic samples.....	150
Figure 6. 10 Th/Y vs Nb/Y plot for Eocene volcanic samples. Reference data is given next to the figure.....	153

Figure 6. 11 La/Nb vs Th/Nb plot for comparing the studied rocks with the other post collisional rocks from the Alpine belt and Basin and Range Province from the USA. Reference data is the same in Figure 6.10. Upper crust value is from Rudnick and Gao, 2004. 154

Figure 6. 12 $^{143}\text{Nd}/^{144}\text{Nd}$ vs $^{87}\text{Sr}/^{86}\text{Sr}$ isotope correlation diagram of Eocene volcanics (DM; Depleted mantle, MORB; Mid Ocean Ridge Basalt, EAR; European Asthenospheric Reservoir Cebria and Wilson (1995), HIMU; High μ (U/Pb) Reservoir, BSE; Bulk Silicate Earth, EMI; Enriched Mantle 1; EMII; Enriched Mantle II) 155

LIST OF ABBREVIATIONS

BSE	Bulk Silicate Earth
CACC	Central Anatolian Crystalline Complex
DM	Depleted Mantle
DMM	Depleted MORB Mantle
EM I	Enriched Mantle I
EM II	Enriched Mantle II
HFSE	High Field Strength Element
HIMU	Mantle having high U/Pb ratio
HT/LP	High Temperature/Low Pressure
HREE	Heavy Rare Earth Element
ICP-AES	Inductively Coupled Plasma-Atomic Emission Spectrometry
ICP-MS	Inductively Coupled Plasma-Mass Spectrometry
LILE	Large Ion Lithophile Element
LREE	Light Rare Earth Element
LOI	Loss on Ignition
Ma	Million Years
NHRL	Northern Hemisphere Reference Line
REE	Rare Earth Element
TAS	Total Alkali versus Silica

CHAPTER 1

INTRODUCTION

Post collisional magmatism with distinct geochemical signature was voluminously developed after the closure of the Neotethyan Ocean during the Late Cretaceous time in Turkey and Cenozoic time within the Alpine-Himalayan orogenic belt including the Mediterranean region (Turner et al., 1996; Zeck et al., 1998; Miller et al., 1999; Turner et al., 1999; Aldanmaz et al., 2000; Maury et al., 2000; Williams et al., 2001; Coulon et al., 2002; Williams et al., 2004; Rosu et al., 2004; Marchev et al., 2004; Duggen et al., 2005; Harangi and Lenkey, 2007). This magmatism is generally characterized by arc-like geochemical signature despite its post collisional geodynamic situation, and exhibits progressive evolution from calc-alkaline to alkaline geochemical character. The geochemical transition from calc-alkaline to intra-plate-type geochemical trend is thought to be derived from a major change in mantle geometry beneath the Mediterranean region (Duggen et al., 2005 and references therein).

In Turkey, being an important part of the Alpine-Himalayan orogenic belt, large amounts of granitic bodies were intruded in the Central Anatolian Crystalline Complex (CACC) during the time span of 95-66 Ma (Göncüoğlu et al., 1994; Eler and Göncüoğlu, 1996; Boztuğ, 1998, 2000, 2003, 2007, 2009; Aydın et al., 2001; Köksal et al., 2001, 2004; İlbeyli et al., 2004; İlbeyli and Pearce, 2005; Köksal and Göncüoğlu, 2008). Their compositions vary from potassic to high-K calc-alkaline, peraluminous and alkaline series (Göncüoğlu et al., 1994; Eler and Göncüoğlu, 1996; Boztuğ, 1998, 2000, 2003, 2007, 2009; Düzgören- Aydın et al., 2001; Köksal et al., 2001, 2004, 2008; İlbeyli et

al., 2004; İlbeyli and Pearce, 2005), suggesting different amount of mantle and crust contributions to their genesis. Although geological character, age and composition of the granitic rocks in the complex have been well documented in the previous studies, their geodynamic setting and the mechanism that triggered the magmatism have remained controversial. Origin of the Late Cretaceous granitic magmatism and its tectonic implication has long been debated. In the previous studies, this granitic magmatism has been regarded as arc magmatism formed during the closure of Inner-Tauride branch of Neotethyan Ocean (Görür et al., 1983; Erdoğan et al., 1996; Kadioğlu and Dilek, 2009). However, other studies indicate that Central Anatolian magmatism is of post-collisional character and related to the post-collisional extension (Göncüoğlu and Türel, 1993; Göncüoğlu et al., 1994; İlbeyli and Pearce, 1997; Çemen et al., 1999; Dirik et al., 1999; Boztuğ, 2000; İlbeyli and Pearce, 2005).

After termination of the common granitic magmatism, there was a hiatus in magmatic activity that lasted for a period of ~15 Myr, when several sedimentary basins were developed in the CACC. The post collisional extension or trans-tension related to these basins evolution especially during the Eocene is accompanied by a volcanic event which has not been seriously considered in the previous studies. Eocene volcanic rocks are commonly observed in the northern and central parts of the Eocene basins namely Çankırı and Central Kızılırmak, and intercalated with Early and Middle Eocene clastics and volcanoclastic rocks, with fossiliferous limestones. Occurrence of the sedimentary basins and the volcanic rocks are also subject of debates. Some authors (Görür et al., 1981 and 1984; Erdoğan et al., 1996; Baş et al., 1996; Kadioğlu and Dilek, 2009) regarded them as products of late stage arc related basins and interpreted the volcanism to be caused by north dipping subduction of the Inner Tauride Ocean beneath Anatolian block. Others (Göncüoğlu et al., 1994; Gürer and Aldanmaz, 2002; Clark and Robertson, 2002; Alpaslan et al., 2006), however, argued that these basins were formed as extensional basins after the closure of the Neo-Tethyan Ocean.

All these speculations regarding the geodynamic evolution of the CACC (i.e. basin formations and accompanied volcanism, relationship between basin formation and tectonic setting, mechanism that causes the magmatism and volcanism in the region) makes the studied area a key region for better understanding of dynamics of post collisional magmatism and volcanism and their source region as well. Moreover, the geochemical features of the Eocene volcanics may be an important tool to clarify the petrological changes in mantle source region beneath central Anatolia after a collision event.

Purpose of the present study is to put new insights into the nature of the source region and evolutionary processes of Eocene calc-alkaline volcanism, and its role in geodynamics of the CACC. In the previous studies, this Eocene volcanic event related to basin formation has not been taken into consideration petrologically. The studies are limited to whole rock geochemical data excluding isotopic compositions (Büyükönal, 1986; Alpaslan et al., 2000). The study is concerned with petrology of Eocene volcanic rocks in the CACC.

1.1 Purpose and Scope

The aim of this study is; 1) to investigate the petrogenesis of the post collisional volcanism within the CACC, by establishing the mineralogical and chemical differences and similarities of Eocene volcanic rocks exposed especially in Çiçekdağ (Kırşehir) and Yozgat areas; 2) to decipher the evolution of the mantle source region of this volcanism during Tertiary time; 3) to search the effects of possible mantle enrichment process by different metasomatizing agents (e.g. mantle and/or subduction related components) 4) to understand the magmatic evolution of the CACC and its surroundings (e.g. Ulukışla basin) during the Early Tertiary that followed the Late Cretaceous post collisional period, and 5) to find out possible geodynamic model that caused this large scale magmatism in the CACC in post- orogenic stage.

In the recent years, a number of geodynamic model have been suggested for the geodynamic evolution of the Central Anatolian Crystalline Complex. The overall goal of this research is also to test these models (e.g. subduction, lithospheric delamination and slab break off) and clarify the origin of the volcanism and possible effects of this volcanism on the evolution of the CACC for the Eocene epoch.

1.2 Methods of Study

1.2.1 Field work

Field works in CACC were performed in summer months of 2006-2007. These works mainly included detailed geological mapping and systematical sampling of critical areas with more or less well-preserved outcrops. The overall geological mapping of studied area was performed by Göncüoğlu et al., (1991, 1992, 1993, and 1994). So that in this study detailed mapping was confined to specific areas. The major effort during the field work was the observation of the relationships of volcanic and associated sedimentary rocks and detailed sampling of the volcanic rocks. Although Eocene volcanic units are widespread in the Tertiary basins in the periphery of CACC, the sampling in this study was mainly restricted to Çiçekdağ (Kırşehir) and Yozgat areas, where the volcanic rocks intrude or overlie the crystalline basement of the CACC (Figure 1.1). The studied area is included in Kayseri I32b3, b4, I32c3, I33c1, c3, I34d4 quadrangles of 1/25000 scale topographic map of Turkey. For petrographical and geochemical purposes, a total of 150 samples representing each area were collected. Sedimentary rocks were also sampled for paleontological dating.

1.2.2 Laboratory work

The first step of the laboratory work includes the microscopic examination of the thin sections of the collected samples. 150 thin sections were prepared at

Department of Geological Engineering laboratories, METU. Mineralogical and textural properties of samples from both areas were established by examining the thin sections under the polarizing microscope.

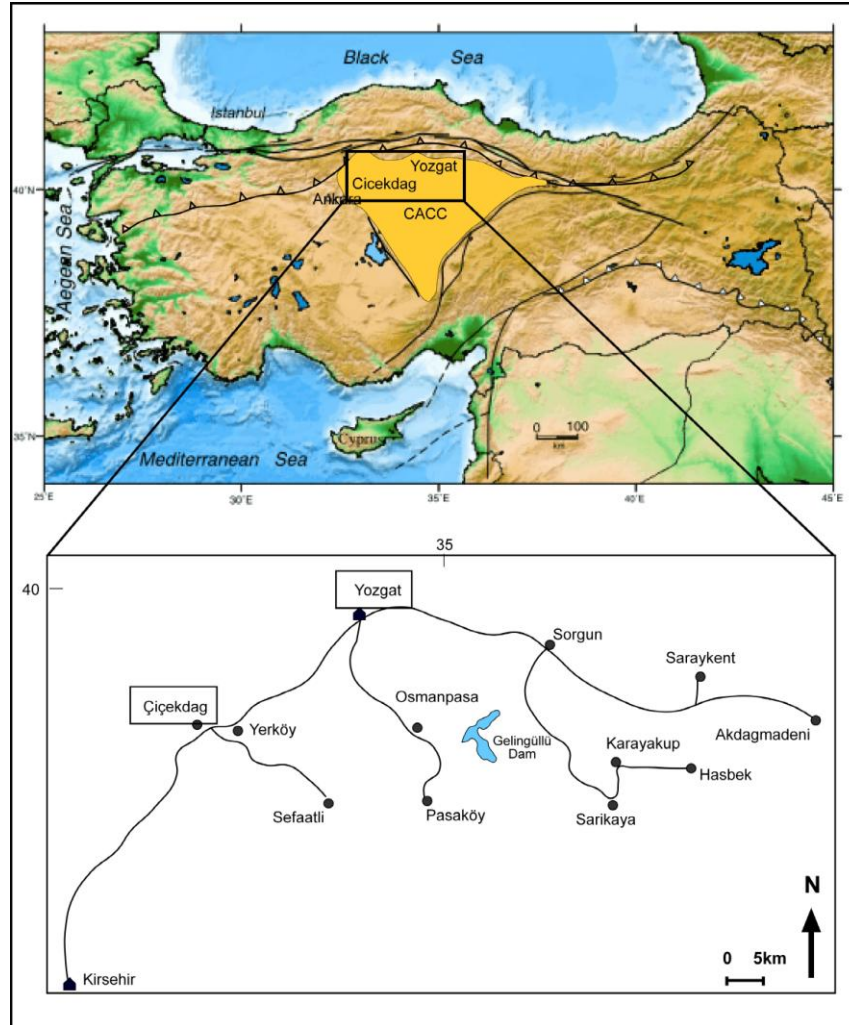


Figure 1. 1 Location map of the studied area (CACC: Central Anatolian Crystalline Complex).

Geochemical analyses were the next step of the laboratory work. Geochemical analyses comprise major oxides, trace and Rare Earth Elements (REE), isotopes (Sr-Nd-Pb). After thin section examination, fresh samples were selected and powdered at the sample preparation laboratory of Department of

Geological Engineering (METU) and analyzed with inductively coupled plasma-mass spectrometer (ICP- AES and ICP-MS). A total of 73 samples representing Çiçekdağ and Yozgat areas were analyzed for major oxides, trace and rare earth elements in the ACME Laboratory in Canada. Sr, Nd and Pb isotope analyses of 20 volcanic and 7 granitic samples were performed at the Isotope Geochemistry Laboratories of the University of Texas at Austin, USA. Besides, 4 samples were analyzed for Sr, Nd and Pb isotopes at Central Laboratory, METU.

1.3. Previous Studies

So far, petrological studies conducted on the CACC generally have been restricted to basement units or metamorphic rocks in relation to paleotectonic period (Göncüoğlu, 1981; Whitney and Dilek, 1998), ophiolitic rocks (Yalınz et al., 1996, Yalınz and Göncüoğlu, 1998; Göncüoğlu et al., 1998; Erdoğan et al., 2000; Koçak et al., 2007; Toksoy- Köksal et al., 2009), granitic magmatism (Akıman et al., 1993; Türeli et al., 1993; Aydın et al., 1998; İlbeyli and Pearce 2005; Boztuğ et al., 2000, 2007) and Quaternary volcanic centers (Pasquare et al., 1988; Toprak and Göncüoğlu, 1993; Vachard et al., 1998; Kürkçüoğlu, 1998; Aydar and Gourgaud, 1998; Gençalioğlu -Kuşcu and Geneli, 2010). Recent studies have focused on the sedimentary basins (Çankırı, Tuzgölü, Sivas and Ulukışla) formed after the closure of the Neotethyan ocean within the CACC (Göncüoğlu et al., 1991) or Kırşehir Block (Görür et al., 1984) during Late Cretaceous time (Kaymakçı et al., 2003; Çemen et al., 1999; Dirik et al., 1999; Görür et al., 1984, 1996; Clark and Robertson, 2002, 2005). However, contemporaneous formation of the extensional or trans-tensional basins (Göncüoğlu, 1992; Dirik et al., 1999) and Eocene volcanism has not been taken into consideration in detail in previous studies. Actually, the sedimentary basins at the margins of the CACC (Çankırı basin in the north, Sivas Basin in the east, Ulukışla Basin in the south and the Tuz Gölü Basin in the west) together with the Central Kızılırmak Basin in the internal part are the locus of extensive Eocene volcanism.

Studies on Eocene volcanic rocks exposed to the north of CACC around Yozgat and Çiçekdağ are basically petrography orientated (Büyükönal, 1986; Alpaslan et al., 2000; Koçbulut et al., 2001) and generally trace element and isotope data were not presented.

The earliest data on Eocene volcanism in the CACC was reported by Ketin, (1955). He defined the Eocene volcanic units around Yozgat region as the “Lutetian volcanic facies” and interpreted them to be composed of lava flows, agglomerates and ashes.

Büyükönal, (1986) described the same rock-units as “Yozgat Volcanics” in her study, focused on their petrographic characteristics and evaluated their geochemical characteristics on the basis of limited major oxide analysis.

Erdoğan et al., (1996) named these volcanic rocks as “Bayat Volcanics” consisting of basaltic and andesitic lavas, breccias and tuffs. They claimed that the volcanic rocks are products of arc related magmatism formed at the north margin of Kırşehir Massif.

Alpaslan and Temel, (2000) were firstly described the trace element geochemistry of the rocks in Yozgat area. They claimed that the rocks are calc-alkaline in nature and magma mixing, fractional crystallization and assimilation are the main petrogenetic processes during the evolution of the volcanic rocks.

Widespread Eocene volcanism is also observed to the east of the CACC in Sivas region. Gökten and Floyd, (1987) examined the petrographical–geochemical properties of the Eocene volcanic rocks within Şarkışla (Sivas) area and classified them as calc-alkaline andesites.

In the vicinity of Sivas, Eocene volcanic rocks called as Pazarcık volcanics and Kaletepe volcanics by Alpaslan, (2000) and Koçbulut et al., (2001),

respectively. In both areas the volcanic rocks are generally composed of basalts, andesites and dacites. In these studies, the authors mainly concentrated on the petrographic features of the volcanic rocks.

Another study regarding Eocene volcanism to the north of CACC in Çankırı basin was carried out by Demirer et al., (1992). They divided the volcanic rocks into four categories; 1) tholeiitic basalts and tholeiitic olivine basalts of mantle origin, 2) basaltic and andesitic lavas indicating crustal origin, 3) tuffs and agglomerates, 4) hornblende biotite andesite, biotite andesite and pumice biotite andesites. The authors made this classification based on the petrographical observations without any geochemical analysis.

Most recently, Eocene volcanic rocks along the North Anatolian Fault Zone in Yuvacık and Armutlu areas, located to the north of the central Anatolia, have been studied by Kürkcüoğlu et al., (2008). In this study, the volcanic rocks vary from calc-alkaline to tholeiitic in nature. The authors pointed out that the differences between lava suits in terms of their geochemistry can be attributed to small degree mantle heterogeneity in the source region. This study also contains radiometric age determinations for the volcanic rocks exposed in those areas. $^{40}\text{Ar}/^{39}\text{Ar}$ data indicates an age of 47.04 ± 1.22 Ma and 51.79 ± 0.38 Ma (Early Eocene, Ypresian) for the rocks from Armutlu and Yuvacık areas, respectively (Kürkcüoğlu et al., 2008).

Keskin et al., (2008) also studied the geochemistry of the Eocene volcanic rocks from Amasya and Çorum regions to the north of Kırşehir. In these areas, the Middle Eocene volcanism produced voluminous sub-aerial lavas from basalt to rhyolite, and their pyroclastic units. Keskin et al., (2008) argued that the mechanism responsible for volcanism is slab break-off which is also proposed to explain the formation of the Eocene magmatism and metamorphism in other parts of the Alpine-Himalayan collision belt.

As Eocene volcanism is spatially related to the evolution of the Eocene basins, it is worth to evaluate also the basin development in and around the CACC. Studies on the structural geology, stratigraphy and sedimentology of these basins in the Central Anatolia are numerous (Görür et al., 1984; Dirik et al 1999; Çemen et al., 1999; Gürer and Aldanmaz, 2002; Kaymakçı et al., 2003).

Ulukışla is one of these basins in which extensive Eocene volcanism is observed. Initial studies on Ulukışla basin started with beginning of the 1980's by Oktay, and most of them are related to the sedimentology and stratigraphy of the basin (Oktay, 1982; İşler, 1988; Çevikbaş and Öztunalı, 1991; Clark and Robertson, 2002; Gürer and Aldanmaz, 2002; Clark and Robertson, 2005), on the other hand, studies focused on the volcanics within this basin are limited to a few investigations (İşler, 1988; Baş et al., 1992; Alpaslan et al., 2004 and 2006; Kurt et al., 2008).

Baş et al., (1992) studied the geochemistry of the volcanic rocks in the Ulukışla basin. The authors suggested that the volcanics are alkaline in character and are supposed to have been formed in arc environment.

Clark and Robertson, (2002) studied geology and stratigraphy of the Ulukışla basin. They defined general tectonic features of the basin and provided some geochemical data on the Late Cretaceous to Early Oligocene volcanic rocks. They further claimed that intrusive and extrusive rocks within the Ulukışla basin are co-genetic and they display within plate character with a certain subduction fingerprint.

One of the most recent study on Eocene volcanic rocks within Ulukışla basin and their tectonic setting was reported by Alpaslan et al., (2004). The rock types in the Ulukışla basin consist of conglomerate, sandstone, marl, pelagic limestone, reefal limestone, claystone and volcanic rocks including pillow lavas, lava flows and pyroclastic rocks (Alpaslan et al., 2004). They suggested that the volcanic rocks exhibit within plate geochemical signature.

Presence of the ultrapotassic lavas indicating enriched mantle source beneath the Ulukışla basin is also documented by Alpaslan et al., (2006). They suggested that the mantle lithosphere beneath the Ulukışla basin was metasomatized during closure of Neotethyan Ocean and enrichment was caused by fluids and subducted sediments.

The most recent study around the Ulukışla basin was conducted by Kurt et al., (2008). The authors studied the late stage dyke swarms of the basin. They are calc- alkaline and shoshonitic in composition and classified as monzo- gabbro, monzo- diorite, and gabbroic diorite. All rock types are characterized by enrichment of LILE and LREE. The authors argued that the formation of the dyke swarms is related with the extensional tectonic regime during Eocene that followed the Late Cretaceous compression and resulted in the opening of the Ulukışla basin.

To understand the different speculations concerning the basin formation in the Central Anatolia, the followings should be considered. The Late Cretaceous and Tertiary period in CACC is characterized by extensive sedimentation deposited within the huge basins surrounding or separating the CACC from the Tauride- Anatolide platform and the Pontides. These are namely; Tuzgözü, Haymana, Ulukışla and Çankırı basins, respectively. The Central Kızılırmak basin is another important structure, which is formed within the CACC. Although in the last 20 years, various studies have been conducted to clarify the formation of the sedimentary basins and their regional geodynamic evolution (Görür et al., 1984, 1998; Tüysüz and Dellaloğlu, 1992; Floyd et al., 1998; Çemen et al., 1999; Dirik et al., 1999; Gürer and Aldanmaz, 2002), in the literature, however, there is a still ongoing debate on their tectonic setting. This is basically derived from the idea that there was another branch of the Tethyan ocean namely Inner Tauride Ocean between the Tauride Carbonate platform to the south and Kırşehir continent to the north during the Jurassic (Şengör and Yılmaz, 1981; Oktay et al., 1981; Görür et al., 1984). Subduction of pieces of the oceanic lithosphere beneath the CACC during Paleocene is believed to

result in formation of fore arc sedimentary basins in the region (i.e. Haymana, Ulukışla, Tuzgölü; Görür et al 1984; Erdoğan et al., 1996; Kadioğlu and Dilek, 2009). However, some others claimed that there was no Mesozoic oceanic area between CACC and the Taurides and the Tertiary basins were formed by post collisional extension and/or trans-tension (Göncüoğlu et al., 1933 and 1994; Dirik et al., 1999; Çemen et al., 1999; Gürer and Aldanmaz, 2002).

CHAPTER 2

GEOLOGY OF THE STUDY AREA

2.1 Regional Geology

Turkey consists of several micro continents represented by continental and oceanic terranes. Oceanic terranes in general, consist of Tethys Oceans, of which the largest and well known is Northern Neotethys. Previous studies on geologic evolution of the Central Anatolia (e.g. Şengör and Yılmaz, 1981; Göncüoğlu et al., 1997; Göncüoğlu et al., 2000) indicate that this branch of Neotethyan Ocean existed between Sakarya continent and Tauride- Anatolide Platform or Central Anatolian Crystalline Complex (CACC, Figure 2.1) during the Late Cretaceous time and subducted under Sakarya continent along İzmir-Ankara- Erzincan suture zone, leading to collision of two continents. The Late Cretaceous time is characterized by allochthonous nappes of ophiolitic sequence and tectonic mélangé that were generated during the closure of the Neotethys Ocean and thrust onto the Tauride-Anatolide platform (Göncüoğlu et al., 1997, 2000). Therefore, geology of the central Anatolia is complex because of the intensive metamorphism, magmatism and deformation process that caused by Alpine subduction and collision events.

The northernmost passive margin of the Tauride- Anatolide Platform bounded by İzmir-Ankara-Erzincan Suture Zone to the north, Sivas Basin to the east, Tuz Gölü basin to the west and Ulukışla basin to the south is called as Central Anatolian Crystalline Complex (CACC) (Göncüoğlu et al., 1991, 1992, 1993, 1994) (Figure 2.2). In the earlier studies, the crystalline unit, composed of the different rock assemblages, was named as Central Anatolian Massif (Ketin,

1955) or Kırşehir Complex (Lünel, 1985); Göncüoğlu et al., (1991) renamed this geological entity as the Central Anatolian Crystalline Complex on the basis of dissimilar lithological assemblages it includes and their structural relations.

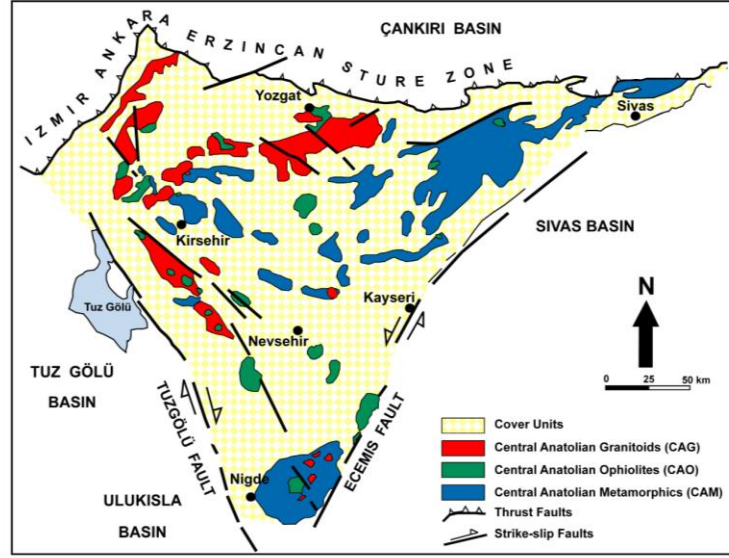


Figure 2. 1 Generalized geological map of the Central Anatolian Crystalline Complex (CACC) (simplified from Göncüoğlu et al., 1994).

In general CACC comprises completely different assemblages such as metamorphic, ophiolitic, magmatic rocks and sedimentary cover (Figure 2.1). It has gained its character as a crystalline complex during the Alpine orogeny. The name “Kırşehir Block” (Görür et al., 1984), on the hand, denotes its Neotectonic character.

Ophiolitic rocks of the CACC, known as Central Anatolian Ophiolites (Mesozoic), consist of ultramafic rocks, cumulates, gabbros, layered gabbros, diabbases, plagiogranites, pelagic sedimentary rocks and exhibit low grade metamorphism (Yalınız and Göncüoğlu, 1998).

The metamorphic assemblages of the complex represent a high temperature-low pressure (HT/LP) metamorphic continental platform sequence and are

tectonically overlain by metamorphic and ophiolitic mélangé and a dismembered ophiolitic nappe. Emplacement of ophiolitic nappes and crustal thickening that took place during the closure of the northern branch of the Neo-Tethyan Ocean led to high grade metamorphism in the Central Anatolian Crystalline Complex.

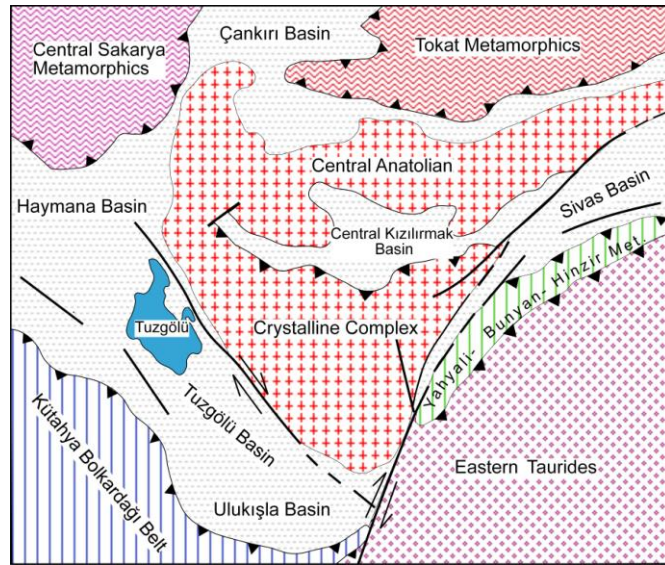


Figure 2. 2 Simplified geological map of the CACC and the sedimentary basins surrounding it (from Göncüoğlu et al., 1994).

Metamorphic rocks of the complex comprises three different assemblages from bottom to top; Paleozoic Gümüşler formation which is mostly composed of gneiss; Mesozoic Kaleboynu formation represented by an alternation of marble, mica schist, calc- silicate marble and gneiss; and Aşıgediği formation consisting of marble (Göncüoğlu et al., 1991). The platform carbonate-dominated is covered by a metamorphic olistostrome with ophiolitic olistolites. The metamorphic assemblage overall is correlated with the Paleozoic-Mesozoic rock units of the Tauride-Anatolide Platform (Özgül, 1976; Göncüoğlu, 1977).

The magmatic activity, mainly granitic in nature, on the CACC began during the Late Cretaceous period (Göncüoğlu, 1986) soon after or penecontemporaneous with the peak of metamorphism. Tectonomagmatic discriminations indicate that this magmatism is post-collisional and mainly comprises a large variety of granitic rocks such as high-K calc-alkaline granitoids as well as peraluminous and alkaline-peralkaline series (Göncüoğlu et al., 1994; Erler and Göncüoğlu, 1996; İlbeyli and Pearce, 1997; Boztuğ, 1998, 2000; Aydın et al., 2001; Köksal et al., 2001, 2004; İlbeyli et al., 2004; İlbeyli and Pearce, 2005). Generalized columnar section of the basement rocks of the CACC is given in Figure 2.3.

Oldest non-metamorphic cover units of the CACC are made up the marine sedimentary, volcanic and volcanoclastic rocks of the Late Cretaceous and Early Tertiary (?Upper Maastrichtian-Paleocene) age formed within the E-W trending basins Late Tertiary continental clastics and volcanics (Central Anatolian Volcanics of Toprak and Göncüoğlu, (1993)) represent the younger cover of the CACC. According to Göncüoğlu et al., (1994) and Dirik et al., (1999) the cover units occur either in a limited number of sedimentary basins formed during the Late Cretaceous-Tertiary period after the closure of the northern branch of the Neo-Tethys within the CACC or in surrounding huge basins and separating it from the main trunk of the Tauride- Anatolide platform. The cover units are mapped as Elmadere, Göynük, Yeşilöz and Mucur formations. The last one includes the Eocene volcanics (Göncüoğlu et al., 1993, 1994). Generalized columnar section displaying the cover units is given in Figure 2.4.

Being the oldest formation in the cover unit, Maastrichtian- Paleocene Elmadere formation is characterized by shallow marine and continental deposits. This unit is defined as representative of the earliest marine transgression in relation with the post-collisional uplifting of the CACC (Göncüoğlu et al., 1991, 1992, 1993, 1994). According to this assumption, sedimentary basins that evolved as extensional basins during Upper

Maastrichtian- Early Paleocene were filled with alluvium deposits and debris flows on the continental platform and by shallow-marine sediments at the margin. From these, Kızılırmak Basin located within the central part of the CACC became an aborted extensional basin (Göncüoğlu et al., 1993), while peripheral basins such as Tuz Gölü, Ulukışla and Sivas continued to expand and became deeper.

Göynük formation consists of a sedimentary sequence with volcanoclastic olistostromes and is dominated by red sandstones at its middle part. The type locality is at Göynük village located northern part of Avanos (Nevşehir, Köksal and Göncüoğlu, 1997). Göynük formation is contemporaneous with Elmadere formation but represents the intra-cratonic deposition with restricted marine influence. Maastrichtian- Paleocene Göynük formation laterally grade into Yeşilöz formation. Red clastics formed as debris flow at the central part of the CACC are named as the Yeşilöz formation (Göncüoğlu et al., 1993). Debris flow deposits together with mud flow dominate at lower parts of the units and they grade upward into shallow marine and continental deposits. The Yeşilöz formation and its Saytepe member are widely distributed in the studied area. They are mainly exposed within the northern part of the CACC and mainly consist of red continental deposits with volcanic clasts. Another member of Yeşilöz formation, characterized by grey- brown coarse grained sandstone, siltstone at the lower part and lacustrine deposits at the upper part is called as the Asaftepe member (Göncüoğlu et al., 1994). Asaftepe member represents lacustrine and shallow marine environment based on its lithological and fauna contents. The Yeşilöz formation contains fossils of Late Paleocene (Thanetian) age (Göncüoğlu et al., 1992, 1993).

Mucur Formation is the next transgressive unit above the CACC. Its main distribution is the E-W trending Central Kızılırmak Basin in the center of the crystalline complex, following more or less the Kızılırmak valley. Mucur formation contains 5 different lithostratigraphic units composed of different rock types namely; Göbekli member representing the by basal conglomerates,

Ayhan member containing fossiliferous limestone, Sarılar member composed of sandstone- shale alternation within a blocky flysch sequence, Keklicek member formed by marl and volcanic member composed of the basaltic andesite and basalt. Volcanic units, the subject of this study, are widely distributed in the northern part of the CACC, especially to the south of the Çankırı basin and are called as Yozgat (Büyükönel, 1986) and Bayat Volcanics (Erdoğan et al., 1996) in the previous studies.

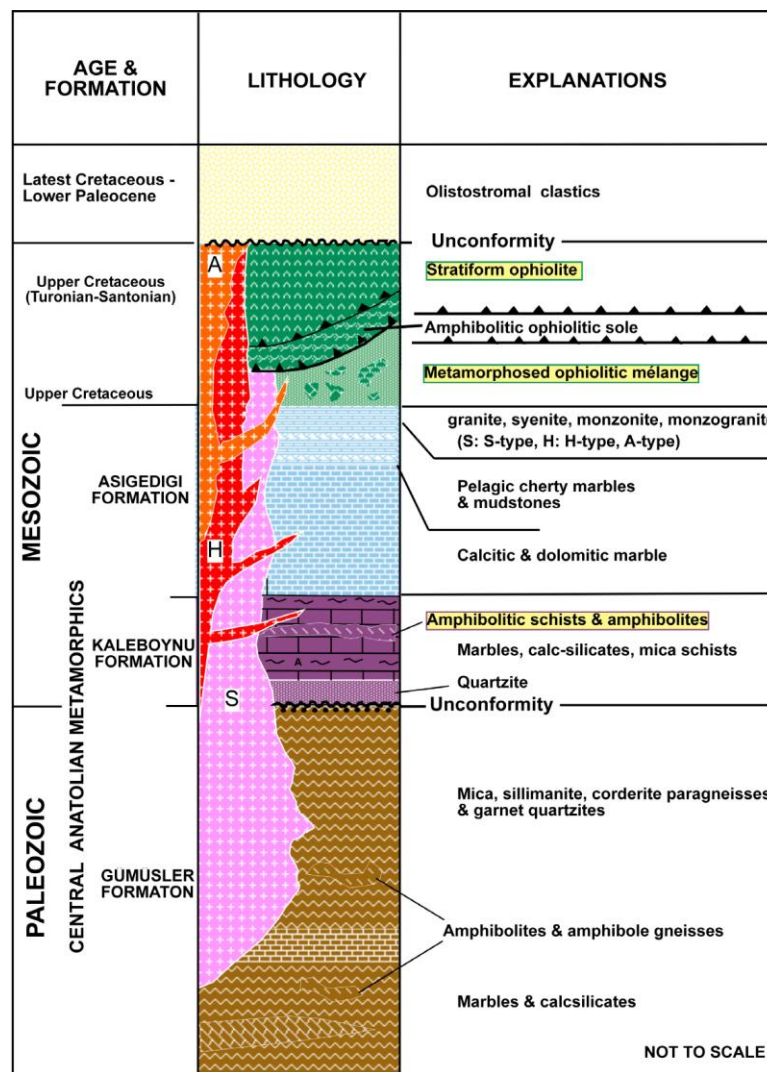


Figure 2. 3 Generalized columnar section of the basement rocks (Göncüoğlu et al., 1994, modified from Toksoy, 1998).

Age and Formation		Lithology	Explanations
N e o g e n e	Lower- Middle Miocene G ü m ü s y a z i		Cover units
			Unconformity
			Conglomerate
			Cross bedded sandstone and conglomerate
			Gypsum and marl
			Marl with coal
			Unconformity
			Green-pinkish and white marl
			Flysh
			Basaltic and andesitic volcanics
E o c e n e	M u c u r		White- grey fossiliferous reefal limestone
			Conglomerate- sandstone
			Unconformity
			White and pink fluvial limestone and marl
			Sandstone
			Volcanoclastic flysh with volcanic and metamorphic blocks
			Unconformity
			Central Anatolian Crystalline Complex
			Paleozoic-Mesozoic
			Central Anatolian Crystalline Complex

Figure 2. 4 Generalized columnar section of the sedimentary cover of the CACC (taken from Göncüoğlu et al., 1994).

2.2 Geological Features of the Eocene Units in the Studied Areas

Since the general geological features of the Eocene units were presented in previous studies (Göncüoğlu et al., 1991, 1992, 1993, 1994), only a brief description of lithological characteristics of the basement rocks and their contact relations with the cover units were given here. The distribution of the

Eocene volcanic rocks in Central Anatolia is shown in Figure 2.5. During this study, only the volcanic samples in undoubted relation with fossiliferous Eocene rocks were collected. The detailed descriptions of the main geological features of the Eocene rocks from two main volcanic profiles are given in the next section.

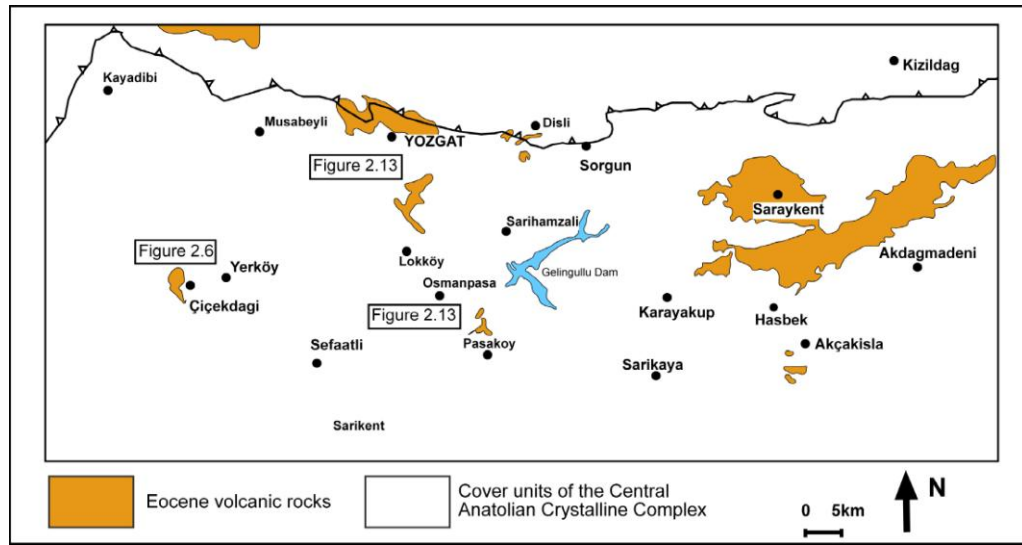


Figure 2. 5 General distribution of the Eocene volcanics in the Central Anatolia (simplified from 1/500.000 scale geological map of MTA and Göncüoğlu et al 1994).

2.2.1 Geology of the Eocene units in the Çiçekdağ area

The geological map of Çiçekdağ (Kırşehir) area is given in Figure 2.6. In this area, the oldest unit observed is the granitic rocks of the CACC basement and exposed eastern and western part of Çiçekdağ. They display frequent changes in mineralogy over short distances. They are represented by granites and granodiorites around Çamlık area; however, they are cut by pinkish syenites around Hamamtepe district. They are equigranular to porphyritic. Porphyritic ones are characterized by large pinkish feldspar crystals. It includes roof-pendants of the Central Anatolian Ophiolites (Yalınz et al., 2000).

Radiometric age determinations performed on granitic rocks gave the age of 71 Ma (Ataman et al., 1972).

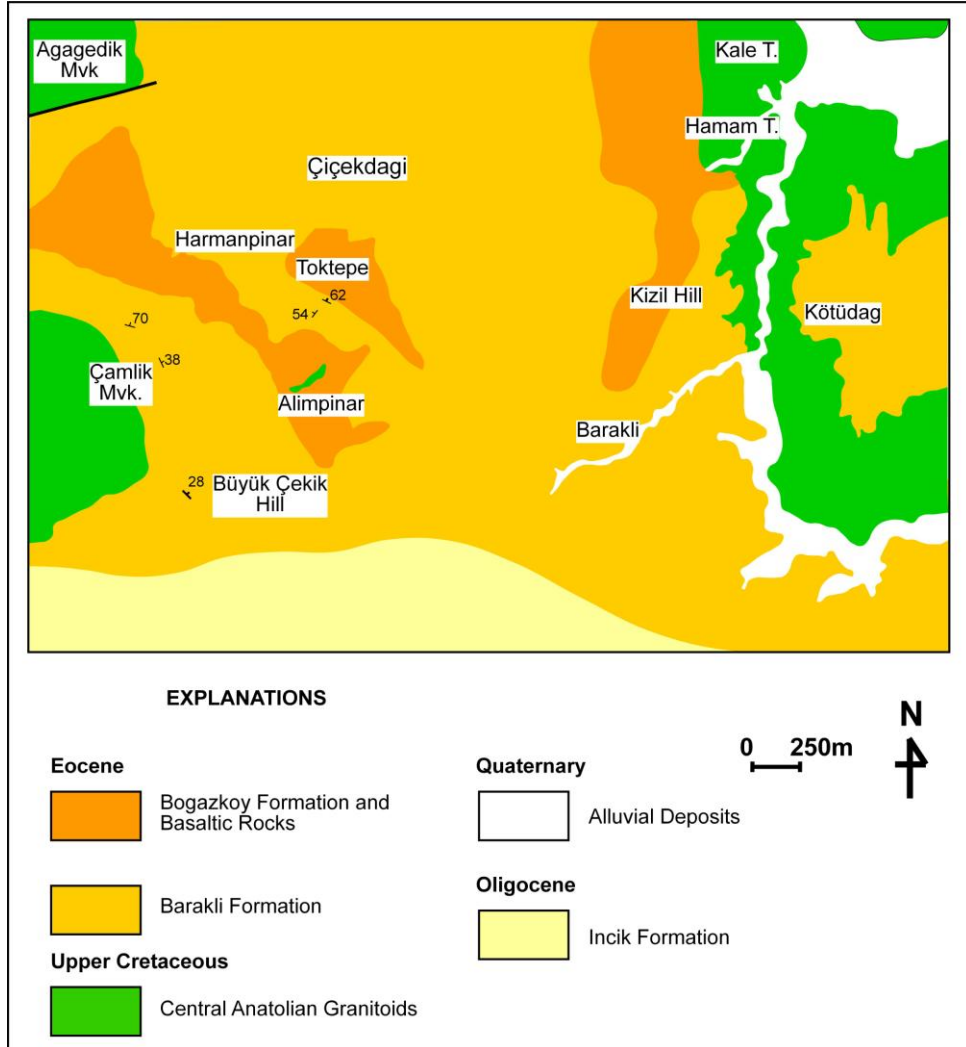


Figure 2. 6 Geological map of Çiçekdağ area (simplified from 1/100.000 geological map of the MTA, Dönmez et al 2005).

The Eocene units within the Çiçekdağ area are represented by Baraklı formation and Boğazköy formation (Figure 2.6), the latter contains also basaltic lava flows and these units unconformably overlie the central Anatolian granitoids. In the previous studies Baraklı formation was named as Hacıhalil

(Birgili et al., 1975) but the name Barakli is used in this study, following Kara and Dönmez, (1990).

The formation contains alternations of conglomerates having metamorphic clasts, yellow- grey sandstones, reddish grey mudstones, and has widespread distribution throughout the study area. Based on its fossil content the formation is assumed to be Middle Eocene (Dönmez et al., 2005).

Boğazköy formation conformably overlies Barakli and consists of white-yellow limestones, pale brown- yellow sandstones intercalated with volcanic rocks and comparatively minor quantities of siltstones (Özcan et al., 1980). Type location of the Bogazköy formation is around Kaletepe area (Figure 2.6) to the N of Yerköy. In this area, the formation starts with red conglomerates and sandstones, continues with grey- greenish sandstone and terminates with yellowish- beige fossiliferous limestones (Figure 2.7). Around Alimpınar and Harmanpınar, there is no fossil observed within the limestones of Boğazköy formation whereas, the formation becomes fossiliferous towards Kaletepe in northern part of the study area. Following fossils were found in limestones at this part of the study area, dating the formation as Bartonian (Middle Eocene) age (det. Dr. Şükrü Acar, MTA).

Nummulites sp,
Asterigerina rotula,
Rotaliidae,
Miliolidae,
Linderia brugesii.

This finding is in accordance with the previously published data (Göncüoğlu et al., 1992, 1993; Erdoğan et al., 1996). Boğazköy formation also contains uniform limestone beds to the south of Çiçekdağ. The Eocene volcanic rocks, distinct member of the Boğazköy formation, crop out within the large area around Alimpınar and Harmanpınar (Figure 2.6). They are intercalated with

volcano-sedimentary and sedimentary rocks characterized by different depositional environments, ranging from fluvial to shallow marine. They are exposed both as massive lava flows and pillow lavas. They are dark grey and black in color and highly altered. In general, the studied volcanic rocks are aphanitic and contain amygdules.

Figures 2.8 and 2.9 display the contact relations between Eocene volcanic rocks and sedimentary units of the Boğazköy formation around Alimpınar area (Figure 2.6). In this area, sedimentary rocks consist of an alternation of sandstone with angular-subrounded marble pebbles, marl and marble. The volcanic rocks lie above the marls as lava flows. The contact between the sediments and the basaltic lava flows are highly altered and oxidized (Figure 2.9). A thin baked-zone of 0.5cm is observed in the marls and the lavas are chilled, darker colored and less altered. The latter also contain rare amygdules and partially filled with quartz.

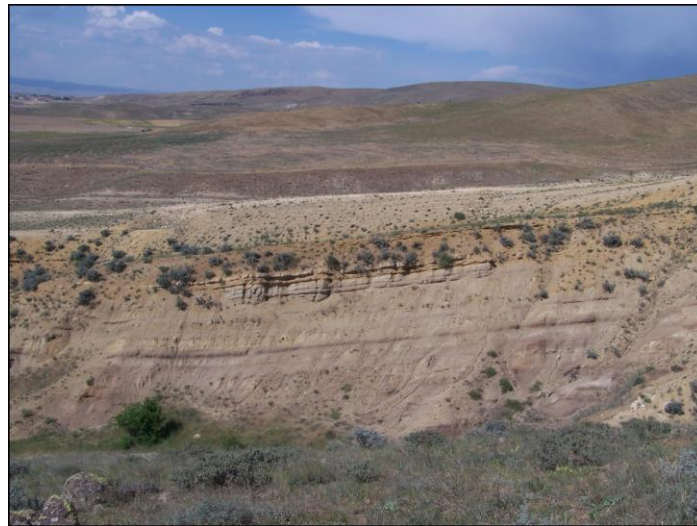


Figure 2. 7 Exposure of the Boğazköy Formation around Kaletepe area. The formation contains alternation of sandstones and limestones. Fossil findings from upper part of the limestone level indicates Middle Eocene age.

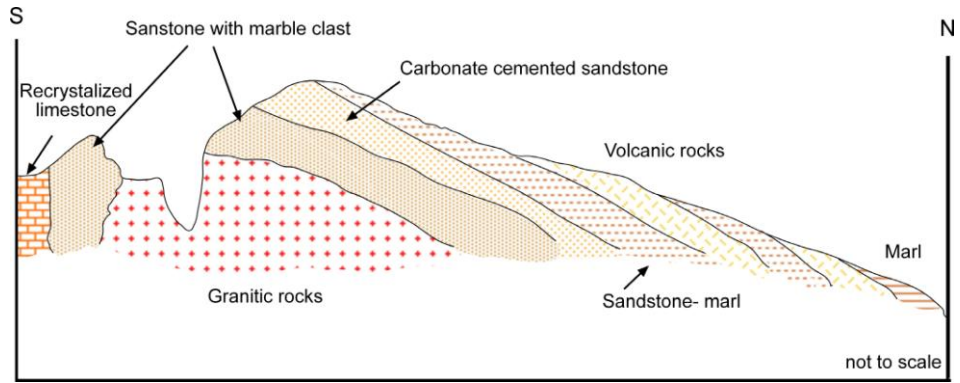


Figure 2. 8 Cross section displaying the contact relationship of the Boğazköy formation with Eocene volcanic rocks around Alimpınar area.

In Çiçekdağ region the studied rocks are generally represented by vesicular basalts and andesites based on macroscopic determination. Along the Çiçekdağ- Kırşehir road they exhibit pillow structures with globular surface. To the west, they grade into dome-like massive intrusions and display columnar jointing which is one of the most characteristics structural feature of basaltic rocks (Figs 2.10 and 2.11). The volcanic rocks are essentially non-porphyrific lavas and amygdaloidal versions of it (Figure 2.12). The Eocene units are overlain by the İncik formation, which is composed of continental clastics i.e. conglomerates, sandstones and mudstones (Birgili et al., 1975). In the study area this formation outcrops around south of the Alimpınar. It is composed of cross-bedded red conglomerates, sandstones and mudstones alternation. The matrix of the sandstone is clearly derived from the underlying basement rocks and is rich in biotite clasts. İncik formation contains white/grey gypsum lenses to the south of the Alimpınar village. The size and shape of the gypsum lenses are variable and range from a few cm to 15-20 cm. The İncik Formation is thought to have been deposited dominantly in fluvial facies (Erdoğan et al., 1996). However gypsum lenses indicates change in depositional environment from time to time to evaporitic basins. There is no consensus on the age of the İncik Formation. In the previous studies, on the basis of the contact relation with underlying and overlying sedimentary units, the age of the formation is considered as Oligocene (Birgili et al., 1975).

Besides, Erdoğan et al., (1996) reported Late Paleocene- Middle Eocene age based on the fossiliferous limestone exposed north of Çiçekdağ. However, the detailed palynological studies on gypsum bearing cover unit of the CACC have yielded Middle Miocene age for the formation (Akgün et al., 1995).

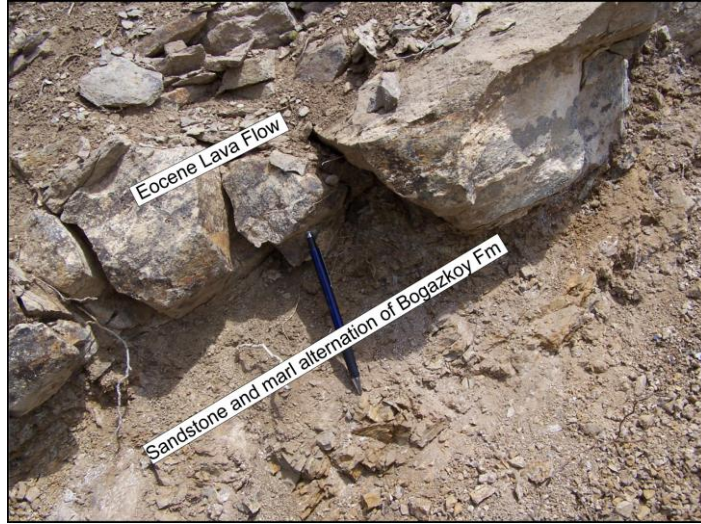


Figure 2. 9 In Alimpınar area Eocene lavas are intercalated with sandstone and marl of Boğazköy Formation.



Figure 2. 10 The studied rocks are observed as pillow lavas along Çiçekdağ-Kırşehir road.



Figure 2. 11 The investigated rocks show weakly developed columnar jointing towards the northern part of the Alimpınar area.

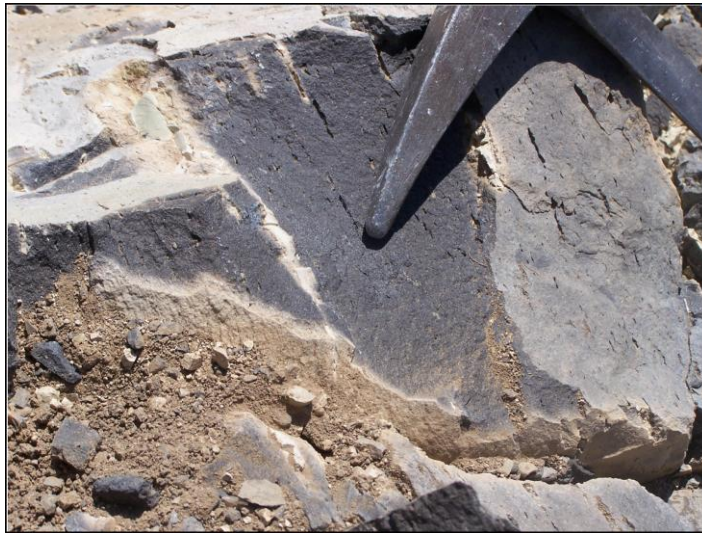


Figure 2. 12 The studied rocks are aphyric and contain vesicles most of which filled with secondary minerals such as quartz.

2.2.2 Geology of the Eocene units in Yozgat area

The simplified geological map of Yozgat area is given in Figure 2.13. Eocene volcanic rocks have extensive outcrops especially north of Yozgat, Divanlı and Azizli, Bayatviran village and Paşaköy in the south of Yozgat.

The oldest unit exposed in this area is rocks of the crystalline complex, which are represented by granitic and ophiolitic rocks, the former being the dominating lithology. Ophiolitic rocks of the basement are generally exposed around southern part of Yozgat as isolated outcrops. They are made up of gabbros, dolerite dykes, and basaltic rocks. Gabbros are the most dominant rock type of the ophiolitic unit observed in the study area. Ophiolitic rocks of the CACC are thought to represent a wide range of tectonic environment from subduction to ensimatic arc (Göncüoğlu et al., 2000). They are cut by the granitic rocks. In the study area, the granitic masses mainly consist of porphyritic alkali feldspar granite and equigranular biotite- hornblende granites. Eocene units within Yozgat area is represented by the Mucur formation, named by Göncüoğlu et al., (1993). In previous studies, Mucur Formation is called as Yoncalı formation (Erdoğan et al., 1996). The formation has widespread distribution within the study area and unconformably overlies the basement rocks. In the studied area, it consists of alternation of conglomerates, fossiliferous sandstones, shale and marl (Figure 2.14). The conglomerates are composed of the clasts mainly derived from the basement rocks including granites and metamorphics. In general, they are subrounded to rounded and their clast size is variable. The sandstones are beige or dark grey in color and fine to medium grained. The sandstones of Mucur Formation contain plant remains and Nummulite fossils (Figure 2.15). The shales are black or dark grey and thin bedded. The fossiliferous yellow- beige limestones, some of which are very thick, occur at various levels of the Mucur Formation (Figure 2.16). They contain abundant Nummulites and are laterally not continuous. In the previous studies, these limestone lenses were described as a different formation, namely Koçaçay by Birgili et al., (1975).

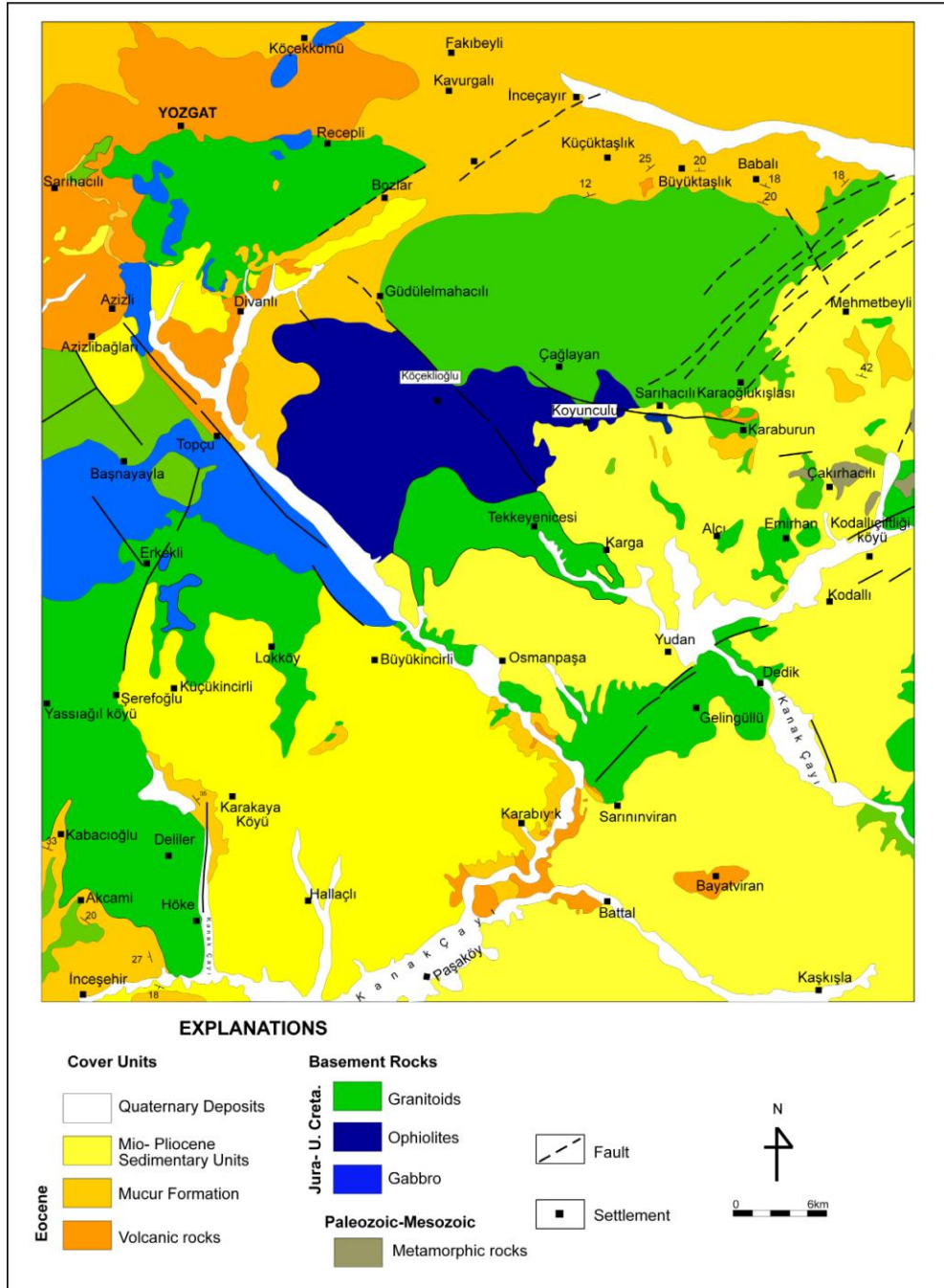


Figure 2. 13 Geological map of Yozgat area (simplified from Göncüoğlu et al., 1994).

Volcanic member of the Mucur Formation that was extruded during the deposition of the formation is called as Bayat volcanics (Erdoğan et al., 1996). Eocene volcanic rocks are in general, basalts and basaltic andesites either black

or dark grey in color. They are highly amygdaloidal filled with quartz, calcite and zeolite. They mainly occur as interbedded with the detrital sedimentary sequences and as dykes. The dominant volcanic lithology is dark colored massive lava flows and alteration is common in those rocks. Figure 2.17 illustrates the schematic cross section of Eocene lavas laying in contact with the sedimentary rocks of the Mucur Formation and Figure 2.18 displays the occurrence of the studied rocks around Paşaköy region.



Figure 2. 14 Alternation of conglomerate, sandstone, shale and marl within Mucur formation around north of Yozgat.

In this area the lava flows lie between the sedimentary units of the Mucur Formation which is composed of sandstones, sandy limestone and fossiliferous limestone at the contact. Although dominant extrusive lithology is dark colored basaltic lava flows in Yozgat and its vicinity, there are a few localities where the volcanic rocks can be observed as dykes (Figure 2.19). Dykes, ranges in thickness from 2 to 4 m, are only observed around Yerköy, the west of Yozgat and they were emplaced within sedimentary rocks. They are purple or grey in color and have chilled margins (1-5 cm) formed at the contact zone. They show

vesicular texture at the contact with sedimentary rock, whereas inner part displays more massive structure.



Figure 2. 15 Sandstones of Mucur Formation contain abundant plant remnants.



Figure 2. 16 Fossiliferous limestones within Mucur formation around Sarıhacılı.

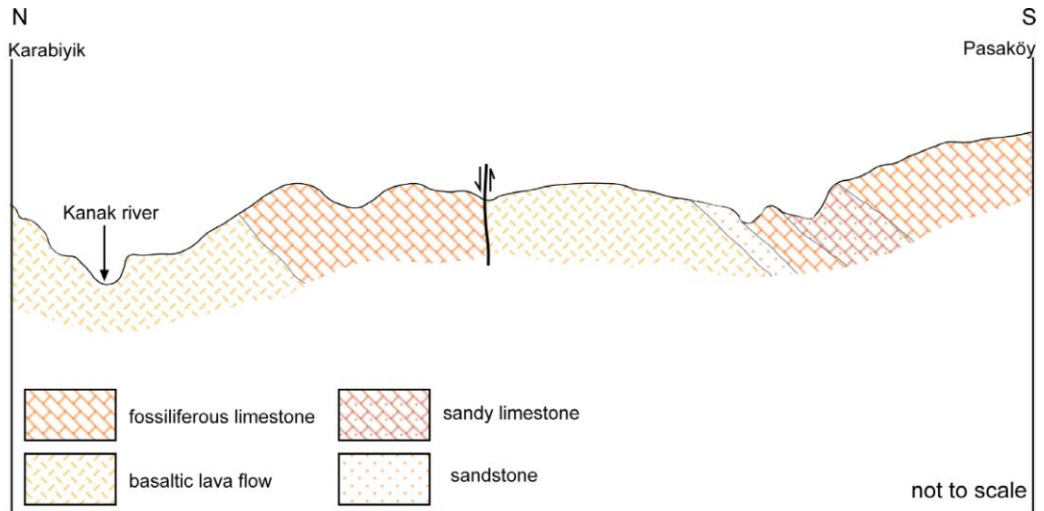


Figure 2. 17 Cross section showing contact relation of Eocene lavas with sedimentary rocks. The area between Paşaköy and Karabiyik lava flows lie above the fossiliferous limestone and sandstone.



Figure 2. 18 In general Eocene volcanic rocks are observed as massive lava flows in Yozgat region. Around Paşaköy studied rocks are intercalated with fossiliferous sandstone.

There are no observed differences between lava flows, pillow lavas and dykes in terms of their lithological and petrographical properties. Typical lava flow

morphologies suggest that the volcanic rocks were emplaced within shallow marine environment. Lavas exhibit typical pillow structures and perfect columnar jointing (Figs 2.20 and 2.21). Flow banding also characterize these rocks (Figure 2.22). They are aphyric and no phenocryst can be defined from the hand specimen. Volcanic rocks display varying degrees of alteration. In general, kaolinization is the most common alteration type. Only, volcanics in Paşaköy south of the Yozgat have been less affected by alteration.



Figure 2. 19 Dykes are not common structures of the Eocene volcanic rocks. However, wherever they are observed, there is a chilled margin at the contact zone.

The association of the volcanic rocks with the sediments indicates that the volcanism must be co-eval with the deposition. Limestone and sandstone associated with the Eocene volcanic rocks contain a rich assemblage of foraminifera characterized by the following: *Alveolina sp.*, *Gyroidinella magna*, *Le Calvez*, *Asterigerina sp.*, *Gypsina sp.*, *Fabiana sp.*, *Fabiana Cassis* (*oppenheim*) *Ratoliidae*, *Discocyclina sp.*, *Sphaerogypsina sp.*



Figure 2. 20 The investigated rocks are also observed as pillow lavas around Kürkçü village located south of Yozgat.



Figure 2. 21 Columnar jointing is the most common feature of the Eocene lava flows. The picture is taken from south of Yozgat around Gelingüllü area.



Figure 2. 22 Flow banding is one of the most diagnostic features of the studied lava flows exposed around Yerköy in Yozgat area.

This assemblage is indicative for Late- Middle Eocene (Bartonian, 37-40 Ma) (Dr. Şükrü Acar, MTA). This age is consistent with the previous studies (Göncüoğlu et al., 1994; Erdoğan et al., 1996). Radiometric age data on these rocks is scarce. However; recently, Atakay, (2009) provided K-Ar dating for the volcanic rocks exposed around Çorum area as $(41.4 \pm 1.4 \text{ Ma})$ indicating Middle Eocene age.

The Eocene volcanic rocks are unconformably overlain by the Middle Miocene (Akgün et al., 1995) Gümüşyazı Formation (Göncüoğlu et al., 1993) that consists of conglomerates, sandstones and limestones.

CHAPTER 3

PETROGRAPHY

3.1 Introduction

For petrographical purposes a total of 150 rock samples from Çiçekdağ and Yozgat areas were collected and examined under the microscope. This number comprises both volcanic and sedimentary rocks taken for paleontological investigation. Given the fact that the distribution of the volcanics is limited around Çiçekdağ, most of the samples were taken from Yozgat and its vicinity. Post magmatic alteration processes made sampling difficult especially in Çiçekdağ region. During the field study, the samples were carefully chosen as free as possible from visible alteration; however, the extent of alteration is variable, from slight to strong.

3.2 Petrographical and Textural Properties of the Volcanic Rocks

Most of the Eocene rocks are massive lava flows in form but pillow lavas are also present. In addition, volcanic rocks occur as dykes. In the field the volcanic rocks were classified as basalt and andesite based on their texture and visible mineral contents, which is further confirmed by the microscopic observations and geochemical analyses as well. The volcanic rocks in the different exposures are mineralogically similar. Although Eocene volcanic rocks crop out in two different regions, they have comparable petrographical and textural characteristics but differ in relative abundances of the minerals that constitute the phenocryst phases. The volcanics that crop out within Yozgat area have, in general, higher phenocryst content than those within

Çiçekdağ area, which can be attributed to relatively rapid ascend of the magmas in that region. For aforementioned reason, they were evaluated together. Their basic mineralogical and textural characteristics are given in Table 3.1.

3.2.1 Basalts

In general, the basalts are the most common rock type in Eocene volcanic rocks in Yozgat area. They are black or dark grey in color in hand specimen and their textures are, in general, aphanitic. Mineralogically, they contain phenocrysts of olivine, clinopyroxene, orthopyroxene, plagioclase and Fe-Ti oxides and titanite as accessory phase. They do not contain any hydrous minerals (e.g. biotite or hornblende). The groundmass texture ranges from hypocrySTALLINE to holocrySTALLINE and its microphenocryst content is akin to that of the phenocrysts assemblage except that the former does not contain olivine. In general, it consists predominantly subhedral plagioclase microlites, subhedral to anhedral clinopyroxene, volcanic glass and minor Fe–Ti oxides. Most of the samples display a slight to a very well-defined parallel orientation of the plagioclase laths (Figure 3.1). The basaltic rocks are characterized by porphyritic to glomeroporphyritic texture which is generally represented by cluster of olivine, pyroxene and plagioclase (Figure 3.2). Vesicular textures are also common, possibly indicating emplacement at a shallow water depth. The degree of vesiculation is strong and these cavities often filled with the secondary zeolites and quartz (Figure 3.3). Some samples display perlitic cracking indicating hydration of glass (Figure 3.4). Most of the rocks display various degrees of alteration which includes kaolinite, replacing plagioclase; calcite, iddingsite and serpentine replacing olivine. One of the most abundant phases is plagioclase and occurs as phenocryst and microphenocryst of variable amount and size in most of the Eocene samples. In the phenocryst phase, plagioclase is represented by two different morphology; sieve textured and normal (clear) type.

Table 3. 1 General petrographical properties of the Eocene basalts and andesites from Yozgat and Çiçekdağ areas.

Sample	Rock Type and Location	Phenocryst	Texture	Groundmass	Miscellaneous
F31	Andesite, Yozgat	cpx, plag	glomeroporphyritic, trachytic, flow, zoned plag, reaction rim to q	cpx, plag	q as xenocryst
F24	Andesite, Yozgat	cpx, opx, plag	glomeroporphyritic, zoned plag, sieved plag,	cpx, plag	
YR17	Basalt, Yozgat	ol, cpx, plag	porphyritic, cpx rims on q, vesicular	cpx, plag	q as xenocryst
F26	Andesite, Yozgat	cpx, plag, hb,	porphyritic, sieved plag,	cpx, plag	poikilitic inclusion of plag in hb
D2	Basalt, Yozgat	ol, cpx, opx, plag	porphyritic, cpx rims on q, vesicular	cpx, plag	q as xenocryst, iddingsitised ol
YS2	Basalt, Yozgat	ol, cpx, opx, plag	glomeroporphyritic	cpx, plag	iddingsitised ol
GE5	Basalt, Yozgat	ol, cpx, opx, plag	glomeroporphyritic	cpx, plag	iddingsitised ol
P6	Basalt, Yozgat	ol, cpx, plag	glomeroporphyritic, flow	plag	calcitised ol
YS7	Basalt, Yozgat	cpx, opx, plag	glomeroporphyritic, flow	cpx, plag	
YR1	Basalt, Yozgat	cpx, opx, plag	glomeroporphyritic	cpx, plag	
FG28	Andesite, Yozgat	cpx, hb, q	porphyritic, flow, vesicular	plag	embayed q
K17	Basalt, Çiçekdağ	cpx, plag	flow, vesicular	plag	
K14	Andesite, Çiçekdağ	cpx, opx, plag	porphyritic, vesicular	plag	
F2	Andesite, Çiçekdağ	cpx, plag	glomeroporphyritic, vesicular	plag	
FG3	Andesite, Çiçekdağ	cpx, opx, plag	porphyritic, flow, vesicular	cpx, plag	
FG1	Andesite, Çiçekdağ	cpx, plag	flow	plag	

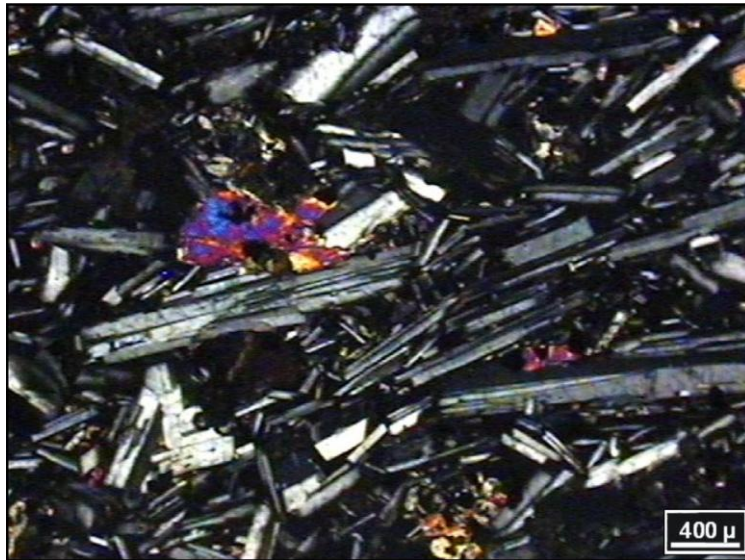


Figure 3. 1 Basalts are characterized by sub parallel to parallel alignment of the tabular plagioclases (10X, XPL).

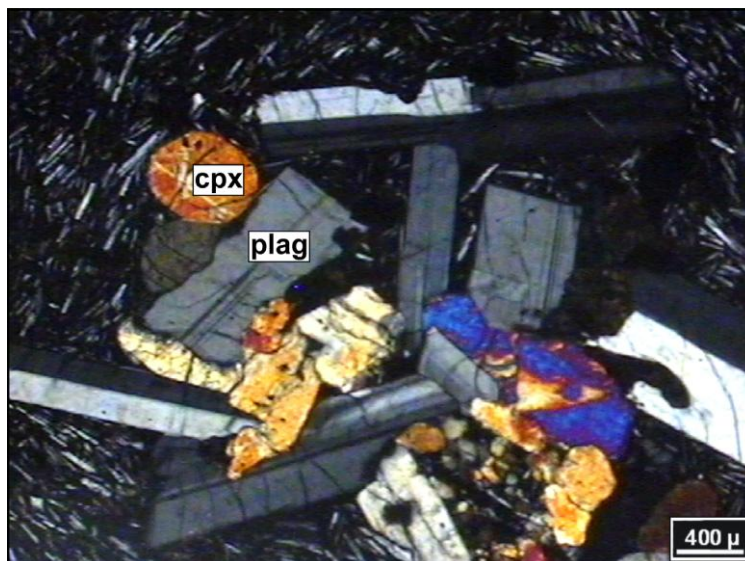


Figure 3. 2 A glomeroporphyritic cluster which contains plagioclases and clinopyroxenes in basalts(10X, XPL, cpx: clinopyroxene; plag: plagioclase).

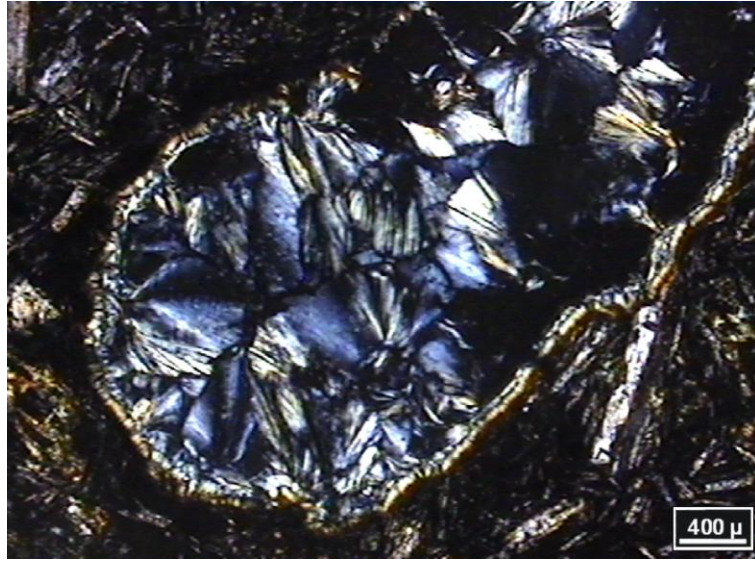


Figure 3. 3 Vesicular texture is a common feature of the basalts and these cavities are filled with zeolites, quartz and calcite. In this microphotograph zeolites are seen (10X, XPL).

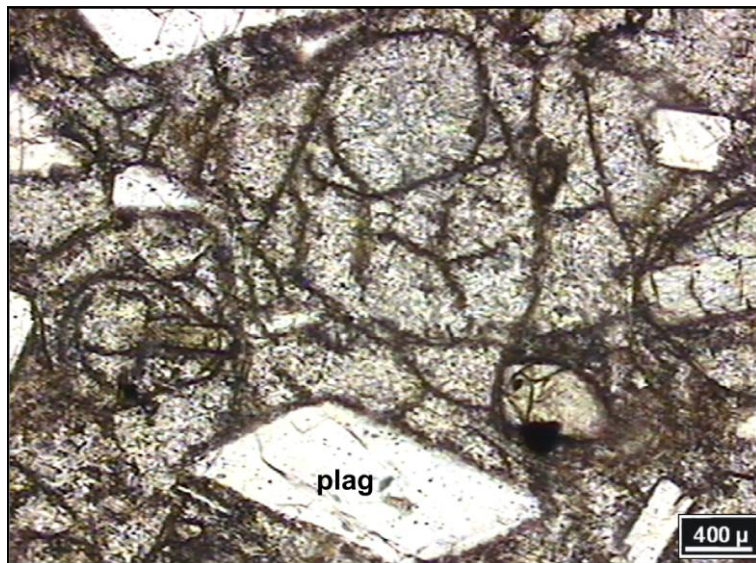


Figure 3. 4 Photomicrograph showing perlitic cracks and plagioclase microlites in the groundmass of basalt (10X, PPL).

Both types can be found together, implying disequilibrium crystallization which will be considered in the next sections. Their compositions are

labradorite which is optically determined. Each type has almost the same composition. Zoning is common in both types. Prismatic plagioclase and subhedral clinopyroxene occur as microphenocryst in some samples and form an intersertal texture. The effects of alteration on plagioclases are evident that they partly or completely turned into clay minerals (Figure 3.5).

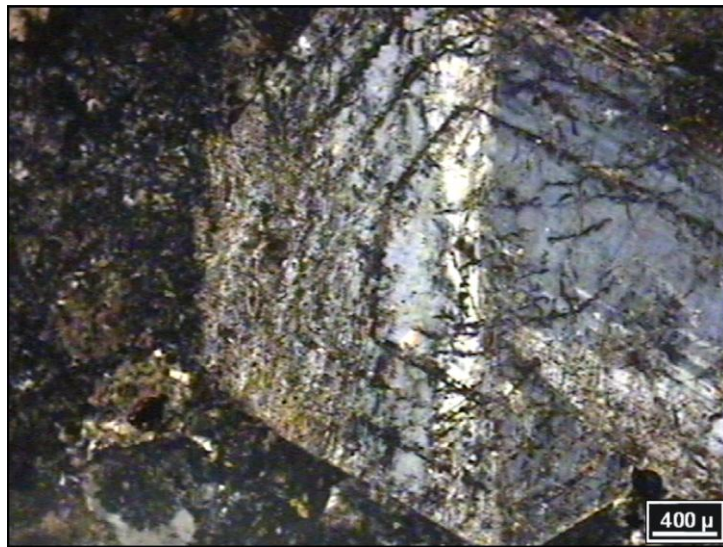


Figure 3. 5 Plagioclase phenocryst shows zonation. Alteration is so intense that plagioclase almost turned into clay (10X, PPL).

Olivine is the most important mafic constituent of basaltic rocks and mostly absent in the evolved rocks. It occurs generally euhedral to subhedral form in phenocryst phase. Olivine crystals do not show any evidence for zoning. In almost all rocks it is partially or completely altered to iddingsite and serpentine, which can be identified by its fibrous form and grayish to blue interference colors along the fractures (Figure 3.6). Alteration degree varies based on the mineral size. It seems that the large phenocrysts are subjected to higher degree of alteration.

It begins around the margin, and proceeds along the fractures and becomes intense at the inner part of the mineral. Whereas in the small ones, alteration is limited to mineral's margin. In addition to this, in some samples it is completely replaced by calcite (Figure 3.7), which exhibit typical rhombohedral twinning. The coexistence of quartz and olivine provides the most significant evidence for disequilibrium condition.

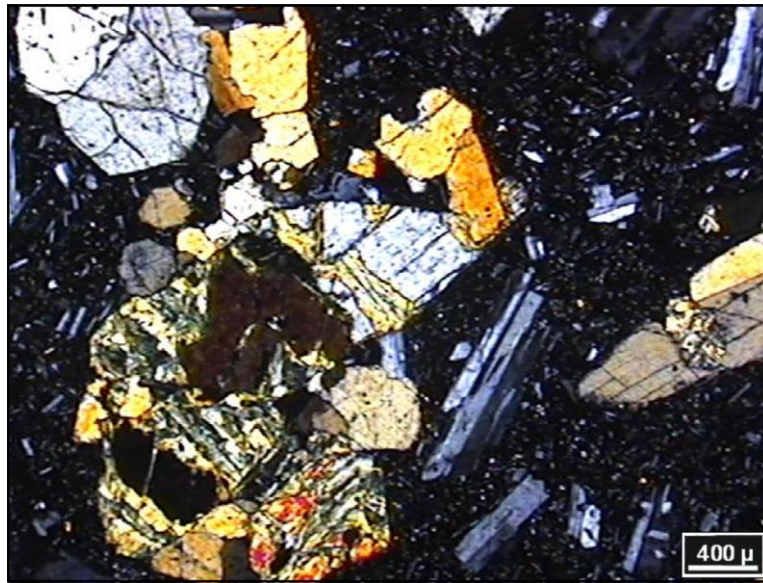


Figure 3. 6 Photomicrograph displaying altered olivine phenocryst. Olivine is replaced by serpentine (10X, XPL).

The pyroxenes occur throughout the Eocene volcanics as both in clinopyroxene and orthopyroxene composition. Based on optical determination their compositions are augite (clinopyroxene) and enstatite (orthopyroxene) (Figure 3.8). Their amount and size are variable. For example, clinopyroxene is predominantly found in both phenocryst and microphenocryst phase whereas, orthopyroxene is observed only within main phenocryst assemblage. Consequently, modal abundance of clinopyroxene is higher than that of the orthopyroxene. Augite occurs as colorless to pale green and subhedral to euhedral prismatic crystals. Its extinction angle varies between 37- 43°. Zoning

and twinning are common in this mineral. Alteration is observed along cleavage planes. However, in some cases, especially in phenocrysts, the interior part of the mineral appears to be more subjected to the alteration. Orthopyroxene phenocrysts are intact relative to clinopyroxene. It occurs as small euhedral crystals and does not show any pleochroism. It is characterized by first order grey birefringence colors.

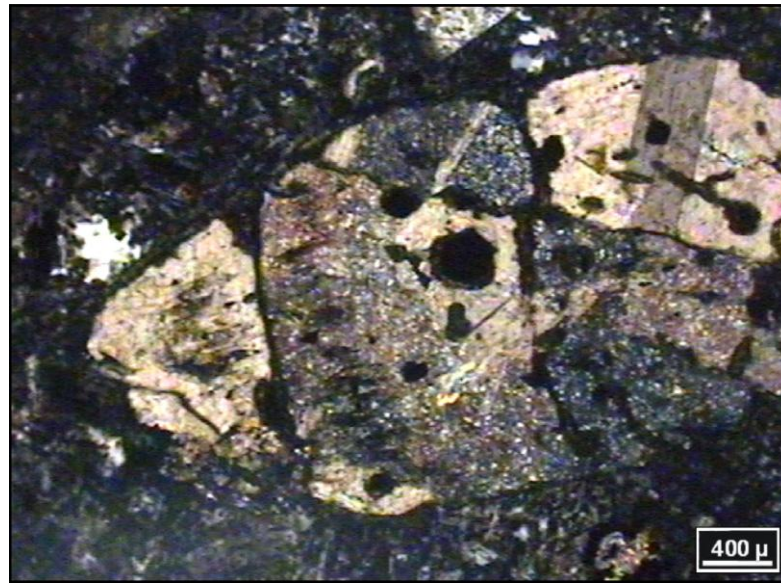


Figure 3. 7 Almost euhedral olivine crystal. It is completely replaced by calcite and also contains opaque inclusions (10X, XPL).

Fe-Ti oxides are present as accessory phase in all rocks. They form small and rounded crystals, but also occur less frequently as inclusions within other phenocryst phases (e.g. pyroxene). Basaltic rocks contain titanite as an accessory mineral. It is less common relative to oxide minerals. It can be regarded to be late crystallization phase since none of them is observed as euhedral form. In addition, mafic mineral phases do not include titanite as inclusion.

3.2.2 Andesites

They are generally found as red to pinkish colored rocks in hand specimen. Some andesites are porphyritic with phenocryst of plagioclase. Phenocryst assemblage of the Eocene andesites is composed of clinopyroxene, orthopyroxene, hornblende, biotite and rarely quartz.

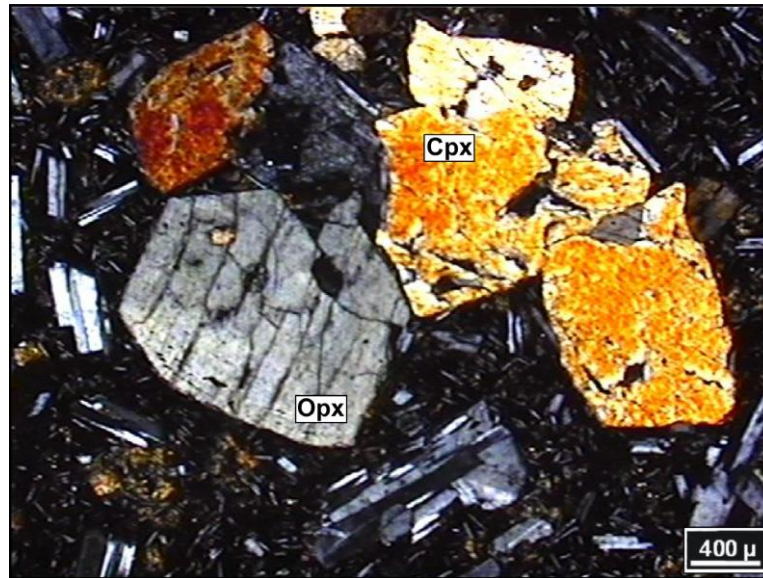


Figure 3. 8 Photomicrograph of glomeroporphyritic clinopyroxene and orthopyroxene. Orthopyroxene is distinguished from clinopyroxene by its low interference color (10X, XPL, opx: orthopyroxene, cpx: clinopyroxene).

Quartz phenocrysts are extremely rare and contain embayments suggesting resorption. In some cases they are surrounded by pyroxene rims which imply reaction with the host magma. Although microphenocryst content of the andesites is composed of pyroxene and plagioclase, some of them have glassy matrix and are distinctive in being free of microlites. Some show also fluidal texture (Figure 3.9). Hydrous phases are not observed as part of the microcryst phase.

Plagioclase seems to be the most abundant phenocrystal phases within the evolved rocks. The size of plagioclase ranges from small microlites to large phenocrystals. The majority of them are elongated and strongly altered to clay minerals. Its composition ranges between andesine to oligoclase on the basis of the optical determination. Plagioclase phenocrystals display typically extensive sieve texture. They form glomeroporphyritic texture together with mafic phases such as pyroxene (Figure 3.10). In some samples few plagioclase phenocrysts contain glass inclusions and pyroxene minerals as poikilitic inclusions, which may also indicate crystallization sequence that firstly pyroxene occurred and then plagioclase crystallized.

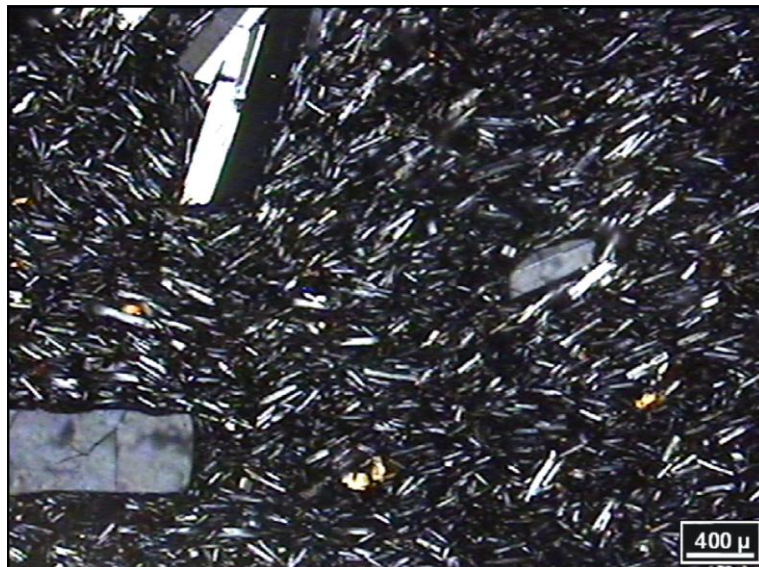


Figure 3. 9 Fluidal texture, represented by almost parallel alignment of the plagioclases, is commonly observed in Eocene rocks (10X, XPL).

Some plagioclase minerals include small inclusions. However, based on the optically determined extinction angle, there is no compositional difference between the plagioclase grains having inclusions and those free of inclusions, which can be attributed to the small differences in crystallization conditions rather than the big change effecting the whole mineral composition.

Pyroxenes are one of the most abundant minerals both in phenocryst and microphenocryst phases. Their compositions do not display a wide range. Based on the optical characteristics, clinopyroxene is augite in composition and orthopyroxene is enstatite, similar to basaltic rocks. Overall, clinopyroxene seems to be the most abundant pyroxene phase since orthopyroxene is not observed in microphenocryst phase. Some of the clinopyroxene crystals are zoned. In some cases clinopyroxene minerals contain opaque minerals as small inclusions (Figure 3.10) that provides valuable information regarding the crystallization history of these minerals. It can be suggested that crystallization of the clinopyroxene took place after formation of the opaque minerals. Orthopyroxene is observed as small rounded crystals and do not contain any Fe-Ti oxide minerals as inclusion.

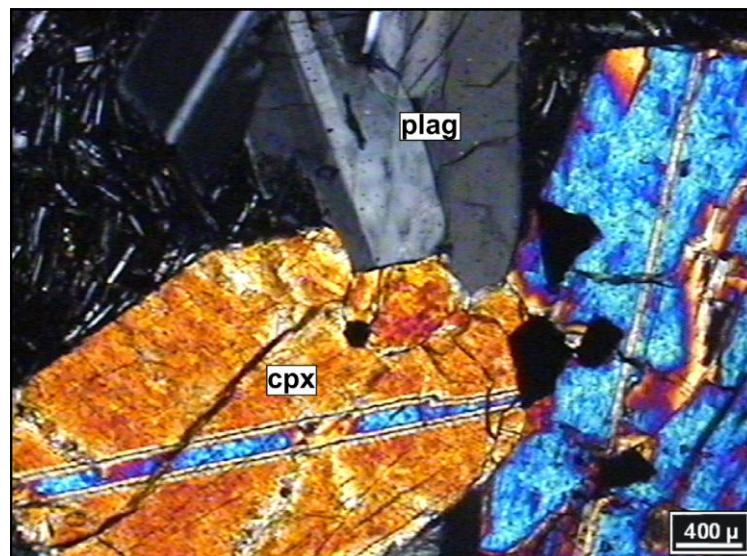


Figure 3. 10 Clinopyroxene minerals are common constituent of the glomeroporphyritic clusters (10X, XPL).

Hornblende is rarely found in the evolved rocks. It occurs as medium to coarse grained, green to dark green in color and found only in phenocryst phase. It is observed as subhedral to euhedral crystals and in some cases encloses small

plagioclases. It appears that hornblende is not in equilibrium with its host magmas since there is a reaction rim around it (Figure 3.11). Unlike the other mafic minerals (e.g. olivine and pyroxene), amphibole does not appear as being part of glomeroporphyritic clusters, e.g. it is found as discrete crystals.

Quartz is not a common component of the whole Eocene suite but it is observed as fine to medium grained and trace amount in andesites. Apart from that, some of the basaltic rocks contain quartz as xenocryst.

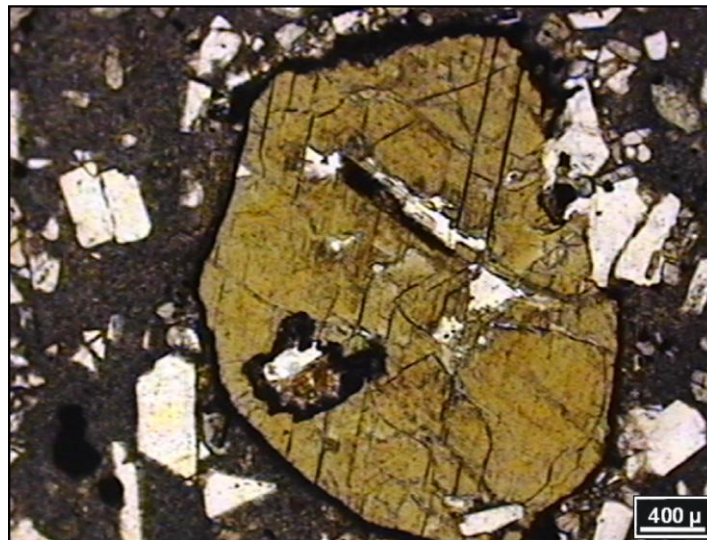


Figure 3. 11 Photomicrograph showing an almost euhedral hornblende phenocryst with reaction rim (10X, PPL).

It is worth to note that these quartz bearing rocks also contain large olivine crystals (Figure 3.12), which is partially replaced by serpentine. In these rocks quartz xenocryst is surrounded by thick clinopyroxene rims. Quartz is not intergrown with other mafic phenocryst phases (e.g. hornblende or biotite). It is thought to be a late phase since it occurs as anhedral grains and includes small fluid inclusions. This striking olivine- quartz coexistence can be attributed to either magma mixing process or crustal assimilation. Although Eocene rocks exhibit several textural characteristics indicating disequilibrium crystallization,

this distinctive feature was interpreted as crustal assimilation based on the quartz structure which displays comparable textural properties with those found in granites. Considering distribution of granitic rocks within the studied area, presence of monomineralic quartz xenoliths should be indicative of silica rich wall rock assimilation.

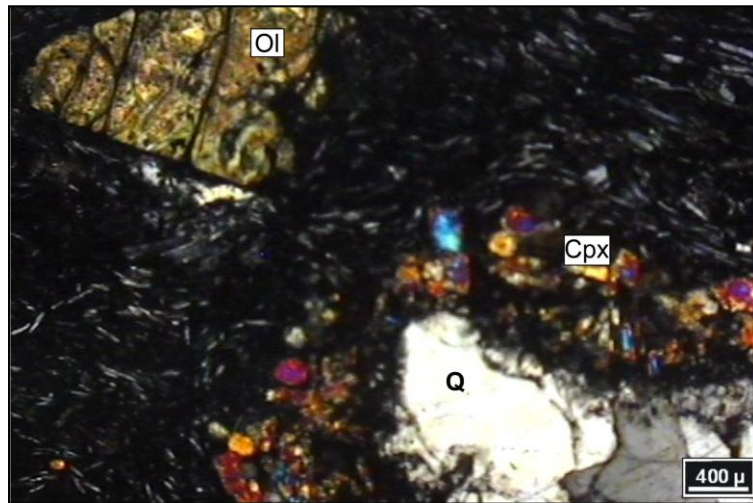


Figure 3. 12 Photomicrograph displaying olivine and xenocryst of quartz coexistence in basaltic rocks. Olivine is entirely replaced by serpentine. Quartz, on the other hand, is surrounded by thick clinopyroxene reaction rim (10X, XPL, Q: quartz, Ol: olivine, Cpx: clinopyroxene).

Based on the textural relationship and observed phenocryst assemblage following crystallization sequence can be inferred; olivine, pyroxene, Fe-Ti oxides, plagioclase and titanite for basaltic rocks and Fe- Ti oxides, pyroxene, plagioclase, hornblende and quartz for andesitic rocks. Eocene rocks are characterized by such a mineral assemblage that contains mainly olivine, pyroxene and plagioclase, implying shallow crystallization depth. Although its occurrence is restricted to evolved rocks, presence of the amphibole indicates hydrous condition in the source region.

3.3 Disequilibrium Textures and Their Petrologic Significance

All Eocene units display striking petrographical and textural evidence indicating crystallization under disequilibrium conditions. Disequilibrium textures are; the sieve texture of plagioclases, coexistence of sieved and normal (clear) plagioclases within the same rock, zoning within the plagioclases, clinopyroxene reaction rims around quartz xenocrystals, reaction rims to mafic minerals; presence of embayed felsic minerals indicate crystallization under disequilibrium conditions. Based on the microscopic determinations, these magma mixing/mingling texture observed within the Eocene suite can be summarized as followings.

3.3.1 Sieve texture on plagioclases and their coexistence with the normal ones

Sieve texture on plagioclases is common in orogenic volcanic rocks. To explain their origin several mechanisms have been proposed; magma mixing and rapid decompression where heat loss is negligible relative to the ascent rate (Nelson and Montana, 1992 and references therein). Magma mixing process is able to modify the mineral composition in terms of albite and anorthite content; on the contrary, in the latter case large compositional diversity is not expected to happen (e.g. Nelson and Montana, 1992).

Most of the studied rocks have plagioclase crystals that display sieve texture. They can also be found together with the normal (clear) ones (Figure. 3.13). Although lack of the mineral chemistry data made the mixing process tough to prove, rapid decompression model is not favored to explain the origin of sieve texture plagioclase since in such a case all plagioclases are supposed to be expected to have sieve texture, which is not the case. Therefore, sieve texture plagioclase and their coexistence with the clear ones can be attributed to the magma mixing process.

Another disequilibrium texture observed within the plagioclase is poikilitic inclusions. Some of plagioclase crystals contain pyroxene minerals (Figure 3.14). This texture is defined as enclosure of small pyroxene crystals by big plagioclase phenocryst. Yılmaz and Boztuğ, (1994) argued that during the mixing of the felsic and mafic magmas there could be small plagioclase, hornblende or biotite crystals which subsequently might be found as inclusions within the quartz and plagioclase crystals that are formed after the mixing process.

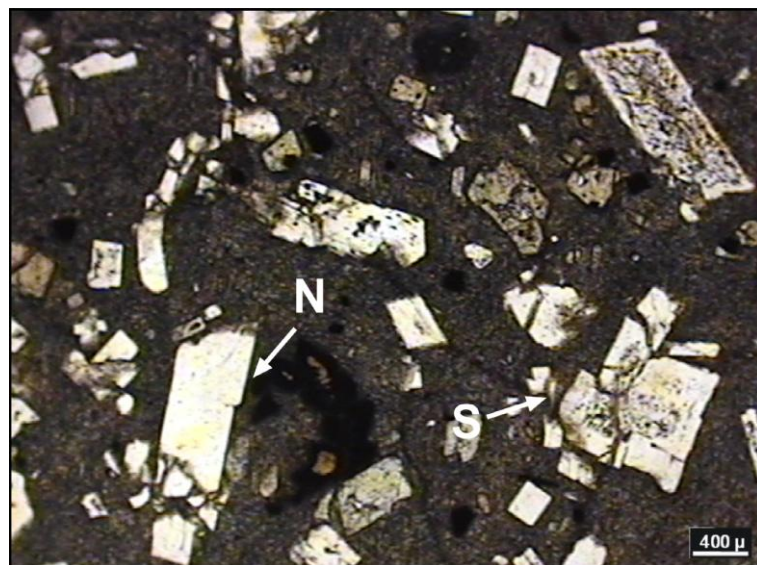


Figure 3. 13 Photomicrograph displaying coexistence of sieve textured and normal (clear) type plagioclases in andesites having glassy groundmass (10X, PPL, S: sieve textured plagioclase, N: normal plagioclase).

3.3.2 Pyroxene reaction rims around quartz xenocrysts

Some of the basaltic rocks typically display quartz crystals surrounded by fine grained pyroxene rims (Figure 3.15). The pyroxenes that constitute the rim around quartz are augite in composition. Orthopyroxene is not involved in this structure. The size of quartz located at the core and the pyroxene rim around it is both variable. Some of the augite rims surrounding quartz are altered but

most of them are recognizable. Ussler and Glazner, (1987) argued that pyroxene rim on quartz crystals derived from Mg, Fe and Ca diffusion into the silicic melts surrounding the quartz and they proposed that this texture occur after extrusion of the hybrid magmas since fragile- appearing rim can no longer grow in a convecting magma.

Similar textures have also been reported from Neogene- Quaternary volcanic centers located within the Central Anatolia, e.g. Karapınar monogenetic volcanoes (Keller, 1973); Kızılcım volcanics (Ercan et al., 1987); Karataş basalts (Ercan et al., 1992); Hasandağ basalts and andesites (Aydar and Gourgaud, 1993, 1998); Çınarlı, Melendiz, (Keçiboyduran-Aydın, 2008). Keller (1973) noted the frequent occurrence of pyroxene crystals around quartz xenocrysts, and suggested that it might be characteristic for central Anatolian basalts.

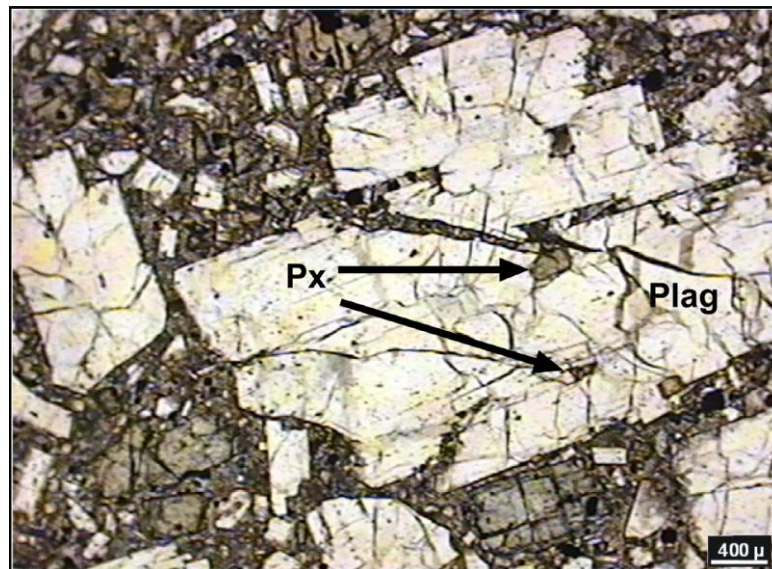


Figure 3. 14 Photomicrograph showing plagioclase phenocryst with pyroxene inclusions (10X, PPL, Px: pyroxene, plag: plagioclase).

3.3.3 Reaction rim around mafic minerals

Another texture indicating disequilibrium crystallization is corona texture. Although the reaction rim is observed around both pyroxene and amphibole crystals, it becomes more pronounced in hornblende phenocrysts (Figure 3.11). The thickness of the Fe-Ti reaction rim is variable based on the mineral size. The hornblendes without reaction rim show yellow- brown pleochroism while those with reaction rim are pleochroic in dark brown-reddish color. In some cases hornblende is found as remnants of opaque pseudomorphs. Coexistence of the hornblende crystals with and without reaction corona also supports the magma mixing/mingling process in the genesis of the studied rocks.

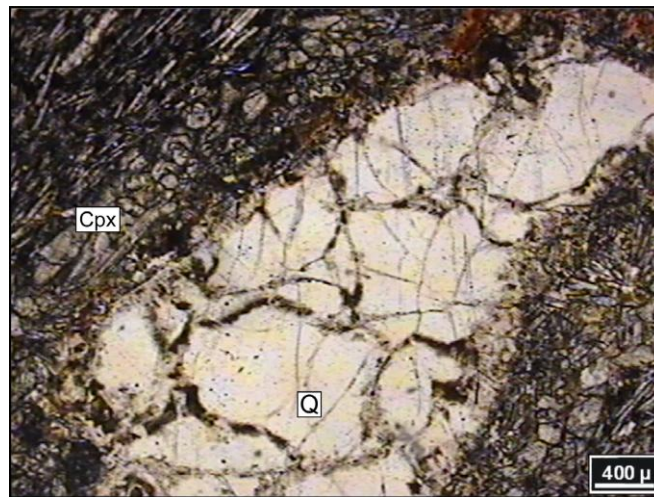


Figure 3. 15 Photomicrograph displaying a quartz xenocrystal which is corroded and rounded and also have augite rims indicating a reaction with surrounding groundmass (10X, XPL, Q: quartz, cpx: clinopyroxene).

3.3.4 Embayed quartz crystals

This texture is observed in quartz phenocrysts in andesitic samples. Quartz crystals are mostly found as rounded and embayed, in some cases cracked (Figure 3.16). Glass or fluid inclusions are also common in quartz crystals.

Basaltic rocks also have quartz crystals with augite rim, indicating a reaction with surrounding host magma; on the other hand, quartz crystals in andesitic rocks do not bear pyroxene rims.

3.3.5 Mineral zoning

Zoning is commonly observed in plagioclase and clinopyroxene minerals, however in the former case; it was mostly masked by mineral's alteration (Figure 3.5). Compositional zoning in minerals is generally attributed to the change in oxygen fugacity of the melt due to the magma mixing (Humphreys et al., 2006).



Figure 3. 16 Photomicrograph illustrating embayed quartz crystals. Mineral contains glass or fluid inclusions but do not have pyroxene rim (10X, XPL, Q: quartz).

3.4 Discussion

Magma mixing and/or mingling phenomenon is considered to be an important process in the evolution of the studied volcanics. Recently, considerable

numbers of studies have demonstrated that magmas with diverse composition may coexist within a single magmatic system (e.g. Clynne et al., 1999; Murphy et al., 2000; Gioncada et al., 2005; Humphreys et al., 2006). Magma mixing is expected to happen during different stages of the magmatic evolution. For example; in magma chamber through the convection (e.g. Couch et al., 2001) or in conduit in the course of ascend (e.g. Synder and Tait, 1996). Besides, recharging of magma chamber by means of the new magma batch, which in turn promote the eruption (e.g. Murphy et al., 2000), can lead to magma mixing (Humphreys et al 2006., and references therein). Magma recharge or new mafic magma intrusion to the existing magma chamber can be recorded by textural properties like mafic enclaves, corroded xenocrysts and presence of the phenocrysts showing zonation (Humphreys et al., 2006 and references therein).

The development of pyroxene rims on quartz crystals (Ussler and Glazner, 1987; Castro et al., 1991); presence of sieved/dusty plagioclases, and their coexistence with the non-sieved ones (Dungan and Rhodes, 1978; Tsuchiyama, 1985; Stimac and Pearce, 1992); presence of embayed felsic minerals (Stimac and Pearce, 1992); reaction rims to mafic minerals (Feeley and Sharp, 1996) are generally considered as evidence for magma mingling/mixing. Besides textural properties, presence of diversity in phenocryst assemblage may indicate mixing of the magmas with different compositional and thermal conditions (Davidson et al., 1990).

Presence of sieve textured plagioclase, zoning patterns of main phenocrystal phases (e.g. plagioclase and pyroxene), embayed felsic crystals and corroded quartz xenocrysts indicate that Eocene rocks may have been subjected to different thermal or cooling history during their evolution. Mixing and/or mingling of the magmas with contrasting compositions such as basic and acidic can explain the textural and mineralogical diversity of the Eocene samples. However, Eocene rocks sampled and analyzed during this study do not contain silicic rocks which would be further used as felsic end member in a possible mixing scenario; for that reason mixing of felsic and mafic magma batches can

not be documented. On the other hand, previous studies on Eocene volcanism in Yozgat area (e.g. Erdoğan et al., 1996 and Alpaslan et al., 2000) reported presence of the dacitic and rhyolitic rocks and mentioned a magma mixing process as well. This gives a strong evidence for that there might be a silicic magma chamber beneath the region. Thus by the help of the previous data the pervasive disequilibrium textures can be explained by magma mixing event, if it can be evidenced that they are coeval with the studied Eocene volcanics. In the previous study crystallization sequence of evolved rocks, which is mainly based on the textural observations, comprises pyroxene, Fe-Ti oxides, hornblende plagioclase and quartz (Alpaslan et al., 2000). On the other hand, more mafic rocks have a mineralogical assemblage dominated by olivine and pyroxene. This observation indicates that parental magmas of the evolved rocks resided in the crustal level magma chamber long enough. Recharging of the preexisting silicic magma chamber by hot and more mafic magmas gave rise to interaction of the two magma batches and consequently resulted in disequilibrium textures in both series. Continuous magma and thus heat supply to the magma chamber promoted the eruption. Crystallization history and mixed origin of the studied samples can be explained by this way. Another issue that needs to be emphasized here is the time of the magma mixing. The time between mixing of the magmas having different compositions and their eruption do not appear to be so long since the quartz and olivine crystals have not been melted completely.

Textural evidence observed from phenocryst assemblage indicates that magma mixing process had played a role in the genesis of the studied rocks; on the other hand, a detailed microprobe studies need to be done to highlight the mixing phenomenon.

CHAPTER 4

GEOCHEMISTRY and PETROGENESIS

4.1 Introduction

This chapter aims to present geochemical characteristics of the studied rocks, classify and evaluate them on the basis of, major, trace and rare earth element variations, and petrogenetic processes. To do so, totally 70 samples were analyzed, 59 of which are from Yozgat and 11 from Çiçekdağ area. Post magmatic alteration processes (weathering and secondary minerals in the cavities) within the Çiçekdağ area made sampling difficult, so only a limited number of samples were analyzed from that region. Petrogenetic processes such as partial melting, fractional crystallization and assimilation have been modeled by using of the geochemical data.

4.2 Analytical Methods

Whole rock geochemical analyses were performed at Acme Analytical Laboratories in Canada. Major oxide analyses were carried out by inductively coupled plasma-atomic emission spectrometry (ICP-AES). Trace and rare earth elements (REE) were determined by inductively coupled plasma-mass spectrometry (ICP-MS).

Sr, Nd and Pb isotopic compositions of the Eocene volcanic rocks have been measured by mass spectrometer at Department of Earth Sciences, University of Texas at Austin, USA. All samples were crushed to about millimeter-scale grain size chips after removal of weathered rims and handpicked under a

magnifier to exclude the xenocrysts and amygdales. Only fresh xenocryst-free and amygdale-free rock chips were selected. These chips were washed with purified water several times in an ultrasonic bath. A split of ~20 mesh chips were leached by HCl about 1 hour at 80 °C before dissolution to remove the effect of late alteration or weathering. The chips were spiked and then dissolved in teflon beakers with 2:1 mixture of HF+HNO₃ acids at 80 °C for 72 hours. Sr, Nd and Pb were extracted from the same solution through a combination of ion-exchange columns. The isotopic ratios corrected for mass fractionation by normalizing to ⁸⁸Sr/⁸⁶Sr= 8.375209 and ¹⁴⁶Nd/¹⁴⁴Nd= 0.7219. During this study NBS 987 Sr standard gave a mean value of 0.71025 ± 0.000006 (n=6) and Nd standard AMES gave a mean value of 0.512069473 ± 0.000004 (n=4) and La Jolla standard gave 0, 51195428 ± 0.000004 (n=2). Fractionation corrected values for SRM 981 Pb standard (n=5) were ²⁰⁶/²⁰⁴Pb 16, 90 ± 0.0005, ²⁰⁷/²⁰⁴Pb 15, 44 ± 0.0005, ²⁰⁸/²⁰⁴Pb 36, 55 ± 0.0007. The Pb data were corrected based on the true NBS 981 value of Baker et al., (2004). Apart from the analyses carried out at University of Texas, 4 volcanic rock samples were analyzed for isotopes at Central Laboratory, METU. Detailed description of sample preparation and analysis method can be found from Köksal and Göncüoğlu, (2008). Whole rock geochemical data, isotope compositions of the studied rocks and trace element ratios used in the text are given in the Appendix A B, and C respectively.

4.3 Alteration Effect

Although the effects of alteration were minimized in the first instance by selection of the freshest samples as possible, Eocene volcanic rocks show petrographic evidence of alteration such as the presence of replacement (iddingsite, calcite and clay) of main phenocrystal phases. Moreover, high (up to 8.3 wt %) loss on ignition (LOI) values indicate that volcanic rocks have undergone variable degree of alteration and weathering during post eruption processes. As a result, some elements may have become mobile. Thus, element mobility has been tested before using geochemical data for petrological

purposes. Zr was used as fractionation index because of its immobile nature to test element mobility. Trace element (Ba, Sr, Pb, U, Th, La, U) variation plots (not shown here) reveal that a significant degree of mobility is only limited to U especially in samples having LOI values higher than 5 wt %. All the samples except for U display coherent positive linear trends, suggesting that geochemical variations are basically related to petrological processes rather than post magmatic alteration. Nevertheless, samples with LOI value higher than 4.5 (wt %) were not used and trace element modeling is based on relatively immobile elements that are likely to be less affected by secondary processes.

4.4 Classification of the Studied Rocks

In an attempt to determine the magma series total alkalis vs silica diagram was used. In this graph all samples from Çiçekdağ exhibit an apparent subalkaline affinity (Figure 4.1a; Irvine and Baragar, 1971), whereas some samples from Yozgat show alkaline nature. On McLean and Barret (1993) classification diagram, subalkaline Çiçekdağ samples plot in the calc-alkaline field. Yozgat volcanics, on the other hand, mostly plot in the calc-alkaline and transitional area (Figure 4.1b). Only one sample with high Y (ppm) and low Zr (ppm) is plotted in the tholeiitic field. To avoid the effects of mobility Winchester and Floyd, (1977) diagram based on the immobile elements was used. On this diagram Yozgat volcanics plotted in the basalt and basaltic andesite field. On the other hand; Çiçekdağ samples, which are more evolved than those from Yozgat, mostly classified as basaltic andesite and andesite (Figure 4.1c).

4.4.1 Normative mineralogy

Normative constituents can provide significant information about parental composition of the source region. The most challenging part of the normative classification is that lavas erupted through continental lithosphere can be interacted with the silica rich wall rocks en route to the surface, which cause

decrease in normative nepheline (ne) content or increase in normative hyperstene (hy) content. By this the resultant rocks would be interpreted to have derived from a shallower depth (DePaolo and Daley, 2000). Therefore, for the normative classification purposes uncontaminated samples should be taken into consideration. Normative compositions of Eocene volcanic rocks are given in Appendix D. Evaluation of the Eocene samples implies that normative constituents of the studied rocks support the geochemical classification and confirm their transitional to mildly alkaline nature. For example, most of the Eocene rocks are quartz (q) - hyperstene (hy) normative (i.e. calc-alkaline). But a few samples from Yozgat area namely A5 and Y5 are nepheline (ne) - olivine (ol) normative (alkaline) and sample Fg20 is ol- hy normative (transitional basalt). Sample Fg20 also contains normative corundum (c), although no modal garnet was observed under the microscope.

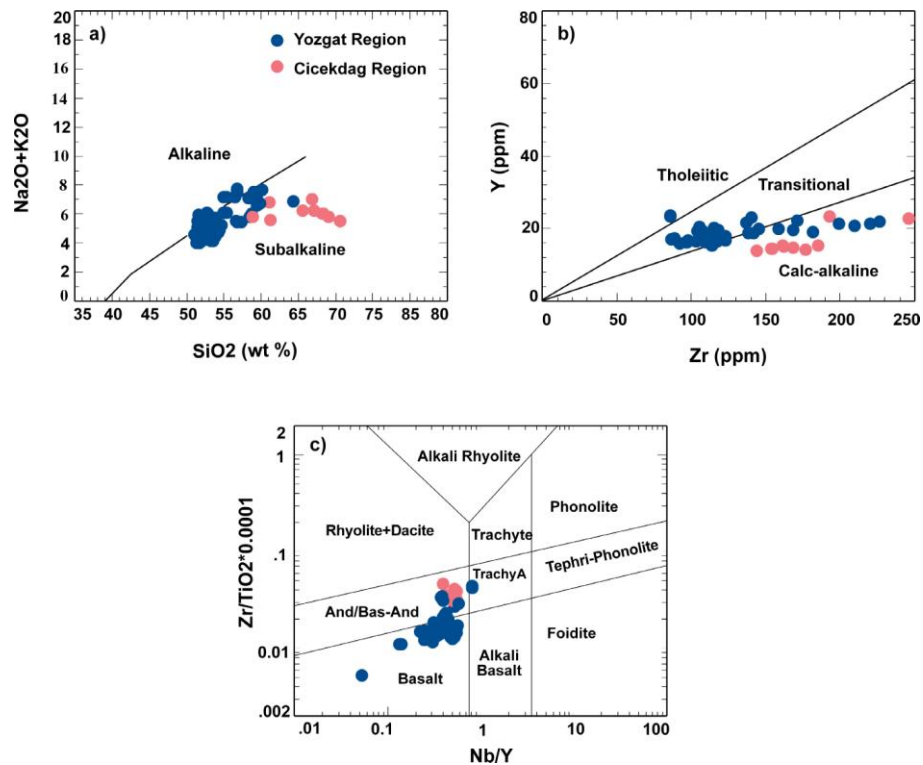


Figure 4. 1 Classification of Eocene volcanic rocks a) on total alkali vs silica (TAS) diagram (Irvine and Baragar, 1971) b) Y vs Zr diagram (McLean and Barret, 1993) c) after Winchester and Floyd, (1977), (Pearce, 1996).

4.5 Major Oxide and Trace Element Variations

Different exposures of the Eocene samples (e.g. lava flows or dykes) display similar geochemical characteristics and they exhibit a wide range of major and trace element composition. For example, Yozgat volcanics have a silica content between from 47.13 to 64.38 (wt. %). On the other hand, Çiçekdağ samples are characterized by a wider range of silica contents changing between from 53.62 to 70.60 (wt. %). Although Yozgat volcanic rocks have quite high $\Sigma\text{Fe}_2\text{O}_3$ contents (4.7 to 9.61 wt. %), Çiçekdağ rocks are characterized by relatively low concentration of $\Sigma\text{Fe}_2\text{O}_3$ which changes between 1.96- 7.17 wt %. A few samples from Yozgat area have relatively high TiO_2 , MgO and P_2O_5 abundances. Trace element concentrations of the rocks also exhibit the same compositional differences. While Yozgat volcanics are represented by enriched trace element compositions for example, 56.5- 300.1 ppm for Zr and 1.4- 19.5 ppm for Nb. These values for Çiçekdağ samples changes between 143.5- 245.9 ppm and 7-19.2 ppm, respectively.

Because the study area is composed of different sampling areas, binary trace element diagrams were used to determine if there were any distinct geochemical groups within the whole suite. The Zr vs Nb and Y plots suggest two main groups within Eocene samples (Figs 4.2 and 4.3). Group 1 is characterized by low to high Nb, moderate to high Y and high Zr concentrations. Çiçekdağ samples are involved in this group with similar Nb abundances with Yozgat samples although they are represented by the lowest Y content within the whole suites.

Group 2 differs from the other group in that it has the lowest and restricted Zr content although its Y concentration is as high as Group 1 and it has low Nb concentration compared to group 1. Both groups display an increasing Nb content with increasing Zr abundances. It appears from these plots that sample location is not a controlling factor in generating these variations.

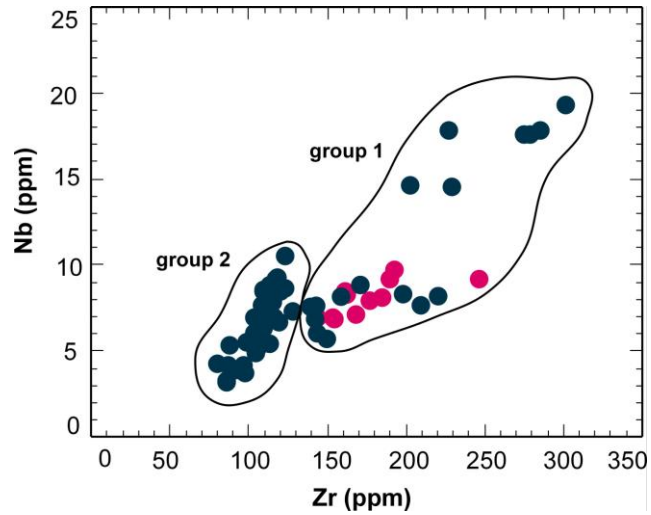


Figure 4. 2 Nb vs Zr diagram for Eocene volcanic rocks (symbols are the same as in Fig. 4.1).

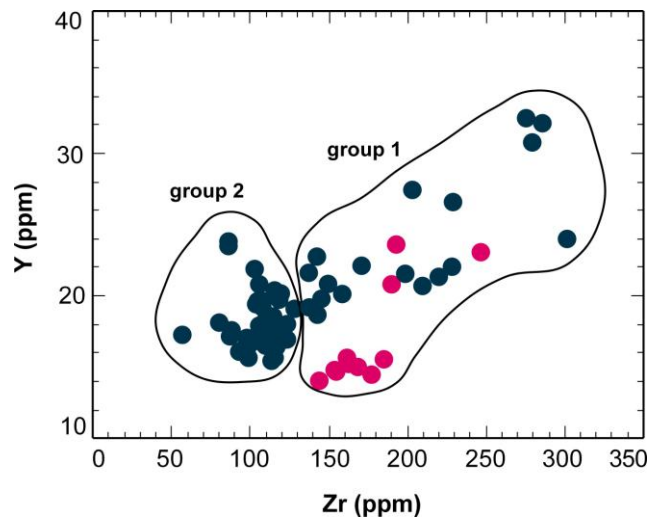


Figure 4. 3 Y vs Zr diagram for the studied rocks.

Because Çiçekdağ samples plot with Yozgat samples; on the other hand, Yozgat area itself contains different geochemical suites represented by different elemental abundances. It is not expected that these variations are related to the post magmatic alteration process because HFSE's are known to be the most immobile elements and simple fractional crystallization process

can not change their abundances. Therefore, observed variations are either source related or reflect the differences in partial melting degrees.

Harker diagrams were conducted to monitor major oxide and trace element variations (Figs 4.4). In these graphs all groups were plotted together to show similarities and differences. Group 2 that contains most of Yozgat samples has the highest content of $\Sigma\text{Fe}_2\text{O}_3$, MgO and CaO whereas, its Al_2O_3 , Na_2O and K_2O abundances are relatively lower than those found in the other group. This is consistent with their primitive nature because Group 2 is characterized by higher Mg numbers among the whole suite (Figure 4.5). Some of the samples from Group 1 have higher TiO_2 , P_2O_5 and Na_2O contents relative to rest of the group. Çiçekdağ samples have the lowest abundances of major oxides, which is compatible with their evolved nature represented by low Mg numbers and high silica content. Despite having low concentration of major elements, they behave similar with Group 1 in most of the variation plots apart from Na_2O and K_2O .

Based on the observed variations fractionation history of the investigated rocks can be summarized as following. $\Sigma\text{Fe}_2\text{O}_3$, MgO, TiO_2 and CaO contents of all groups decrease with increasing silica, which can be attributed to fractionation of olivine, plagioclase and Fe-Ti oxides. $\text{Al}_2\text{O}_3/\text{CaO}$ content of all Eocene samples increases with increasing silica. This can be explained by fractionation of clinopyroxene and plagioclase. This is supported by petrographic observations, where most of the samples from Group 2 are olivine- and pyroxene-phyric, whereas pyroxene and plagioclase population dominate the more evolved rocks of the Group 1. Small negative Eu/Eu* anomaly with the ratio of 0.65- 1.00 for Yozgat and 0.65- 0.88 for Çiçekdağ is also consistent with plagioclase fractionation in both areas. Na_2O abundances show weak correlation with increasing silica content, indicating plagioclase crystallization to some extent. It appears that fractionation of accessory phases such as apatite is insignificant according to random variations on the P_2O_5 vs silica diagram.

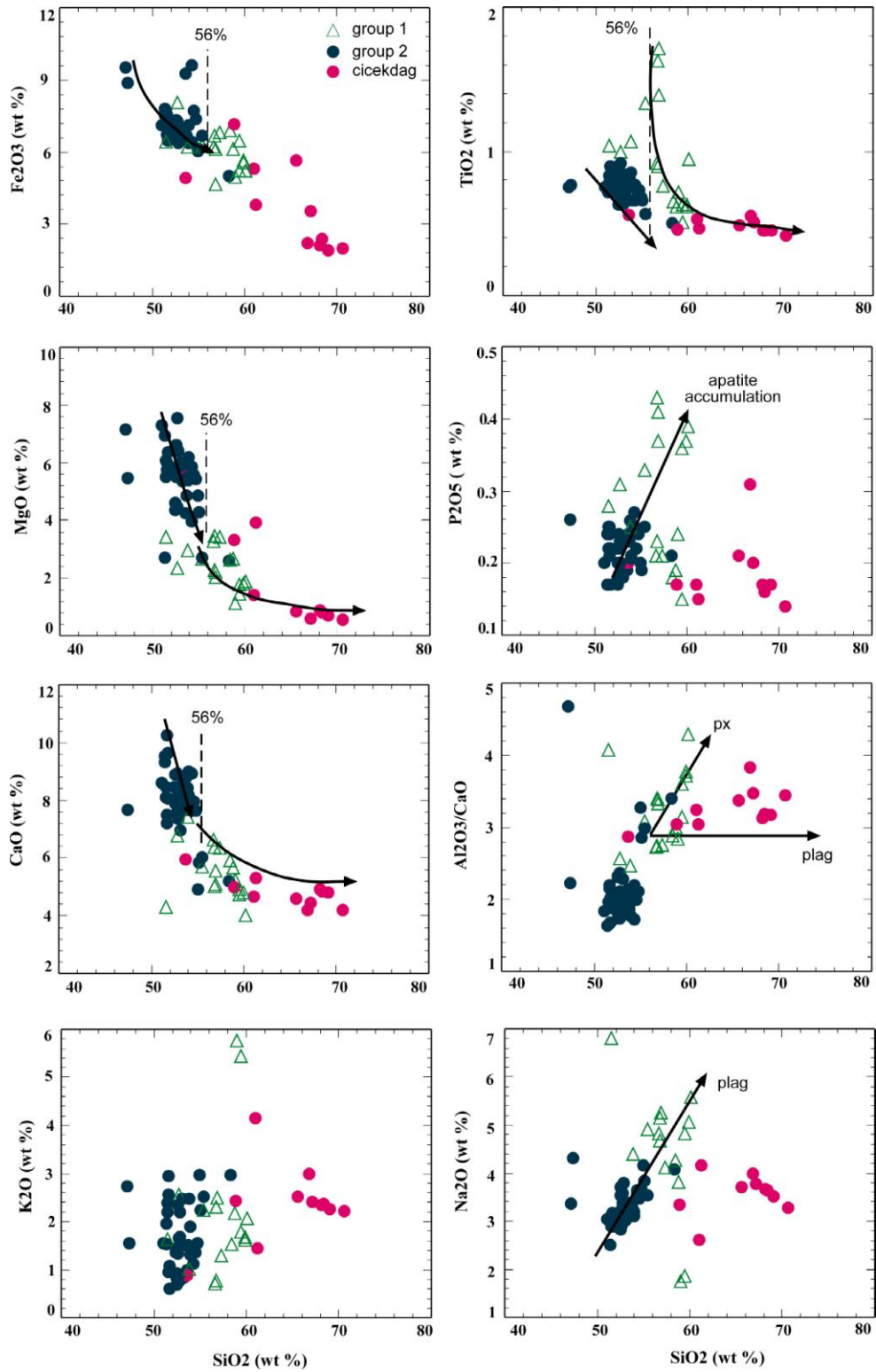


Figure 4. 4 Major oxides variation plots for the studied rocks. Green triangles represent Yozgat samples falling into the Group 1 in Nb-Y vs Zr diagram.

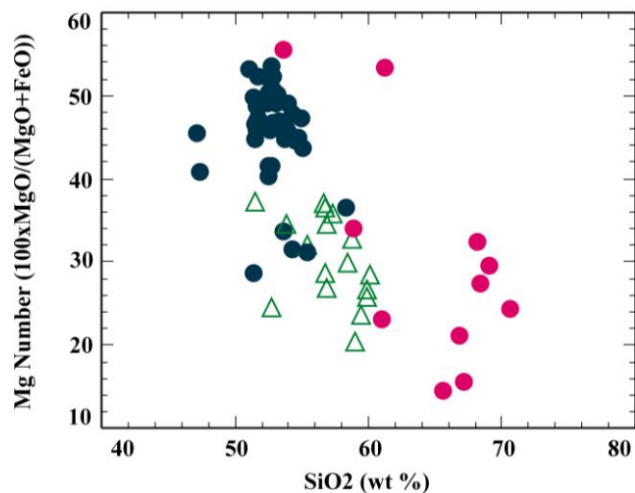


Figure 4. 5 SiO₂ vs Mg number plot for Eocene samples. Rocks from group 2 are characterized by high Mg #s (Symbols are the same in Figure 4.4).

Although some of the major oxide variations can be attributed to the fractional crystallization, scattered trends on some of the major oxide plots (especially those in P₂O₅ and to some degree TiO₂) combined with the petrographic observations imply disequilibrium crystallization and can be attributed to magma mixing/mingling process. Scattered trend in K₂O diagram might be related to post magmatic alteration.

Trace element variation plots (Figure 4.6) display the same trends as those observed in the major oxide diagrams. Group 2 is characterized by the highest concentration of Sr, Ni, V, Sc, Co among all groups, whereas its incompatible element concentrations such as Th, Hf, Zr, La and Y are the lowest. Most of Çiçekdağ samples have the lowest abundances of compatible elements, which is in agreement with their evolved nature. Incompatible elements (Rb, Th, Hf, Ba and La) generally display an increasing trend with the degree of differentiation. Marked increase in Ba content in Group 2 at a given SiO₂ could not be an alteration effect, since some of the compatible trace element variations display the same trend (i.e. Ni). Relatively less incompatible

elements such as Zr show positive correlation with the silica content, whereas Y and Sr have scattered trends.

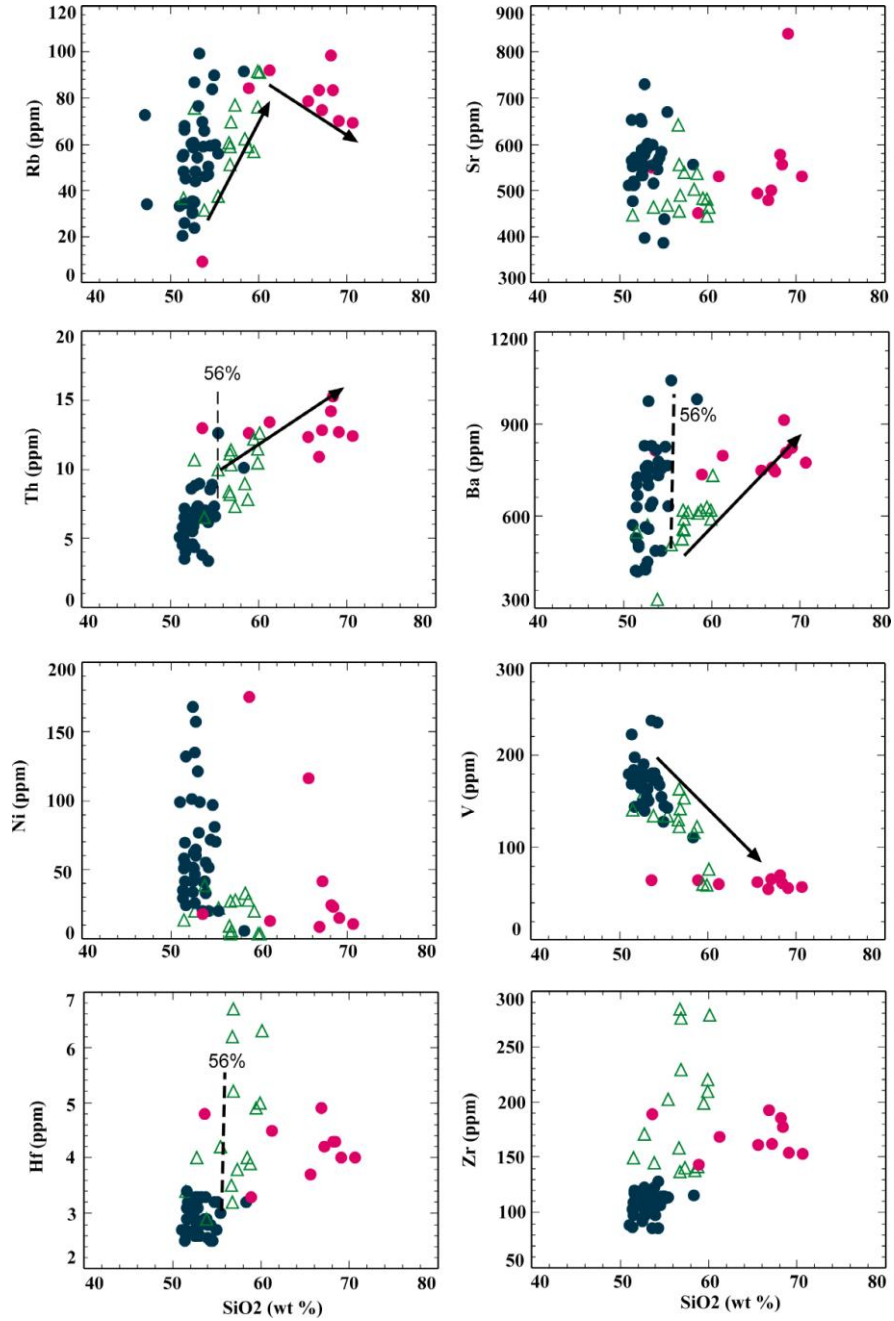


Figure 4. 6 Trace element variation plots for Eocene samples (Symbols are the same as in Figure 4.4).

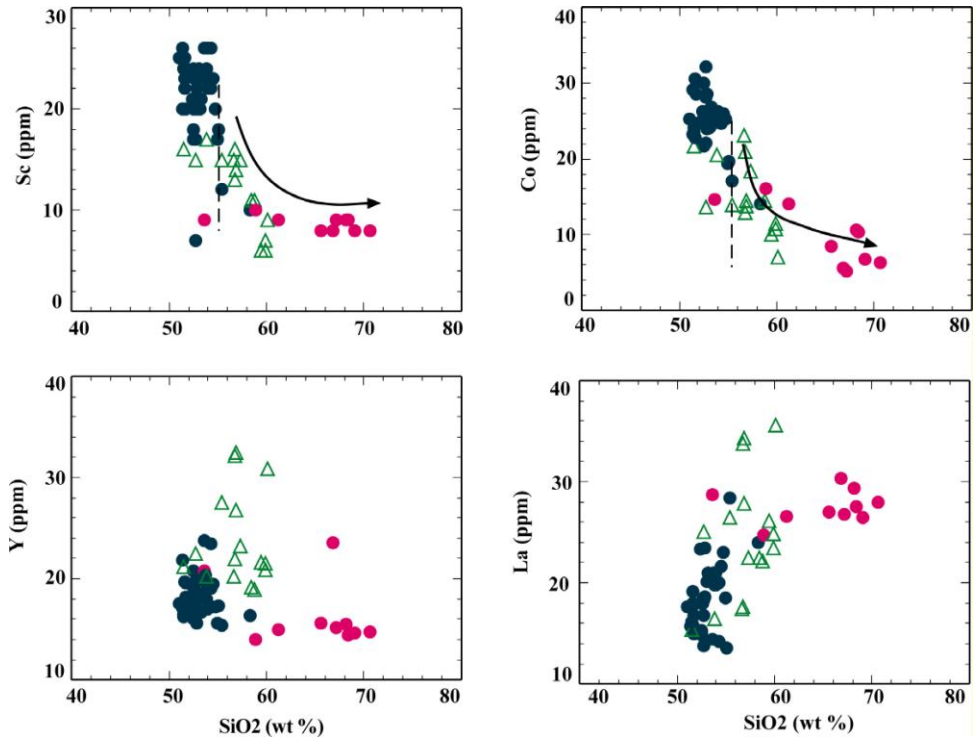


Figure 4.6 (continued).

Both groups show negative correlation between strongly compatible trace elements such as Ni and V, Sc and Co. Marked decrease in Sc content is compatible with pyroxene fractionation throughout the fractionation sequence of Group 1 and 2, whereas Çiçekdağ samples have relatively flat Sc concentrations. Ni shows sharp decrease at a given silica content for Group 2, which supports the olivine dominated phenocryst content of this group. Ni concentration is mainly governed by olivine, while V is controlled by pyroxene and opaque oxides. Therefore, their low abundances are consistent with the fractionation of these phases. Again, concentration of Co is hosted by mafic phases such as olivine and pyroxene (diopside). The negative correlations of these elements with the fractionation index indicate formation of these minerals.

The most striking feature regarding the Harker variation plots is that most of the major and trace element plots appear to show a kink at around 56 wt % SiO₂, which may suggest that Group 1 and Çiçekdağ samples can be evolved products of Group 2. A similar feature has already been reported by Keskin et al., (2008) for Middle Eocene volcanic rocks within the northern part of the study area. They attributed the kinked trends at around 57 wt % SiO₂ to the fractionation of the hydrous phases. This seems to be also applicable to the studied rocks, as Group 1 rocks contain variable amount of amphibole phenocrysts, whereas Group 2 rocks have olivine and pyroxene as the dominated phenocryst assemblage.

Nevertheless, it can be argued that compositional variations observed among the groups require different petrogenetic processes besides simple fractional crystallization event. These could be magma mixing, crustal contamination, and different degrees of partial melting or small scale heterogeneities in the mantle source.

4.6 Trace and Rare Earth Element (REE) Geochemistry

Chondrite (McDonough and Sun, 1995) normalized REE patterns of the studied rocks are presented in Figure 4.7. Both groups are enriched in the REE, with total REE ranging from 100.95- 231.57 ppm for Çiçekdağ, 77- 124.9 ppm for group 2, 85.72- 163.11 ppm for group 1. Overall, the REE patterns of the Eocene volcanic rocks are strongly light REE (LREE) enriched. However, the extent of enrichment is not only variable between two volcanic fields but also among both groups. For example, (La/Yb)_N ranges from 8.5 – 18.40 for Çiçekdağ samples; 4.18- 13.42 for group 2; 4.27- 18.44 for Group 1. Group 2 has the lowest abundances of REE, whereas Group 1 is the most REE enriched (Figure 4.7). The LREE of all groups have 80-120 times the chondritic values, whereas HREE 8- 10 times. Although Çiçekdağ samples were plotted with Group 2, their La/Yb and total REE concentrations significantly differ from it.

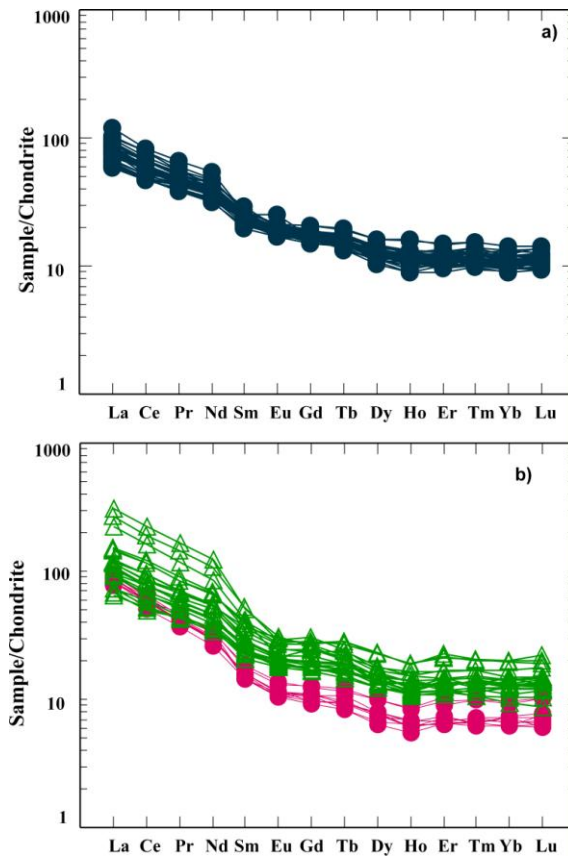


Figure 4. 7 Chondrite normalized REE patterns of investigated rocks a) for Group 2, b) for Group 1 and Çiçekdağ samples (Normalizing values are taken from McDonough and Sun, 1995).

Group 2 rocks show small Eu anomaly, which may indicate that plagioclase was one of the fractionating phases during their formation. The most diagnostic feature of the residual garnet in the source is depleted HREE pattern mainly because of the fact that Yb and Lu have high partition coefficient for garnet (Rollinson, 1993). The relatively flat HREE patterns of all suites in chondrite normalized REE diagram (Figure 4.7) preclude garnet as residual phase in the mantle source region. Instead, observed patterns are consistent with the derivation from a shallower depth. Besides concave shape that Group 1 and Çiçekdağ samples display may be indicative of clinopyroxene and hornblende fractionations.

In addition to REE diagrams, primitive mantle normalized multi element diagrams were also plotted for the samples from all groups (Figure 4.8). The primitive mantle (McDonough and Sun, 1995) normalized trace-element patterns of the Eocene volcanic rocks show significant enrichments in large ion lithophile elements (LILE) and LREE but depletion in Nb and Ta content and a pronounced Pb peak, especially for Çiçekdağ volcanics. Nb and Ta depletions become more pronounced in Çiçekdağ samples (Figure 4.8).

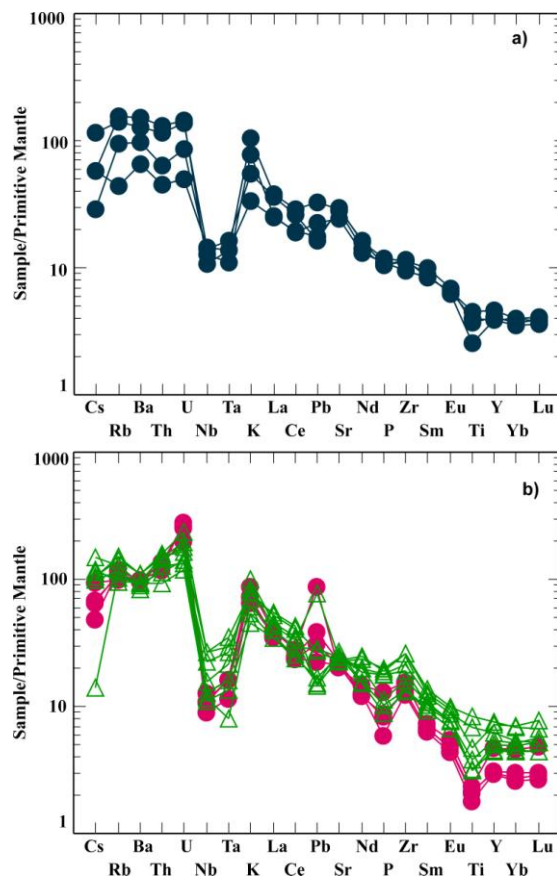


Figure 4. 8 Primitive mantle normalized multi element patterns of the studied rocks a) for Group 2, b) for Group 1 and Çiçekdağ samples (primitive mantle normalized values are from McDonough and Sun, 1995).

None of the groups shows negative Zr anomaly but Group 1 and 2 including Çiçekdağ samples display variable degree of negative Ti anomaly ($Ti/Ti^* =$

0.13- 0.75) which can be explained by either crustal contamination (Taylor and McLennan, 1985) or fractionation of the Ti bearing phases such as Fe- Ti oxides. Eocene volcanic rocks show small negative Ce anomaly (Ce/Ce^*) ranging between from 0.87 to 1.04. In the primitive mantle normalized diagram negative P anomaly that observed only within group 1 containing Çiçekdağ samples (Figure 4.8) could reflect apatite fractionations for these samples.

In general, all rocks, regardless of location, have similar patterns as in the REE diagrams, which suggest derivation from similar or the same source region.

4.7 Isotope Geochemistry

In addition to bulk geochemical analyses, isotope determinations were performed on 24 rock samples, 3 of which from Çiçekdağ and the rest from Yozgat region, encompassing full range of chemical diversity from both regions. The age of the Eocene (Bartonian; 37-41 Ma, Ogg, 2004) volcanic rocks is taken as 39 Ma according to the fossil findings to calculate the initial isotopic ratios and ϵNd values. Analytical and age corrected Sr, Nd and Pb isotopes of Eocene volcanic rocks are given in the appendix section.

There is no clear geographic control on the isotopic compositions since all Eocene samples are very homogeneous with regard to their Nd and Sr isotopic compositions in contrary to their highly variable trace element characteristics.

Çiçekdağ samples are characterized by isotope ratios of $^{87}Sr/^{86}Sr$ - $^{143}Nd/^{144}Nd$ ranging from 0.70522- 0.70538 and 0.51261- 0.51263, respectively. Their Pb isotopic compositions are 18.58- 18.77 for $^{206}Pb/^{204}Pb$; 15.63- 15.67 for $^{207}Pb/^{204}Pb$ and 38.85- 38.89 for $^{208}Pb/^{204}Pb$. The $^{87}Sr/^{86}Sr$ and $^{143}Nd/^{144}Nd$ isotope compositions of Group 2 range between from 0.70466- 0.70559 and 0.51263- 0.51277, respectively. The $^{206}Pb/^{204}Pb$, $^{207}Pb/^{204}Pb$ and $^{208}Pb/^{204}Pb$ ratios of Group 2 are 18.32- 18.79; 15.57- 15.65; 38.58- 38.90 respectively. The $^{87}Sr/^{86}Sr$ ratios of group 1 vary between 0.70404 to 0.70531. Its

$^{143}\text{Nd}/^{144}\text{Nd}$ ratios range from 0.51261 to 0.51280. Pb isotopic compositions are 18.01- 19.01 for $^{206}\text{Pb}/^{204}\text{Pb}$; 15.61- 15.67 for $^{207}\text{Pb}/^{204}\text{Pb}$; 38.69- 38.90 for $^{208}\text{Pb}/^{204}\text{Pb}$. All groups show similar $\Delta 7/4$ and $\Delta 8/4$ ($\Delta 7/4$ and $\Delta 8/4$ notations symbolize to vertical deviation from the Northern Hemisphere Reference Line (NHRL, Hart 1984) in the $^{206}\text{Pb}/^{204}\text{Pb}$ vs $^{207}\text{Pb}/^{204}\text{Pb}$ and $^{208}\text{Pb}/^{204}\text{Pb}$ diagram)) values that range between 10.42- 17.31 and 24.66- 128.92, respectively. Çiçekdağ samples have ϵNd values clustering around 0.53 to 0.83 and all groups from Yozgat samples have ϵNd values ranging between 0.55 to 4.33.

In the initial $^{87}\text{Sr}/^{86}\text{Sr}$ versus $^{143}\text{Nd}/^{144}\text{Nd}$ isotope correlation diagram (Figure 4.9), Eocene volcanic rocks fall into the mantle array line, overlapping with the Bulk Silicate Earth (BSE). In the plot of $\Delta 7/4$ vs $^{206}\text{Pb}/^{204}\text{Pb}$ diagram (Figure 4.10) they plot within the area between MORB and EMII source although most of the samples are close to the EM II area which is defined as enriched mantle source modified by terrigenous sediments (Weaver, 1991). In this diagram all samples fall above the northern hemisphere reference line (NHRL; Hart, 1984).

4.8 Differentiation Processes

Shallow level crustal differentiation processes for example, fractional crystallization, crustal contamination and magma mixing may significantly modify the chemical compositions of the magmas. Therefore, the extent of the crustal input and fractional crystallization on the elemental concentration should be evaluated to avoid uncertainty in establishing the source composition. For this purposes, in the following section, it is aimed to quantify all processes involved in the genesis of the studied rocks in terms of trace element and isotope compositions.

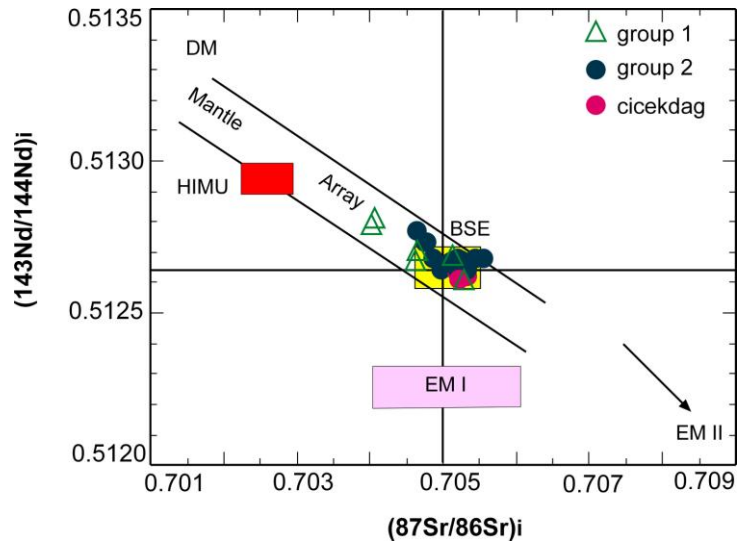


Figure 4. 9 $^{87}\text{Sr}/^{86}\text{Sr}$ vs $^{143}\text{Nd}/^{144}\text{Nd}$ plot of the studied samples. Most of the rocks placed on BSE (BSE; bulk silicate earth, EMI and EMII; enriched mantle I and II, DM; depleted mantle, HIMU; mantle having high U/Pb ratio). Different mantle reservoirs are from Zindler and Hart, (1986).

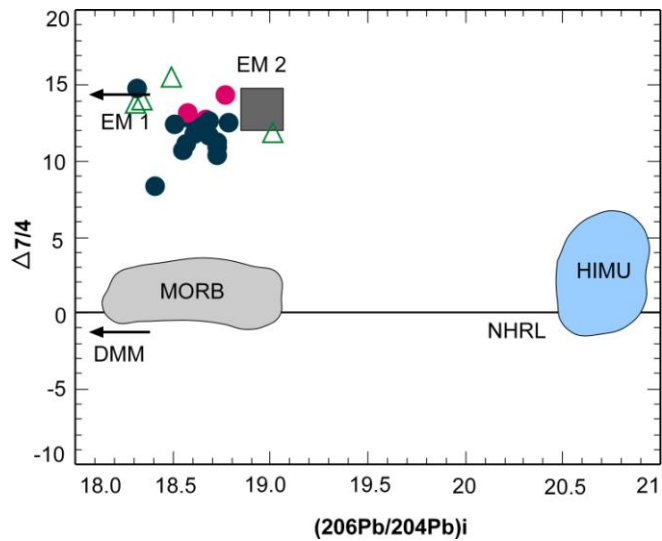


Figure 4. 10 $\Delta 7/4$ vs $^{206}\text{Pb}/^{204}\text{Pb}$ plot for Eocene samples. Data sources; DMM, HIMU, EM I, EM II are from Zindler and Hart (1986) and Hofmann (1997). Northern Hemisphere Reference Line (NHRL) from Hart, (1984). (Symbols are the same as in the Figure 4.4).

4.8.1 Fractional crystallization

Mantle derived primary magmas are commonly assumed to have Mg numbers of 68-72 (Green et al., 1974; Frey et al., 1978; Hart and Davies, 1978; Baker et al., 1997) and low ratio of LILE/HFSE (e.g. Weaver, 1991). The studied rocks are characterized by high phenocryst contents, low Mg numbers (19.57- 55.57) and low compatible trace element concentrations (Ni 5-166 ppm; Co 7-32 ppm). The observed phenocryst assemblage indicate to low pressure fractionating phases and geochemical characteristics point out that the volcanic rocks can not be regarded as representative of the primary melts. On the other hand, evolved affinity of the studied rocks requires fractional crystallization of variable phases during magma evolution. Based on the petrographic observations and Harker variation diagrams, rocks from Group 2 are characterized by fractionation of the mafic phases such as olivine and clinopyroxene whereas fractional crystallization sequence is governed by clinopyroxene, plagioclase and lesser amount of hornblende in the more evolved samples i.e. Group 1.

To show the effect of the fractional crystallization on the Eocene volcanic rocks FC vectors based on the bivariate element plots were used (Figure 4.11). Theoretical Rayleigh fractionation vectors were drawn by using FC Modeler program of Keskin, (2002). The program is based on the 50 % crystallization of given mineral assemblage. Partition coefficients of the minerals used in the model were taken from Rollinson (1993), Keskin (2002) and GERM (Geochemical Earth Reference Model, home page <http://earthref.org/databases/KDD/>).

In this diagram, Rb was used as fractionation index due to its highly incompatible nature during fractional crystallization. Besides, it is not partitioned into main mineral assemblages given on the diagram. As a result, fractional crystallization of the main mineral phases such as pyroxene, olivine and plagioclase, can not change the Rb concentration. The major oxides and

trace element variation plots, REE and spider diagrams indicate that mafic mineral fractionation is important in the genesis of the Eocene volcanic rocks. Because of the fact that Sc is partitioned into ferromagnesian minerals, Sc was selected for displaying mafic mineral fractionation in particular pyroxene and amphibole. Since Group 1 and Çiçekdağ samples behave similarly in most of the Harker variation plots, they were regarded as one single suite.

On the Sc vs Rb diagram, samples from Group 2 have trends that show compatibility with the vector 2 and 3 indicating mainly the olivine, clinopyroxene and plagioclase whereas, group 1 is distinguished by plagioclase, pyroxene and small amount of amphibole fractionations which are represented by the vector 6, 7, and 8.

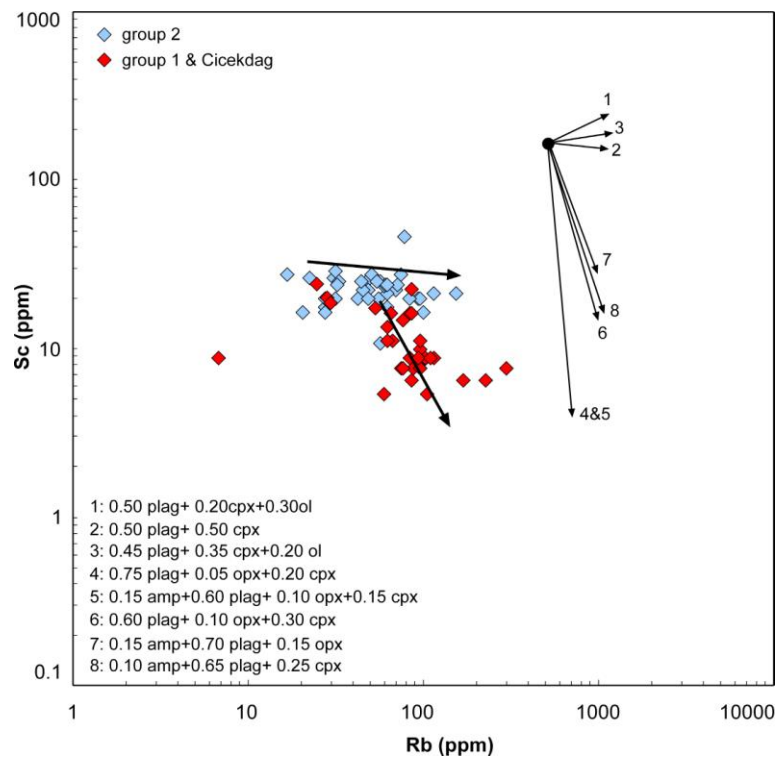


Figure 4. 11 Sc vs Rb bivariate plot displaying Rayleigh fractionating vectors. Phase combinations are given in inset. Abbreviations: plag; plagioclase, cpx; clinopyroxene, ol: olivine, opx; orthopyroxene, amp; amphibole.

On the basis of observed phenocryst assemblages and geochemical trends, it can be argued that the crystallization sequence seems to have begun with olivine, continued by pyroxene and plagioclase for Group 2, while it started with pyroxene, plagioclase and finished with amphibole for Group 1. Most of the variations in major and trace element compositions of the Eocene volcanic rocks are likely to be a result of fractional crystallization either in magma chambers or en route to the surface.

4.8.2 Crustal contamination

In the literature there are two types of contamination processes; low pressure crustal contamination involving chemical reactions between mantle derived magmas and crustal material during the emplacement of magmas and source contamination which modify the chemical composition of the mantle source prior to the partial melting (e.g. Hollanda et al., 2003). Source contamination could be related to the addition of subducted material (e.g. sediments) to the source region (Davidson and Harmon, 1989). Before discussing source characteristics, it is essential to find out the role and the extent of the crustal input on the magma genesis. In this section contamination by crustal rocks will be considered and source or sediment contamination will be evaluated in further sections.

It is commonly accepted that mantle derived magmas passing through a crustal section may have undergone variable degrees of crustal assimilation in magma chambers and during their movement to the surface (Hergt et al., 1991; McDonald et al., 2000). The geochemical data indicates that Eocene volcanic rocks are not primary magmas in composition and have erupted through a thick granitic basement; accordingly, assimilation processes might have modified the observed elemental compositions. This can be further emphasized by using trace element data. The studied rocks display some elemental ratios which were mainly attributed to crustal contamination. For example, low Nb/La ratio is regarded as a proxy of crustal contamination (Kieffer et al., 2004). Eocene

samples have Nb/La ratios changing between from 0.21 to 0.62, which indicates that they may have experienced some degree of crustal contamination en route.

Before quantifying assimilation and fractional crystallization process (AFC), it is necessary to establish the composition of the crustal rocks in the study area. The lack of the geochemical data regarding the lower crustal rocks in the CACC made the comparison difficult. Therefore, emphasize will be placed on the upper crust, mainly composed of voluminous granitic rocks that were emplaced during the Late Cretaceous time. A piece of evidence for contamination from granitic rocks comes from the presence of quartz xenocrysts surrounded by clinoproxene rims (Figure 3.12). To quantify the amount of assimilated local rocks 7 granite samples, of which 3 are from Çiçekdağ and the rest from Yozgat, as representative of the upper crustal basement in the CACC were analyzed for whole rock data and Sr, Nd and Pb isotope compositions and given in the Appendix E and F. Analyzed granitic rocks are metaluminous to peraluminous. They have radiogenic Sr and Pb isotopic compositions and are characterized by negative ϵNd values (-6.51 to -7.91) in contrast to Eocene lavas having positive ϵNd values (0.53 to 4.33).

Figure 4.12 shows the comparison of the studied Eocene volcanics and Upper Cretaceous granitic rocks. Eocene volcanic rocks have comparable $^{206}\text{Pb}/^{204}\text{Pb}$ vs $^{207}\text{Pb}/^{204}\text{Pb}$ ratios with the granitic basement. Negative correlation observed in the diagram of Ba/Nb vs $^{206}\text{Pb}/^{204}\text{Pb}$ points towards granite values (Figure 4.12b). However, there is no correlation between Ba/Nb ratio and $^{87}\text{Sr}/^{86}\text{Sr}$ or $^{143}\text{Nd}/^{144}\text{Nd}$, implying that crustal contamination has not affected all isotopic systems but was enough to overprint Pb isotopes. Similarly, some other trace element ratios (Nb/La, Ba/La and Ba/Ta, Ce/Pb; not shown here) exhibit good negative correlation only with the Pb isotopes, not other systems. This, suggest that aforementioned trace elements have been little affected by basement contamination or crustal assimilation is not main process in the genesis of Eocene volcanic rocks.

Upper crustal assimilation that affected only Pb isotope system can be explained by the elemental concentration of the contaminants and the volcanics. For instance, analyzed granitic rocks have lower Sr contents (ranging between 67- 1101 ppm) than the Eocene rocks (444- 1299 ppm) but comparable Nd concentration (15.68- 67.47 for granites and 14.2- 47.9 for volcanics) and as a result, assimilation of the upper crustal rocks having similar Sr and Nd concentrations has not caused significant change in Sr and Nd isotopic systems. On the other hand, granites have higher Pb concentration (22- 91 ppm) than Eocene samples (1.4- 19.9 ppm), which may well explain the observed trends in Figure 4.12a, b and relatively radiogenic Pb isotope composition of the Eocene samples.

To constrain better the contribution of the local granitic basement to the genesis of the Eocene volcanic rocks, assimilation and fractional crystallization (AFC) modeling was performed in terms of Rb/Sr ratios and Sr isotopic compositions by using equations derived by DePaolo, (1981). In this model two end members were used as the parental magma and contaminant. Sample PK1 was chosen for parental magma because of its relatively primitive nature with lower $^{87}\text{Sr}/^{86}\text{Sr}$ ratios and high Mg number. One of the granite samples from Yozgat region namely MCG 119 was selected for the contaminant. The curve on the diagram was calculated using a bulk D value of 0.05 for Rb and 0.94 for Sr for the average mineralogical assemblage of 50% plagioclase, 15% olivine, 30% clinopyroxene, 5% orthopyroxene. Distribution coefficients were taken from Rollinson, (1993). The results of modeling are shown in Figure 4.13 for r values of 0.1. The “r” value equals the ratio of assimilated wall rock to the rate fractionating phases, which are being separated from the original magma (i.e. assimilation rate/ fractionation rate). Therefore; the higher r value, the higher crustal input. Most of the samples were plotted between $r=0.1$ and $r=0$. Based on the AFC modeling it can be concluded that variable degrees of fractionation and small percentages of assimilation can successfully account for the observed isotopic compositions in the Eocene rocks.

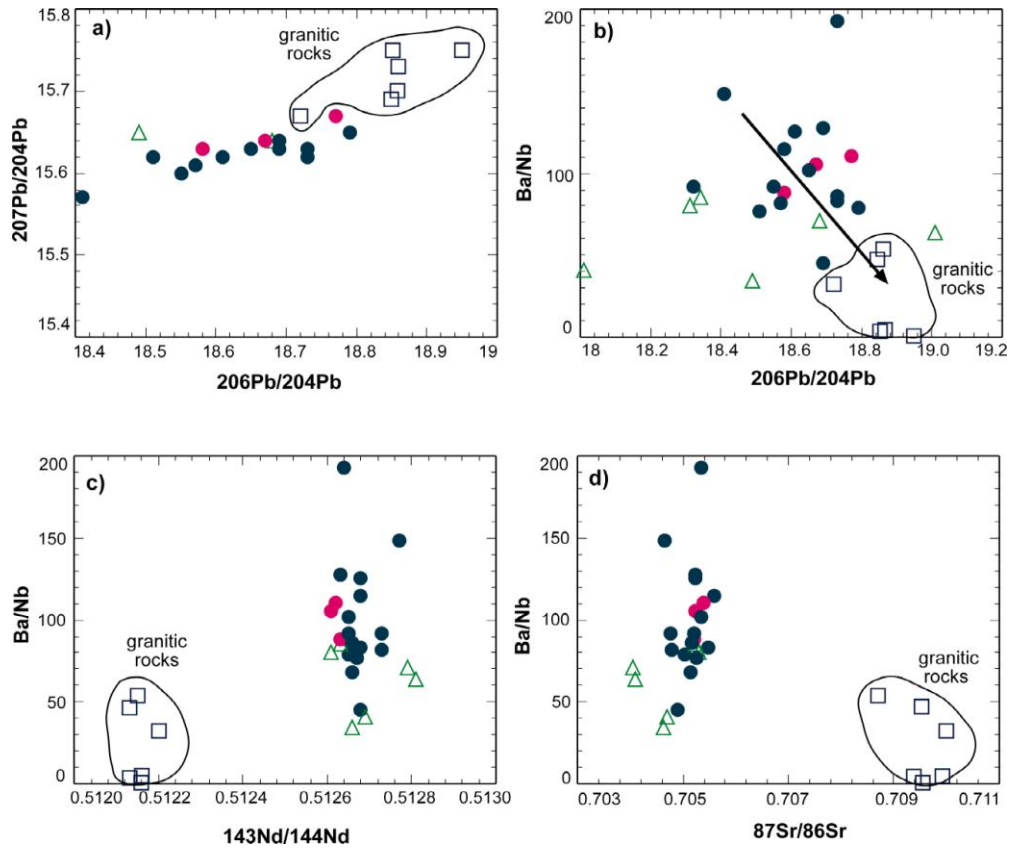


Figure 4. 12 a) $^{207}\text{Pb}/^{206}\text{Pb}$ vs $^{206}\text{Pb}/^{204}\text{Pb}$ plot for the studied rocks b) Ba/Nb vs $^{206}\text{Pb}/^{204}\text{Pb}$ c) Ba/Nb vs $^{143}\text{Nd}/^{144}\text{Nd}$ d) Ba/Nb vs $^{87}\text{Sr}/^{86}\text{Sr}$ ratios. (Symbols are the same as in Figure 4.4).

A further aspect to be considered is that AFC process involving Rb/Sr ratio could be problematical since the calculated AFC curves will be sensitive to distribution coefficient of Sr which can easily change depending on the plagioclase abundances in the fractionating assemblage. Besides, Rb/Sr ratio is likely to change depending on the source composition or residual phases in the source (e.g. presence of phlogopite). Therefore, to avoid uncertainty another AFC model based on the Pb isotope ratios and Pb concentration were performed (Fig 4.14).

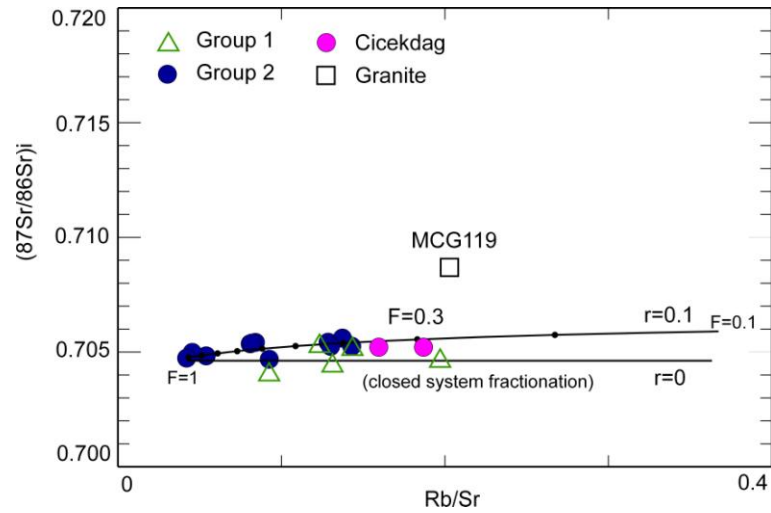


Figure 4.13 Initial $^{87}\text{Sr}/^{86}\text{Sr}$ vs Rb/Sr plot for assessing crustal assimilation process. The composition of the contaminant (MCG119) and the parental (Pk1) are ($^{87}\text{Sr}/^{86}\text{Sr}$: 0.70869, Rb: 207 ppm; Sr: 1009 ppm and 0.70477; 23.9; 552.4 respectively). The tick marks and numbers on the curve show the percentage of the melt (F) remained in the system.

For this second modeling calculation of different end members was realized. Sample F26 which has the lowest $^{206}\text{Pb}/^{204}\text{Pb}$ ratio was chosen for the parental end member and the sample MCG23-21 was selected for the contaminant, due to its highest Pb concentration and $^{206}\text{Pb}/^{204}\text{Pb}$ isotope ratio. The results of AFC calculation are given in Figure 4.14. The curve on the diagram was calculated using a bulk D value of 0.9 for Pb based on the mineralogical assemblage used in the first model. According to diagram the AFC curve (D=0.9 and r=0.4) is representative for most of the samples.

One of the drawbacks of the DePaolo's equation is that it does not give a certain amount of crustal input. On the other hand, Sheth and Ray, (2002) defined a mathematical expression based on the r and F value, which yield degree of contamination as percentage. $C (\%) = r (1-F) / (1-r)$, where F is defined as the ratio of final volume of magma to initial volume of magma.

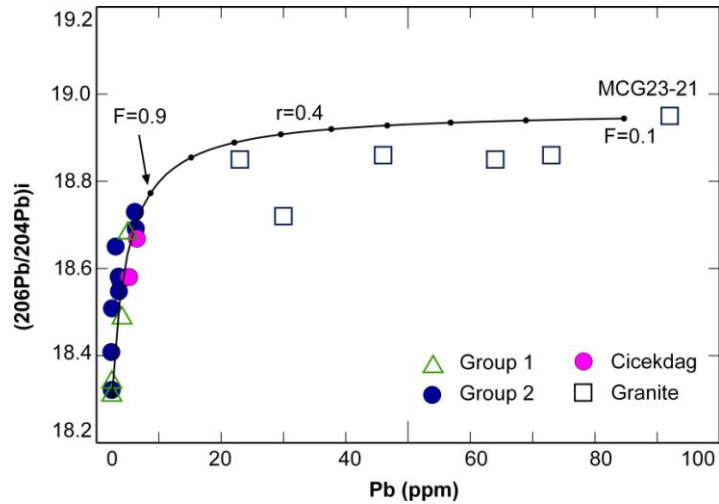


Figure 4. 14 $^{206}\text{Pb}/^{204}\text{Pb}$ vs Pb plot for evaluating the effect of crustal assimilation. The compositions of the end members are (MCG23-21 $^{206}\text{Pb}/^{204}\text{Pb}$ 18.95 and Pb 91 ppm; F26 $^{206}\text{Pb}/^{204}\text{Pb}$ 18.31 and Pb 2.5 ppm).

Using this expression, the degree of crustal input can be calculated. The most contaminated Eocene samples have the F value of 0.3 in the first model and 0.9 in the second one. Accordingly, the equation of Sheth and Ray, (2002) produces crustal assimilation value of 8 % and 7 %, respectively.

AFC curves calculated using different contaminants and parental compositions do not significantly differ from each other in terms of the amount of crustal material (7-8%) needed to produce the isotopic and trace element compositions of Eocene samples. Although calculated amount of the crustal input seems to be high enough to shift the Pb isotope compositions of the studied rocks, it is not responsible for the variations observed in the Sr-Nd systems so they must be inherited from the source.

4.8.3 Magma mixing/mingling

Studied volcanic samples are characterized by various textures indicating disequilibrium crystallization such as glass inclusions in plagioclase and sieved textured and poikilitic plagioclase, coexistence of sieved and normal (clear)

plagioclases within the same rock (Figure 3.13), reaction rim around the mafic minerals (Figure 3.11), zoning in pyroxene and plagioclase phenocrysts (Figure 3.5), and quartz phenocryst surrounded by pyroxene (Figure 3.12). Therefore, Eocene magmas appear to have mixed in shallow magma chambers based on the petrographic observations. Lack of evolved samples with high silica contents (i.e. rhyolite or dacite) within whole suite makes the mixing modeling difficult. Therefore, binary mixing modeling based on the felsic and mafic end members could not be realized.

4.9 Source Region and Petrogenesis

As shown in the previous chapters, the mantle source components and degree of partial melting in source region/regions are the most critical aspects to evaluate the geochemical characteristics of the Eocene volcanic rocks. For this the possible processes will be modeled and discussed in the following chapter. To minimize the effects of fractional crystallization the rocks with intermediate in composition are excluded and only relatively more mafic rocks ($\text{MgO} > 6 \text{ wt } \%$) are considered for the modeling and evaluation.

4.9.1 Melting conditions and partial melting process

Although several petrological process such as fractional crystallization, magma mixing and crustal assimilation may have been involved in the genesis of the studied rocks, positive correlation between La/Yb ratio and La (Figure 4.15) content and large variations in (La/Yb 6.28- 25.42) ratios -which can not be largely affected by small amount of fractional crystallization- indicate that partial melting is the dominant process that caused the compositional variability in the Eocene samples.

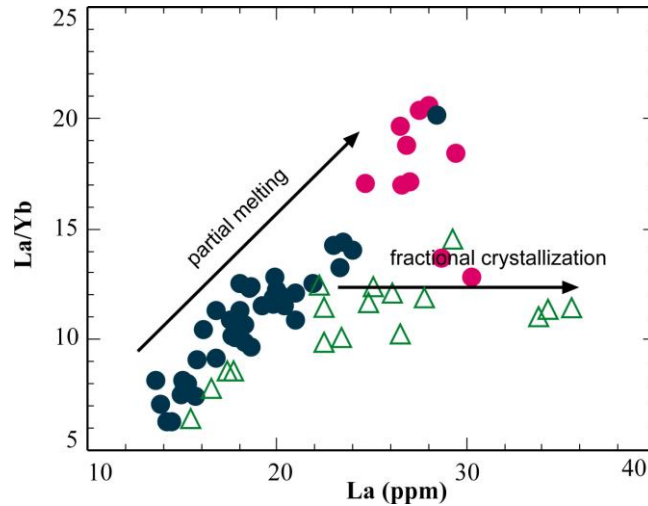


Figure 4. 15 La/Yb vs La plot for the investigated rocks (Symbols are the same as in Figure 4.4).

Before quantifying partial melting process, residual minerals that may have retained in the mantle source region during partial melting process, which can also provide valuable information on melting depth, should be evaluated. For example, the presence of garnet in the source is recorded by the steep HREE pattern in the chondrite normalized REE plots. The flat HREE patterns of the studied rocks, however, indicate derivation from a garnet free source i.e. shallower than 80 km since garnet is thought to be unstable above 60 and 80 km in anhydrous mantle and plume mantle, respectively (e.g. McKenzie and O’Nions, 1991). Therefore, relatively high middle REE (MREE) and heavy REE (HREE) contents of the studied rocks give a strong evidence for melting in the spinel stability field.

Another constraint regarding the residual minerals in the source region comes from LILE data. Furman and Graham, (1999) argued that relative abundances of alkali and alkaline earth elements such as Rb, Ba, Sr can be used to assess the presence of amphibole or/and phlogopite in the mantle source region. Primitive mantle normalized trace element patterns of the studied rocks reveal significant enrichment in LILE and LRE. In addition to this, the evolved rocks

contain hornblende phenocryst, which give a line of evidence that source region of the Eocene magmas may contain K bearing phases such as amphibole and/or phlogopite. In the literature there are several criteria that can be used to distinguish phlogopite bearing source from amphibole bearing source. For example, phlogopite is thought to have high K/Nb (>3000), Ba/Nb (>50) (Tommasini et al., 2005), high Rb/Sr (>0.1) and low Ba/Rb (<20) (Hawkesworth et al 1990; Furman and Graham, 1999; Davies et al., 2006) and low K/Rb (Kempton et al., 1991) ratios, whereas moderate K/Nb (200-400), low Ba/Nb (<5 ; Tommasini et al., 2005), low Rb/Sr and low Rb/Ba are interpreted as amphibole bearing source region (Furman and Graham, 1999; Davies et al., 2006). The studied rocks are characterized by high K/Nb (up to 3500), high Ba/Nb (up to 200), high Rb/Sr (up to 0.3) and low Ba/Rb (<20), implying that residual K bearing phase in the source region was phlogopite rather than amphibole.

Rare Earth Elements (REE) or their ratios (e.g. Dy/Yb, La/Yb or Sm/Yb) have been widely used to show the upper mantle composition, mineralogy and magma segregation depth since they have different partition coefficients for spinel and garnet lherzolites (Thirlwall et al., 1994; Baker et al., 1997; Shaw et al., 2003). The Dy/Yb vs Dy diagram offers a good opportunity to address the degree of partial melting and source compositions (Figure 4.16).

To quantify the source compositions and degrees of partial melting involved in producing Eocene magmas, trace element modeling (Figure 4.16) was performed using the batch melting equations derived by Shaw (1970). Calculations were made using model source composition of primitive mantle (McDonough and Sun, 1995) since MORB like mantle does not have elemental abundances to reproduce Eocene magmas that were likely to have been generated from an enriched source based on the trace element data. Modeling was performed using two different mantle mineral assemblages, garnet facies lherzolite and phlogopite bearing spinel facies lherzolite. Source compositions

of different mantles and partition coefficients used in the calculation are given in Table 4.1.

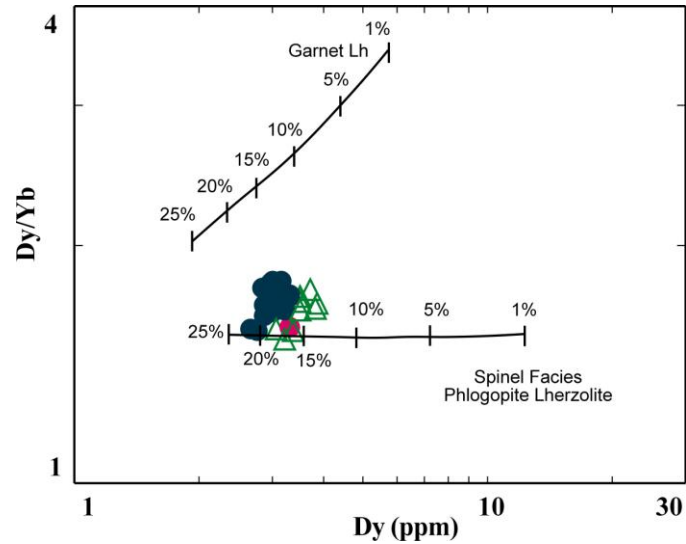


Figure 4. 16 Calculated partial melting curves assuming batch melting of garnet facies and phlogopite bearing spinel facies sources. Source compositions ($Dy=0.674$ ppm, $Yb= 0.441$ ppm) are from McDonough and Sun, (1995). Partition Coefficient (K_d) values are from McKenzie and O’Nion, (1991 and 1995) and GERM (Geochemical Earth Reference Model), home page <http://earthref.org/databases/KDD/>.

It appears that the REE patterns of the calculated hypothetical melts, which are formed by 15-20 % melting of a 2 % phlogopite bearing spinel lherzolitic source, can account for the observed REEs since they closely match the most primitive rocks of the Eocene unit. It is also inferred from the Figure 4.16 that variations in the REE of the studied rocks can be attributed to different degrees of partial melting since Group 1 and Çicekdag samples seem to have generated by lower melting degree.

Table 4. 2 Partition coefficient (D) and source model composition data used in batch melting modeling calculation.

Elements	Partition Coefficient (D)				
	Olivine	Orthopyroxene	Clinopyroxene	Spinel	Phlogopite
Dy	0.0017	0.0220	0.3300	0.0100	0.290
Yb	0.0015	0.0600	0.2800	0.0100	0.030

	Source Mode	
	Garnet Facies	Spinel Facies Phlogopite
Olivine	0.60	0.564
Orthopyroxene	0.20	0.24
Clinopyroxene	0.15	0.116
Spinel	-	0.06
Phlogopite	-	0.02
Garnet	0.05	-

4.9.2 Source characteristics

Source region of post collisional magmatism may involve several components including deep asthenospheric mantle (MORB or OIB like), lithospheric mantle metasomatized during previous subduction events, upper and/or lower crust which can be involved by means of anatectic melting or crustal contamination of mantle derived magmas, and subducted oceanic crust which may produce adakitic magmas (Maury et al., 2004 and references therein). Therefore, in order to show the geochemical similarities and differences between different source components chondrite normalized REE and primitive mantle normalized multi element diagrams were conducted (Figs 4.17 and 4.18). For comparison purposes; MORB, OIB, upper continental crust and average arc composition were also plotted in these diagrams.

In the chondrite normalized REE diagram, Eocene volcanic rocks show enriched values similar to ocean island basalts and average arc basalts. Upper crust compositions have also comparable REE patterns with Eocene samples. In the primitive mantle normalized multi element plot, Eocene volcanic rocks are characterized by a pattern different from the N type MORB that is thought to be representative of the mantle.

The studied rocks display large ranges in trace element patterns, lying between those found in OIB and subduction zone lavas; the former generally characterized by positive Nb and Ta and negative Pb anomaly in the primitive mantle normalized plots (e.g. Hofmann 1988). In contrast, Eocene samples display negative Nb, Ta, P, Ti and positive Pb anomaly (Figure 4.18).

Regardless of their region and group, the whole Eocene volcanic suite is represented by elevated LILE (Rb, Ba, and K), LREE and low HFSE (especially Nb, Ta) contents relative to neighboring elements, suggesting derivation from a mantle source different from the asthenosphere-derived magmas (i.e. MORB or OIB).

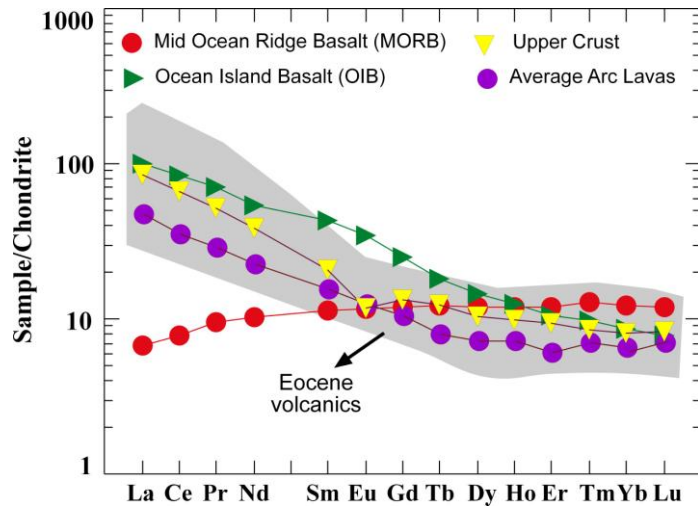


Figure 4. 17 C1 Chondrite (McDonough and Sun, 1995) normalized REE patterns for the Eocene volcanic samples. For comparison purposes, Upper crust, average arc lavas, ocean island basalts and mid ocean ridge basalts were also plotted (Upper crust value from Rudnick and Gao, 2004; OIB and MORB from Sun and McDonough, 1989 and average arc lavas composition represents Aegean arc (<http://georoc.mpch-mainz.gwdg.de/georoc/Start.asp>)).

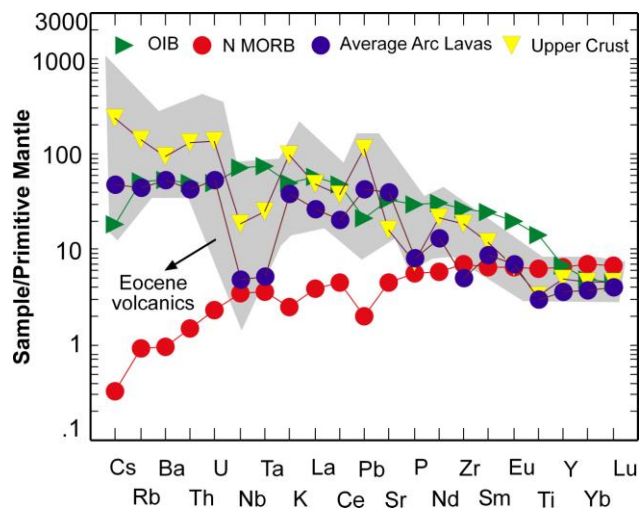


Figure 4. 18 Primitive mantle (McDonough and Sun, 1995) normalized multi element patterns for the Eocene volcanics (Data set and reference values are the same as in Figure 4.17).

As a general consensus, low HFSE contents and high LILE abundances are considered to be the most diagnostic characteristics of the rocks formed in subduction zone environment (Thirlwall et al., 1994; Pearce and Peate, 1995; Davidson, 1996). However, Eocene volcanics have following characteristics which make them different from arc-related rocks;

- 1) they are characterized by relatively high Zr (up to 300 ppm) and Nb (up to 19.5 ppm) contents that are higher than those found in conventional subduction related rocks (i.e. Aegean arc which has average Zr and Nb contents of 171 ppm and 7.54 ppm, respectively). Moreover, in the plot of Zr vs Zr/Y (Figure 4.19 Pearce and Norry, 1979), they plot within the intraplate field.
- 2) Besides, as stated previously in geology section there is no evidence for Eocene volcanic rocks to be part of an active subduction process. Moreover, several lines of evidence indicate a post collisional extension-related environment.

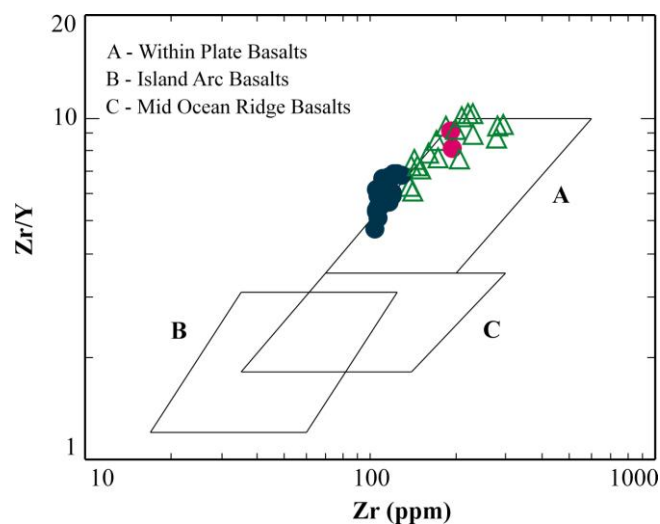


Figure 4. 19 Zr/Y vs Zr diagram (Pearce and Norry, 1979) for Eocene volcanics. All samples fall into field A representing within plate setting (Symbols are the same as in Figure 4.4).

The origin of the HFSEs depletion and LILE enrichment of the studied rocks appear to be the most important key in establishing the mantle source region. Such geochemical properties are well defined for many continental flood basalt provinces (Arndt et al., 1993; Ewart et al., 2004) and post collisional extension related volcanic rocks (Waters and Erlank, 1988; Hergt et al., 1991; Jahn et al., 1999; Turner and Hawkesworth, 1995; Hawkesworth et al., 2000) throughout the world. Distinctive geochemical features of those rocks are commonly represented by low HFSE contents are interpreted to have been derived from;

- 1) contamination of ascending mantle-derived magmas with crustal wall rocks (Cox and Hawkesworth, 1984; Arndt et al., 1993; Mahoney et al., 1995),
- 2) asthenosphere or deep mantle plume derived melts mixed or contaminated by lithospheric mantle (Arndt and Christensen, 1992; Frey et al., 1996),
- 3) enriched lithospheric mantle modified by metasomatizing agents during previous geodynamic event (Hergt et al., 1991; Hawkesworth et al., 1995; Fan et al., 2003).

In the following these possibilities will be discussed.

4.9.2.1 Crustal contamination

One of the possible reasons for depleted HFSE abundances might be crustal contamination since the crustal rocks are also characterized by low content of HFSE (Taylor and McLennan, 1985).

However, as discussed in the section above on crustal contamination, assimilation of the Upper Cretaceous granitic rocks seems to have affected only the Pb isotopic system. No correlation exists between trace element ratios sensitive to crustal contamination (e.g. Ba/Nb, Nb/La and Ba/La) and Sr and Nd isotopic composition of the granites. Similarly, if crustal contamination had

affected the overall geochemistry of the studied rocks, aforementioned ratios would not be so high since the granites have comparable alkali content with the Eocene samples. Addition of the 8% upper crustal granitic rocks (MCG 119; Ba= 1206 ppm and La= 71.73) to the least contaminated Eocene volcanic sample (P5; Ba= 591.6 and La= 34.33) did not cause a marked change in the LILE geochemistry, as Ba/La ratio of the sample P5 remained the same. Moreover, binary mixing calculation between the MORB as representative of the mantle derived magmas and granites as representative of the upper crust in the CACC failed to reproduce isotopic and trace element compositions of the Eocene samples. Besides, Ormerod et al., (1988) claimed that low Nb abundances of the Basin and Range (USA) magmas (between 10-20 ppm) can not be derived from crustal contamination since to reduce Nb abundance (assuming an OIB type parental magma), from 50 ppm to 20 ppm would require an addition of 150-400% crustal material. Thus, the elevated LILE/LREE and HFSE/LREE ratios and Sr and Nd isotopic signature of the studied rocks together with the HFSE depletion must be inherited from the source rather than being related to crustal contamination.

4.9.2.2 Asthenosphere or plume component contaminated by lithospheric mantle

Relative contribution of the lithospheric and sub- lithospheric mantle source (plume or asthenosphere) to the genesis of the basic rocks has been reported by previous studies (Baker et al., 1997; Shaw et al., 2003; Duggen et al., 2005; Jourdan et al., 2006). McKenzie and Bickle, (1988) argued that mantle lithosphere contains two parts as mechanical boundary layer (MBL) which tends to behave a rigid plate and thermal boundary layer (TBL) acting a barrier between convecting asthenosphere and MBL. Only the mechanical boundary layer of the lithosphere can be stable without any interaction with asthenosphere and consequently, able to accumulate enriched isotopic composition with time; on the other hand, thermal boundary layer is thought to have MORB like depleted isotopic signature (McKenzie and Bickle, 1988).

Fitton et al., (1991) argued that continental rocks formed within the TBL of the lithosphere could have similar elemental and isotopic composition with the asthenospheric melts. But they can not be assumed to have generated entirely within the asthenosphere, their elemental and isotopic compositions must have interacted considerably with the lithosphere. This process has been widely applied to explain the major variations in both trace element and isotope geochemistry of the continental flood basalts throughout the world (e.g. Sana'a Yemen, Baker et al., 1997; Zimbabwe, Jourdan et al., 2006) as well as within the Alpine belt (Rhodope volcanics Bulgaria, Marchev et al., 2004). It appears that all these rocks have depleted HFSE patterns inherited within the lithospheric mantle although their trace element geochemistry reflects (Ba/Nb, Ce/Pb, Nb/U) the OIB like asthenospheric mantle properties. Aforementioned rocks also display wide range of isotopic composition, suggesting mixing of the two different mantle sources (e.g. Shaw et al 2003). Asthenospheric trace element signature is thought to be derived from either melting of the underlying mantle plume (Baker et al., 1997; Jourdan et al., 2006) or mantle diapirism due to lithospheric removal (Marchev et al 2004). Jourdan et al., (2006) argued that the sub- lithospheric components (OIB like mantle plume or relatively depleted asthenospheric mantle) are expected to have isotopic composition between bulk silicate earth (BSE) and isotopically depleted ocean island basalt (OIB) and the authors suggested that mixing of the enriched lithospheric mantle and plume component would result in negative ϵ_{Nd} and unradiogenic Pb isotope composition due to the chemical contrast between two components.

In case of the studied Eocene volcanics, several lines of evidence based on the trace element and isotope signature argue against asthenospheric contribution for the genesis of the studied rocks. For example, Eocene rocks are characterized by elemental ratios (Nb/La, Ce/Pb, Nb/U; 0.3, 10, 3, respectively) that are different from OIB like mantle sources (1, 20, 43, respectively; Hofmann, (1997); Hofmann, (1988)). Homogeneous Sr and Nd isotope compositions and positive ϵ_{Nd} values are also inconsistent with the

mixing of two different mantle sources. Relatively unmodified Sr and Nd isotopic compositions (plotted on the BSE in the Sr- Nd isotopic space) of the Eocene samples have more enriched values compared to asthenosphere derived magmas. This is evident from Figure 4. 20 where all samples are plotted within the region of lithosphere derived melts. Relatively high Pb isotope compositions of the Eocene samples similar to those of European Asthenospheric Reservoir (EAR, Cebria and Wilson, 1995) must be related to crustal contamination as indicated AFC model. Another line of evidence for arguing against this hypothesis can be provided from the partial melting modeling. Presence of the residual hydrous phases (e.g. phlogopite) limits the melting depth to mechanical boundary layer of the lithospheric mantle since K bearing phases can not be stable within the convecting asthenosphere (Class and Goldstein, 1997).

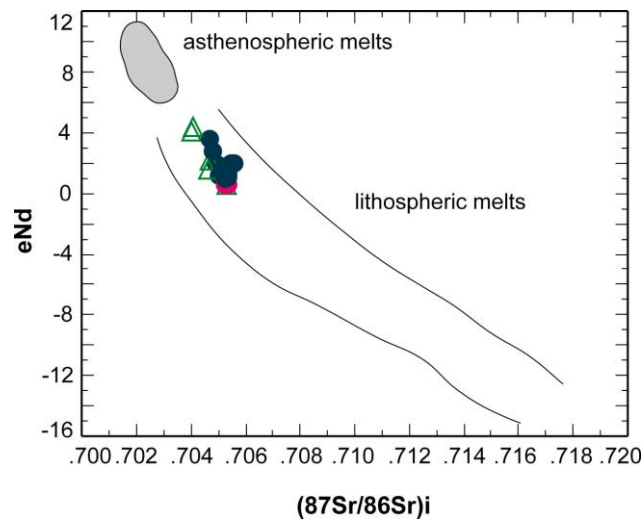


Figure 4. 20 ϵ_{Nd} vs $^{87}Sr/^{86}Sr$ plot for Eocene volcanic samples. Asthenospheric and lithospheric melt fields are taken from Davies and Van Blanckenburg, (1995). (Symbols are the same as in Figure 4.4).

Consequently; based on the trace element and isotopic compositions of the studied rocks, asthenospheric contribution to the genesis of the Eocene

volcanism appears to be unlikely. On the other hand, extraordinary heat influx is required to generate widespread volcanism in the region in such a short period of time (Bartonian), which will be considered in the forthcoming sections.

4.9.2.3 Lithospheric mantle source

In general, high LILE, LREE abundances and low Nb/La ratios are attributed to melting of the lithospheric mantle enriched by subduction derived fluids and melts (Waters and Erlank, 1988; Hergt et al., 1991; Turner and Hawkesworth, 1995; Peate and Hawkesworth, 1996; Jahn et al., 1999; Hawkesworth et al., 2000). Geochemical characteristics of the Eocene volcanism are consistent with the derivation from an enriched lithospheric mantle source. The main evidence for the generation from the enriched lithospheric mantle comes from the high LILE, low HFSE abundances and relatively radiogenic Sr and Nd isotopic ratios. Several studies indicate that low content of the Nb and Ta would be the diagnostic feature of the lithospheric mantle itself. For example, Bradshaw and Smith, (1994) argued that HFSE, especially La, tends to have low concentration in the lithospheric mantle relative to REE. Hence high HFSE/LREE (Nb/La) ratios, generally >1 indicates asthenospheric mantle source while low ratios of these elements are indicative of lithospheric origin. In Figure 4.21 all Eocene rocks have low Nb/La ratios, which is in good agreement with the lithospheric derivation. In this plot, all Eocene rocks are represented by variable Zr/Y ratios, indicating different degrees of partial melting.

Geochemical characteristics similar to the studied Eocene volcanics are reported for the volcanic rocks from extensional environments. For example in Basin and Range Province (BR, USA; Hawkesworth et al., 1995) where the Tertiary post collisional volcanism does not have any genetic relation with an active subduction event. Crustal-like signature of the BR volcanic rocks (e.g. high Ba/Nb ratios) is widely attributed to source regions in the continental

mantle lithosphere (Hawkesworth et al., 1995, and references therein). Recently, numerous studies indicate that lithospheric mantle can also be the source of flood basalt province having low HFSE and high LREE abundances (Hergt et al., 1991; Lighthfoot et al., 1993; Hawkesworth et al., 2000; Wang et al., 2007). Harangi and Lenkey, 2007 also reported low Nb, Ti and High LREE contents for the rocks from the Pangolian Basin (Carpathian) which is also characterized by extensional regime.

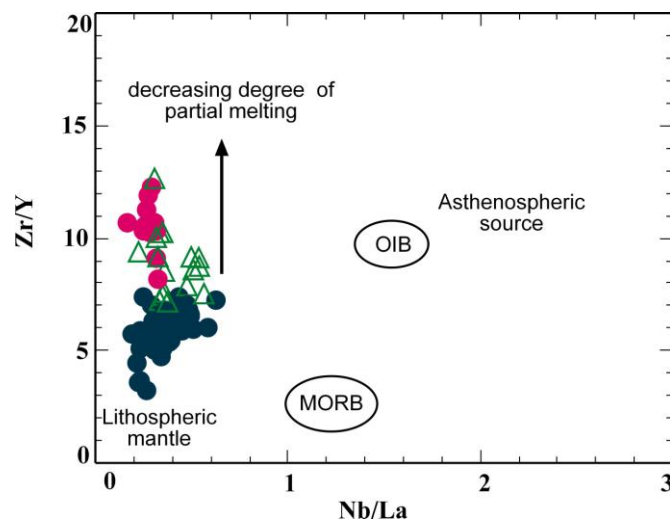


Figure 4. 21 Zr/Y vs Nb/La plot for Eocene volcanic rocks. All samples are characterized by relatively low Nb/La and variable Zr/Y ratios.

In the following section, Eocene volcanic rocks will be compared with the rocks having the lithospheric mantle as the dominant source region for better understanding of geochemical evolution of the studied rocks. Data set contains a number of flood basalt provinces and post collisional volcanic rocks from extensional environments. Flood basalts data comes from Ferrar low Ti Flood basalts, Australia (Hergt et al., 1991), Parana flood basalt province (Peate and Hawkesworth, 1996) and West Siberian flood basalts (Reichow et al., 2005). Post collision- extension related data includes Basin and Range Province, USA (Hawkesworth et al., 1995; Rogers et al., 1995), Apuseni volcanics, Romania

(Rosu et al., 2004). All these volcanic provinces are characterized by low Nb/Zr ratio.

Nb, Ti, Zr, Y and Yb are mainly assumed to be mantle derived (prior to the metasomatism, Pearce and Parkinson, 1993) and their concentration and ratios do not change with simple fractional crystallization or crustal contamination process (Davidson, 1996; Singer et al., 1996). Therefore diagrams involving these elements are likely to reflect the mantle compositions prior to the metasomatism and can give useful information about the mantle source region of the magmas. It is inferred from Figure 4.22 that Eocene volcanic rocks have the Nb and Zr abundances higher than those of the N MORB, implying derivation from an enriched mantle source relative to MORB. The studied rocks overlap with all rock groups, which suggest the same source characteristics.

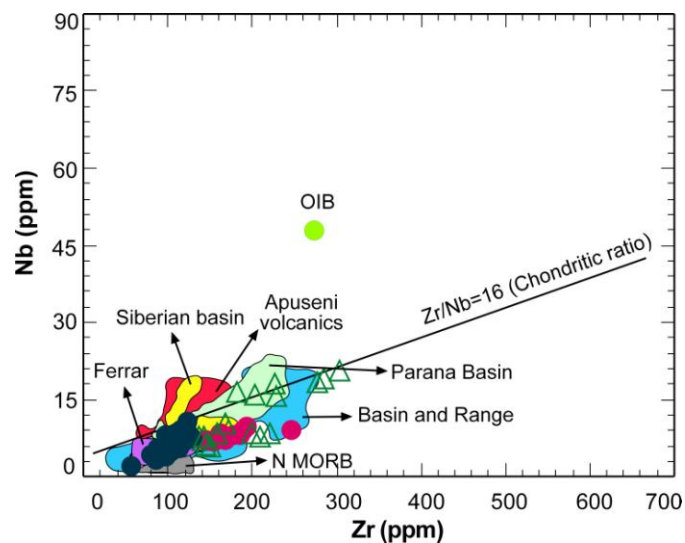


Figure 4. 22 Nb vs Zr plot for Eocene volcanic rocks in comparison with data for Normal Mid Ocean Ridge Basalts (N MORB), Ocean Island Basalts (OIB), West Siberian Basin (Reichow et al., 2005), Ferrar low Ti basalts (Hergt et al., 1991), Parana (Peate and Hawkesworth, 1996) Apuseni Mt (Rosu et al., 2004). (Symbols are the same as in Figure 4.4).

Primitive mantle normalized multi element diagram and incompatible trace element ratios point out that crustal or arc like signature of the Eocene rocks are entirely lithospheric in origin and unrelated to the subduction process. Consequently, the combined trace element and isotope geochemistry of the Eocene volcanic rocks leads to conclusion that they were derived from an enriched lithospheric mantle.

4.10 Trace Element Enrichment

An enriched mantle source relative to N- MORB is required to explain the trace element patterns of the studied rocks on the multi element and ratio- ratio diagrams. Enrichment process could be derived from any of the followings;

1. low degree partial melting,
2. metasomatic agents.

4.10.1 Low degree partial melting

In general, small degrees partial melting would cause enriched trace element patterns in the resultant rocks. However, considerably high contents of the trace elements and LREs of the Eocene magmas (Ba and Sr up to 1400 and 1299 ppm, respectively) can not be completely attributed to partial melting process. On the contrary, selective enrichment of the trace element abundances (i.e. LILE and LRE over the HFSE) requires the enrichment to have happened before the partial melting process. An extremely small degree of partial melting is required to produce such a high incompatible trace element contents by partial melting of mantle derived magmas (i.e. MORB or OIB). For instance, one of the Eocene samples has 1299 ppm Sr, to produce this value the degree of partial melting would be about 0.5% based on the batch melting equations of Shaw, (1970), assuming the source composition (C_0) as 19.9 (primitive mantle, McDonough and Sun, 1995) and bulk partition coefficients (D) given in the Table 4.1.

On the other hand, partial melting modeling shows relatively high melting degrees that change between 15- 20%. Therefore, low degree partial melting can not account for observed enriched values. In other words, mantle enrichment process seems to be related to metasomatizing agents that modified the trace element budget.

4.10.2 Mantle metasomatism

The metasomatizing agents which modify the chemical composition of the mantle source can be divided into three groups: (1) Carbonate or carbonatitic melts or fluids (Furman and Graham, 1999; Downes et al., 2001; Xu et al., 2003; Zeng et al., 2005; Ionov and Harmer, 2002 and Ionov, 2007); (2) silicate melts (Zangana et al., 1999; Downes et al., 2001; Ionov and Harmer 2002; Witt-Eickschen et al., 2003); (3) subduction derived components (Downes et al., 2001; Johnson et al., 1996). The effects of the carbonatite and silicate metasomatism on the trace element contents and/or isotope abundances could be different because aforementioned agents carry different type of elements, which result in different kind of trace element abundances in the mantle source region with different enrichment levels (i.e. Menzies et al., 1987).

The metasomatic signature that characterize the geochemistry of the Eocene volcanic rocks can be summarized as follows; (1) high LILE contents (e.g. Ba, Sr), (2) LREE enrichment with high La/Sm ratios (1.54- 6.17), (3) High LILE/LREE and high LILE/HFSE ratios (high Ba/La and Ba/Nb) (4) Relatively high Zr/Hf ratios and (5) Low HFSE content

4.10.2.1 Silicate and carbonate metasomatism

The metasomatizing magmas for silicate melts are believed to be derived from deeper asthenospheric mantle (Downes et al., 2001) whereas carbonatite melts are suggested to have two possible sources; recycled subducted slab and deep mantle derived melts (Su et al 2010). In general carbonate metasomatism is

characterized by enrichment in LREE, Ba, Sr and greater depletion in Rb, K, Zr and Ti (Su et al 2010) while the rocks metasomatized by silicate melts are represented by enrichment in LREE, Sr, Zr, Hf and often Nb in the bulk rocks (Downes et al., 2001). Therefore, if a mantle source is metasomatized by carbonate derived fluids or melts, the resulting magmas would have low Rb/Sr, Sm/Nd ratios and low HFSE contents (Dupuy et al., 1992; Rudnick et al., 1993). Although studied Eocene volcanics have low content of HFSE, their Rb/Sr and Sm/Nd are quite high (up to 0.4 and 0.3, respectively). However, to make this clear, another constraint can be used. For example, the Ti/Eu ratio together with the $(La/Yb)_N$ ratios can be useful indicators of the carbonatite metasomatism which is assumed to have Ti/Eu ratios less than 1500 and $(La/Yb)_N$ higher than 3-4 (Su et al., 2010). In Figure 4.23 $(La/Yb)_N$ is plotted vs. Ti/Eu ratios for Eocene rocks. Most of the data have Ti/Eu ratios between 2300-6700, which is well in excess of the values that characterize the carbonatite metasomatism. From the trace element geochemistry, silicate and carbonatite metasomatism appear to have insignificant role on the genesis of the Eocene volcanics.

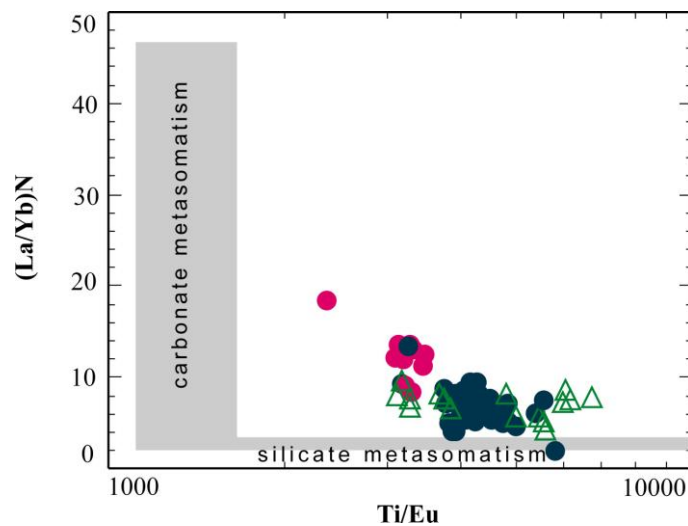


Figure 4. 23 $(La/Yb)_N$ vs Ti/Eu diagram (Su et al., 2010) for Eocene volcanics. The studied rocks are characterized by relatively high Ti/Eu and low $(La/Yb)_N$ ratios.(Symbols are the same as in Figure 4.4).

4.10.2.2 Subduction derived components

The complete geochemical and isotopic study of the Eocene volcanic rocks (high LILE and LREE, high Ba/Nb (34- 208) and Ba/La (17-46) demonstrate that mantle source of the Eocene magmas might have been variably modified by LILE and LREE rich metasomatic agents. The most likely candidate could be subduction related components; subducted sediments, melts or hydrous fluids. The most probable way by which subduction related components may involve into the mantle source is the subduction of an oceanic lithosphere. In general, sediment subduction is considered as a kind of source contamination. However, fluids and melts derived from subducted slab tend to affect mantle source region at different scale on the basis of their physical properties. In the next section possible effects of the metasomatizing agents derived from subducted slab on the Eocene magmas will be discussed.

4.10.2.2.1 Melt related enrichment

Melts derived from subducted slab result in adakite-like trace element composition in the mantle source region (i.e. Fan et al., 2007). Although adakites are thought to be derived from partial melting of the subducted slab (Defant and Drummond, 1990; Kay et al., 1993; Martin et al., 2005), recent studies indicate that adakitic rocks can also be formed in extensional area by partial melting of the thickened lower crust (Wang et al., 2006 and references therein).

Geochemical characteristics of adakite can be summarized as follows; high Al_2O_3 content (> 15 wt %), high Sr (>400 ppm) content and Sr/Y ratios (>40), high La/Yb ratios, low Yb content (1.9 ppm $<$) and Y content (18 ppm $<$) and low $^{87}\text{Sr}/^{86}\text{Sr}$ ratios (<0.7040) (Defant and Drummond, 1990). Some of the geochemical properties of the studied Eocene rocks such as high Al_2O_3 (14.5- 18.48 wt %) and Sr (240- 1299 ppm) contents are in accord with the adakite geochemistry. However, high Y (14- 32.5 ppm with an average of 19.40), Yb

(1.35- 3.16 ppm with an average of 1.87) and Sr/Y ratios (14.03- 66.35) and relatively high $^{87}\text{Sr}/^{86}\text{Sr}$ ratios ranging between from 0.7040 to 0.7053 are not consistent with the standards mentioned above. Especially Y and Yb concentrations of the Eocene rocks are considerably higher than those of the adakites. Although a few samples from Çiçekdağ region plot in the adakite field on the Sr/Y vs. Y diagram (Figure 4.24), most of the samples fall into normal calc- alkaline field with high Y content. Besides, in the La/Yb vs. Yb diagram (Figure 4.24), most of the samples fall into normal calc- alkaline field with high Y content. As a result, trace element geochemistry argues against metasomatism induced by the melts derived from subducted slab.

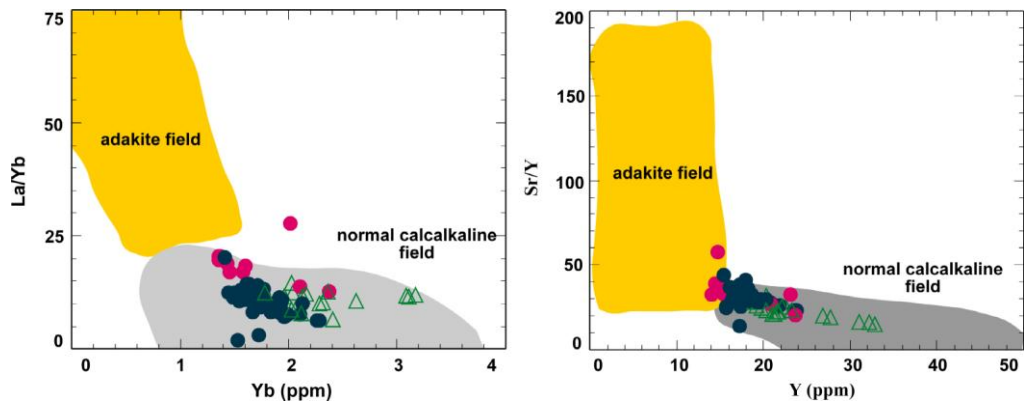


Figure 4. 24 La/Yb vs Yb and Sr/Y vs Y diagram for Eocene volcanic samples. The studied rocks are characterized by higher Yb content and lower La/Yb ratios than those of adakitic rocks. Adakite fields are taken from Defant and Drummond (1990).

4.10.2.2.2 Sediment addition

Although distinguishing crustal contamination from assimilation of recycled subducted sediment is not straightforward (Ewart et al., 2004), several chemical tracers can be used to clarify the sediment addition into the mantle source. Elliot et al., (1997) argued that addition of pelagic sediments to the mantle source has effects similar to aqueous fluids; however, it can result in

enrichment of Th relative to Nb. Moreover, elemental ratios such as Ce/Pb and Th/Yb can be used as indications of sediment contribution to magma source (Handley et al., 2007), since LREE and Th are known to be less mobile in aqueous fluids than the LILE and their abundances in the source region are thought to be derived from either by bulk addition of the sediments or by melt (Leat et al., 2000). Eocene volcanic rocks are characterized by high and variable Ce/Pb (3.45- 34.92) and Th/Yb (0.2- 18) ratios, which can be attributed to the sediment contribution to their mantle source. To show the possible sediment input to the mantle source a parameter, Nb/Nb*, is defined by Eisele et al., (2002). Based on the calculation, Eocene samples have relatively low but variable Nb/Nb* ratios (0.14-0.45), implying effect of the sediments on the source. Beside trace element geochemistry, isotope ratios also support the sediment contamination. Because of its fluid mobile nature, Sr is not commonly used to show subducted sediment effect on the mantle source region, on the other hand, Pb isotopes are thought to be the most sensitive one to sediment contamination (Davis et al., 1998). In the diagram of $^{207}\text{Pb}/^{204}\text{Pb}$ vs $^{206}\text{Pb}/^{204}\text{Pb}$ the rocks under investigation plot almost exclusively within the range of the GLOSS area (Plank and Langmuir, 1998, Figure 4.25), which suggests that source region of the Eocene magmas may have been modified by addition of the subducted sediment. In summary, several aspects of the trace elements and isotope ratios suggest that sediment contribution had played a role on the genesis of Eocene magmas.

4.10.2.2.3 Slab derived fluids

Slab derived hydrous components preferentially host fluid mobile elements such as Rb, K, Ba, Sr and U, but have low concentration of REE, HFSE and Th. As a result, a mantle enriched by slab derived metasomatizing agents is characterized by high content of U and Rb/Sr, moderately Sm/Nd ratios but depletion of HFSE (Hawkesworth et al., 1997; McDonald et al., 2000). Recent experimental determination suggests that the addition of significant amounts of

HFSEs via a fluid phase is generally considered unlikely because of their low solubility in hydrous fluids (Stolz et al., 1996).

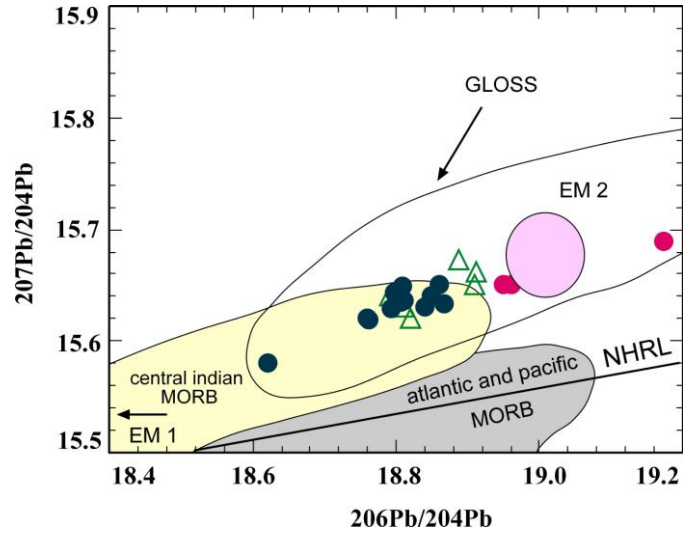


Figure 4.25 $^{207}\text{Pb}/^{204}\text{Pb}$ vs $^{206}\text{Pb}/^{204}\text{Pb}$ plot for Eocene volcanic samples. Field for Central Indian MORB is from Mahoney et al. (1989) and Hofmann (1997). Field for Atlantic and Pacific MORB is from White et al., (1987) and Hofmann, (1997). The field of GLOSS (global subducted sediment composition, which is based on large number of comprehensive dataset (Plank and Langmuir, 1998). The NHRL (Northern Hemisphere Reference Line; Hart, 1984), EM1 and EM2 (enriched mantle end-members; Zindler and Hart, 1986; Hofmann, 1997; Zou et al., 2000) are plotted for reference (Symbols are the same as in Figure 4.4).

Based on the above discussion, some geochemical characteristics of Eocene volcanics such as low Nb, high LILE consequently high LILE/HFSE and LILE/LRE can be taken as evidence for slab derived fluid metasomatism. This can be further supported by ratio-ratio graphs. For example, Ba/La vs Nb/Zr plot provide good opportunity to show hydrous fluids involvements. In this diagram majority of the Eocene rocks are aligned along the fluid related enrichment line with relatively high Ba/La ratios (Figure 4.26).

Given the high mobility of Sr in fluids generated during subduction processes (Pearce and Peate, 1995), Sr isotopic ratios can also be used as subduction component tracer. Therefore, differences in melt versus fluid-induced enrichments in the source region can be further emphasized by the $^{87}\text{Sr}/^{86}\text{Sr}$ vs Ba/TiO₂ and Ba/La graphs (Figure 4.27).

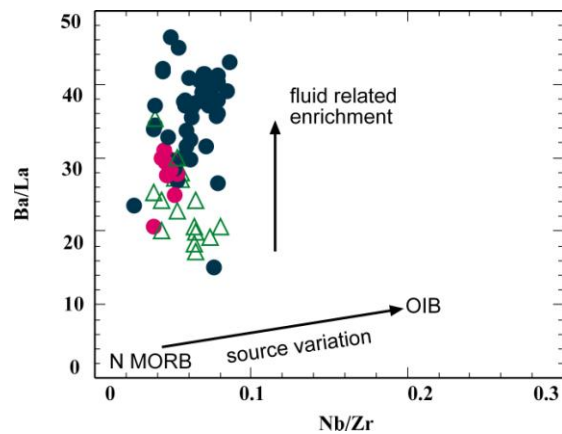


Figure 4. 26 Ba/La vs Nb/Zr plot for the studied Eocene rocks. High Ba/La ratios of the Eocene samples can be attributed to fluid related metasomatism. (N- MORB and OIB data are from Sun and McDonough, 1989).

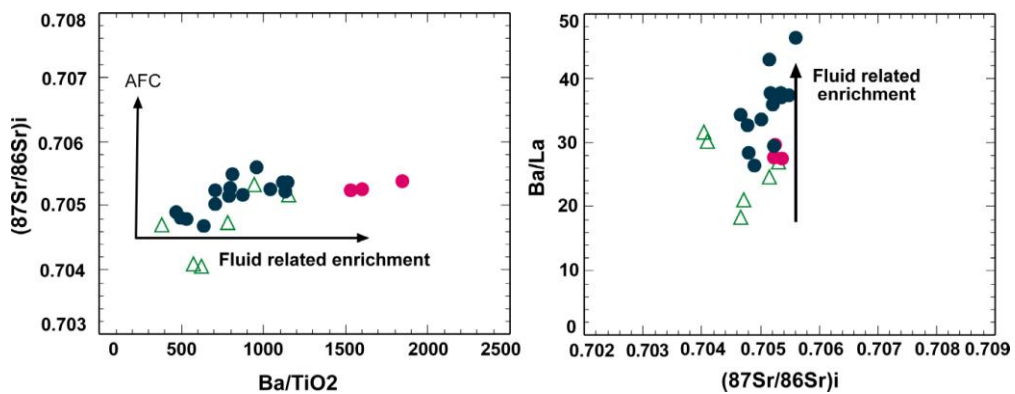


Figure 4. 27 $^{87}\text{Sr}/^{86}\text{Sr}$ vs Ba/TiO₂ and Ba/La plots for Eocene volcanic rocks (Symbols are the same as in Figure 4.4).

Eocene volcanic rocks are generally characterized by relatively radiogenic Sr isotopic ratios and in these diagrams they are shifted toward high Ba/TiO₂ and Ba/La ratios which are widely regarded as fluid mobile elements during subduction process (Gill, 1981; McCulloch and Gamble, 1991). In conclusion, mantle source enrichment of the Eocene magmas can be linked with the cryptic metasomatism mainly governed by subduction related aqueous fluids and sediments, which modified concentration of fluid mobile elements (LILE and LREE) in the mantle source region without changing the HFSE contents of the source.

4.10.3 Timing of metasomatism

Having confirmed the dominant metasomatic agent modifying the mantle source region, the next issue that needs to be solved is timing of the metasomatism. Recently, Sm- Nd isotope ratios has been widely used to decide when the enrichment process happened (Hollanda et al., 2003, and references therein). Hollanda et al., (2003) argued that high ¹⁴³Nd/¹⁴⁴Nd ratios and low Sm/Nd ratios indicate a recent metasomatism (metasomatism took place just before crystallization) on the other hand, if both ratios are low, metasomatism must be old so that low ¹⁴³Nd/¹⁴⁴Nd ratios may develop with time.

Although the age and nature of the metasomatism process that modified the lithospheric mantle have been poorly constrained, the metasomatic enrichment beneath the CACC is unlikely to be ancient because the ⁸⁶Sr/⁸⁷Sr ratios are not as high as what would be expected in an old metasomatic event. Although there is a weak correlation between Sm/Nd and ¹⁴³Nd/¹⁴⁴Nd (Figure 4.28), ⁸⁷Sr/⁸⁶Sr ratios of the Eocene samples do not correlate with Rb/Sr ratios, suggesting that time integrated growth of radiogenic ⁸⁷Sr is little; consequently, metasomatism in the source region must have taken place before the eruption of the Eocene lavas. Subduction related enrichment during the closure of the IAEO (65-72 Ma) seems to be most likely mechanism responsible for the mantle enrichment process.

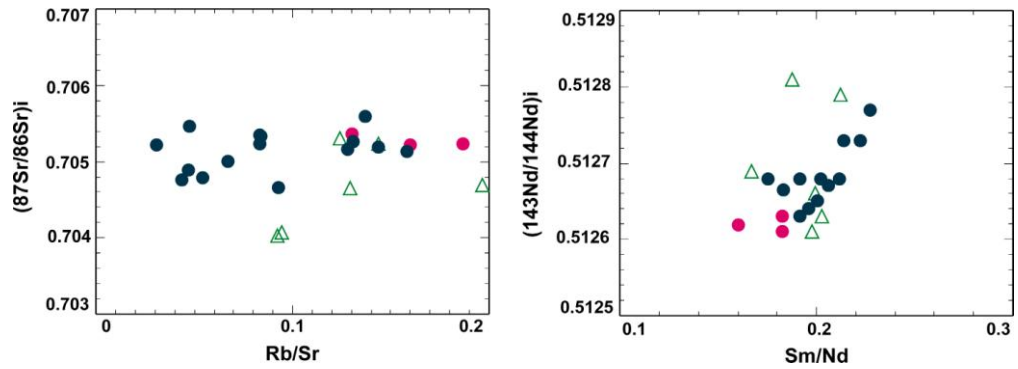


Figure 4.28 $^{87}\text{Sr}/^{86}\text{Sr}$ vs Rb/Sr and $^{143}\text{Nd}/^{144}\text{Nd}$ vs Sm/Nd plots for the studied rocks. $^{143}\text{Nd}/^{144}\text{Nd}$ ratios increase with increasing Sm/Nd ratios; however, there is not such trend in the Sr isotope.

4.11 Review on Geochemistry of Late Cretaceous Magmatism

Late Cretaceous granitic magmatism with distinct geochemical characteristics is widespread in the central Anatolia and regarded as the basement of the CACC. Apart from being the contaminant for the Eocene volcanic rocks, this magmatism is considered to be a significant key to clarify the geodynamic evolution of the region. Therefore, in order to make reliable interpretations in regional scale Eocene volcanism and Late Cretaceous granitic magmatism, which are somehow connected with each other, must be considered as a whole. For that reason, this section will provide a brief summary of late Cretaceous magmatism in terms of its geochemical characteristics. The detailed geochemical and isotopic characteristics of the Central Anatolian granites have already been reported in previous studies (e.g. İlbeyli et al., 2004; Boztuğ et al., 2000; Köksal and Göncüoğlu, 2008) thus here only a brief summary of their geochemical characteristics will be given to begin with and then main effort will focus on comparison of them with Eocene rocks. Representative whole rock geochemical and isotope data of granitic rocks performed during this study are given in appendix.

The Late Cretaceous granitic rocks are characterized by high silica concentrations. Analyzed samples have silica content ranging between 52.87-76.33 (wt %). They are, similar to Eocene volcanism, mostly subalkaline, despite a few samples plotted within the alkaline field (Figure 4.29). Their total alkali ($\text{Na}_2\text{O}+\text{K}_2\text{O}$) contents are higher than those observed in Eocene samples. The peraluminosity index ($\text{Al}_2\text{O}_3/\text{K}_2\text{O}+\text{Na}_2\text{O}+\text{CaO}$) of the analyzed samples ranges between 0.6 to 1.1, indicating their metaluminous to weakly peraluminous compositions (Figure 4.30). All samples generally have similar REE patterns (Figure 4.31) represented by enriched LREE.

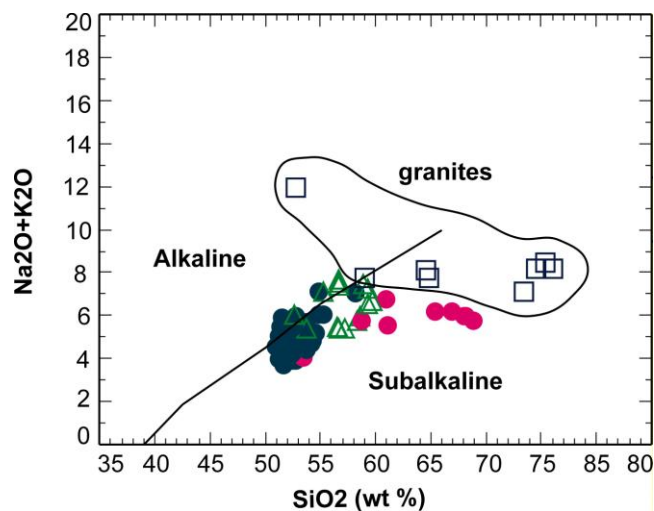


Figure 4. 29 Total alkalis vs silica diagram for Late Cretaceous granitic rocks. Eocene volcanic rocks are plotted for comparison (Dividing line from Irvine and Baragar, (1971) and symbols are the same as in Figure 4.4).

However, some of them display strong Eu anomaly. Besides, the samples having Eu anomaly also show depletion in the Sr on the multi element patterns (Figure 4.32), which suggests plagioclase fractionation during their evolution. The lack of the significant Eu anomaly in the Eocene volcanics makes these rocks different from the granites. All analyzed samples are enriched in LILE (Cs, Rb, and Th) except for Ba which shows negative anomaly for all samples. Depletion in HFSE is straightforward but degree of anomaly is variable.

Compared to Eocene rocks, the granites show higher Rb, Th, U and Pb contents. Besides REE and multi element plots, ratio-ratio diagrams are also employed to compare the Eocene rocks and granites.

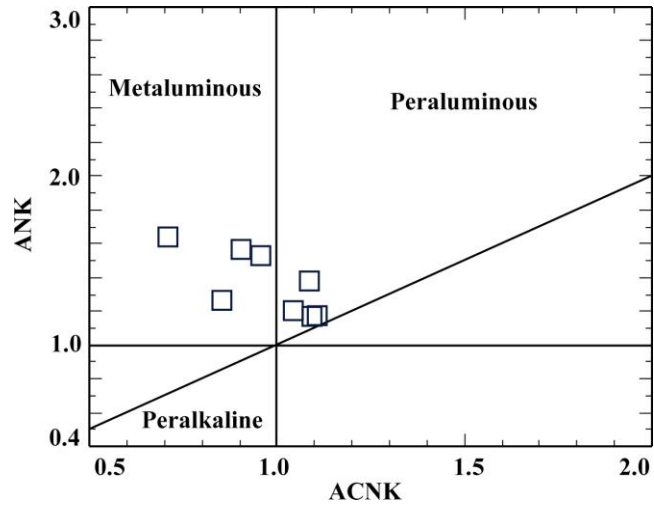


Figure 4. 30 Shand index for the analyzed Central Anatolian granites.

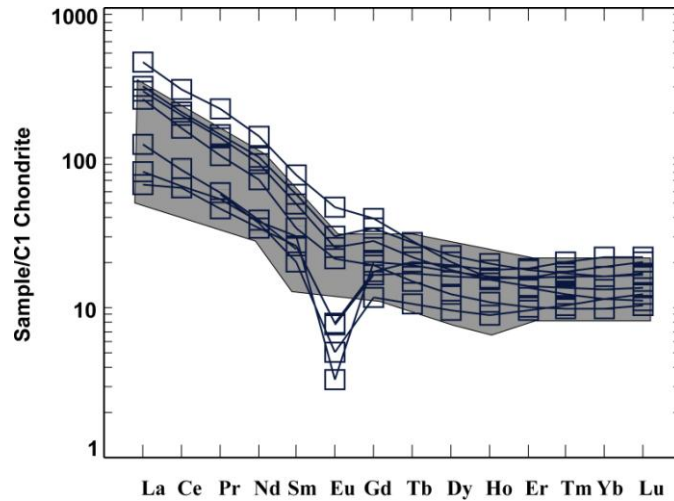


Figure 4. 31 C1 Chondrite (Sun and McDonough, 1995) normalized REE plot for the Late Cretaceous granites. Shaded area represents Eocene volcanic rocks.

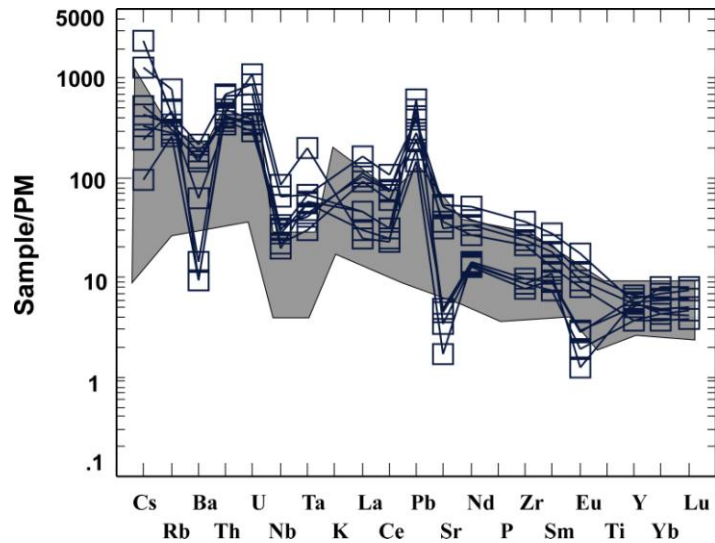


Figure 4.32 Primitive mantle normalized (Sun and McDonough, 1995) multi element patterns for Late Cretaceous granitic rocks.

The Th/Yb vs Ta/Yb plot of the Pearce, (1983) can be safely used to show source variations and assimilation effects. In this ratio-ratio diagram, Eocene volcanic samples are aligned along mantle metasomatism trend (Figure 4.33). Another aspect need to be emphasized here is that although Eocene samples have relatively narrow range of Th/Yb ratios, their Ta/Yb ratios are variable, which, as seen in Figure 4.33, can be in favor of either mantle metasomatism or AFC process. Granitic rocks, on the other hand, have wider range of Th/Yb ratios. Their Ta/Yb ratios are higher than those of the volcanic rocks. None of the samples including granites plot within the mantle array. Sr-Nd isotopic compositions of the Late Cretaceous granites and the Eocene rocks can be correlated with related to the geodynamic evolution of the CACC. The plot of $^{143}\text{Nd}/^{144}\text{Nd}$ vs $^{87}\text{Sr}/^{86}\text{Sr}$ provides a comprehensive picture of the isotopic variations between granitic magmatism and Eocene volcanism. Late Cretaceous granitic magmatism are characterized by low ϵNd values (Köksal and Gönçüoğlu, 2008), indicating derivation from an enriched mantle source while Eocene volcanic rocks have relatively high ϵNd values between 0.53-4.33, which point out an isotopically depleted mantle (Figure 4.34).

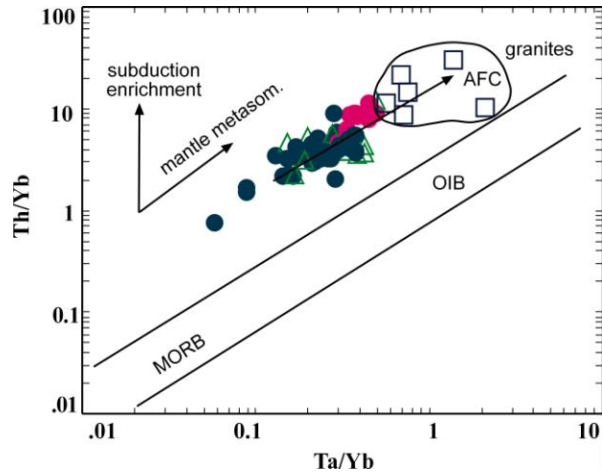


Figure 4. 33 Th/Yb vs Ta/Yb (Pearce, 1983) diagram for the Late Cretaceous granites and the Eocene volcanic rocks.

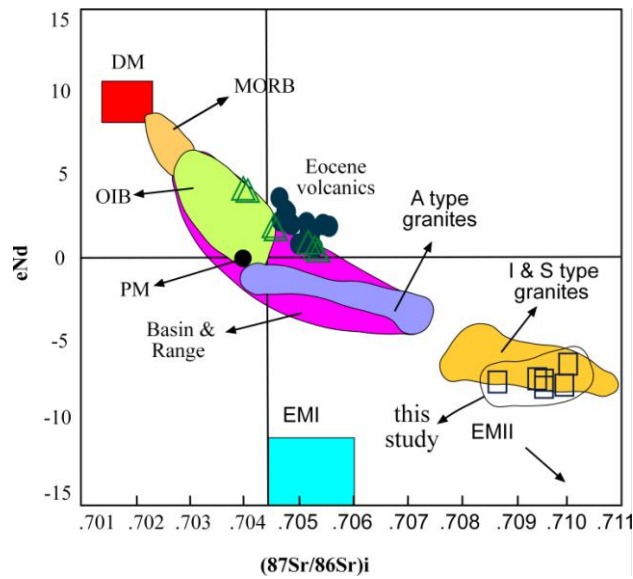


Figure 4. 34 ϵ_{Nd} vs $^{87}Sr/^{86}Sr$ plot for Eocene volcanic rocks and Late Cretaceous granitic rocks. Data source for granites are taken from İlbeyli et al., (2004), Boztuğ et al., (2007), Köksal and Göncüoğlu, (2008) and this study.

S and I types granites, whose origin is attributed to crustal sources, are plotted away from the mantle array while A type granites, source of which is mainly assumed to be mantle derived rather than crustal sources, fall into the mantle

array field. The clear difference between isotopic compositions of the Late Cretaceous granites and Eocene volcanic rocks suggest an evolutionary trend from crustal sources to the mantle during Eocene time.

CHAPTER 5

GEODYNAMIC IMPLICATIONS

5.1 Orogenic vs Anorogenic volcanism

Alpine- Himalayan orogenic belt is considered to be one of the most complex orogenic systems in the world and locus of the extensive post collisional magmatism during the Mesozoic and Cenozoic times (i.e. Wilson and Downes, 1991; Duggen et al., 2005; Lustrino and Wilson, 2007; Harangi and Lenkey, 2007). Lustrino and Wilson, (2007) argued that the volcanic rocks with distinctive geochemical signature from calc- alkaline to alkaline that occurred in many parts of the Mediterranean region including Algeria, Spain, Carpathian-Pannonian region, Bulgaria, and Turkey during Mesozoic-Quaternary time can be divided into two groups: orogenic (calc-alkaline through potassic and ultrapotassic) and anorogenic (alkaline-sodic). Anorogenic magmatism generally observed at periphery of the Mediterranean region whereas orogenic magmatism dominates the middle part of the Mediterranean region (Harangi and Lenkey, 2007). There are some age constraints between two types of magmatism. For instance, orogenic magmatism is regarded to be older than Pliocene while anorogenic magmatism extends from Pliocene to Recent although both types display some local exceptions (Lustrino and Wilson, 2007; Lustrino et al., 2007). Calc-alkaline affinity for subalkaline magmas and potassic-ultrapotassic character for alkaline magmas are distinctive for the orogenic stage.

Geochemically, orogenic magmatism differs from anorogenic one in that it is characterized by arc like geochemical signature (e.g. high LILE, low HFSE

contents and high LILE/HFSE ratios) and has distinctive isotope composition (Sr isotope ratios are higher than (>0.70445) Bulk Silicate Earth (BSE); Nd isotope ratios are lower than (< 0.51264) Chondritic uniform reservoir (CHUR); Pb isotope composition is mildly radiogenic and relatively high ($^{206}\text{Pb}/^{204}\text{Pb} = 18.6- 19.3$; $^{207}\text{Pb}/^{204}\text{Pb} = 15.65- 15.72$) (Wilson and Lustrino, 2007; Lustrino et al., 2007). Therefore, orogenic signature of the volcanism or mantle source region of the orogenic magmatism is thought to require a subduction component mostly inherited from previous subduction events (Lustrino et al 2007 and references therein).

A transition between both types is also observed in some part of the Mediterranean region (Turner et al., 1999; Coulon et al., 2002; Duggen et al., 2005). This transition from orogenic to anorogenic is generally attributed to contrasting tectonic process such as convective removal of lithospheric mantle (Turner et al., 1999), slab break off (Coulon et al., 2002) and, delamination of the lithosphere (Duggen et al., 2005). Duggen et al., (2005) argued that the geochemical transition from calc- alkaline to intra plate type geochemical trend is derived from major change in mantle geometry beneath the Mediterranean region whereas Harangi et al., (2007) suggest that such transition in West Carpathian Volcanic Field does not necessarily require a change in tectonic regime from compression to extension. They argued that both orogenic and anorogenic type of magmatism can be attributed to lithospheric extension and calc-alkaline magmas were formed by melting of metasomatized lithospheric mantle, and then were contaminated by lower crustal melts. On the other hand, mafic alkaline magmas were generated by low-degree melting of the shallow asthenospheric mantle during the post-extensional stage.

In general, Eocene volcanism in CACC is represented by calc-alkaline to mildly alkaline rocks and they range from basalt to andesite. They are mostly quartz-hyperstene normative i.e. calc- alkaline. However a few samples have normative olivine-nepheline and olivine- hyperstene, indicating mildly alkaline and transitional nature, respectively. The studied rocks exhibit apparent

subduction signature represented by negative Nb-Ta anomaly on the multi element diagram (Figure 4.18). The extent of the anomalies varies slight to moderate (e.g. Nb/Nb* = 0.12- 0.43). Their isotopic compositions are 0.70404- 0.70559 for $^{87}\text{Sr}/^{86}\text{Sr}$; 0.51261- 0.51281 for $^{143}\text{Nd}/^{144}\text{Nd}$; 18.01-19.01 for $^{206}\text{Pb}/^{204}\text{Pb}$; 15.57- 15.67 for $^{207}\text{Pb}/^{204}\text{Pb}$. Based on the geochemical data mentioned above Eocene volcanic rocks can be considered as transitional between orogenic and anorogenic types in the context of Wilson and Lustrino, (2007).

5.2 The Mechanism That Triggered Eocene Volcanism

The mechanism that triggers magmatism in post orogenic areas is debatable and generally thought to be derived from decompression melting of the lithospheric mantle enriched by previous geodynamic event (Hawkesworth et al., 1995; Fan et al., 2004). McKenzie and Bickle, (1988) argued that dry asthenosphere can melt only when the lithosphere is adequately thinned (less than 70km), which requires a number of mechanisms that are able to lower the thickness of the lithosphere and also overlying lower crust. Several processes have been suggested to explain the reason for lithospheric thinning and consequently genesis of magmatism in orogenic or post collisional settings. These include slab break off (Davies and von Blanckenburg, 1995), convective thinning or removal (Houseman et al., 1981; England and Houseman, 1987; Turner et al., 1992; Platt and England, 1993), and lithospheric delamination (Bird, 1979; Sacks and Secor, 1990). All these mechanisms are based on the idea that lithosphere tends to readjust its thermal and mechanical condition after crustal thickening caused by previous event, subduction or collision. Readjustment comprises asthenospheric upwelling, which induces melting of overlying lithospheric mantle. In general, volatiles decrease the solidus temperature of the mantle and consequently lithospheric mantle previously enriched by volatiles tends to melt when asthenosphere reach its base (Turner et al., 1992, 1996; Platt and England, 1994).

Slab break off or slab detachment model was firstly suggested to explain the genesis of the post collisional magmatism in the Alpine- Himalayan orogenic belts by Davies and von Blanckenburg, (1995). It predicts a limited and narrow range of magmatism and melting occurs when upwelling of the hot asthenosphere reach to the base of the metasomatized, hydrous lithosphere (Davies and von Blanckenburg, 1995). Low degree partial melting of the enriched lithosphere results in alkaline to ultrapotassic magmas, whereas higher degrees of melting produce calc- alkaline melts (Davies and von Blanckenburg, 1995). Decompression melting of the dry asthenosphere is expected at depth shallower than 50 km (Davies and von Blanckenburg, 1995).

Convective thinning or removal is described as removal of the dense and unstable lithospheric root beneath the orogenic area (Houseman et al., 1981; England and Houseman, 1987; Turner et al., 1992; Platt and England, 1993). Removal of the whole lithospheric mantle allows rapid upwelling of the hot asthenosphere, which may result in fast uplift in the orogenic area (Turner et al., 1999). Turner et al., (1999) argued that if the extension rate and consequently lithospheric thinning amount are high enough to bring the asthenosphere to the 50 km of the surface, decompression melting of the dry asthenosphere could happen, which lead to higher degree of crustal contamination since hot asthenosphere starts melting of the crustal rocks firstly.

Another mechanism that brings hot asthenosphere into contact with MOHO is lithospheric delamination which has become one of the most popular models for rapid regional uplift and widespread magmatism in the post orogenic areas (Bird, 1979; Sacks and Secor, 1990; Kay and Kay, 1993). According to Kay and Kay, (1993) large scale magmatism can be used as the most diagnostic feature of the delamination process since there is no direct evidence for delamination model. Large scale magmatism seems to be compatible with CACC the case. Delamination model involves, similar to other mechanism,

heating of the lower crust and lithospheric mantle due to the rapid upwelling of hot asthenospheric mantle to the shallow depths (Kay and Kay, 1993).

All above mentioned processes that induce the melting of the hydrated and metasomatized lithospheric mantle involves several geological indications. For instance, they cause important amount of uplift of the region before extension, conductive heating of the lithosphere, and consequently magmatism induced by decompressional melting (Turner et al., 1999 and references therein); therefore their distinction in terms of extension, magmatism and geochemistry may not be straightforward. However, according to Houseman and Molnar, (1997) there are a few criteria that can be used to distinguish the convective thinning process from delamination. First of all, convective thinning is expected to form symmetrically so migrating delamination front is not observed. In addition to this, it is based on the assumption that only lower part of the mantle is removed so that direct contact between asthenosphere and crust is prevented.

As a first approach, all aforementioned mechanisms seem to be consistent with the geochemical signature of post collisional Eocene volcanism; on the other hand, some of them can be ruled out on the geological ground. The source region of the Eocene magmas is likely in subcontinental mantle enriched in LILE and LREE during a previous geodynamic event based on the combined trace elements and isotopic studies. Besides, thermal and geochemical studies also indicate that melt generation by means of the continental extension is little, unless β value, the amount of extension, is higher than 2 (Mc Kenzie and Bickle, 1988). Widespread but volumetrically small distribution of the Eocene volcanic rocks mainly within the E-W trending sedimentary basins supports derivation in relation with extension. Therefore, asthenospheric mantle (i.e. OIB like mantle source) or mantle diapirism (active asthenospheric upwelling or deep mantle plume) can not account for the observed elemental and isotopic variations of the studied rocks.

In the context of the geodynamic evolution of the CACC region Late Cretaceous granitic magmatism and Eocene volcanism that show compositional variations with time should be considered as a whole as discussed in the section 4.11. For that reason, any theory concerning genesis of the regional magmatic activity including Eocene volcanism and geodynamic evolution of the CACC is supposed to explain some geological and geochemical observations such as the formation of contemporaneous calc-alkaline and mildly alkaline spectrum, geochemical signature with a distinctive subduction fingerprint despite the geodynamic setting, large scale granitic magmatism and volumetrically small but widespread distribution of the volcanism. As mentioned before, several popular hypotheses have been proposed to explain regional magmatic activity in the CACC. The first involves a subduction mechanism in which the Late Cretaceous granitic intrusions and Late Eocene volcanism have been considered to have formed as arc products after closure of Inner Tauride Ocean thought to have existed between CACC and Tauride- Platform (Figure 5.1; Görür et al 1984; Erdoğan et al., 1996; Kadioğlu et al., 2003; Kadioğlu and Dilek, 2009). The available age and geochemical data for the magmatism are not consistent with this argument. The geochemical characteristics indicating a subduction fingerprint on the genesis of Late Cretaceous magmatism and Eocene volcanism do not necessarily indicate that these rocks are part of an active subduction process or derived from melting of a subducted slab; however, it should be considered that melting of the lithospheric mantle enriched in selective trace elements can cause “arc like geochemical signature” in post collision extension related environment (e.g. Hawkesworth et al., 1995; Coulon et al., 2002; Fan et al., 2003).

More recently, slab break off mechanism has been suggested to locally explain the formation of Eocene volcanic rocks exposed to the north of CACC by Keskin et al., (2008; Figure 5.2). Some of the geochemical properties of the Eocene volcanic rocks in that area might be attributed to slab break off model which requires melting of the metasomatized and hydrated layers of the

lithospheric mantle (Davies and von Blanckenburg, 1995). In this scenario, the volcanic rocks are supposed to have formed within the accretionary prism of the İzmir- Ankara- Erzincan Ocean.

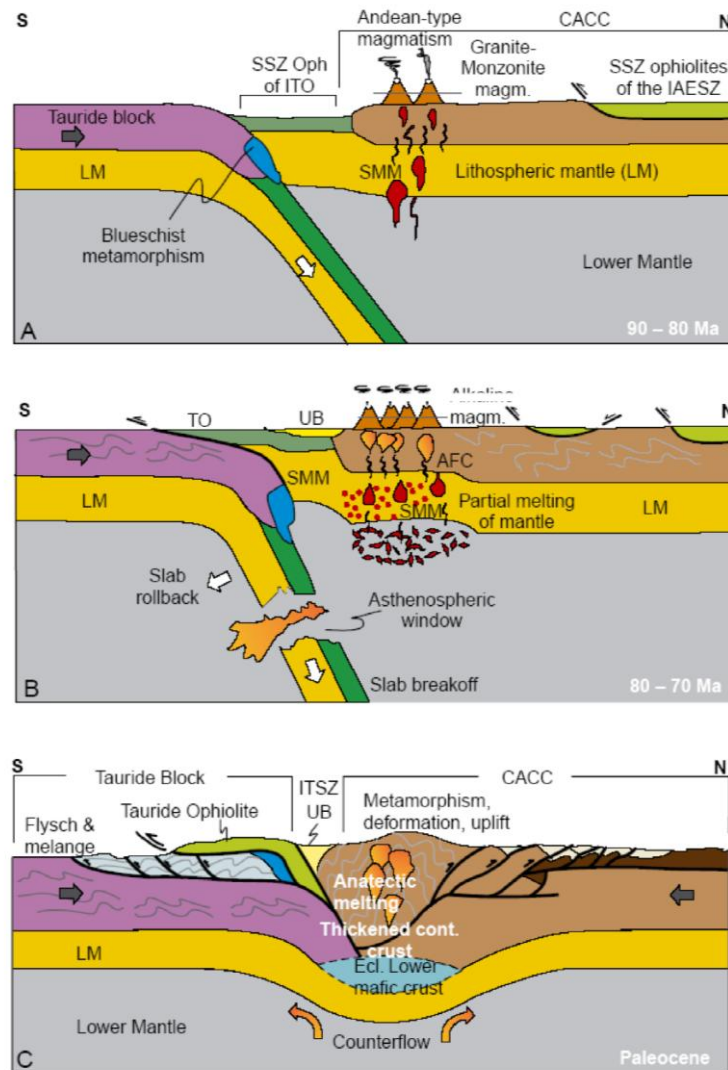


Figure 5. 1 (A to E) Schematic tectonic diagram displaying evolution of the Tauride platform (from Kadioğlu and Dilek, 2009). AFC; assimilation and fractional crystallization; AHO; Alihoca ophiolite; CACC; Central Anatolian Crystalline Complex, EF; Ecemiş Fault, HG; Horoz Granitoid, ITO; Inner Tauride Ophiolite, ITSZ; Inner Tauride Suture Zone, Kızıtepe Blue Schist, MO; Mersin Ophiolite, SMM; Subduction Metasomatized Mantle, SSZ; Supra-subduction Zone, TO; Tauride Ophiolite, UB; Ulukışla Basin, UG; Üçkapılı Granite.

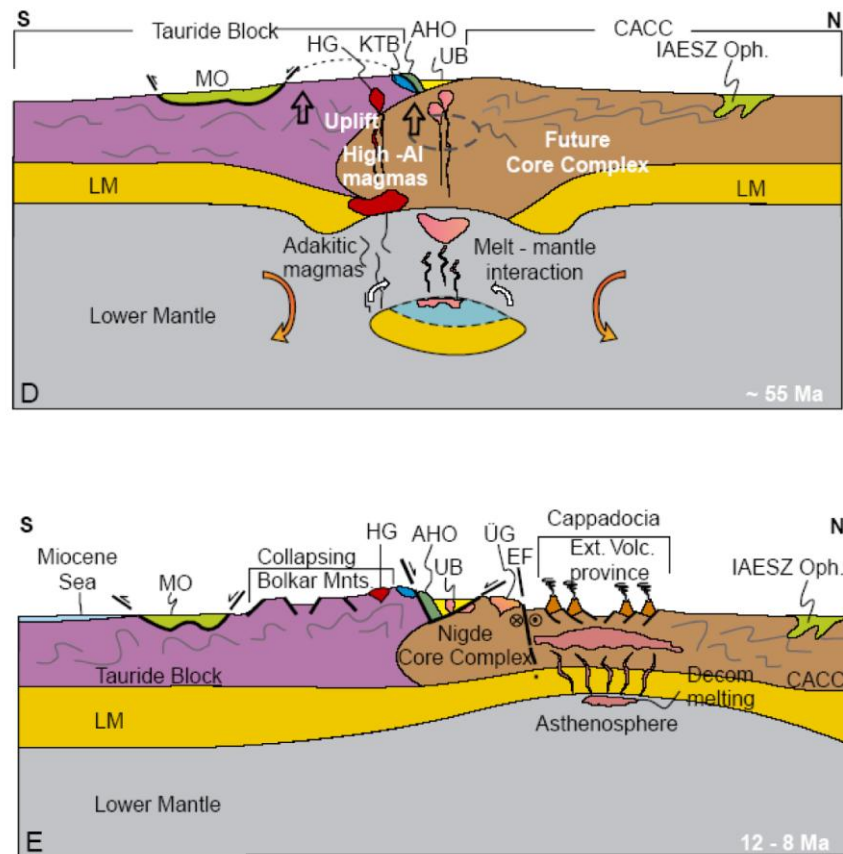


Figure 5.1 Continued.

However, proposed slab break off model is unable to explain a number of geological and geochemical observations about the volcanism in CACC. First of all, detachment process predicts a narrow linear zone of magmatism with limited extent. However, it should be noted that Eocene volcanism is not restricted to that area; it crops out throughout the CACC and in basins surrounding it. Hence, the formation of the Eocene volcanic rocks with homogenous geochemical signature exposed within the CACC can not be explained by detachment model.

Moreover, studied Eocene volcanic rocks have limited range of isotopic compositions, which are not compatible with break off model that is characterized by the wide range of isotopic composition, indicating melting of

the different enriched layers of the mantle (Davies and von Blanckenburg, 1995). On the other hand, quite narrow range of isotopic composition of the studied rocks can be ascribed to their source region. In these respects, break off model seems inappropriate to explain genesis of the widespread Eocene volcanism within the CACC.

The change in composition of magmatism (from calc-alkaline to alkaline) in the CACC is still not well understood. The progressive evolution from calc-alkaline to alkaline nature is largely variable in space and time and thought to be consequences of the extensional tectonic regime caused by closure of the IAEO. However, studies on genesis of the post collisional magmatism and geodynamic evolution of the CACC should be reconsidered in the light of many new geochronological and geochemical data, because subduction and detachment models can not satisfactorily explain the overall characteristics of the magmatism and volcanism in the region. Therefore, a two stage lithospheric delamination model (Figure 5.3) is favored to explain magmatism and volcanism in the CACC based on the wide spatial distribution and distinctive geochemical properties. The first stage delamination in the region resulted in large scale crustal melting and consequently led to calc-alkaline to alkaline granitic magmatism as proposed in previous studies (Aydin et al., 1998 and Düzgören- Aydın et al., 2001; İlbeyli et al., 2004; Köksal and Göncüoğlu, 2008). During Late Cretaceous time CACC crust was strongly thickened due to the final closure of the IAEO and ophiolite obduction caused by collision between CACC and Sakarya continent. Thickened crust of the CACC experienced HT/LP metamorphism (Göncüoğlu et al., 1994; Fayon et al., 2001), resulting in an increase in the lower crustal density, which promotes delamination process (Rudnick and Fountain, 1995). First stage syn- collisional S type granitic magmatism within the CACC, which are thought to be derived from partial melting of the upper crustal sedimentary protolith (Aydin et al., 1998), also caused some changes in the crustal structure of the region.

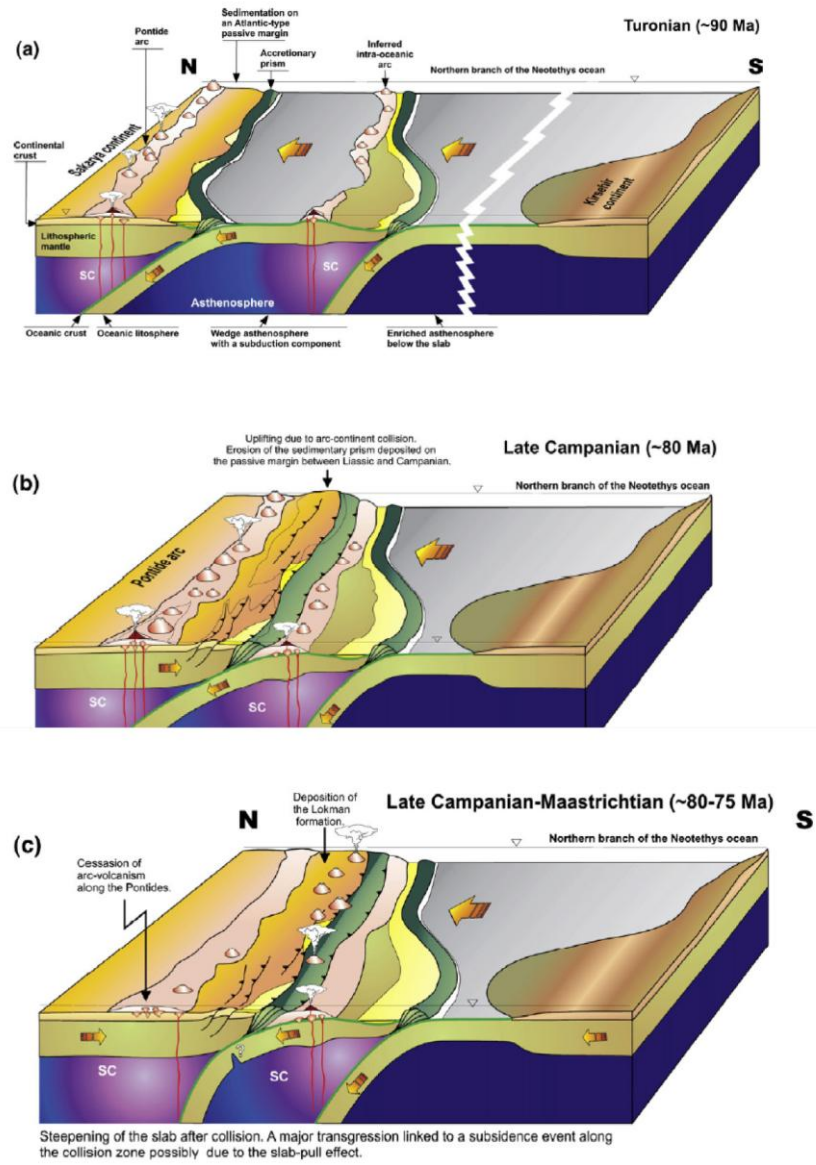


Figure 5. 2 (A to H) Block diagram showing geodynamic evolution of the northern part of the CACC during the period of Late Cretaceous- Early Miocene (from Keskin et al., 2008).

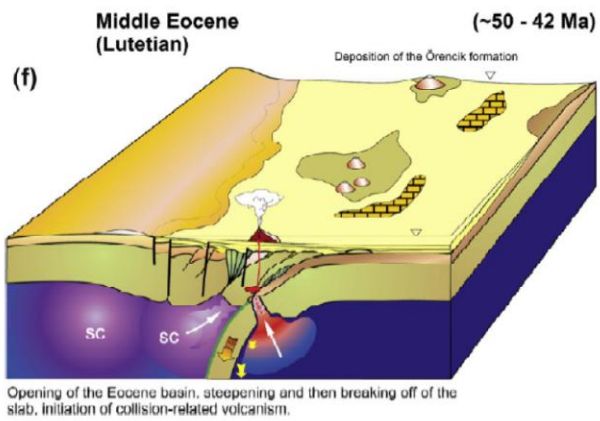
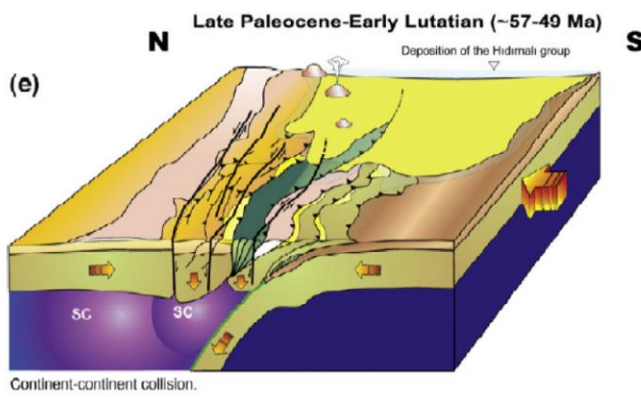
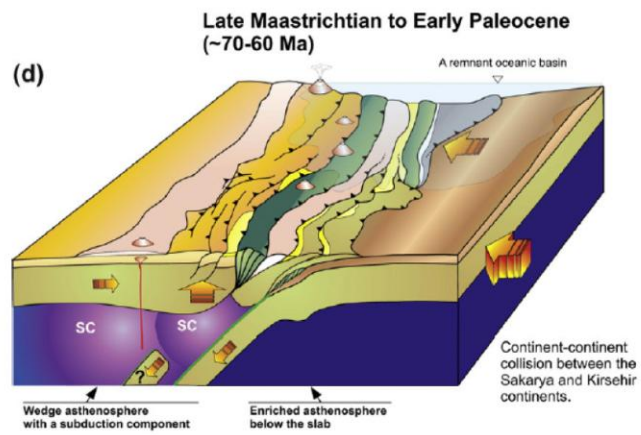


Figure 5.2 Continued.

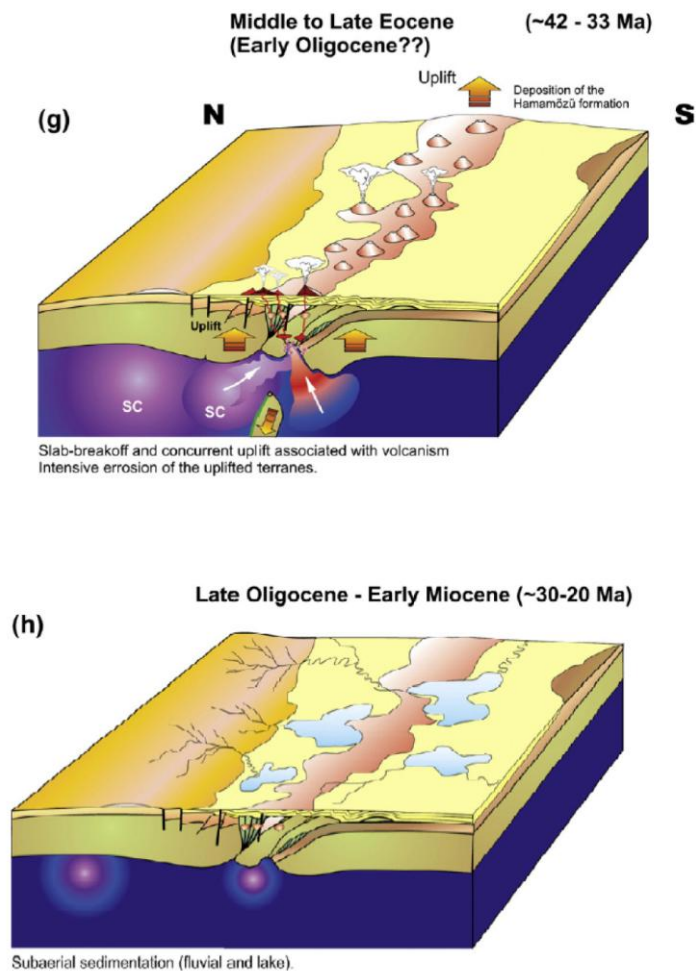


Figure 5.2 Continued.

Metamorphism of the basement rocks and granitic intrusions resulted in increased lower crustal density which also led to rheological and compositional differences between the lower and upper part of the crust and as a result, lithospheric delamination occurred. Exhumation of the metamorphic basement of the crystalline complex before the Maastrichtian time (Göncüoğlu et al., 1991, Floyd et al., 2000) suggests that delamination process most probably happened during Campanian- Maastrichtian time. Due to this delaminated part of the lithospheric mantle beneath the CACC, asthenospheric upwelling took place, which induces melting of overriding lithospheric mantle. This period also corresponds to a change in tectonic regime from compression to extension

marked with the large scale granitic magmatism with the different compositions in the CACC. Second delamination event took place after granitic magmatism terminated and gave way to formation of the Eocene magmas. Asthenospheric upwelling has provided required heating and melting conditions in the shallow mantle for both cases.

Figure 5.3 summarizes the geodynamic evolution of the CACC during Late Cretaceous- Eocene period. During the early Late Cretaceous time, İzmir-Ankara- Erzincan Ocean (IAEO) started to close with multiphase subduction (Göncüoğlu et al., 1994). During these subduction events subduction components, mostly aqueous fluids, derived from the subducted slab may be stored as small masses within the lithospheric mantle. These discontinuous masses were transported into the mantle by means of the mantle flow. Northward movement of the CACC due to its thick crustal structure also promoted this motion. As a result, subduction components enriched in LILE and LREE modified the lithospheric mantle beneath the region. In the meantime, ophiolitic units derived from this subduction event were emplaced onto Tauride- Anatolide platform represented by CACC (Figure 5.3). Final closure of the IAEO during Paleocene was represented by arc magmatism in the Sakarya continent. Crustal thickness of the CACC increased due to the ophiolite obduction, which led to the thermal instability. This in turn, resulted in lithospheric delamination during Eocene time. Delaminated lithospheric mantle sunk into the asthenosphere and the opening gap, occupied earlier by lithosphere, filled with asthenospheric mantle. This induced partial melting of the previously enriched lithospheric mantle. Melting of the lithospheric mantle gave rise to formation of the Eocene volcanism. Delamination of the lithospheric mantle can also account for isotopic variations between Late Cretaceous magmatism and Eocene volcanism.

As shown in the geochemistry section, Eocene volcanic rocks have isotope compositions plotted on the bulk silicate earth area within the Sr-Nd isotope space (Figure 4.34).

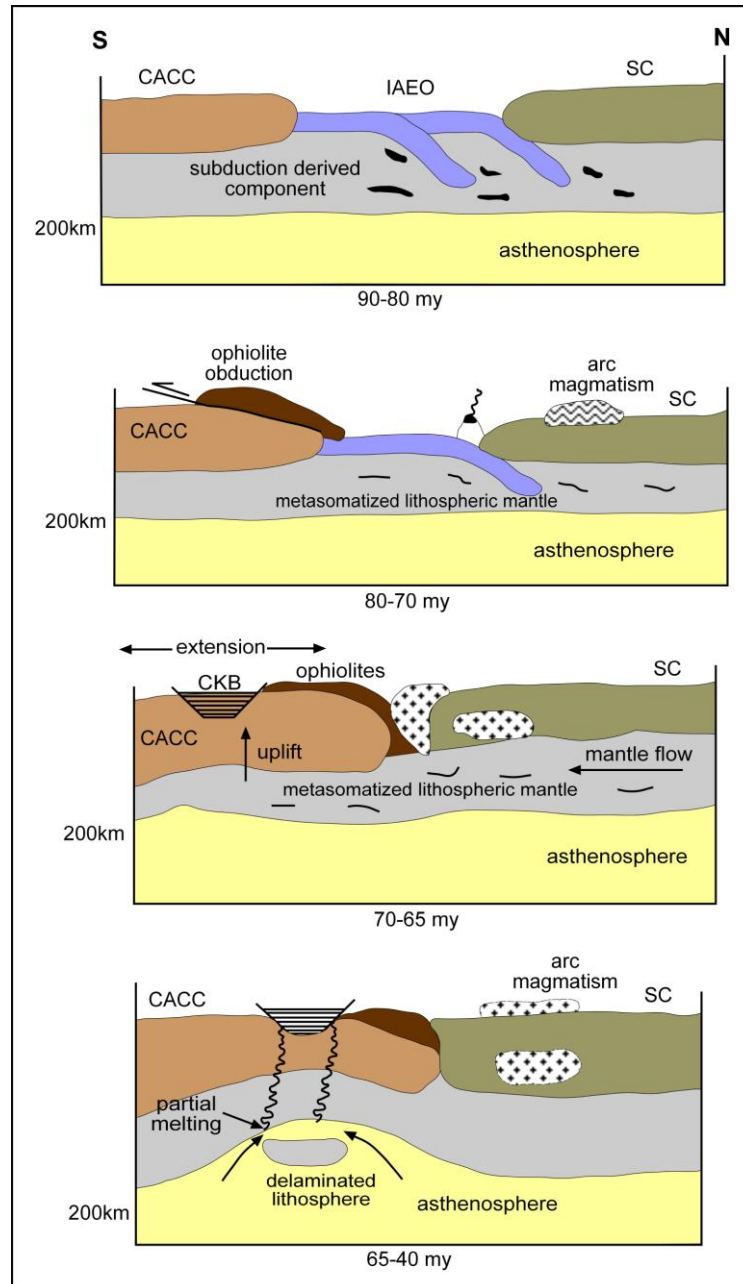


Figure 5. 3 Schematic cross section displaying proposed geodynamic evolution of the CACC during Late Cretaceous and Eocene time (CACC: Central Anatolian Crystalline Complex, SC: Sakarya Continent, CKB: Central Kızılırmak Basin).

On the other hand, Late Cretaceous magmatism is characterized by high Sr and low Nd isotope compositions relative to Eocene rocks, plotting close to the

crustal sources. This may suggest increasing mantle contribution to the genesis of the magmatism within the region during Eocene time.

Seismic investigations within the Central Anatolia are restricted to a few studies which suggest that crustal thickness of the central Anatolia varies between 37-42 km and changes laterally (Kuleli et al., 2004). This may suggest that thinning caused by extensional tectonics may not be uniform beneath the whole region. In this regard, the lack of comprehensive seismic tomography indicating crust-mantle structure beneath the central Anatolia makes the delamination model impossible to verify. Consequently, there is no consensus on the age of the lithospheric delamination and how much lithosphere delaminated. However, partial melting modeling based on the trace element data (Figure 4.16) indicates that melting has happened in the spinel stability field or mechanical boundary layer of the lithosphere (shallower than 80 km), hence substantial upwelling of the asthenosphere should have occurred (up to 60- 70 km), which imply unusual amount of the lithosphere was removed beneath the CACC.

Lithospheric delamination model has been widely applied to explain the formation of the widespread volcanism and magmatism with calc- alkaline to intraplate geochemical affinity in the Alpine- Himalayan orogenic belt. For instance, formation of the A- type granite and adakitic granite in the Tibetan Plateau was explained by lithospheric delamination model by Zhang et al., (2007). Furthermore, Duggen et al., (2005) linked the generation of Si rich subduction related and Si poor intraplate type lavas to delamination of the lithospheric mantle beneath the Alboran basin, Iberia.

Nevertheless, to answer all questions mentioned above the combination of geological, geophysical, geochronological and geochemical studies are required. On the other hand, based on the available data lithospheric delamination model can explain the best genesis of the widespread post

collisional magmatism within the CACC during the Late Cretaceous and Middle Eocene time and its compositional diversity as well.

CHAPTER 6

DISCUSSION

The aim of this thesis is to constrain the petrogenetic processes responsible for the formation and evolution of Eocene volcanics and also clarify the role of the volcanism on geodynamic evolution of the CACC during Early Tertiary time. Therefore, this chapter will first describe tectonic and geologic evolution of the central Anatolian basins in which Eocene volcanic rocks were exposed and then continue with a discussion on petrological characteristics of the Eocene volcanic rocks and finish with comparison of them with the rocks thought to be formed within post collision- extensional environment from Turkey and the Alpine belt.

6.1 Evolution of the Sedimentary Basins

As mentioned before, previous studies on geology of Turkey indicate that there was an oceanic branch of Neotethys between Sakarya continent and the Central Anatolian Crystalline Complex (CACC) during Late Triassic to Late Cretaceous. Although there is an ongoing debate regarding the geologic evolution of this Neotethyan Ocean, recent studies indicate that this oceanic seaway closed with multi- phase subduction (i.e. an intra- oceanic subduction creating the supra-subduction-type oceanic crust (Yalınız et al., 1996), and the main subduction of the oceanic lithosphere beneath Sakarya continent; e.g. Göncüoğlu et al., 1991). Therefore, the geological evolution of the CACC during Cretaceous time is governed by a complex chain of events including subduction, metamorphism, magmatism and deformation processes, which in turn lead to continental thickening caused by arc-continent collision, granitic

magmatism, ophiolite obduction onto the CACC and consequently metamorphism of the basement rocks.

In addition to these complex geological processes, normal fault controlled sedimentary basins related to the post-collisional extension were formed within the CACC or its margins (Göncüoğlu et al., 1993 and 1994), which was accompanied by calc-alkaline to mildly alkaline volcanic activity. For better understanding of contemporary formation of sedimentary basins and the volcanism, it is necessary to evaluate the basin formation and its tectonic effects on regional geodynamic history. Sedimentary basins within the CACC or surrounding it are collectively described as Central Anatolian Tertiary Basins and named as Çankırı, Sivas, Tuzgölü and Haymana basin (Göncüoğlu et al., 1993; Görür et al., 1998). These sedimentary basins are characterized by basin fill deposits reaching up to 1000 meters thickness and accompanied by volcanism, which indicate a transitional period from tensional to extensional tectonic regime after the closure of İzmir- Ankara- Erzincan branch of the Neo-Tethyan Ocean during Upper Cretaceous time.

Being intercalated with shallow marine sandstones and limestones, Eocene volcanism is thought to be active in the course of sedimentation. In addition to Tertiary peripheral basins of CACC, the Eocene basin located in central part of the crystalline complex parallel to the Kızılırmak River is defined as the Central Kızılırmak basin (Göncüoğlu et al., 1993a, b). The initial stage of sedimentation in all peripheral basins started during Late Maastrichtian. This period was characterized by sedimentation of reefal limestones following a regional transgression. Formation of lagoon deposits followed by red conglomerates and fossil bearing sandstones (Göncüoğlu et al., 1993) indicate a regression covering throughout the CACC during Thanetian (Late Paleocene). This regressive sequence points to the termination of post collisional extensional period, marked by Upper Cretaceous granitic magmatism, during Paleocene time. The whole middle Eocene period apart

from a few outcrops of lower Eocene units was characterized by a transgressive succession all over the CACC.

Eocene sedimentation within the Tuzgölü Tertiary basin located west of the CACC and its relation with CACC has been comprehensively studied by Görür and Derman, (1978), Derman, (1980) and Çemen et al., (1999). Tuzgölü basin was not considered in this study because of limited outcrops of Eocene volcanism within this basin (Eskipolatli formation, Sincik member Göncüoğlu et al., 1997). Overall, the Tuzgölü basin is regarded to have been formed as a fault-controlled trans-tensional basin during the Upper Cretaceous extensional tectonic regime and became deeper with Eocene extension (Çemen et al., 1999).

Ulukışla basin, located to the south of the CACC has comparable characteristics with the Central Kızılırmak basin. Within this basin extensive volcanic rocks are exposed (Oktay, 1982; Çevikbaş, 1991; Clark and Robertson, 2002; Alpaslan et al., 2004 and Kurt et al., 2008). There have been several different ideas regarding the evolution of this basin. Kadioğlu and Dilek, (2009) argued that the basin has been formed in the latest Cretaceous as foreland and/or fore arc basin when the compressional tectonic regime was dominated. However, in recent studies, formation of Eocene volcanism within this basin was linked with lithospheric thinning and consequently upwelling of the asthenospheric mantle (Alpaslan et al., 2004). Contrary to Görür et al., (1998) who argued a fore arc tectonic setting for the basin, Ulukışla basin is considered to be an extensional basin dominated by flysh sediments and intercalated volcanic rocks (Clark and Robertson, 2002; Kurt et al., 2008).

Sivas basin is located in the eastern part of the study area. The basement of this basin is represented by different rock units. For example, it is floored by the rocks derived from Sakarya continent to the north, while the basement is composed of recrystallized limestones and clastics of Bunyan metamorphics to the south and HT/LP metamorphics and granitic rocks of the CACC to the west

(Cater et al., 1991; Gökten et al., 1993; Yılmaz., 1994; Poisson et al 1996; Dirik et al., 1999). Late Cretaceous- Late Eocene period was characterized by deposition of turbiditic sequences with olistoliths in the central part of the basin, while at the basin margins fluvial deposits of Paleocene was unconformably overlain by Eocene transgressive successions, mainly represented by intercalation of shallow marine sediments and volcanic rocks. Products of Middle Eocene regional transgression dominate the southern margin of the CACC (Tekeli et al., 1992; Gökten et al., 1993), which is interpreted to be an indication of extensional episode in regional scale. There are small and isolated volcanic rocks within the Middle Eocene sedimentary deposits exposed in narrow strips lying in east-west direction within the southwestern part of the Sivas basin from western edge of the basin to Cayıralan area in CACC (Göncüoğlu et al., 1994). The presence of these strips, their geometry and the abrupt change in depositional facies indicate that formation of these basins was governed by normal faults (Dirik et al., 1999). Formation of the volcanic rocks exposed within the Middle Eocene units is thought to be associated with the regional trans-tensional systems. There is no published geochemical data on Eocene volcanic rocks exposed western margin of the Sivas basin.

Çankırı basin, located north of the study area, is regarded as a collisional basin and Eocene deposits within this basin are thought to be derived from the mélangé of the İzmir- Ankara- Erzincan Ocean (Erdoğan et al., 1996). The sedimentary fill of the Çankırı basin is composed of marine and continental deposits intercalated with the volcanic rocks and range from Paleocene to Pleistocene in age (Erdoğan et al., 1996). Erdoğan et al., (1996) called the Eocene volcanic rocks exposed within this basin as Bayat volcanics. On the basis of their origin and composition, Bayat volcanics are divided into 4 groups ranging between tholeiitic basalts to andesites (Demirer et al., 1992). Origin and evolution of this basin is also debatable. Kaymakçı et al., (2009) suggested arc related environment for this basin. They put forward a two stage evolutionary scenario to explain the evolution of the basin. According to the

authors, Upper Cretaceous deposits of the basin formed within fore-arc environment while the Paleocene and younger units are interpreted as having been formed within foreland setting. The authors suggested that termination of the fore-arc setting and beginning of the foreland basin is related to the complete subduction of the Neotethyan Ocean which subsequently led to collision of Pontides (Laurasia) and Taurides (Gondwana) in the Paleocene. Based on the local unconformities, they separated the basin fill deposits into two sequences as Upper Cretaceous and Paleocene. However, stratigraphically no depositional hiatus was observed between these two units and they can be regarded as stratigraphically conformable (Kaymakçı et al., 2009). Sedimentary sequence of the Çankırı basin does not show any difference in terms of depositional environment and stratigraphical succession those found within other Tertiary basins of the CACC (e.g. Göncüoğlu et al., 1994).

Another sedimentary basin developed after closure of the IAEO is Kızılırmak basin which is, unlike the peripheral basins, completely formed within the CACC. Eocene units exposed in this basin are called as Mucur Formation (Göncüoğlu et al 1994). Mucur formation starts with Göbekli member that contains coarse clastics mainly derived from the basement rocks and transported to the basin as alluvial fans and gravity flow deposits within the northern part of the study area. Sarılar member is characterized by a proximal turbiditic sequence, olistoliths and mega blocks, which indicates that the basin was tectonically active during deposition of the Sarılar member. Clastics with huge recrystallized limestone blocks of the Central Anatolian Metamorphics overlie the Middle Eocene transgression series especially in Çiçekdağ area. They indicate that normal faults promote the basin formation. Existence of granitic bodies within the Mucur Formation in Kızılırmak basin and gabbro blocks within the Eocene clastics in Felahiye area are interpreted as indication of the same normal fault system in the region (Dirik et al., 2004). Keklice member representing the upper level of the Mucur Formation contains blocks derived from basement rocks of the complex and the oldest cover units, which imply that the regional compression started during the final deposition of the

Mucur formation. Investigated volcanic rocks are observed in close association with any member of the Mucur Formation, which therefore, suggest that their eruption must have been going on during the deposition.

The evolutionary process of the sedimentary basins within the CACC and its tectonic implications has been intensively debated in previous studies (Görür et al., 1984 and 1998; Göncüoğlu et al., 1994; Dirik et al., 1999; Gürer and Aldanmaz, 2002). Due to the contrasting ideas, on the other hand, there is no consensus on the tectonic control that led to formation of the sedimentary basins in the region. This is mainly because of the fact that there is no agreement on the subduction history of the Tethys oceans (how many Tethys Ocean existed, their subduction direction etc.) in the central Anatolia. Consequently, a direct link between regional magmatic activity, basin formation and extensional tectonic has not been certainly established. Several different models and tectonic environment have been suggested to explain the formation of the sedimentary basins in the region. For instance, some authors argued that there was another branch of the Tethyan Ocean existed between Kırşehir continent and Menderes- Taurus Platform during the Cretaceous-Eocene time. Subduction of pieces of the oceanic lithosphere beneath the CACC during the Paleocene is believed to result in formation of fore arc/intra-arc basins (i.e. Tuzgölü, Haymana and Ulukışla) in the region (Şengör and Yılmaz, 1981; Oktay et al., 1981; Görür et al., 1984 and 1998). However, the most recent studies indicate that there is no need in placing an oceanic area between CACC and Tauride Platform to explain the geodynamic history of the region (Göncüoğlu et al., 1994; Çemen et al., 1999; Dirik et al., 1999; Gürer and Aldanmaz, 2002) since the stratigraphic succession of the CACC is almost the same to that of the Tauride Platform (e.g. Dirik et al., 1999; Gürer and Aldanmaz, 2002). As a result, this theory does not fully account for the geodynamic evolution of the basins.

Recently, besides these stratigraphic and structural analyses of the sedimentary basins, fission track ages were also used to decipher the formation of the

sedimentary basins in the region. Based on the apatite fission track ages performed on the Baranadağ and Hamit granitoids, Boztuğ et al., (2009) suggested that basement rocks were exhumed close to the surface around 57-61 Ma, which equals to Middle Paleocene (Selandian) and argued that this fast tectonic uplift has resulted from a compressional regime induced by the collision between Tauride- Anatolide platform and Sakarya continent and this compressional regime has also led to formation of the peripheral foreland basins in Central Anatolia. However, as stated by Boztuğ et al., (2009) there is no evidence in the field (i.e. deformation, faults or metamorphism) suggesting compressional tectonic regime in the region during that time. Moreover, fission track data of Boztuğ et al., (2009) do not show any consistency with those published in previous studies (e.g. Fayon et al 2001; Köksal et al 2004), which also makes reliability of those data open to discussion. Contrary to Boztuğ et al., (2009), Fayon et al., (2001) proposed fission track ages of 32- 47 Ma from Kırşehir and Akdağmadeni massifs, which is consistent with the Middle Eocene (Bartonian) age obtained from fossil data during this study. Since the cover units of the CACC do not provide any evidence for supporting apatite fission track data of Boztuğ et al., (2009), the compressional tectonic regime theory does not seem suitable to explain the origin of the basins.

The sedimentary basins within the CACC are required to be considered in the same geodynamic environment since they have some characteristics in common. First of all, they all formed during Late Cretaceous- Early Tertiary which post dates the final closure of the İzmir- Ankara- Erzincan Ocean (IAEO). They have a volcanic succession intercalated with the sedimentation despite the fact that the volume of volcanism displays some changes depending on the basin location. Besides, the deposition within these basins, in general, started with continental clastics followed by marine sediments during the Paleocene- Eocene time and ended with the Oligocene-Miocene shallow marine-lacustrine deposits (Göncüoğlu et al., 1994). Calc- alkaline volcanism exposed within these basins give a line of evidence that they were formed during the extensional regime after the closure of the IAEO. In the light of the

previous works, geodynamic evolution of these basins can be explained as follows. Closure of the IAEO during the late Cretaceous resulted in the ophiolite obduction which led to crustal thickening in the CACC. Thermal relaxation after the collision of two continents resulted in extensional sedimentary basins in the region (Göncüoğlu et al., 1993). Late Paleocene-Early Eocene period is represented by the deposition of the continental clastics in all basins and during this time subsidence of the basins continued. During the Middle Eocene time, asymmetrical development of the basins mainly represented by presence of gravity flow deposits within southern part of the basins and regional transgression to the north can be attributed to the formation of half graben systems associated with transtensional movements (Dirik et al 1999). Late Eocene- Oligocene time is characterized by compressional tectonic regime that thought to be related to the final collision of the basement of the CACC and Pontide units (Göncüoğlu et al., 1994; Dirik et al., 1999). Geodynamic evolution of the sedimentary basins is given in Figure 6.1.

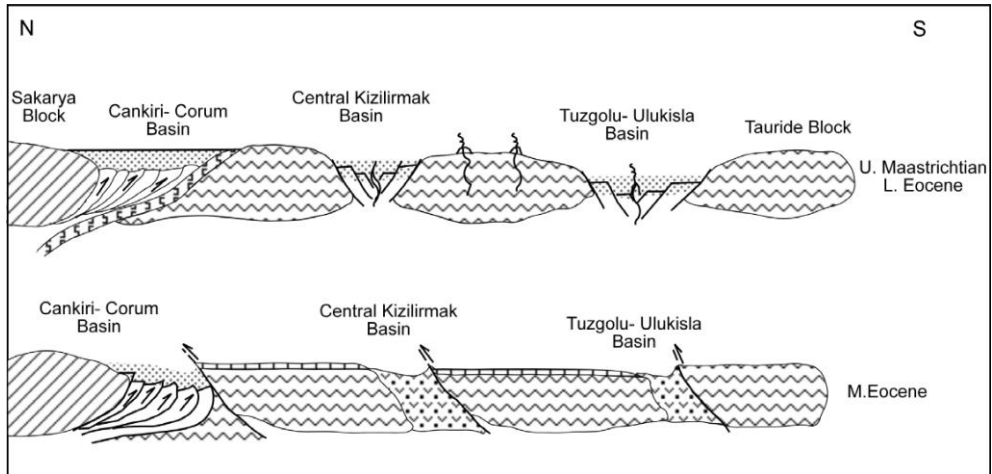


Figure 6. 1 Schematic cross section displaying evolution of the Tertiary basins within the CACC (from Göncüoğlu et al., 1994). As a whole, all basins show comparable features. They were formed within the northern part of the Tauride- Anatolide platform which has experienced significant amount of the crustal thickening during the final closure of the IAEO which in turn resulted in extensional tectonic regime accompanied by calc- alkaline volcanism exposed within these basins.

Consequently, regional geodynamics by which Eocene volcanism was controlled can be summarized as follows;

- Early- Late Cretaceous: crustal thickening caused by continental collision,
- Late Cretaceous, post collisional extension and widespread post collisional granites,
- Paleocene, demise of the extensional phase and relaxation
- Mid Eocene (Bartonian), renewed regional transtension induced by existing fault systems and associated volcanism,
- Late Eocene, compressional tectonic regime and deformation process.

6.2 Structural Control on Volcanism

As stated previously, final closure of the IAEO is believed to be the cause of most of the geological events in the CACC. This is also supported by the recent paleomagnetic studies suggesting that variable rotational movements affected the region after the closure of the IAEO and the rate of the rotation is likely to increase with time (Gürsoy et al., 1997; Tatar et al., 2002 and references therein). On the other hand, one of the most significant evidences for this extensional period comes from the regional structural components; widespread magmatism and formation of fault controlled sedimentary basins separating the CACC from the Tauride platform. Accordingly, there is a close association between regional geodynamics and the volcanism, in this respect several concerns should be taken into consideration. First of all, temporal relationship between the volcanism and the basin formation should be documented. Secondly, the question “what is the mechanism that causes the volcanism?” should be answered.

It appears that the volcanism in all Tertiary basins occurred more or less at the same time i.e. Early to Middle Eocene (e.g. Bayat volcanics in Çankırı basin, Demirer, 1992; Erdoğan et al., 1996; Ulukışla volcanics in Ulukışla Basin,

Clark and Robertson, 2002, Alpaslan et al., 2004 and 2006, Kurt et al., 2008; Sincik Formation in Tuzgözü basin, Göncüoğlu et al., 1997 and Mucur Formation in Kızılırmak basin, Göncüoğlu et al., 1994 and this study), which suggest that the volcanism is directly associated with the basin formation. As stated previously, all Tertiary basins in the central Anatolia share some common characteristics. Among them, however, the Ulukışla Basin appears to be the most important one in which voluminous Eocene calc-alkaline to alkaline through ultrapotassic rocks were exposed. Therefore, this basin can be regarded as prototype for other Tertiary basins in terms of sedimentation and large volume of volcanism. According to Clark and Robertson (2002) the Ulukışla Basin displays successive phases of transgression, subsidence, volcanism, evaporite deposition, deformation and uplift, which is also comparable with the other basins. The structural history of the Ulukışla Basin is summarized into several stages by Clark and Robertson, (2002). The first stage is represented by the emplacement of the ophiolitic basement of the basin during the Late Cretaceous which also corresponds to the same process in other basins. The second stage contains rapid subsidence, fault controlled sedimentary deposition and within plate type volcanism during the late Paleocene- Early Eocene. As emphasized before, the volcanism in all basins started Early- Mid Eocene. Besides, Eocene sedimentary units within the Central Kızılırmak basins contain carbonate dominated clasts derived from the Tauride Platform, indicating that the CACC and the Tauride Platform so close to each other during this time (Göncüoğlu et al., 1994). This argues against the presence of an oceanic area to south of the CACC. The third stage includes deformation process including thrust faults in Late Eocene. This compressional period continued to Early Miocene followed by extensional period represented by normal faulting.

To conclude, having been covered by the same sedimentary sequences represented by the same age and depositional environment, all Tertiary basins within and/or around the CACC are thought to be formed by the same geodynamic event. It appears that sedimentary basins provided weak zones for

the basaltic volcanism to erupt and extensional/ transtensional faults within and/or bordering these basins acted as suitable pathways. Therefore, basin formation, fault controlled sedimentation and accompanied volcanism is believed to have developed in response to the regional E-W extensional regime.

From the tectono-magmatic point of view, based on the regional geological relationships and the results of this study, the following scenario is proposed for the formation of Eocene magmas within the CACC. The upwelling of hot asthenosphere to the base of the lithosphere took place in response to the foundering some of the lithospheric mantle. Delamination process enhanced decompression melting of metasomatized lithospheric mantle beneath the CACC because the lithospheric mantle enriched by volatiles has a lower solidus relative to anhydrous asthenospheric mantle (i.e. Turner et al., 1992) and as a result early magmas were formed. Normal faults might have provided a weak zone for emplacement of the magmas formed by decompressional melting of the lithospheric mantle. These magmas underwent significant residence time in the shallow level magma chamber until suitable pathways were available to the surface. In the mean time, they experienced some degree of low pressure fractionation and also interacted with the upper crustal rocks. Extensional tectonic regime promoted ascent of magmas to the surface. The spatial distributions of the Eocene magmas argue against the presence of a single magma chamber beneath the region. Instead, isolated occurrences of the Eocene rocks require limited source volume, which subsequently leads to the idea that there were several small magma batches beneath the whole region. These magma batches must have been fed by the same or similar parental sources since all the volcanic rocks show similar geochemical characteristics. The distribution of the studied rocks also implies that Eocene magmas rose to the surface through the preexisting weak zones extending parallel to the major fault systems. The most important petrogenetic processes involved in magma generation in the CACC seem to be probably variable degrees of partial melting of a heterogeneous lithospheric source and then assimilation and

fractional crystallization process (AFC). Short eruption time and compositional similarities between the rocks from both regions suggest that Eocene volcanic rocks have experienced the same geochemical process and geodynamic events and formed from a common primary magma. Consequently, the most likely trigger for the Eocene volcanism in the CACC was extensional tectonic regime and lithospheric thinning that followed the closure of the Neo- Tethyan Ocean along IAE suture zone.

The indication of the extensional period after the Eocene time is also reported within the Central Anatolian Volcanic Province (CAVP). As known, the eastern and western margin of the CACC is bounded by two major fault systems; Tuzgölü and Ecemiş faults. The spatial association between main fault systems and the Quaternary volcanism has been discussed in previous studies (Pasquare et al 1988; Toprak and Göncüoğlu, 1993; Toprak, 1998). Pasquare et al., (1988) argued that considering distribution of the volcanic centers in the CAVP, volcanism is likely to occur either along the main fault systems (e.g. Hasandagi and Erciyes) or the ones parallel to them formed during the extensional phases. Apart from being a pathway to the surface, these transcurrent fault systems are also thought to have a control on the residence time and coexistence of the complete spectrum of volcanic rocks (calc-alkaline, tholeiitic through alkaline series) within the CAVP explained by this way (Gençalioglu-Kuşcu and Geneli, 2010).

Besides the Central Anatolia, the temporal and spatial association of extension and magmatism is also documented in the Alpine belt by several studies (e.g. Carpathian-Pannonian Region including Apuseni Mountains, Romania; Rosu et al., 2004; Harangi and Lenkey, 2007, Eocene- Oligocene basaltic rocks from Bulgaria; Marchev et al., 2004). These all suggest that extensional tectonics had played a role on the regional magmatism and its compositional diversity as well. It is a well known truth that extensional or strike slip tectonic regime make the magma transport easy from the deep mantle to the surface (Shaw, 1980; Maury et al., 2004).

6.3 Discussion on Petrology of Eocene Volcanism

Before discussing geochemical characteristics of the studied rocks in detail the petrographical properties will be summarized. The investigated rocks are generally plagioclase + pyroxene \pm olivine \pm hornblende-pyrrhic, indicating shallow crystallization level. They are characterized by various textures indicating disequilibrium crystallization such as glass inclusions in plagioclase, sieved textured plagioclase, coexistence of sieved and normal (clear) type plagioclases within the same rock, reaction rim around the mafic minerals, zoning in pyroxene and plagioclase phenocrysts, and quartz phenocrysts surrounded by pyroxene. These disequilibrium textures could be result of either the mixing of felsic and mafic magma batches or bulk mixing of the silica rich local crustal rocks.

Besides petrographical properties, geochemical signature of the volcanic rocks from Çiçekdağ and Yozgat areas also displays comparable characteristics. Eocene volcanic rocks are calc- alkaline to mildly alkaline in nature with mainly basaltic and basaltic andesitic compositions. Small negative Eu anomaly indicates that both plagioclase fractionation and crustal assimilation have been involved in the genesis of the volcanic rocks. The flat REE concentration which is above 10 times chondrite values indicates a garnet free source for all rocks. Based on the Nb and Zr contents, Eocene rocks from both regions can be divided into 3 groups. The compositional variations among all these groups can be attributed to several reasons which include (1) insignificant amount of assimilation (2) various amount of fractional crystallization (FC) process during ascending of the magmas (3) different degrees of partial melting of chemically heterogeneous mantle source.

As discussed in the geochemistry section, one of the major issues in dealing with the petrology of within plate volcanics is the effect and extent of the crustal input. Crustal contamination might cause significant depletion in HFSE especially Nb and Ta and enrichment in Th and U in the mantle normalized

multi element diagrams (Taylor and McLennan, 1985). As stated previously, Eocene volcanic rocks display petrographical and geochemical features that imply the crustal assimilation had happened during their evolution. As known, besides enriched trace element abundances crustal material involved into genesis of the ascending magmas results in elevated isotope ratios. The convention to check whether the isotope composition of the rocks has been modified by crustal contamination during magma ascent is to plot isotopic ratios against an index of differentiation (i.e. SiO₂ or MgO) or to plot 1/Sr vs ⁸⁷Sr/⁸⁶Sr ratios which would produce a linear correlation if mixing with crustal material had happened. It is clear from Figure 6.2 that there is no strong correlation between silica and isotope ratios. The lack of correlation might be attributed to several reasons. For example, Eocene samples have limited isotope ratios that they could not be able to make an obvious correlation in the isotope vs silica diagram and consequently, can not be sensitive to show crustal contribution. Second possible cause could be that crustal contamination might not be one of the important processes involved in the genesis of Eocene magmas. The second hypothesis can not be favored here, as discussed in previous sections; Eocene rocks bear petrographical and geochemical evidence for that at least some of the isotope ratios have been little (7-8%) affected by the crustal assimilation. In this respect, the lack of correlation between indices of fractionation and isotopes is therefore no guarantee that contamination has not occurred. On the other hand, another support for the crustal contribution to the genesis of the studied rocks comes from the isotope analyses of the local crustal rocks within the CACC.

If the fractionation index is not suitable to display the crustal contribution then trace element ratios sensitive to crustal contamination (e.g. Ba/Nb, Nb/La and Ba/La) might be useful to show subtle crustal effects on the volcanic rocks. Contamination of Late Cretaceous granitic rocks is evident from Figure 6.3, as the positive correlation between studied rocks and Pb isotopes of the granites obviously exist, which is also evidenced by Figure 4.12, where Eocene samples trend towards the basement rocks of the CACC in the Pb isotope space.

Consequently, relatively high Pb isotopic compositions of the studied rocks can be attributed to crustal contamination. Assimilation of 8% local crustal rocks seems to account for some of the isotope and trace element abundances of the studied rocks. On the other hand, local upper crustal rocks clearly have Sr and Nd isotopic compositions different from the Eocene samples (Figure 6.3).

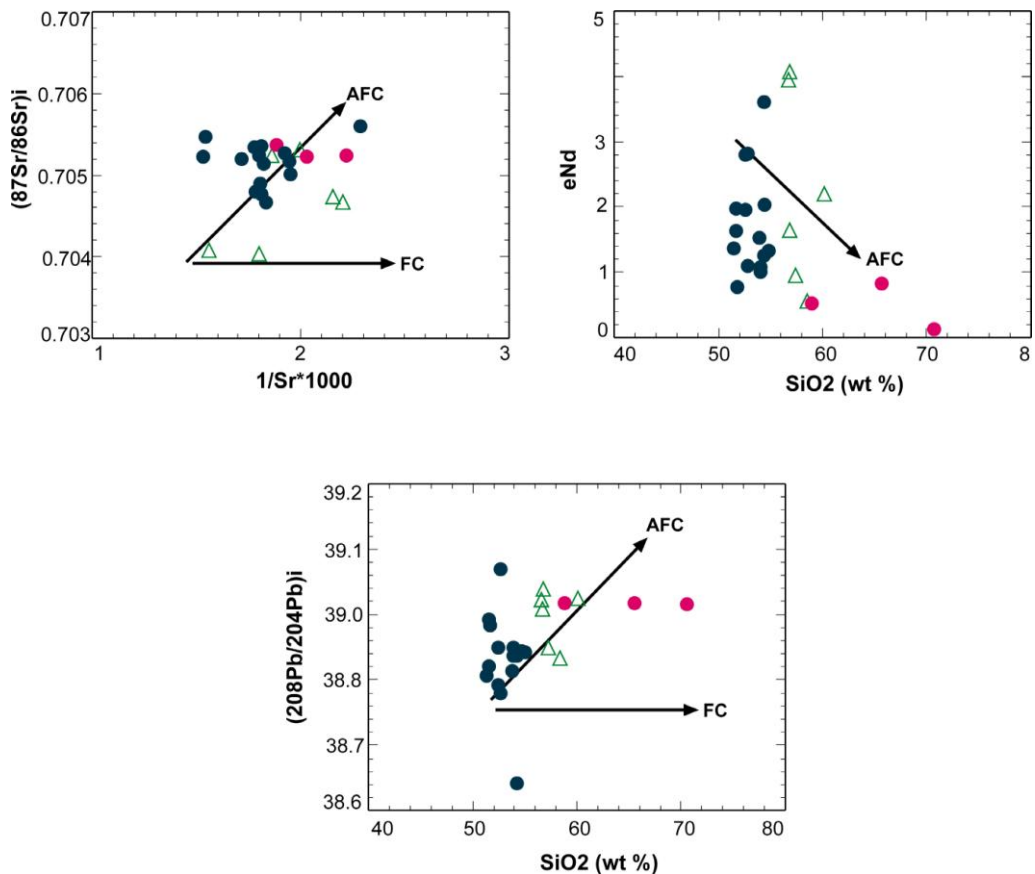


Figure 6. 2 Sr- Nd- Pb isotopes vs silica- $1/\text{Sr} \times 1000$ diagram for Eocene samples (AFC: assimilation and fractional crystallization; FC: fractional crystallization).

The variations in Sr and Nd isotopic compositions can not be attributed to the crustal contamination since the lack of correlation between isotope ratios and trace element ratios weakens the possibility of large scale crustal effects on these systems. Thus, this suggests that upper crustal contamination has

negligible effect on the studied rocks compared to the mantle source heterogeneities. On the basis of the discussion above, it can be considered that some of the compositional variations observed in the Eocene volcanic rocks especially those in Pb isotopes can be explained by crustal contamination; on the other hand, the whole range of the trace element and isotope variations can not be attributed to the crustal assimilation. As discussed in geochemistry section, these variations should mostly be related to the mantle source heterogeneities and/or partial melting process rather than crustal contamination.

Since the trace element data seems to be unaffected by the large degree of crustal assimilation, they can be a good proxy for mantle source region. Based on the trace element geochemistry, mantle source region or melting depth can be estimated. As stated in geochemistry section, Eocene volcanic samples highly enriched K and Rb relative to Ba in the multi element diagrams (Figure 4.8), indicates that residual phase in the source region was phlogopite rather than amphibole. A similar situation has been reported by Miller et al., (1999) for the lamproites from Spain.

Furman and Graham, (1999) argued that both Rb and Ba are compatible in phlogopite whereas, Rb, Sr and Ba are moderately compatible in amphibole. Thus; melts derived from phlogopite bearing source are assumed to have higher Rb/Sr and lower Ba/Rb values, while melts in equilibrium with amphibole are characterized by extremely high Ba and Ba/Rb ratios. In the Rb/Sr vs Ba/Rb diagram (Figure 6.4) most of the studied rocks are characterized by high Rb/Sr ratios up to 0.3, which also supports derivation from phlogopite rich source.

Partial melting calculations indicate that both Çiçekdağ and Yozgat volcanics were derived from a common mantle source by different degrees of partial melting in the presence of the residual phlogopite. In general, Çiçekdag samples and some of Yozgat samples display slightly higher trace element

abundances. As indicated by partial melting modeling these elemental variations might have been derived from lower degree partial melting during the formation of parental melts of these rocks.

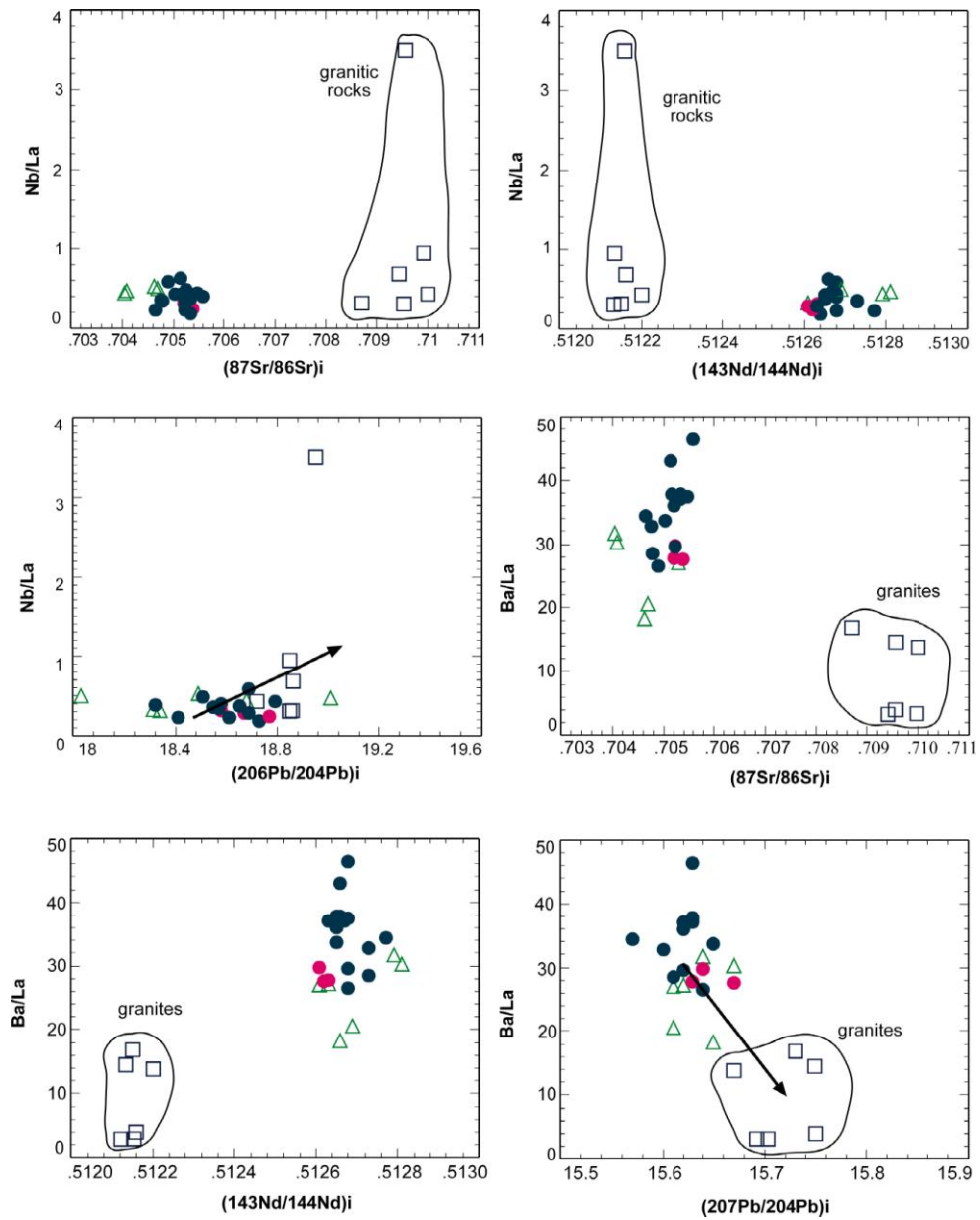


Figure 6. 3 Nb/La, Ba/La vs isotope diagrams for the studied rocks. Note that trace element ratios show good correlation only with Pb isotopes (Symbols are the same as in Figure 4.4).

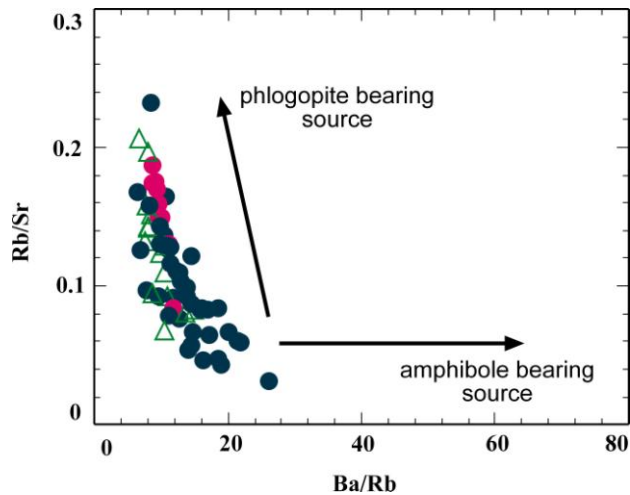


Figure 6. 4 Ba/Rb vs Rb/Sr diagram for Eocene volcanic samples. All samples are shifted towards phlogopite bearing source.

In general, low degree melts are believed to be generated at greater depths and have lower silica, higher FeO and higher incompatible trace element abundances than higher degree melts (e.g. Langmuir et al., 1992; Shaw et al., 2003). Whole rock geochemistry and partial melting calculations indicate that Eocene volcanic rocks are relatively large degree partial melts of phlogopite bearing spinel lherzolite source. On the basis of the trace element and REE signature (the HREE 10 times the chondritic values) and partial melting modeling, it appears that Eocene magmas were formed from a garnet free source, which requires the melting region to be within the lithospheric depth. Presence of residual phlogopite can also provide significant implications for melting depth. K bearing phases such as amphibole and phlogopite thermally can not be stable in both convecting asthenospheric mantle and sublithospheric plume component but stable in oceanic and continental lithospheric mantle (Foley, 1992; Class and Goldstein, 1997). According to these findings melting depth can be estimated approximately. The spinel facies and garnet facies transition in the upper mantle occurs between 60 and 80 km depth (Ellam, 1992). Lack of garnet in the mantle source, which is recorded by flat HREE and low $(Dy/Yb)_N$ ratios of the samples indicate derivation from mechanical boundary layer of the lithosphere (<80 km). But no further depth

resolution can be conducted due to deficiency of deep seismic studies in the central Anatolia.

Another point that needs to be discussed here is that although Eocene samples were formed within plate setting, they show geochemical characteristics similar to arc related environment. Arc like geochemical signature is represented by high LILE/HFSE and low HFSE especially Nb and Ta abundances. However, compared to arc products the studied rocks are characterized by high Sr content (up to 1300 ppm), La/Nb (0.7- 4.6), Zr/Y (3.61- 12.45) and Ba/Nb ratios (33-208). Although HFSE depletion is mostly attributed to the magmas derived from subduction process (Thirlwall, 1994; Parkinson and Pearce, 1993), Nb and Ta depletion in the mantle normalized pattern could be explained by several ways. For example, Jochum et al., (1989) argued that depleted Nb and Ta concentrations relative to La seem to be diagnostic feature of lherzolite xenoliths from the lithospheric mantle. Another possible explanation for the Nb depletion is the presence of residual titanite phase such as rutile, titanite (sphene), ilmenite or perovskite to retain Nb in the source region during partial melting, on the other hand, the difficulty of this process is that high content of the TiO_2 is required (up to 7 or 9 % TiO_2) for rutile saturation in basaltic melts to stabilize these phases, which seems theoretically impossible (McCulloch and Gamble, 1991). In addition to these, Gill, (1981) argued that modification of a MORB like mantle source by LILE-enriched but HFSE-depleted agents such as slab derived fluids also cause Nb-Ta depletion in the resulting magmas. However, in the recent literature these geochemical characteristics are mostly explained as indication of the enriched lithospheric mantle source. Lithospheric origin of the studied rocks can be further emphasized by Nb/La vs Ba/La (Figure 6.5) diagram. In this diagram all samples plot away from the field of mantle derived rocks and shifted towards to lithospheric area with relatively high Ba/La ratios. Lithospheric mantle might be involved in the genesis of the intraplate volcanic rocks either as the contaminant for the asthenosphere derived magmas or direct melting of the lithosphere itself.

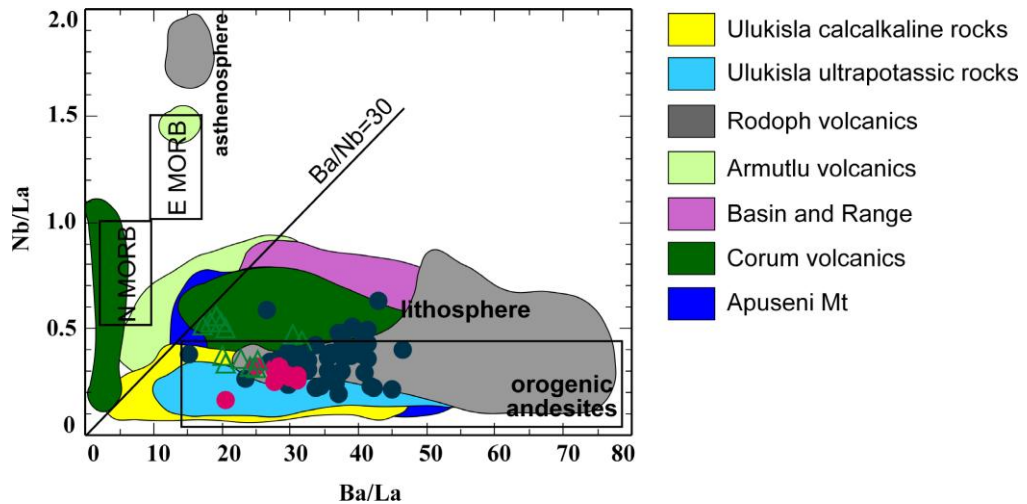


Figure 6. 5 Nb/La vs Ba/La plot for the studied rocks (E MORB, MORB and orogenic andesite reference fields are taken from Sun and McDonough, 1989 and Gill, 1981 respectively). Data from other extensional area are also plotted. Ulukışla calc- alkaline and ultrapotassic rocks, Alpaslan et al., 2004; 2006 respectively; Rhodope volcanics Marchev et al., 2004; Armutlu volcanics Kürkcüoğlu et al., 2008; Basin and Range Province Hawkesworth et al., 1995, Rogers et al., 1995; Çorum volcanics Keskin et al., 2008; Apuseni Mt Rosu et al., 2004.

In either case resultant magmas will have inherited LILE enrichment and negative HFSE anomalies in the mantle normalized patterns. The possibility of the lithospheric contamination of the asthenosphere derived magmas has already been discussed in the geochemistry section. Despite of the heterogeneous trace element signature, slightly homogeneous isotopic compositions of the studied rocks give strong evidence against asthenosphere-lithosphere interaction. This argument can be further supported by an isotope vs ratio diagrams. For example, mixing of the melts from different mantle source (asthenosphere and lithosphere) would be expected to result in reverse relationship in the diagram of ϵNd vs Sm/Nd ratios. However, Eocene samples show linear trend in this diagram. That means the sample having the highest ϵNd values also have the highest Sm/Nd ratios (Figure 6. 6), which basically argue against the mixing of two different mantle sources. The restricted

variations in isotope ratios suggest that the mantle source of the different groups (e.g. Çiçekdağ and Yozgat) can not be distinct from each other.

Another line of evidence again comes from trace element data. Different mantle domains are characterized by different trace element and isotope compositions (e.g. Weaver, 1991). Table 6.1 summarizes the trace element ratios of different mantle sources.

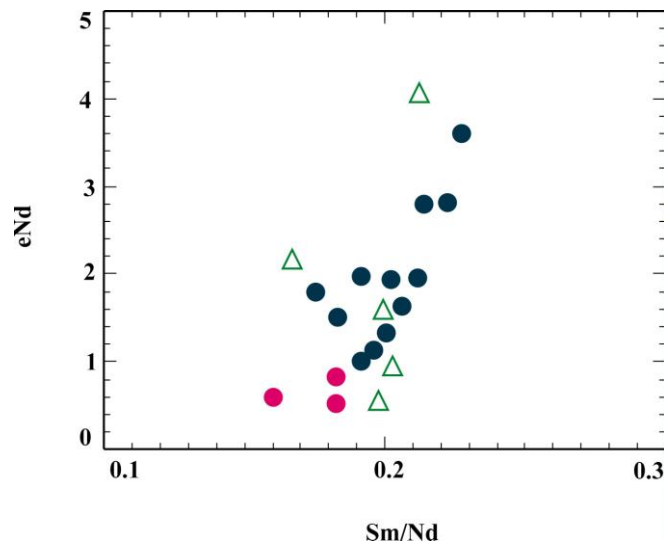


Figure 6. 6 ϵNd vs Sm/Nd plot. Linear trend that Eocene volcanic samples show suggests derivation from single source.

The studied rocks have considerably high LILE/HFSE element ratios relative to mantle derived rocks e.g. OIB and MORB. On the other hand they have comparable trace element ratios with continental crust and global subducted sediments (GLOSS). As discussed in geochemistry section, trace element especially LILE enrichment can be explained by several ways. Although low degree partial melting is capable of producing enriched trace element abundances, partial melting calculations and mostly Q- Hy normative nature of the studied rocks rule out being derived from the low degree melting. So, selective enrichment of the trace element concentrations requires some

additional process other than partial melting. Most of the geochemical characteristics indicate that source of the Eocene magmas had been modified by metasomatic agents. Mantle enrichment process could be related to any of the following; silicate metasomatism, carbonate metasomatism and subduction related components. High K_2O/TiO_2 ratios of the studied rocks (up to 5) thus imply that the origin of the subduction component involved in the genesis of the studied rocks was H_2O - rich fluids. High LILE and K_2O/TiO_2 ratios are thought to be indicative of H_2O - rich fluids whereas high TiO_2/K_2O is linked with silicate-melt metasomatism (Hawkesworth et al 1984; Kempton et al., 1991). Besides, relatively low $(La/Yb)_N$, low Zr/Hf high Ti/Eu and high $(Hf/Sm)_N$ ratios eliminate the possibility of silicate and carbonate metasomatism (Figure 4.23). Figure 6.7 shows the relative contribution of the subduction derived components into the genesis of the studied rocks. It seems from the figure that the dominant metasomatizing agent is subduction derived fluids although some of the samples are plotted within the melt related enrichment. This enrichment can be attributed to sediment contamination, since subducted sediments might have been involved into the mantle source region either bulk or melt in form. Besides this, Eocene volcanic rocks have comparable Pb isotope compositions with global subducted sediments (GLOSS, Plank and Langmuir, 1998; Figure 4.25). Another line of evidence can be again provided by Pb isotopes; Eocene samples have relatively high $\Delta 7/4$ values (8.41-17.31) which is also interpreted as an effect of subducted sediment component in the mantle source (Shaw et al., 2007).

Consequently, the complete geochemical and isotopic study of the Eocene rocks reveals that their source enrichment (i.e. LILE and LREE) and depletion (HFSE; Nb, Ta) can be attributed to the addition of variable amounts of subduction derived fluids and sediments into the mantle source. It is well known truth that addition of the H_2O - rich agents to mantle peridotite significantly lowers its solidus temperature and lead to crystallization of the hydrous phases such as amphibole and phlogopite (Gallagher and

Hawkesworth, 1993) and such a mantle could preferentially melt during the initial stage of thermal perturbation due to extension (e.g. Wang et al., 2002).

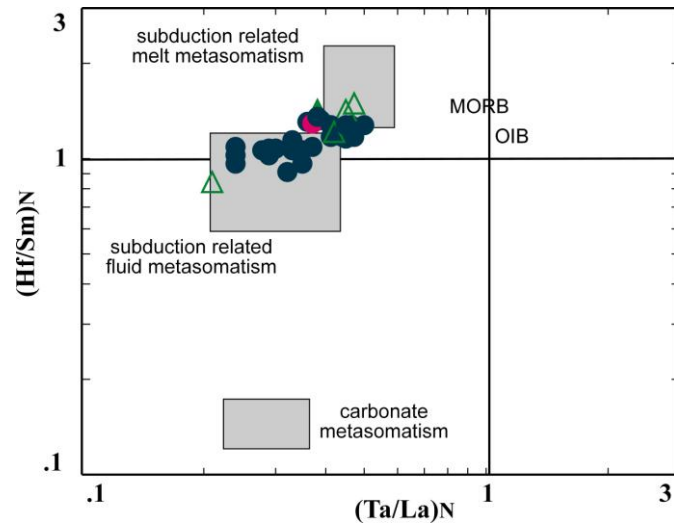


Figure 6. 7 $(\text{Hf}/\text{Sm})_N$ vs $(\text{Ta}/\text{La})_N$ plot for the studied rocks. Most of the Eocene samples fall into the subduction related fluid metasomatism area which is consistent with overall geochemical signature of the rocks. Fields are from Wang et al., (2004).

The dominant factors that control the composition of the Eocene magmas are derivation from a metasomatized lithospheric mantle source, the degree of partial melting of the source and fractional crystallization of the mafic phases with negligible amount of the crustal assimilation. Enrichment of the source region is considered to have taken place during subduction of the oceanic lithosphere beneath the Sakarya continent. A continental collision caused by subduction of the Neo-Tethyan oceanic lithosphere, took place before Eocene volcanism, during Late Cretaceous time. Subduction fluids released from subducted slab might be the most convenient explanation for modification of the lithospheric mantle beneath the CACC.

6.4 Tectonic Discrimination Diagrams for the Studied Rocks

Diagrams based on the trace elements and/or their ratios are commonly used for tectonic discrimination purposes. However, there are some restrictions on the use of them. Therefore, diagrams based on the immobile elements stable under the hydrothermal conditions must be employed.

Another point that should be taken into consideration is that the rocks either affected by crustal contamination or derived from lithospheric mantle tend to show arc like geochemical signature and hence might be plotted in the arc related environments in tectonic discrimination diagrams (Ernst et al., 2005).

For the discrimination purposes, only mafic samples ($\text{SiO}_2 < 54$ (wt %)) having low LOI values were used. Most of the Çiçekdağ samples being more felsic than those from Yozgat were not included to the classification. As a result, relatively fresh 30 samples, most of which are from Yozgat, were selected.

The projection of the geochemical characteristics of the Eocene samples into various geotectonic discrimination diagrams proves the calc-alkaline to post orogenic, within plate signature of these rocks. For example, in the diagram of Zr–Zr/Y plots (Pearce and Norry, 1979; Figure 4.24), all the samples fall into the field of within-plate-basalt consistent with their post collisional- extension related intraplate environment.

On the discrimination diagram of Meschede, (1986, Figure 6.8), most of the samples plotted in the AII and C field, which stand for the alkali within-plate and within-plate tholeiites- volcanic arc, respectively. For the Eocene rocks Cabanis and Lecolle, (1989, Figure 6.9) diagram was also applied. In this diagram most of the studied rocks plotted in the calc-alkaline basalt area.

Table 6. 1 Incompatible trace element ratios in Eocene samples and major mantle reservoirs (PM: Primordial Mantle, N MORB: Normal Mid Ocean Ridge Basalt, CC: Continental Crust, GLOSS: Global Subducted Sediments, OIB: Ocean Island Basalt, HIMU, EM I and EM II are isotopically defined OIB end members. PM, N MORB, OIB and OIB end members are taken from Weaver 1991, GLOSS composition is from Plank and Langmuir 1998, “Eocene” represents the average values of the studied rocks).

Ratios	Zr/Nb	La/Nb	Ba/Nb	Ba/Th	Rb/Nb	K/Nb	Th/Nb	Th/La	Ba/La
PM	14.8	0.94	9	77	0.91	323	0.117	0.125	9.6
N MORB	30	1.07	4.3	60	0.36	296	0.071	0.067	4
CC	16.2	2.2	54	124	4.7	1341	0.44	0.204	25
GLOSS	14.54	3.2	86.8	112	6.40		0.77	0.240	26.9
HIMU OIB	3.2-5	0.66-0.77	4.9-5.9	63-77	0.35-0.38	179	0.78-0.101	0.107-0.133	6.8-8.7
EM I OIB	5-13.1	0.78-1.32	9.1-23.4	80-204	0.69-1.41	432	.094-.130	0.089-0.147	11.2-19.1
EM II OIB	4.4-7.8	0.79-1.19	6.4-11.3	57-105	0.58-0.87	378	0.105-0.168	0.108-.0183	7.3-13.5
Eocene	18.22	9.93	93.89	87.77	8.82	2193.68	1.11	0.38	31.78

As indicated in the diagrams, some of the Eocene volcanic rocks plot in within plate environment whereas some of them fall into the calc-alkaline basalt field. This might be explained by geochemical signature of the lithospheric mantle on the investigated rocks.

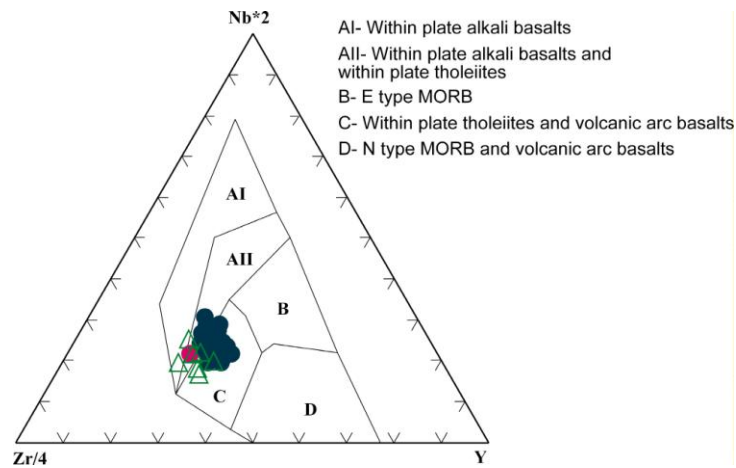


Figure 6. 8 Nb*2-Zr/4-Y diagram (Meschede, 1986) for the studied Eocene basaltic rocks.

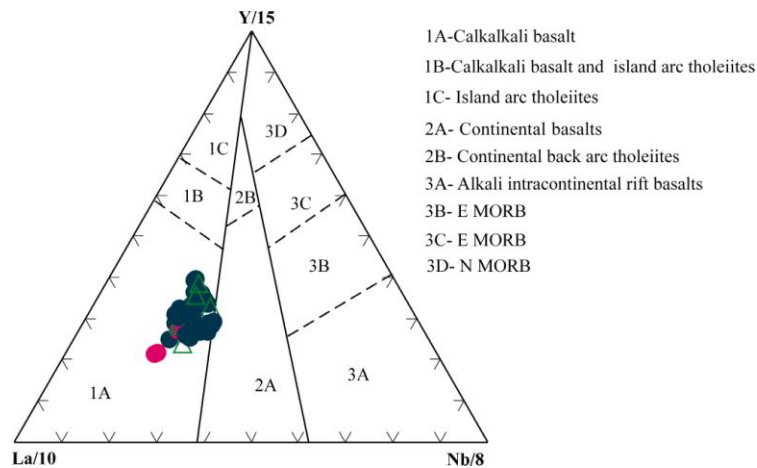


Figure 6. 9 Y/15- La/10-Nb/8 plot (Cabanis and Lecolle, 1986) for Eocene basaltic samples.

6.5 Comparison with Other Post Collision- Extension Related Rocks

The Eocene volcanic data was compared with the rocks from post- collisional extension related environments for better understanding of geochemical and geodynamic evolution. Although Eocene volcanism in CACC is widespread and crops out throughout the whole region, the available geochemical data is restricted. The lack of the geochemical studies within the other sedimentary basins limits the data only to the Ulukışla Basin (UB).

In this sense, the volcanic rocks exposed within the UB are essential since both Ulukışla and Central Kızılırmak basin are thought to be formed by the same geodynamic event. Besides calc- alkaline volcanic rocks, Eocene ultrapotassic rocks from UB have been also reported by Alpaslan et al., (2006) and used in this study as well. In addition to these data, Keskin et al., (2008) and Kürkcüoğlu et al., (2008) described Late Eocene volcanism within the N and NW part of the CACC, Çorum and Armutlu areas respectively. As being part of the whole Eocene volcanism within the central Anatolia, they were also included to the correlations. All aforementioned rocks share the common geochemical properties such as LILE enrichment and HFSE depletion.

Besides, Eocene volcanic rocks can be compared with the evolution of the Alpine- Himalayan orogenic belt to show spatial and temporal variations of the rocks that formed during the extensional regime throughout the region. Therefore, the comparison also includes extension related rocks from Alpine- Himalayan orogenic belt. Data set is taken from various parts of the Alpine- Himalayan region such as mafic volcanic rocks from the Eastern Rhodope (Bulgaria, Marchev et al., 2004); Apuseni volcanics (Romania, Rosu et al., 2004). In addition to these regions extensional data also includes Basin and Range Province (B&R, USA) one of the well known post collision- intra plate extensional zone in the world. The data also include the upper crust composition (Rudnick and Gao, 2004) for comparison purpose.

The mafic volcanism in the Eastern Rhodope is supposed to have formed in a post collisional extension related environment (Marchev et al., 2004). The authors explained the genesis of the calc-alkaline to alkaline rocks by convectonal removal of the lithosphere and argued that asthenospheric mantle contaminated by lithospheric mantle is the possible source for volcanic rocks having Nb-Ta anomaly. Neogene Apuseni Mountains (Romania) is another volcanic province within the Alpine- Himalayan orogenic belt and characterized by the same geochemical signature with Eocene rocks. Apuseni Mt is also considered to be formed within post collisional extension related environment after the closure of Neo- Tethyan Ocean (Rosu et al., 2004). The authors argued that the subduction signature of the magmas, shown by negative Nb-Ta anomaly, emphasizes the significant involvement of fluids inherited during previous geodynamic events. Basin and Range Province (B&R) is also one of the well known extension related volcanic provinces in the USA. Origin of the B&R rocks attributed to the melting of the lithospheric mantle previously enriched by subduction related component (Hawkesworth et al., 1995; Rogers et al., 1995).

To compare the geochemical characteristics ratio-ratio diagrams were employed. For example, diagrams involving Th and Nb can be useful for determining the source characteristics of magmas and degree of crustal involvement (Pearce, 1983). On Th/Y vs Nb/Y diagram Eocene volcanic rocks are placed toward subduction enrichment field with high Th/Y ratio (Figure 6.10), which can be interpreted as either crustal involvement or metasomatized mantle source because Th tends to be concentrated in the continental crust, while Nb and Ta are generally depleted (i.e. Kempton et al., 1991). Although Armutlu volcanics were interpreted as having crystallized from a metasomatized lithospheric mantle (Kürkçüoğlu et al., 2008), they display the lowest Nb/Y ratios within the entire set. They have comparable Th/Y ratios with the studied rocks, but their low Nb/Y ratios might be related to partial melting process. Besides, their crustal basement is poorly known; consequently

this may suggest that crustal processes might have also contributed to these differences.

Another important point on this diagram that needs to be emphasized is that Rhodope (Marchev et al., 2004) and Çorum volcanics (Keskin et al., 2008) differ from the whole data set in having relatively high Nb/Y ratios plotted within the mantle array field. Marchev et al., (2004) attributed this to increasing asthenospheric input into the source region of the volcanics. Although source region of the Çorum volcanics is argued as enriched lithospheric mantle, the few samples having OIB like characteristics was explained by mantle heterogeneities (Keskin et al., 2008). Even if both explanations are acceptable, low degree partial melting and uncontaminated nature could be other alternatives. Apart from a few samples that belong to these two volcanic areas, all groups are characterized by comparable trace elemental ratios.

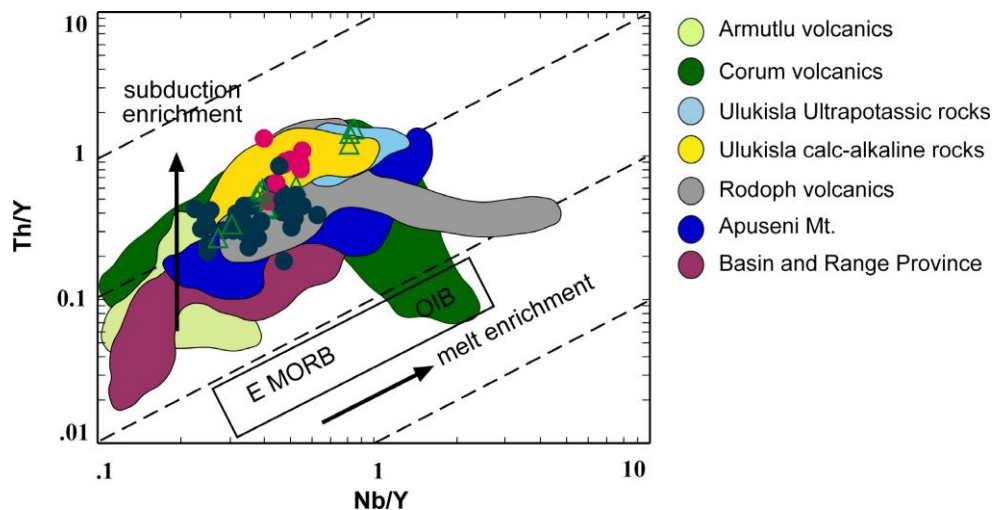


Figure 6. 10 Th/Y vs Nb/Y plot for Eocene volcanic samples. Reference data is given next to the figure.

Highly incompatible trace elements or their ratios provide good opportunity to compare the geochemical data since their concentration do not change with the secondary processes such as fractional crystallization. In this respect La/Nb vs Th/Nb plot can be useful. In this diagram most of the Eocene rocks are characterized by the same elemental ratios with the rocks from Apuseni Mt and Basin and Range Province (Figure 6.11). It is again noteworthy here that a few samples from Bulgaria and Çorum area are characterized by high and variable range of La/Nb ratios and could not be correlated any of the studied rocks or the data set. This may indicate again an increase of asthenospheric effect on their genesis. It is also clear from the diagram that there is a considerable compositional overlap between the rocks from extensional environment and the upper crust. In addition, active continental margin data also shows similar trace element signature with the extension related rocks.

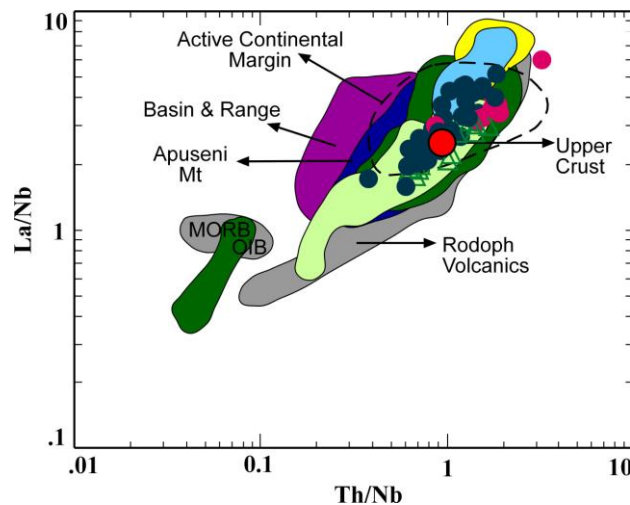


Figure 6. 11 La/Nb vs Th/Nb plot for comparing the studied rocks with the other post collisional rocks from the Alpine belt and Basin and Range Province from the USA. Reference data is the same in Figure 6.10. Upper crust value is from Rudnick and Gao, 2004.

Although the rocks investigated have comparable trace element signature with other extension related rocks, their isotope compositions are moderately

different from them (Figure 6.12). Apart from a few samples, all Eocene rocks are plotted within the Bulk Silicate Earth region. Armutlu volcanics also display similar pattern with the studied rocks. On the other hand, the rocks from Ulukışla Basin have higher Sr isotopic compositions which were interpreted as being derived from enriched mantle source (Alpaslan et al., 2004; 2006). Some of the rocks from Bulgaria are plotted close to the HIMU mantle although the rest of them are aligned toward EM II, similar to Ulukışla Basin's rocks. Origin of the Bulgaria volcanics, as stated previously, is attributed to the asthenospheric mantle contaminated by lithosphere (Marchev et al., 2004). Ultrapotassic rocks from Ulukışla basin (Alpaslan et al., 2006) have the most radiogenic Sr isotope compositions. The differences between isotopic compositions of the studied rocks and those of Ulukışla basin can be attributed to the mantle enrichment process, its timing and the extent of the shallow level processes such as assimilation and fractional crystallization. In this diagram, isotope space European Asthenospheric Reservoir (EAR) composition is also plotted for reference.

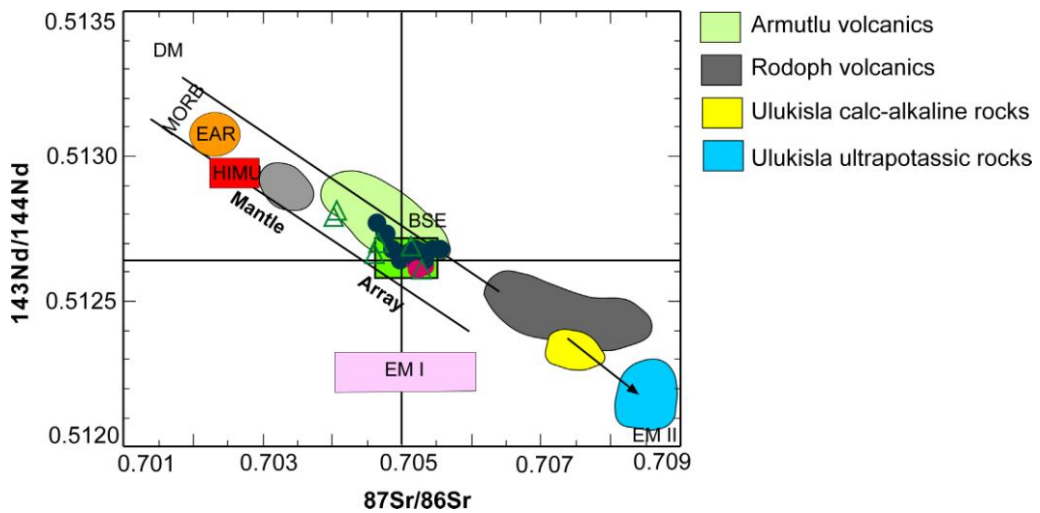


Figure 6. 12 $^{143}\text{Nd}/^{144}\text{Nd}$ vs $^{87}\text{Sr}/^{86}\text{Sr}$ isotope correlation diagram of Eocene volcanics (DM; Depleted mantle, MORB; Mid Ocean Ridge Basalt, EAR; European Asthenospheric Reservoir Cebria and Wilson (1995), HIMU; High μ (U/Pb) Reservoir, BSE; Bulk Silicate Earth, EMI; Enriched Mantle I; EMII; Enriched Mantle II)

This isotopic reservoir is defined by Cebria and Wilson, (1995) and regarded as an isotopically distinct mantle reservoir similar to plume component beneath Europe. It is placed between MORB mantle and HIMU component. Compositional similarity of the studied rocks and Late Eocene rocks from Ulukışla Basin and Çorum area suggests that their primary magmas may have been derived from similar sources which have inherited subduction related components. Besides, it is also important to note that on the whole, geochemical characteristics of the Eocene samples resemble those of post collisional lavas emplaced in the Alpine- Himalayan/ Tethyan orogenic belt (Apuseni volcanics, Rosu et al., (2004) and Basin and Range Province (western USA, Hawkesworth et al., 1995, Rogers et al., 1995), which are widely considered to have originated from enriched lithospheric mantle source. This also suggests a similar source and/or process for the generation of the Eocene volcanic rocks. Some of the Rhodope volcanics, on the other hand, display geochemically quite different properties. This can be attributed their source region since those rocks have been interpreted as having been derived from asthenospheric mantle source (Marchev et al., 2004), which is also evident from their HIMU like isotope compositions.

CHAPTER 7

CONCLUSIONS

Central Anatolia is a typical area where Late Cretaceous post-collisional magmatism is followed by Eocene extension and basin formation. These basins are locus of extensive volcanism. Calc- alkaline to mildly alkaline and ultra-potassic rocks formed coeval within these basins although they were erupted different part of the complex. This suggest that lithospheric mantle beneath the CACC is considerably heterogeneous, which make it possible to produce distinct magma types at the same time.

The Eocene volcanic rocks within the Central Anatolian Crystalline Complex CACC are represented by basaltic and andesitic rocks and have calc- alkaline to mildly alkaline character. Petrographical examination of these rocks suggests crystallization under disequilibrium conditions.

REE and multi element patterns of the studied rocks exhibit pronounced depletion in HFSE especially Nb and Ta and enrichment in LRE and LILE. HREE pattern of these rocks suggest derivation from a garnet free source.

Eocene samples display similar isotope compositions. Pb isotope compositions of the studied rocks seem to be related to the crustal contamination; on the other hand Sr and Nd isotope ratios reflect the source region.

Different degrees of partial melting from a common magma source then fractional crystallization of variable phases and crustal contamination are

important factors in controlling in compositional variations of the Eocene magmas.

The combined trace element and isotopic abundances of the studied rocks are consistent with derivation from a lithospheric source region that had been variably enriched in LILE and LRE before the eruption of the magmas.

Geochemical properties suggest that Eocene volcanism within the CACC was result of decompressional melting of phlogopite bearing enriched mantle source and lithospheric delamination is the most probable trigger that caused volcanism in the region.

Despite the fact that Eocene volcanic samples display subduction related geochemical signature, there is no evidence for being related to the contemporaneous subduction event, as suggested in previous works. But this signature is a consequence of paleo- subduction.

REFERENCES

- Aldanmaz, E., Pearce, JA., Thirlwall, MF., and Mitchell, JG., 2000. Petrogenetic evolution of late Cenozoic, post-collision volcanism in western Anatolia, Turkey. *Journal of Volcanology and Geothermal Research* 102, 67-95.
- Angus, D., A., Wilson, DC., Sandvol, E., and Ni, JF., 2006. Lithospheric structure of the Arabian and Eurasian collision zone in eastern Turkey from *S*-wave receiver functions *Geophys. J. Int.* 166, 1335–1346
- Akgün, F., Olgun, E., Kuşcu, İ., Toprak, V., and Göncüoğlu, M.C., 1995. Orta Anadolu Kompleksi'nin "Oligo-Miyosen" örtüsünün stratigrafisi, çökelme ortamı and gerçek yaşına ilişkin yeni bulgular: *Türkiye Petrol Jeologları Derneği Bülteni*, 6-1, 51-68.
- Akıman, O., Erler, A., Göncüoğlu, M.C., Güleç, N., Geven, A., Türeli, K., and Kadioğlu, Y., 1993. Geochemical characteristics of granitoids along the western margin of the Central Anatolian Crystalline Complex and their tectonic implications: *Geological Journal*, 28, 371-382.
- Alpaslan, M., 2000. Pazarcık Volkanitinin (Yıldızeli-Sivas) Mineralojik-Petrografik and Jeokimyasal Özellikleri, *Türkiye Jeoloji Bülteni*, Sayı: 43-2, 49-60.
- Alpaslan, M., Frei, R., Boztuğ, D., Kurt, M.A., and Temel, A., 2004. Geochemical and Pb-Sr-Nd Isotopic Constraints Indicating an Enriched Mantle Source for Late Cretaceous to Early Tertiary Volcanism, Central Anatolia, Turkey, *International Geology Review* 46, 1022-1041.

- Alpaslan, M., Boztuğ, D., Frei, R., Temel, A., and Kurt, MA., 2006. Geochemical and Pb–Sr–Nd isotopic composition of the ultrapotassic volcanic rocks from the extension-related Camardı-Ulukışla basin, Nigde Province, Central Anatolia, Turkey *Journal of Asian Earth Sciences* 27, 613-627.
- Alpaslan, M., and Temel, A., 2000. Petrographic and Geochemical Evidence for Magma Mixing and Crustal Contamination in the Post Collisional Calc-Alkaline Yozgat Volcanics, Central Anatolia, Turkey, *International Geology Review* 42, 850-863.
- Arndt, N.T., and Christensen, U., 1992. The role of lithospheric mantle in continental flood volcanism: thermal and geochemical constraints. *Journal of Geophysical Research* 97, 10967–10981.
- Arndt, N.T. Gerald K. Czamanske, J.L.W., and Valeri, A. F., 1993. Mantle and crust contributions to continental flood volcanism, *Tectonophysics* 213, 39-52.
- Atakay, Evren., 2009. Çorum güney batısındaki volkanik kayaçların jeolojik ve petrolojik özellikleri ve Alacahöyük kazısında arkeolojik çalışmalar. Doktora tezi (unpublished), Ankara Üniversitesi 194s.
- Ataman, G., 1972. Ankara'nın güneydoğusundaki granitik/granodiyoritik kütlelerden Cefalıkdağın radyometrik yaşı hakkında ön çalışma Hacettepe Üniv. Fen ve Müh. Bilimleri Dergisi, 2-1, 44-49.
- Aydar, E., and Gourgaud A 1993. Evolution of magma chambers and related petrogenetic processes of the Hasandag stratovolcano. *Yerbilimleri* 16, 101-113 (in Turkish with English abstract)

- Aydar, E., and Gourgaud, A., 1998. The geology of Mount Hasan stratovolcano, central Anatolia, Turkey. *Journal of Volcanology and Geothermal Research* 85, 129-152.
- Aydın, N.S., Göncüoğlu, M.C. and Erler, A., 1997. Granitoid magmatism in Central Anatolia. In: Boztuğ, D., Yılmaz-Şahin, S., Oflu, N. and Tatar, S. (Eds.) *Proceedings of TUBITAK-BAYG/NATO-D Program on "Alkaline Magmatism" (theoretical Consideration and a Field Excursion in Central Anatolia) 2-10 October, 1997*, 202, Department of Geological Engineering Sivas University, Sivas.
- Aydın, N.S, Göncüoğlu, M.C., and Erler, A., 1998 Latest Cretaceous magmatism in the Central Anatolian Crystalline Complex: brief review of field, petrographic and geochemical features. *Turkish Journal of Earth Science* 7-3, 258-268.
- Bacon, C. R., 1986 Magmatic inclusions in silicic and intermediate volcanic rocks. *Journal of Geophysical Research* 91, 6091-6112.
- Baker, J. A., Menzies, M. A., Thirlwall, M. F., and Macpherson, GC., 1997. Petrogenesis of Quaternary intraplate volcanism, Sana'a, Yemen: Implications for plume–lithosphere interaction and polybaric melt hybridization. *Journal of Petrology* 38, 1359–90.
- Baker, J., Peate, D., Waight, T., and Meyzen, C., 2004. Pb isotopic analysis of standards and samples using a ^{207}Pb – ^{204}Pb double spike and thallium to correct for mass bias with a double-focusing MC-ICP-MS. *Chemical Geology* 211, 275-303.
- Be'dard, J.H., 1999. Petrogenesis of boninites from the Betts Cove Ophiolite, Newfoundland, Canada: Identification of subducted source components. *Journal of Petrology* 40, 1853–1889.

- Bird, P., 1979. Continental delamination and the Colorado Plateau. *Journal of Geophysical Research* 84, 7561–71.
- Birgili, Ş., Yoldaş, R., and Ünalın, G., 1975. Çankırı- Çorum havzasının jeolojisi ve petrol olanakları, MTA rapor no: 5621, Ankara.
- Boztuğ, D., 1998. Post-collisional central Anatolian alkaline plutonism, Turkey. *Turkish Journal of Earth Sciences* 7, 145–165.
- Boztuğ, D., 2000. S-I-A type intrusive associations: geodynamic significance of synchronism between metamorphism and magmatism in Central Anatolia, Turkey. In *Tectonics and Magmatism in Turkey and the Surrounding Areas* (eds E. Bozkur, J.A. Winchester and J.A.D. Piper), pp 441-485. Geological Society of London, Special publication no. 173.
- Boztuğ, D., Tatar, S., Yılmaz- Şahin, S., and Harlavan, Y., 2003. The coexistence of S-type and I-type granitoids in the crustal thickening-related Felahiye pluton in the Anatolide-Tauride Terraine, NE Kayseri, Central Turkey. *International Conference the South Aegean Active Volcanic Arc: Present Knowledge and Future Perspectives, SAAVA-2003, 17-20 September, 2003, Milos Island, Greece, Book of Abstracts*, 47–48.
- Boztuğ, D., Harlavan, Y., Arehart, G.B., Satır, M. and Avcı, N. 2007. Kar age, whole-rock and isotope geochemistry of A-type granitoids in the Divriği-Sivas region, eastern-central Anatolia, Turkey. *Lithos* 97, 193–218.
- Boztuğ, D., Güney, Ö., Heizler, M., Jonckheere, RC., Tichomirowa, M., and Otlı, N., 2009. ^{207}Pb - ^{206}Pb , ^{40}Ar - ^{39}Ar and Fission-Track Geothermochronology Quantifying Cooling and Exhumation History of the Kaman- Kırşehir Region Intrusions, Central Anatolia, Turkey. *Turkish Journal of Earth Sciences* 18, 85-108.

- Bradshaw, TK., and Smith, E. I., 1994. Polygenetic Quaternary volcanism at Crater Flat, Nevada. *Journal of Volcanology and Geothermal Research* 63, 165–82.
- Büyükönel, G., 1986. Yozgat Yöresi Volkanitlerinin Asal ve İz Element Dağılımları, *MTA Dergisi*, 105/106, 97 -111.
- Cabanis, B., and Lecolle, M., 1989. Le diagramme La/10-Y/15-Nb/8: un outil pour la discrimination des series volcaniques et la mise en evidence des processus de melange et/ou de contamination crustale: *Comptes Rendus de l'Academie des Sci*, ser. II, 309: 2023–2029.
- Castro, A., Moreno-Ventas. I. and De La Rosa, 1991. Multi stage crystallization of tonalitic enclaves in granitoid rocks (Hercynian belt, Spain): implication for magma mixing. *Geo. Rund*, 80,109-120.
- Cebria, J.M., Wilson, M., 1995. Cenozoic mafic magmatism in western/central Europe: a common European asthenospheric reservoir? *Terra (Abstract)*, EUG 7, p. 162.
- Clark, M., and Robertson, A., 2002. The role of Early Tertiary Ulukışla Basin, southern Turkey, in suturing of the Mesozoic Tethys Ocean, *Journal of Geological Society, London* 159, 673-690.
- Clark, M., and Robertson, A., 2005. Uppermost Cretaceous–Lower Tertiary Ulukışla Basin, south-central Turkey: sedimentary evolution of part of a unified basin complex within an evolving Neotethyan suture zone. *Sedimentary Geology* 173, 15-51.
- Class, C., and Goldstein, S.L., 1997. Plume-lithosphere interactions in the ocean basins: constraints from the source mineralogy. *Earth and Planetary Science Letters* 150 3- 4, 245–260

- Clyne, A. M., 1999. complex magma mixing origin for rocks erupted in 1915, Lassen Peak California. *Journal of Petrology* 40, 105-232.
- Conticelli, S., Guarnieri, L., Farinelli, A., Mattei, M., Avanzinelli, R., Bianchini, G., Boari, E., Tommasini, S., Tiepolo, M., Prelevic, D., and Venturelli, G., 2009. Trace elements and Sr–Nd–Pb isotopes of K-rich, shoshonitic, and calc-alkaline magmatism of the Western Mediterranean Region: genesis of ultrapotassic to calc-alkaline magmatic associations in a post-collisional geodynamic setting. *Lithos* 107, 68–92.
- Couch, S., Sparks, R. S. J., and Carroll, M. R., 2001. Mineral disequilibrium in lavas explained by convective self-mixing in open magma chambers. *Nature* 411, 1037–1039.
- Coulon, C., Megartsi, M., Fourcade, S., Maury, R.C., Bellon, H., Louni-Hacini, A., Cotton, J., Coutelle, A., and Hermitte, D., 2002. Post-collisional transition from calc-alkaline to alkaline volcanism during the Neogene in Oranie (Algeria): magmatic expression of a slab breakoff. *Lithos* 62,87–110.
- Cox, K.G., Bell, J.D., and Pankhurst, R.J., 1979. The interpretation of igneous rock. George Allen and Unwin, London 450pp.
- Cox, K. G., and Hawkesworth, C., J., 1984. Relative contribution of crust and mantle to flood basalt magmatism Mahababeshwar area, Deccan traps. *Phil. Trans. R. Soc. London*, A310, 627-641.
- Cox, K.G., and Hawkesworth, C.J., 1985. Geochemical stratigraphy of the Deccan Traps at Mahabaleshwar, Western Ghats, India, with implications for open system magmatic processes. *Journal of Petrology* 26, 355–377.

- Çemen, İ., Göncüoğlu, M.C., and Dirik, K., 1999. Structural Evolution of the Tuz Gölü Basin in Central Anatolia, Turkey, *The Journal of Geology* 107, 693-706.
- Çevikbaş, A. and Öztunalı, Ö. 1991. Ore deposits in the Ulukışla- Çamardı (Niğde) Basin. *Jeoloji Mühendisliği*, 39, 22-40 (in Turkish with English abstract).
- Davidson, J.P., and Harmon, R.S., 1989. Oxygen isotope constraints on the origin of volcanic arc magmas from Martinique, Lesser Antilles. *Earth and Planetary Science Letters* 95, 255-270.
- Davidson, J.P., De Silva, S.I., Holden, P., and Halliday, A.N., 1990. Small-scale disequilibrium in a magmatic inclusion and its more silicic host. *Journal of Geophysical Research* 95, 17661-17676.
- Davidson, J.P., 1996. Deciphering mantle and crustal signatures in subduction zone magmatism. *Subduction Top to Bottom. Geophys. Monogr. 96*, American Geophysical Union, Washington, DC, 251–262.
- Davis, A. S., David, A.C., and White, W.M., 1998. Geochemistry of basalts from Escanaba trough for sediment contamination. *Journal of Petrology* 39, 841-858.
- Davies, J. H., and Von Blanckenburg, F. S., 1995. Slab break off: A model of lithosphere detachment and its test in the magmatism and deformation of collisional orogens. *Earth and Planetary Science Letters* 129, 327–43.
- Davies, G. R., Stolz, A. J., Mahotkin, I. L., Nowell, G. M., and Pearson, D. G., 2006. Trace Element and Sr–Pb–Nd–Hf Isotope Evidence for Ancient, Fluid-Dominated Enrichment of the Source of Aldan Shield Lamproites. *Journal of Petrology* 47-6, 1119-1146.

- Defant, M. J., and Drummond, M. S., 1990. Derivation of some modern arc magmas by melting of young subducted lithosphere. *Nature* 347, 662–665.
- Demirer, A., Özcelik, Y., and Özkan, R., 1992. Çankırı- Çorum basenindeki Eosen volkanitlerinin petrografisi. TPAO Rap. No. 1810 (unpublished).
- Deniel, C., Aydar, E., and Gourgaud, A., 1998. The Hasandag stratovolcano (central Anatolia, Turkey): evolution from calc-alkaline to alkaline magmatism in a collision zone. *Journal of Volcanology and Geothermal Research* 87, 275–302.
- DePaolo, D.J., 1981. Trace element and isotopic effects of combined wall rock assimilation and fractional crystallization. *Earth and Planetary Science Letters* 53, 189–202.
- DePaolo, D., and Daley, E. E., 2000. Neodymium in basalts of the southwest basin and range and lithospheric thinning during continental extension. *Chemical Geology* 169, 157-185.
- Ding, L., Kapp, K., Yue, Y., Lai, Q., 2007. Post collisional calc- alkaline lavas and xenoliths from the southern Qiangtang terrane, central Tibet. *Earth and Planetary Science Letters* 254, 28-38.
- Dirik, K. and Göncüoğlu, M.C., 1996. Neotectonic characteristics of the Central Anatolia: *International Geology Review* 38-9, 807-817.
- Dirik, K., Göncüoğlu, M. C., and Kozlu, H., 1999. Stratigraphy and Pre Miocene Tectonic Evolution of the Southwestern Part of the Sivas Basin, Central Anatolia, Turkey. *Geological Journal* 34, 303-319.

- Downes, H., Upton, B.G.J., Handisyde, E., and Thirlwall, M.F. 2001. Geochemistry of mafic and ultramafic xenoliths from Fidra (Southern Uplands, Scotland): implications for lithospheric processes in Permo-Carboniferous times, *Lithos* 58, 105-124.
- Dungan, MA, and Rhodes, JM., 1978. Residual glasses and melt inclusions in basalts from DSDP Legs 45 and 46: evidence for magma mixing. *Contributions to Mineralogy and Petrology* 67, 417–431.
- Duggen, S., Hoernle, K., van den Bogaard, P., Garbe-Schönberg, D., 2005. Post-collisional transition from subduction- to intraplate type magmatism in the westernmost Mediterranean: evidence for continental-edge delamination of subcontinental lithosphere. *Journal of Petrology* 46, 1155–1201.
- Dupuy, C., Liotard, JM., Dostal, J., 1992. Zr/Hf fractionation in intraplate basaltic rocks - carbonate metasomatism in the mantle source. *Geochimica et Cosmochimica Acta* 56(6):2417–2423.
- Düzgören, Aydın, N., Malpas, W., Göncüoğlu, M.C. and Erler, A., 2001. Post collisional magmatism in Central Anatolia, Turkey: field, petrographic and geochemical constraints. *International Geology Review* 43-8, 695-710.
- Eisele, J., Sharma, M., Galer, S. J. G., Blichert-Toft, J., Devey, C. W., and Hofmann, A. W., 2002. The role of sediment recycling in EM-1 inferred from Os, Pb, Hf, Nd, Sr isotope and trace element systematics of the Pitcairn hotspot. *Earth and Planetary Science Letters* 196, 197-212.
- Ellam, R. M., 1992. Lithospheric thickness as a control on basalt geochemistry, *Geology* 20, 153-156.

- Elliott, T., Planck, T., Zindler, A., White, W., and Bourdon, B., 1997. Element transport from slab to volcanic front at the Mariana arc. *Journal of Geophysical Research* 102, 14991–15019.
- England, P., and Houseman, G., 1987. Extension during Continental Convergence, With Application to the Tibetan Plateau. *Journal of Geophysical Research* 94, 17561-17579.
- Ercan, T., Yıldırım, T., Akbaşlı, A., 1987. Gelveri (Niğde)-Kızılçın (Nevşehir) arasındaki volkanizmanın özellikleri (Characteristics of volcanism between Gelveri (Niğde)- Kızılçın (Nevşehir)), *Jeomorfoloji Dergisi* 15, 7-36.
- Ercan, T., Tokel, S., Matsuda, JI., Ui, T., Notsu, K., Fujitani, T., 1992. New geochemical, isotopic and radiometric data of the Quaternary volcanism of Hasandağı-Karacadağ (Central Anatolia). *TJK Bülteni*, 7, 8-21 (in Turkish with English abstract).
- Erdoğan, B., Akay, E., Uğur, M.S., 1996. Geology of the Yozgat Region and Evolution of the Collisional Çankırı Basin, *International Geology Review* 38, 788-806.
- Erler, A., and Göncüoğlu, M.C., 1996. Geologic and tectonic setting of Yozgat Batholith, Northern Central Anatolian Crystalline Complex, Turkey. *International Geology Review* 38, 714-726.
- Ernst, R.E., Buchan, K.L., Campbell, I.H., 2005. Frontiers in large igneous province. *Lithos* 79, 271–297.
- Ewart, A., Marsh, J. S., Milner, S. C., Duncan, A. R., Kamber, B. S., and Armstrong, R. A., 2004. Petrology and Geochemistry of Early Cretaceous Bimodal Continental Flood Volcanism of the NW Etendeka,

Namibia. Part 1: Introduction, Mafic Lavas and Re-evaluation of Mantle Source Components. *Journal of Petrology* 45, 59-105.

Fan, WM., Guo, F., Wang, YJ., Lin, G., 2003. Late Mesozoic calc-alkaline volcanism of post-orogenic extension in the northern Da Hinggan Mountains, northeastern China. *Journal of Volcanology and Geothermal Research* 121,115-135.

Fan, WM., Guo, F., Wang, YJ., Zhang, M., 2004. Late Mesozoic volcanism in the northern Huaiyang tectono-magmatic belt, central China: partial melts from a lithospheric mantle with subducted continental crust relicts beneath the Dabie orogen? *Chemical Geology* 209, 27-48.

Fan, W., Guo, F., Wang, Y., and Zhang, H., 2007. Late Mesozoic mafic magmatism from the North China Block: constraints on chemical and isotopic heterogeneity of the subcontinental lithospheric mantle. *Geological Society of London, Special Publications* 280; p. 77-100.

Fayon, A.K., Whitney, D.L., Teyssier, C., Garver, J.I., and Dilek, Y., 2001. Effects of plate convergence obliquity on timing and mechanisms of exhumation of a mid-crustal terrain, the Central Anatolian Crystalline Complex: *Earth and Planetary Science Letters* 192, 191-205.

Feeley, T.C., and Sharp, Z.D., 1996. Chemical and hydrogen isotope evidence for in situ dehydrogenation of biotite in silicic magma chambers. *Geology* 24, 1021-1024.

Feeley, T, C., Dungan, M, A., Frey, F, A., 1998. Geochemical constraints on the origin of mafic and silicic magmas at Cordon El Quadel, tatará- San Pedro complex, central Chile. *Contributions to Mineralogy and Petrology* 131, 393- 411.

- Fitton, J.G., James, D., and Leeman, W.P., Basic Magmatism Associated With Late Cenozoic Extension in the Western United States: Compositional Variations in Space and Time. *Journal of Geophysical Research* 96, 13693- 13711.
- Floyd, P.A., Göncüoğlu, M.C., Winchester, J.A., and Yalınız, M.K., 2000. Geochemical character and tectonic environment of Neotethyan ophiolitic fragments and metabasites in the Central Anatolian Crystalline Complex, Turkey. Bozkurt, E., Winchester, J. A. and Piper, J. D. A. (eds) *Tectonics and Magmatism in Turkey and the Surrounding Area*. Geological Society, London, Special Publications, 173, 183-202.
- Frey, F.A., Green, D.H., and Roy, S.D., 1978. integrated models of basalt petrogenesis: a study of quartz tholeiites to olivine melilitites from southeastern Australia utilizing geochemical and experimental petrological data. *Journal of Petrology*, 19, 463-513.
- Frey, F.A., McNaughton, N.J., Nelson, D.R., de Laeter, J.R., Duncan, R.A., 1996. Petrogenesis of the Bunbury basalt, Western Australia: interaction between the Kerguelen plume and Gondwana lithosphere? *Earth and Planetary Science Letters* 144, 163–183.
- Furman, T., and Graham, D., 1999. Erosion of lithospheric mantle beneath the east African rift system: geochemical evidence from the Kivu volcanic province. *Lithos* 48, 237–262.
- Gallagher, K., Hawkesworth, C., 1993. Dehydration melting and the generation of continental flood basalts. *Letters to Nature* 358, 57-59.
- Gençaliolu Kuşcu, G., Geneli, F., 2010. Review of post-collisional volcanism in the Central Anatolian Volcanic Province (Turkey), with special

reference to the Tepekoy Volcanic Complex. *International Journal of Earth Science* 99, 593–621

Gertisser, R., and Keller, J., 2000. from basalt to dacite: origin and evolution of the calkalkaline series of Salina, Aeolian Arc, Italy. *Contributions to Mineralogy and Petrology* 139, 607-626.

Gill, JB., 1981. *Orogenic Andesites and Plate Tectonics*. Springer Verlag, New York, pp 385.

Gioncada, T., A., Mazzuolia, R., Milton, A.J., 2005. Magma mixing at Lipari (Aeolian Islands, Italy): Insights from textural and compositional features of phenocrysts, *Journal of Volcanology and Geothermal Research* 145, 97– 118.

Gök, R., Pasyanos, EM, and Zor, E., 2007. Lithospheric structure of the continent–continent collision zone: eastern Turkey *Geophysical Journal International* 169, 1079–1088.

Gökten, E., and Floyd, P., 1987. Geochemistry and tectonic environment of Şarkışla area volcanic rocks in central Anatolia: Turkey. *Mineralogical Magazine* 51, 553-559.

Göncüoğlu, M.C., 1977. *Geologie des westlichen Niğde Massivs*. PhD Thesis, University of Bonn, 181p.

Göncüoğlu, M.C., 1981. Niğde Masifinin Jeolojisi. *Türkiye Jeoloji Kurumu, İç Anadolu'nun Jeolojisi Simpozyumu*, 16-19.

Göncüoğlu, M.C., 1986. Geochronological data from the southern part (Ni.de Area) of the Central Anatolian Massif. *Mineral Research and Exploration Institute (MTA) of Turkey Bulletin* 105/106, 83–96.

- Göncüođlu, M.C., 1992. Structural and stratigraphical framework of the Central Anatolian Tertiary Basins. Guide Book: Introduction to the Early Paleogene of the Haymana-Polatlı Basin, 1-11, MTA Genel Müdürlüğü Yayını, Ankara.
- Göncüođlu, M.C. and Türeli, T.K., 1994. Alpine collisional-type granitoids from western Central Anatolian Crystalline Complex: Journal of Kocaeli University, 1, 39-46.
- Göncüođlu, M.C. and Toprak, V., 1992. Neogene and Quaternary volcanism of Central Anatolia: a volcano- structural evaluation: Bull.de la Section Volcanologie, Soc. Geol. France, 26, 1-6..
- Göncüođlu, M.C., Toprak, V., Kuşcu, İ., Erler, A., and Olgun, E., 1991. Orta Anadolu Masifinin Batı Bölümünün Jeolojisi, Bölüm I: Güney Kesim, TPAO Proje Rapor No: 2909, 140s.
- Göncüođlu, M.C., Erler, A., Toprak, V., Yalınız, K., Olgun, E., and Rojay, B., 1992. Orta Anadolu Masifinin Batı Bölümünün Jeolojisi, Bölüm II: Orta Kesim, TPAO Proje Rapor No: 3155, 76s.
- Göncüođlu, M.C., Erler, A., Toprak, V., Olgun, E., Yalınız, K., Kuşcu, İ., Köksal, S., and Dirik, K., 1993a. Orta Anadolu Masifinin Orta Bölümünün Jeolojisi, Bölüm III, Orta Kızılırmak Tersiyer Baseninin Jeolojik Evrimi, TPAO Proje Rapor No: 3313, 104.
- Göncüođlu, M.C., Toprak, V., Olgun, E., Kuşcu, İ., Erler, A. and Yalınız, K., 1993b. Tertiary Evolution of Central Kızılırmak Basin: 8th Meeting, Assoc. European Geological Soc., 19-26 Sept. Budapest, Abstracts, p 19.

Göncüoğlu, M.C., Dirik, K., Erler, A., and Yalınız, K., 1994a. Orta Anadolu Masifinin Doğu Bölümünün Jeolojisi Bölüm IV, Orta Anadolu Masifinin Sivas Baseni ile İlişkisi, TPAO Rapor No:3535, 135s.

Göncüoğlu, M.C., Olgun, E., Kuşcu, İ., Toprak, V., Kozlu, H., Dirik, K., Erler, A. and Yalınız, K., 1994b. Orta Kızılırmak Tersiyer Baseninin Jeolojisi and Orta Anadolu'nun Tersiyer Tektonik Olaylarındaki Rolü: Türkiye 10. Petrol Kongresi, Ankara, Bildiriler, 77.

Göncüoğlu, M.C., Dirik, K., Olgun, E., Kuşcu, İ., and Kozlu, H., 1995. Evolution of the Kızılırmak Basin: a prototype of Tertiary Basins in Central Anatolia: EUG 8. Biennial Meeting; Strasbourg, 9-14 April 1995, Terra Abstracts, 5, 275.

Göncüoğlu, M.C., Köksal, S. and Floyd, P.A., 1997. Post-collisional A-type magmatism in the Central Anatolian Crystalline Complex; petrology of the İdişdağı Intrusives (Avanos, Turkey). Turkish Journal of Earth Science 6, 65-76.

Göncüoğlu, M. C., Dirik, K.; Erler, A.; Toprak, V., Yalınız, K.; Özgül, L., and Çemen, I. 1997. Tuzgölü Havzasının batı kesiminin temel jeolojik sorunları. Unpubl. TPAO rep. no. 3753.

Göncüoğlu, M.C., Yalınız, K., Özgül, L. and Toksoy, F., 1998. Orta Anadolu Ofiyolitlerinin petrojenezi: İzmir-Ankara-Erzincan Okyanus kolunun evrimine bir yaklaşım. (Petrogenesis of the Central Anatolian Ophiolites: an approach to the evolution of the İzmir-ankara-Erzincan Branch of Neotethys) TUBITAK- Rap. No.:YDABCAG-85, 61p.

Göncüoğlu, M.C., Turhan, N., Şentürk, K., Özcan, A., Uysal, S., Yalınız, M.K. 2000. A geotraverse across northwestern Turkey: tectonic units of the Sakarya region and their tectonic evolution. in: Bozkurt, E., Winchester,

J., A., Piper, J., D., A., (eds), Tectonics and Magmatism in Turkey and the Surrounding Area. Geological Society of London, Special Publications, 173, 139-161.

Görür, N., Oktay, F. Y., Seymen. İ., and Şengör, A.M.C., 1984. Paleotectonic evolution of the Tuzgözü Basin complex, central Anatolia (Turkey): Sedimentary record of Neo-Tethyan closure. In the geological evolution of the eastern Mediterranean (eds. J.E. Dixon and A.H.F. Robertson), pp 467-482. Geological Society of London, Special publications 17.

Görür, N., and Şengör, A.M.C., 1998. Tectonic evolution of the central Anatolian basins. International Geology Review, 40831-850.

Green D.H., Edgan, H.D., Beasley, P., Kiss, E., and Ware, N.G., 1974. Upper mantle source for some hawaiites, mugarites and benmorites. Contrib. Mineral and Petrol., 48, 33-43.

Gürer, Ö., F., and Aldanmaz, E., 2002. Origin of the Upper Cretaceous - Tertiary basins within the Tauride Anatolide platform in Turkey. Geological Magazine 139, 191-197.

Gürsoy, H., Piper, J.D.A., Tatar, O., and Temiz, H., 1997. A palaeomagnetic study of the Sivas Basin, central Turkey: Crustal deformation during lateral extrusion of the Anatolian Block. Tectonophysics 271, 89-105.

Handley, H. K., Macpherson, C. G., Davidson, J.P., Berlo, K., and Lowry, D., 2007. Constraining Fluid and Sediment Contributions to Subduction-Related Magmatism in Indonesia: Ijen Volcanic Complex. Journal of Petrology (48), 1155-1183.

Harangi, Sz., and Lenkey, L., 2007. Genesis of the Neogene to Quaternary volcanism in the Carpathian–Pannonian Region: role of subduction,

extension and mantle plume. In: Cenozoic volcanism in the Mediterranean area (L. Beccaluva, G. Bianchini and M. Wilson, eds.). Geological Society of America Special Paper, 418, 67–92.

Harangi, L., Downes, H., Thirlwall, M., and Gmeling, K., 2007. Geochemistry, Petrogenesis and Geodynamic Relationships of Miocene Calc-alkaline Volcanic Rocks in the Western Carpathian Arc, Eastern Central Europe. *Journal of Petrology* 48, 2261- 2287.

Hart, S.R., 1984. A large-scale isotope anomaly in the Southern Hemisphere mantle. *Nature* 309, 753–757.

Hart, S, R., and Davies, K., E., 1978. Nickel partitioning between olivine and silicate melt. *Earth and Planetary Science Letters* 40, 213-219.

Hawkesworth, C., Rogers, NW., Van Calsteren, PWC., and Menzies, MA., 1984. Mantle enrichment processes. *Nature* 311, 331- 335.

Hawkesworth, C., Erlank, AJ., Kempton, PD., and Waters, FG., 1990. Mantle metasomatism: Isotope and trace-element trends in xenoliths from Kimberley, South Africa. *Chemical Geology* 85, 19-34.

Hawkesworth, C., and CJ, Turner S, Gallagher K, Hunter A, Bradshaw T, Rogers N 1995. Calc-alkaline magmatism, lithospheric thinning and extension in the Basin and Range. *Journal of Geophysical Research* 100, 10271-10286.

Hawkesworth, C., Turner, S., Peate, D., McDermott, F. and van Calsteren, P. 1997. Elemental U and Th variations in island arc rocks: implications for U-series isotopes. *Chemical Geology* 139, 207–221.

- Hawkesworth, C. J., Blake, S., Evans, P., Hughes, R., MacDonald, R., Homas, L. E., Turner, S. P. & Zellmer, G. 2000. Time scales of crystal fractionation in magma chambers – Integrating physical, isotopic and geochemical perspectives. *Journal of Petrology* 41, 991–1006.
- Hergt, J.M., Peate, D.W., Hawkesworth, C.J., 1991. The petrogenesis of Mesozoic Gondwana low-Ti flood basalts. *Earth and Planetary Science Letters* 105, 134–148.
- Hibbard, M.J., 1991. Textural anatomy of twelve magma-mixed granitoid systems. In: Didier, J., Barbarin, B. (Eds.), *Enclaves and Granite Petrology*. *Developments in Petrology* 13. Elsevier, pp. 431–444.
- Hofmann, A.W., 1988. Chemical differentiation of the Earth: the relationship between mantle, continental crust, and oceanic crust. *Earth and Planetary Science Letters* 90, 297–314.
- Hofmann, A. W., 1997. Mantle geochemistry: the message from oceanic volcanism. *Nature* 385, 219–229.
- Holland, M. H. B. M., Pimentel, M. M., Sa, E. F. J., 2003. Paleoproterozoic subduction-related metasomatic signatures in the lithospheric mantle beneath NE Brazil: inferences from trace element and Sr–Nd–Pb isotopic compositions of Neoproterozoic high-K igneous rocks *Journal of South American Earth Sciences* 15, 885–900.
- Houseman, G.A., McKenzie, D.P., Molnar, P.J., 1981. Convective instability of a thickened boundary layer and its relevance for the thermal evolution of continental convergent belts. *Journal of Geophysical Research* 86, 6115– 6132.

- Houseman, G.A., Molnar, P., 1997. Gravitational (Rayleigh-Taylor) instability of a viscosity and convective thinning of continental layer with non-linear lithosphere. *Geophysical Journal International* 128, 125-150.
- Humphreys, M. C.S., Jon D. Blundy, J. D., and Sparks, R.S. J., 2006. Magma evolution and open-system processes at Shiveluch Volcano: insights from phenocryst zoning, *Journal of Petrology* 47, 2303-2334.
- İlbeyli, N., 2005. Mineralogical–geochemical constraints on intrusives in central Anatolia, Turkey: tectono-magmatic evolution and characteristics of mantle source. *Geol Mag* 142-2, 187–207
- İlbeyli, N., and Pearce, J., 1997. Petrogenesis of collision related Anatolian granitoids, Turkey. *European Union of Geoscience (EUG)*. Strasbourg, France 9, 502.
- İlbeyli, N., and Pearce, J., 2005. Petrogenesis of igneous enclaves in plutonic rocks of the Central Anatolian Crystalline Complex, Turkey. *International Geology Review* 47, 78-97.
- İlbeyli, N., Pearce, J.A., Thirlwall, M.F., and Mitchell, J.G., 2004. Petrogenesis of collision-related plutonics in Central Anatolia, Turkey. *Lithos* 72, 163–182.
- Ionov, D.A., O'Reilly, S.Y., and Griffin, W.L., 1997. Volatile-bearing minerals and lithophile trace elements in the upper mantle. *Chemical Geology* 141, 153–184.
- Ionov, D.A., and Harmer, R.E., 2002. Trace element distribution in calcite–dolomite carbonatites from Spitskop: inferences for differentiation of carbonatite magmas and the origin of carbonates in mantle xenoliths. *Earth and Planetary Science Letters* 131, 341–356.

- Irvine, T.N., and Baragar W.R.A., 1971. A guide to the chemical classification of the common volcanics rocks. *Canadian Journal of Earth Science* 8, 523-548.
- İşler, F., 1988. Mineralogical-petrographical and geochemical investigation of Çiftehane (Niğde) volcanics: *Earth Science- Geosound* 26, 47-56. (in Turkish with English abstract).
- Jahn, B.M., Wu, F.Y., Lo, C.H., Tsai, C.H., 1999. Crust–mantle interaction induced by deep subduction of the continental crust: geochemical and Sr–Nd isotopic evidence from post-collisional mafic–ultramafic intrusions of the northern Dobie complex, central China. *Chemical Geology* 157, 119–146.
- Jochum, K.P., McDonough, W.F., Palme, H., and Spettel, B., 1989. Compositional constraints on the continental lithospheric mantle from trace elements in spinel peridotite xenoliths. *Nature* 340, 548– 550.
- Jourdan, F., Bertrand, H., Scha Rer U., Blichert-Toft, J., Feraud, G., and Kampunzu, A. B., 2007. Major and Trace Element and Sr, Nd, Hf, and Pb Isotope Compositions of the Karoo Large Igneous Province, Botswana Zimbabwe: Lithosphere vs Mantle Plume Contribution. *Journal of Petrology* 48, 1043-1077.
- Kadioğlu, Y. K., and Güleç, N., 1997. Triple relations of the granitoid enclaves and gabbro of the Ağaçören Intrusive Suite (Central Anatolia–Turkey): geological, petrographic and geochemical constraints. *Geoenviron '97*, International Symposium on Geology and Environment, İstanbul, Abstract, 54.

- Kadiođlu, Y. K., Dilek Y, Güleç, N., Foland, KA., 2003. Tectonomagmatic evolution of bimodal plutons in the Central Anatolian Crystalline Complex, Turkey. *Journal of Geology* 111-6, 671–690.
- Kadiođlu, Y. K., and Dilek, Y., 2009. Structure and geochemistry of the adakitic Horoz granitoid, Bolkar Mountains, south-central Turkey, and its tectonomagmatic evolution. *International Geology Review*, 1-31.
- Kara, H., and Dönmez, 1990. 1/100.000 ölçekli açınısama nitelikli Türkiye Jeoloji Haritaları Serisi, Kırşehir G17 Paftası, No:34 MTA, Ankara.
- Kay, S.M., Ramos,V.A., and Marquez, M., 1993. Evidence in Cerro Pampa volcanic rocks for slab-melting prior to ridge-trench collision in Southern South America. *Journal of Geology* 101, 703–714.
- Kay, R. W., and Kay, S. M., 1993. Delamination and delamination magmatism. *Tectonophysics* 219, 177–189.
- Kaymakçı, N., White, S. H., and Van Dijk, P.M., 2003. Kinematic and structural development of the Çankırı Basin (Central Anatolia, Turkey): a paleostress inversion study. *Tectonophysics*, 364, 85–113.
- Kaymakçı, N., Özçelik, Y., White, SH., and Van Dijk, P.M., 2009. Tectono-stratigraphy of the C, ankırı Basin: Late Cretaceous to early Miocene evolution of the Neotethyan Suture Zone in Turkey. Van Hinsbergen, D. J. J., Edwards, M. A. and Govers, R. (eds): *Collision and Collapse at the Africa–Arabia–Eurasia Subduction Zone*. The Geological Society, London, Special Publications, 311, 67–106.
- Keller, J., 1974. Quaternary maar volcanism near Karapınar in central Anatolia. *Bulletin of Volcanology*, 38 378-396.

- Kempton, P.D., Fitton, J.G., Hawkesworth, C., and Ormerod, D.S., 1991. Isotopic and Trace Element Constraints on the Composition and Evolution of the Lithosphere Beneath the Southwestern United States. *Journal of Geophysical Research* 96, 13713- 13735.
- Kepezhinskas, P., Mcdermott, F., Defant, M.J., Hochstaedter, A., Drummond, M.S., Hawkesworth, C.J., Koloskov, A., Maury, R.C., Bellon, H., 1997. Trace element and Sr–Nd –Pb isotopic constrains on a three component model of Kamchatka arc petrogenesis *Geochimica et Cosmochimica Acta* 61, 577– 600.
- Keskin, M., 2002. FC-Modeler: a Microsoft® Excel© spreadsheet program for modeling Rayleigh fractionation vectors in closed magmatic systems. *Computers and Geosciences* 28- 8, 919–928.
- Keskin, M., Genç, S., C., and Tüysüz, O., 2008. Petrology and geochemistry of middle Eocene volcanic units in north- central Turkey: Evidence for magma generation by slab break off following the closure of northern Neotethys ocean. *Lithos* 104, 267-305.
- Ketin, İ., 1955. Yozgat bölgesinin jeolojisi and Orta Anadolu Masifinin tektonik durumu, *TJK Bülteni*, C. VI, sayı 1, 1-40.
- Kieffer, B., Arndt, N., Lapierre, H., Bastien, F., Bosch, D., Pecher, A., Yirgu, G., Ayalew, D., Weise, D., Jerram, D.A., Keller, F., Meugniot, C., 2004. Flood and shield basalts from Ethiopia: magmas from the African superswell. *Journal of Petrology* 45, 793–834.
- Koçak, K., Kurt, H., Zedef, V., and Ferre, E.C., 2007. Characteristics of the amphibolites from Nigde metamorphics (Central Turkey), deduced from whole rock and mineral chemistry. *Geochemical Journal* 41, 241- 257.

- Koçbulut, F., Şahin-Yılmaz, S., Tatar, O., 2001. Akdağmadeni (Yozgat)-Yıldızeli (Sivas) arasındaki Kaletpe volkanitinin mineralojik-petrografik and jeokimyasal özellikleri, İst. Üniv. Müh. Fak. Yerbilimleri Dergisi 14;1-2, 77-91.
- Köksal, S., and Göncüoğlu, M. C., 1997. Geology of the İdiş Dağı–Avanos area (Nevşehir–Central Anatolia): Mineral Research and Exploration Institute Bulletin 119, 41–58.
- Köksal, S., Göncüoğlu, M.C., and Floyd, P.A., 2001. Extrusive members of post collisional A-type magmatism in Central Anatolia: Karahıdır Volcanics, İdiş Dağı-Avanos area, Turkey. International Geology Review 43-8, 683-694.
- Köksal, S., Romer, R.L., Göncüoğlu, M.C., and Toksoy-Köksal, F., 2004. Timing of the transition from the post-collisional to A-type magmatism: titanite U/Pb ages from the alpine Central Anatolian Granitoids, Turkey. International Journal of Earth Science 93, 974-989.
- Köksal, S., and Göncüoğlu, MC., 2008. Sr and Nd isotopic characteristics of some S- I- and A-type granitoids from Central Anatolia. Turkish Journal of Earth Science 17,111–127.
- Kuleli, S., Toksöz, M., Gürbüz, C., Gök, R., and Schultz, C., 2004. Crustal Structure Study in Turkey with Controlled Seismic Sources. American Geophysical Union, Fall Meeting 2004, abstract #S13B-1058.
- Kurt, M.A., Alpaslan, M., Göncüoğlu, M.C., and Temel, A., 2008. Geochemistry of Late Stage Medium to High-K Calc-Alkaline and Shoshonitic Dykes in the Ulukışla Basin (Central Anatolia, Turkey): Petrogenesis and Tectonic Setting. Geochemistry International 46, 1145-1163.

- Kürkçüoğlu, B., Şen, E., Aydar, E., Gourgaud, A., and Gündoğdu, N., 1998. Geochemical approach to magmatic evolution of Mt. Erciyes stratovolcano Central Anatolia, Turkey. *Journal of Volcanology Geothermal Research* 85, 473–494.
- Kürkçüoğlu, B., Furman, T., and Hannan, B., 2008. Geochemistry of post collisional mafic lavas from the north Anatolian fault zone, northwestern Turkey. *Lithos* 101, 416-434.
- Langmuir, CH., and Klein, EM., 1992. Petrological systematics of mid-ocean ridge basalts: constraints on melt generation beneath ocean ridges. In: Morgan JP, Blackman DK, Sinton JM (eds) *Mantle flow and melt generation at mid-ocean ridges*. American Geophysical Union, Washington, DC, *Geophysical Monograph* 71, 183–280.
- Leat, P.T., Livermore, L.A., Millar, I.L., and Pearce, J.A., 2000. Magma Supply in Back-arc Spreading Centre Segment E2, East Scotia Ridge. *Journal of Petrology* 41, 845-866.
- Lightfoot, P.C., Hawkesworth, C.J., Hergt, J., Naldrett, A.J., Gorbachev, N.S., Fedorenko, V.A., Doherty, W., 1993. Remobilization of the continental lithosphere by a mantle plume: major-, trace-element, and Sr-, Nd-, and Pb-isotope evidence from picritic and tholeiitic lavas of the Noril'sk District, Siberian Traps, Russia. *Contribution to Mineralogy and Petrology* 114, 171–188.
- Lindsay, J., M., Trumbull, R., B., and Siebel, W., 2005. Geochemistry and petrogenesis of late Pleistocene to Recent volcanism in Southern Dominica, Lesser Antilles. *Journal of Volcanology and Geothermal Research* 148, 253-294.

- Lustrino, M., Wilson, M., 2007. The circum-Mediterranean anorogenic Cenozoic igneous province. *Earth Science Reviews* 81, 1-65.
- Lustrino, M., Morra, V., Fedele, L., and Serracino, M., 2007. The transition between “orogenic” and “anorogenic” magmatism in the western Mediterranean area: the Middle Miocene volcanic rocks of Isola del Toro (SW Sardinia, Italy). *Terra Nova* 19, 148- 159.
- Lünel, AT., 1985. An approach to the naming, origin and age of Baranadağ monzonite of the Kırşehir intrusive suite. *METU Journal of Pure and Applied Sciences* 18, 385–404.
- Mackenzie, W.S., Donaldson, C.H., and Guilford, C., 1988. *Atlas of igneous rocks and their textures*. Longman Scientific and Technical, Londra, 148p.
- MacLean, WH., and Barrett, TJ., 1993. Lithochemical techniques using immobile elements. *Journal of Geochemical Exploration* 48,109–133.
- Mahoney, J.J., Natland, J.H., White, W.M., Poreda, R., Bloomer, S.H., Fisher, R.L. and Baxter, A.N., 1989. Isotopic and geochemical provinces of the Indian Ocean spreading centers. *Journal of Geophysical Research* 94: 4033- 4052.
- Mahoney, J. J., Jones, W. B., Frey, F. A., Salters, V. J. M., Pyle, D. G., and Davies, H. L., 1995. Geochemical characteristics of lavas from Broken Ridge, the Naturaliste Plateau and southernmost Kerguelen Plateau: Cretaceous plateau volcanism in the southeast Indian Ocean: *Chemical Geology* 120, 315–345.
- Marchev, P., Raicheva, R., Downes, H., Vaselli, O., Chiaradia, M., and Moritz, R., 2004. Compositional diversity of Eocene–Oligocene basaltic

magmatism in the Eastern Rhodopes, SE Bulgaria: implications for genesis and tectonic setting. *Tectonophysics* 393, 301–328.

Martin, H., Smithies, R. H., Rapp, R., Moyen, J. F. and Champion, D. 2005. An overview of adakite, tonalite–trondhjemite–granodiorite (TTG), and sanukitoid: relationships and some implications for crustal evolution. *Lithos* 79, 1–24.

Maury, R. C., Fourcadeb, S., Coulon C., El Azzouzia, M, Bellona, H., Coutellea Al., Ouabadib A., Semroude, B., Megartsie M., Cottena J., Belanteure O., Louni-Hacinie A., Piquéa A., Capdevilab R., Hernandezf J., and Réhaulta, J.-P., 2000. Post collisional Neogene magmatism of the Mediterranean Maghreb margin; a consequence of slab break off. *Earth and Planetary Sciences* 331, 159-173.

Maury, RC., Pubellier, M., Rangin, C., Wulput, L., Cotton, J., Socquet, A., Bellon, H., Guillaud, J-P., and Htun, HM., 2004. Quaternary calc-alkaline and alkaline volcanism in an hyper-oblique convergence setting, central Myanmar and western Yunan. *Bull Soc Ge'ol Fr.*,t 175, no 5:461–472.

McDonald, R., Hawkesworth, C.J., Heath, E., 2000. The Lesser Antilles volcanic chain: a study in arc magmatism. *Earth Science Reviews* 49, 1-76.

McCulloch, M. T., and Gamble, J. A., 1991. Geochemical and geodynamical constraints on subduction zone magmatism. *Earth and Planetary Science Letters* 102, 358–74.

McDonough, W.F., 1990. Constraints on the composition of the continental lithospheric mantle. *Earth and Planetary Science Letters* 101, 1–18.

- McDonough, WF., and Sun, SS., 1995. The composition of the Earth. *Chemical Geology* 120:223–253.
- McKenzie, D., and O’Nions, R.K., 1991. Partial melt distributions from inversion of rare earth element concentrations. *Journal of Petrology* 32, 1021–1091.
- McKenzie, D.P. and O’Nions, R.K. 1995. The source regions of ocean island basalts. *Journal of Petrology* 36, 133–159.
- McKenzie, D.P., and Bickle, M.J., 1988. The volume and composition of melt generated by extension of the lithosphere. *Journal of Petrology* 29, 625–679.
- Menzies, MA., Rodgers, N., Tindle, A., and Hawkesworth, CJ., 1987. Metasomatic and enrichment processes in lithospheric peridotites, and effect of asthenosphere-lithosphere interaction. In: Menzies M, Hawkesworth CJ (eds) *Mantle Metasomatism*. Academic Press, London, 313–361.
- Meschede, M., 1986. A method of discriminating between different types of mid-ocean ridge basalts and continental tholeiites with the Nb–Zr–Y diagram. *Chemical Geology* 56, 207–263.
- Miller, C., Schuster, R., Klotzli, U., Frank, W., and Purtscheller, F., 1999. Post-collisional potassic and ultrapotassic magmatism in SW Tibet: geochemical and Sr–Nd–Pb–O isotopic constraints for mantle source characteristics and petrogenesis. *Journal of Petrology* 40, 1399–1424.
- Molnar, P., England, P., and Martinod, J., 1993. Mantle dynamics, uplift of the Tibetan plateau, and the Indian Monsoon. *Reviews of Geophysics* 31- 4, 357-396.

- Murphy, M. D., Sparks, R. S. J., Barclay, J., Carroll, M. R., and Brewer, T. S., 2000. Remobilization of andesite magma by intrusion of mafic magma at the Soufrière Hills Volcano, Montserrat, West Indies. *Journal of Petrology* 41, 21–42.
- Nelson, S.T., and Montana, A., 1992. Sieved textured plagioclase in volcanic rocks produced by rapid decompression. *Am. Mineral.* 77, 1242-1249.
- Ogg, J.G., 2004. Status of divisions of International Geological Time scale, *Lethaia* 37, pp 183-194 Oslo ISSN 0024-1164.
- Oktay, F. Y., 1982. Stratigraphy and geological history of Ulukışla and its surroundings. *Bulletin of Turkish Geological Society*, 25, 15-23 (in Turkish with English abstract).
- Ormerod, D.S., Hawkesworth, C.J., Rogers, N.W., Leeman, W.P., Menzies, M.A., 1988. Tectonic and magmatic transitions in the Western Great Basin, U.S.A. *Nature* 333, 349–353.
- Özcan, A., Erkan, A., Keskin, A., Oral, A., Özer, S., Sümengen, M., Tekeli, O., 1980. Kuzey Anadolu Fayı- Kırşehir masifi arasının temel jeolojisi, MTA Der. Rapor no: 6722 (unpublished), Ankara.
- Pasquare, G., Poli, S., Vezzoli, L., and Zanchi, A., 1988. Continental arc volcanism and tectonic setting in central Anatolia, Turkey. *Tectonophysics* 146, 17–230
- Pearce, J.A., 1996. Sources and settings of granitic rocks. *Episodes* 19:120–125
- Pearce, J.A., 1983. The role of sub-continental lithosphere in magma genesis at destructive plate margins. In: Hawkesworth, C.J., and Norry, M.J., (eds.), *Continental basalts and mantle xenoliths*, 230-249. Nantwich: Shiva.

- Pearce, J.A., and Cann, J.R., 1973. Tectonic setting of basic volcanic rocks determined using trace element analyses. *Earth and Planetary Science Letters* 19, 290–300.
- Pearce, J.A., and Norry, M., 1979. Petrogenetic implications of Ti, Zr, Y and Nb variations in volcanic rocks. *Contributions to Mineralogy and Petrology*, 69, 33-47.
- Pearce., JA., and Peate., DW., 1995. Tectonic implication of the composition of volcanic arc magmas, *Annual Review of Earth and Planetary Science* 23, 251-285.
- Pearce, J. A., and Parkinson, I. J., 1993. Trace element models for mantle melting: application to volcanic arc petrogenesis. In: Prichard, H. M., Alabaster, T., Harris, N. B. W. & Neary, C. R. (eds) *Magmatic Processes and Plate Tectonics*. Geological Society, London, Special Publications 76, 373–403.
- Peate, D. W., and Hawkesworth, C. J., 1996. Lithospheric to asthenospheric transition in low-Ti flood basalts from southern Parana, Brazil. *Chemical Geology* 127, 1-24.
- Plank, T., 2005. Constraints from Thorium/Lanthanum on Sediment Recycling at Subduction Zones and the Evolution of the Continents. *Journal of Petrology* 46, 921-944.
- Plank, T., and Langmuir, C. H., 1998. The chemical composition of subducting sediment and its consequences for the crust and mantle. *Chemical Geology* 145, 325–394.

- Platt, J.P., and England, P.C., 1994. Convective removal of lithosphere beneath mountain belts: thermal and mechanical consequences. *Am. J. Sci.* 293, 307– 336.
- Reichow, M. K., Sounders, A.D., White, R.W., Mukhamedov, A.A., and Medvedev, A.Y., 2005. Geochemistry and petrogenesis of basalts from the West Siberian Basin: an extension of the Permo–Triassic Siberian Traps, Russia. *Lithos* 79, 425-452.
- Rogers, N.W., Hawkesworth, C.J., and Ormerod, D.S., 1995. Late Cenozoic basaltic magmatism in the western Great-Basin, California and Nevada. *Journal of Geophysical Research-Solid Earth* 100, 10287–10301.
- Rollinson, H., 1993. Using geochemical data: evaluation, presentation, Interpretation University of Zimbabwe, 352p.
- Rosu, E., Seghedi, I., Downes, H., Alderton, DHM., Szakacs, A., Pecskey, Z., Panaiotu, C., and Panaiotu, N. L., 2004. Extension related Miocene calc-alkaline magmatism in the Apuseni Mountains, Romania: origin of magmas. *Schweizerische Min. Pet. Mitteilungen*, 84153-172.
- Rudnick, R. L., McDonough, W. F., and Chapell, B. W., 1993. Carbonatite metasomatism in the northern Tanzanian mantle: petrographic and geochemical characteristics. *Earth and Planetary Science Letters*, 114, 463–475.
- Rudnick, RL., and Gao, S., 2004. Composition of the Continental Crust. In: Holland HD Turekian KK (eds) *Treatise on Geochemistry*. Elsevier, Amsterdam 3, 1-64.

- Rudnick, R.L., and Fountain, D.M., 1995. Nature and composition of the continental crust: a lower crustal perspective. *Reviews of Geophysics* 33, 267–309.
- Sacks, P. E., and D, T., Secor, 1990. Delamination in collisional orogens, *Geology*, 18, 999-1002.
- Seghedi, I., Downes, H., Pecskey, Z., Thirlwall, M.F., Szakas, A., Prychodko, M., and Matthey, D., 2001. Magma genesis in a subduction- related post-collisional volcanic arc segment: the Ukrainian Carpathians. *Lithos* 57, 237–262.
- Seymen, İ., 1982. Kaman dolayında Kırşehir masifinin jeolojisi, İTÜ Maden Fakültesi, doçentlik tezi, 164 s (unpublished), İstanbul.
- Shaw, D.M., 1970. Trace element fractionation during anatexis. *Geochimica et Cosmochimica Acta* 34, 237–243.
- Shaw, H.R., 1980. The fracture mechanisms of magma transport from the mantle to the surface. In: Hargraves RB (ed) *Physics of magmatic processes*. Princeton University Press, Princeton, pp 201–264.
- Shaw, J.E., Baker, J.A., Menzies, M.A., Thirlwall, M.F., and Ibrahim, K.M., 2003. Petrogenesis of the largest intraplate volcanic field on the Arabian plate (Jordan): a mixing lithosphere–asthenosphere source activated by lithospheric extension. *J. Petrol.* 44, 1657–1679.
- Shaw, JE., Baker, JA., Kent, AJR., Ibrahim, KM., and Menzies, MA., 2007. The geochemistry of the Arabian lithospheric mantle - a source for intraplate volcanism? *Journal of Petrology* 48, 1495–1512.

Sheth, H.C., Ray, J.S., 2002. Rb/Sr-⁸⁷Sr/⁸⁶Sr variations in Bombay trachytes and rhyolites (Deccan Traps): Rb–Sr isochron, or AFC process? *International Geology Review* 44, 624–638.

Singer, B.S., Leeman, W.P., Thirlwall, M.F. and Roger, N.W.E., 1996. Does fracture zone subduction increase sediment flux and mantle melting in subduction zones? Trace element evidence from Aleutian arc basalt. In: Bebout, G.E., Scholl, D.W., Kirby, S.H. & Platt, J.P. (eds), *Subduction Top to Bottom. Geophysical Monograph* 96, 285–291.

Snyder, D. and Tait, S. 1996. Magma mixing by convective entrainment. *Nature* 379, 529–531.

Sparks, R.S., and Marshall, L.A., 1986. Thermal and mechanical constraints on magma mixing between mafic and silicic magmas. *Journal of Volcanology and Geothermal Research* 29, 99-124.

Stimac, J.A., and Pearce, 1992. Textural evidence of mafic–felsic magma interaction in dacite lavas, Clear Lake, California. *Am Mineral* 77,795–809.

Stolz, A. J., Jochum, K. P., Stettel, B. and Hofmann, A. W. 1996. Fluid- and melt-related enrichment in the sub arc mantle: evidence from Nb/Ta variations in island-arc basalts. *Geology* 24, 587-590.

Su, B. X., Zhang H.F., Sakyi, A.P., Ying, J. F., Tang, Y. J., Yang, Y.,H., Qin, K. Z., Xiao Y., and Zhao., X.,M., 2010. Compositionally stratified lithosphere and carbonatite metasomatism recorded in mantle xenoliths from the Western Qinling (Central China), *Lithos* 116 111-128.

Sun, S.S., and McDonough, W.F., 1989. Chemical and isotopic systematics of oceanic basalts: implication for mantle composition and processes. In:

Saunders, AD, Norry MJ (eds) Magmatism in the ocean basins. Geological Society London Special Publication 42,313–345.

Şengör, A.M.C., and Yılmaz, Y., 1981. Tethyan evolution of Turkey: A plate tectonic Approach. *Tectonophysics* 75, 181-241.

Tatar, O., Gürsoy, H., Piper, JDA., 2002. Differential neotectonic rotations in Anatolia and the Tauride Arc: palaeomagnetic investigation of the Erenlerdag Volcanic Complex and Isparta volcanic district, south-central Turkey. *Journal of Geological Society London* 159, 281- 294.

Taylor, S.R., and McLennan, S.M., 1985. The continental crust; its compositions and evolution, 312pp. Blackwell, Oxford.

Taylor, S.R., McLennan, S.M., 1995. The geochemical evolution of the continental crust. *Review of Geophysics* 33, 241–265.

Thirlwall, M.F., Smith, T.E., Graham, A.M., Theodoru, N., Hollings, P., Davidson, J.P., and Arculus, R.J., 1994. High field strength element anomalies in arc lavas: source or process? *Journal of Petrology* 35, 819-838.

Toksoy, F., 1998. Petrography and mineralogy of the vermiculitized phlogopitic metagabbro from the Kurançalı Area (Kırşehir-Central Anatolia). M.Sc Thesis, Middle East Tech. University., Ankara, 175p, (unpublished).

Toksoy-Köksal, F., Oberhaensli, R., and Göncüoğlu, M.C., 2009. Hydrous aluminosilicate metasomatism in an intra-oceanic subduction zone: Implications from the Kurançalı (Turkey) ultramafic-mafic cumulates within the Alpine Neotethys Ocean. *Mineralogy and Petrology* (in press) DOI: 10.1007/s00710-009-0044-7.

- Tommasini, S., Manetti, P., Innocenti, F., Abebe, T., Sintoni, MF., and Conticelli, S., 2005. The Ethiopian subcontinental mantle domains: geochemical evidence from Cenozoic mafic lavas. *Minerology and Petrology* 84, 259-281.
- Toprak, V. and Göncüoğlu, M.C., 1993. Tectonic control on the development of Neogene-Quaternary Central Anatolian Volcanic Province, Turkey: *Geological Journal*, 28, 357-369.
- Toprak, V., 1998. Vent distribution and its relation to regional tectonics, Cappadocian Volcanics, Turkey. *Journal of Volcanology and Geothermal Research* 85, 55- 67.
- Tsuchiyama, A., 1985. Dissolution kinetics of plagioclase in the melt of the system diopside-albite-anorthite, and the origin of dusty plagioclase in andesites. *Contributions to Mineralogy and Petrology* 89, 1-16
- Turner, S., Sandiford, M., and Foden, J., 1992. Some geodynamic and compositional constraints on post-orogenic magmatism. *Geology* 20, 931– 934.
- Turner, S., Arnaud, N., and Liu, J., 1996. Post collision, shoshonitic volcanism on the Tibetan Plateau: Implications for convective thinning of the lithosphere and the source of oceanic basalts. *Journal of Petrology* 37, 45–71.
- Turner, S.P., Platt, J.P., George, R.M.M., Kelley, S.P., Pearson, D.G., and Nowell, S.M., 1999. Magmatism associated with orogenic collapse of the Betic–Alboran domain, SE Spain. *Journal of Petrology* 40, 1011 – 1036.

- Turner, S., and Hawkesworth, C., 1995. The nature of sub continental mantle: constraints of major element composition of continental flood basalt, *Chemical Geology*, 120,295-314.
- Türeli, T.K., Göncüoğlu, M.C., and Akıman, O., 1993. Orta Anadolu Kristalen Kütlesi batısındaki Ekecikdag Granitoyitinin petrolojisi and kökeni. *MTA Dergisi*, 115, 15-28.
- Ussler, WIII., and Glazner, AF., 1987. Origin of augite coronas around quartz xenocrysts in basalts and andesites. *Geol Soc Am Abst with Programs* 19, 874.
- Xu, Y-G., Menzies, MA., Thirlwall, MF., Huang, X-L., Liu, Y., Chen, X-M., 2003. “Reactive” harzburgites from Huinan, NE China: products of the lithosphere-asthenosphere interaction during lithospheric thinning? *Geochimica et Cosmochimica Acta* 67, 487–505
- Walker, J.D., and Geissman, J.W., 2009. (compilers) *Geologic Time Scale: Geological Society of America*, doi: 10.1130/2009.CTS004R2C.
- Wang, KL., Chung, SL., O’reilly, SY., Sun, SS., Shinjo, R., and Chen, CH., 2002. Geochemical Constraints for the Genesis of Post-collisional Magmatism and the Geodynamic Evolution of the Northern Taiwan Region. *Journal of Petrology* 45, 975- 1011.
- Wang, Y., Fan, W., Zhang, Y., Guo, F., Zhang, H., Peng, T., 2004. Geochemical, $^{40}\text{Ar}/^{39}\text{Ar}$ geochronological and Sr–Nd isotopic constraints on the origin of Paleoproterozoic mafic dikes from the southern Taihang Mountains and implications for the ca. 1800 Ma event of the North China Craton. *Precambrian Research* 135, 55-77

- Wang, Q., Xu, J. F., Jian, P., Bao, Z., Zhao, Z. H., Li, C. F., Xiong, X. L., and Ma, J., 2006. Petrogenesis of Adakitic Porphyries in an Extensional Tectonic Setting, Dexing, South China: Implications for the Genesis of Porphyry Copper Mineralization, *Journal of Petrology* 47, 119-144.
- Waters, F.G., and Erlank, A.J., 1988. Assessment of the vertical extent and distribution of mantle metasomatism below Kimberley. *South African Journal of Petrology Special*, 185-204.
- Weaver, B. L., 1991. The origin of ocean island basalt end-member compositions: trace element and isotopic constraints. *Earth and Planetary Science Letters* 104, 381-397.
- White, W. M., Hofmann, A. W., and Puchelt, H., 1987. Isotope geochemistry of Pacific mid-ocean ridge basalt. *Journal of Geophysical Research* 92, 4881–4893.
- Whitney, DL., and Dilek, Y., 1998. Metamorphism during Alpine Crustal Thickening and Extension in Central Anatolia, Turkey: the Niğde Metamorphic Core Complex. *Journal of Petrology* 39, 1385- 1403.
- Williams, H., Turner, S., Kelley, S., and Harris, N., 2001. Age and composition of dikes in southern Tibet: new constraints on the timing of east–west extension and its relationship to postcollisional volcanism. *Geology* 29, 339– 342.
- Williams, H.M., Turner, S.P., Pearce, J.A., Kelley, S.P., Harris, N.B.W., 2004. Nature of the source regions for post-collisional, potassic magmatism in Southern and Northern Tibet from geochemical variations and inverse trace element modeling. *Journal of Petrology* 45- 3, 555–607.

- Wilson, M., and Downes, H., 1991. Tertiary- Quaternary extension related alkaline magmatism in western and central Europe. *Journal of Petrology* 32, 811- 849.
- Winchester, J.A., and Floyd, P.A., 1977. Geochemical discrimination of different magma series and their differentiations products using immobile elements. *Chemical Geology* 20, 325-343.
- Witt-Eickchen, G., Seck, H. A., Mezger, K., Eggins, S. M. and Altherr, R., 2003. Lithospheric mantle evolution beneath the Eifel (Germany): Constraints from Sr, Nd, Pb isotopes and trace element abundances in spinel peridotite and pyroxenite xenoliths. *Journal of Petrology* 44, 1077-1095.
- Wood, D.A., 1980. The application of a Th-Hf-Ta diagram to problems of tectonomagmatic classification and to establishing the nature of crustal contamination of basaltic lavas of British Tertiary volcanic province. *Earth and Planetary Science Letters* 50, 11–30.
- Yalınız, M.K., Floyd, P.A., and Göncüoğlu, M.C., 1996. Supra-subduction zone ophiolites of Central Anatolia: geochemical evidence from the Sarıkaraman Ophiolite, Aksaray, Turkey: *Mineralogical Magazin*, 60, 697-710.
- Yalınız, K., and Göncüoğlu, M.C., 1998. General geological characteristics and distribution of Central Anatolian Ophiolites. *H.Ü. Yerbilimleri*, 20, 19-30.
- Yılmaz, S., and Boztuğ, D., 1994. Granitoyid petrojenezinde magma mingling/mixing kavramı, *Jeoloji Mühendisliği*, 44-45, 1-20.

- Zangana, N.A., Downes, H., Thirlwall, M.F., Marker, G.F., and Bea, F., 1999. Geochemical variation in peridotite xenoliths and their constituent clinopyroxenes from Ray Pit (French Massif Central): implications for the composition of the shallow lithospheric mantle. *Chemical Geology* 153, 11–35.
- Zeck, H. P., Kristensen, A. B. and Williams, I. S., 1998. Post-collisional volcanism in a sinking slab setting—crustal anatexis origin of pyroxene-andesite magma, Caldear volcanic province, southeastern Spain. *Lithos* 45, 499–522.
- Zhang, HF., Parrish, R., Zhang, L., Wang, CX., Yuan, HL., Gao, S., Crowley, QG., 2007. A-type granite and adakitic magmatism association in Songpan–Garze fold belt, eastern Tibetan Plateau: Implication for lithospheric delamination. *Lithos* 97, 323- 335.
- Zheng, J.P., Zhang, R.Y., Griffin, W.L., O'Reilly, S.Y., 2005. Heterogeneous and metasomatized mantle recorded by trace elements in minerals of the Donghai garnet peridotites, Sulu UHP terrane, China. *Chemical Geology* 221, 243–259.
- Zindler, A., and Hart, S.R., 1986. Chemical geodynamics. *Annual Review of Earth and Planetary Science* 14, 493–571.
- Zou, H. B., Zindler, A., Xu, X. S. & Qi, Q. 2000. Major, trace element, and Nd, Sr and Pb isotope studies of Cenozoic basalts in SE China: mantle sources, regional variations and tectonic significance. *Chemical Geology* 171, 33–47.

APPENDIX A

Major oxides and trace element compositions of the studied rocks.

Sample	K17	K14	K19	K12	K6	K10	K11
Major Oxides (wt %)							
SiO ₂	53.62	70.6	66.79	69.04	61.24	68.21	68.37
Al ₂ O ₃	17.15	14.5	16.13	15.3	16.26	15.46	15.45
Fe ₂ O ₃	4.94	2.03	2.24	1.96	3.82	2.14	2.41
MgO	5.56	0.59	0.54	0.74	3.93	0.92	0.82
CaO	5.98	4.21	4.21	4.83	5.35	4.94	4.86
Na ₂ O	3.24	3.3	4.01	3.53	4.19	3.69	3.67
K ₂ O	0.88	2.22	3	2.26	1.44	2.34	2.37
TiO ₂	0.56	0.42	0.55	0.45	0.47	0.45	0.45
P ₂ O ₅	0.2	0.14	0.31	0.17	0.15	0.17	0.16
MnO	0.07	0.03	0.02	0.03	0.06	0.07	0.04
LOI	7.5	1.8	1.9	1.5	2.9	1.4	1.2
Total	99.74	99.9	99.73	99.87	99.86	99.86	99.88
Mg#	55.57	24.41	21.13	29.55	53.34	32.33	27.43
Trace Element (ppm)							
Ni	18	11.2	8.9	15.5	10.9	24.4	23.1
Sc	9	8	8	8	9	9	9
Ba	814.5	774	756.7	822.9	811.2	913.1	807.2
Co	14.6	6.4	5.6	6.7	14.2	10.6	10.3
Cs	0.5	2.3	1.2	1.8	4	2.5	1.7
Ga	15.9	13.5	16.1	13.9	15	16.3	15.8
Hf	4.8	4	4.9	4	4.5	4.3	4.3
Nb	9.2	7	9.8	6.9	7.3	8.2	8
Rb	9.3	69.2	83.6	70.2	90.1	98.4	83.5
Sr	549.7	531.3	477.7	539.7	535.3	577.3	556
Ta	0.7	0.5	0.7	0.6	0.6	0.6	0.6
Th	13	12.4	10.9	12.7	12.8	14.2	15.3
U	3.3	6.3	6.6	7.6	4.9	7.4	6.6
V	65	57	55	56	62	70	61
Zr	189.2	153.3	192.5	154.4	166.4	185	177
Y	20.8	14.8	23.6	14.6	15.4	15.5	14.4
La	28.7	28	30.3	26.5	26.8	29.4	27.5
Ce	49	48.8	54.8	49.3	49.1	52.9	53

Pr	5.88	5.11	5.71	5.23	5.17	5.44	5.43
Nd	20.8	18.7	21.4	18.8	19.4	20.5	19.4
Sm	3.7	3	3.5	3.1	2.9	2.9	2.9
Eu	1.04	0.8	1	0.81	0.81	0.87	0.82
Gd	3.35	2.47	3.45	2.63	2.65	2.86	2.95
Tb	0.57	0.41	0.59	0.46	0.44	0.52	0.48
Dy	3.3	2.11	3.33	2.51	2.36	2.63	2.55
Ho	0.62	0.41	0.64	0.46	0.43	0.49	0.45
Er	2.13	1.4	2.26	1.41	1.46	1.61	1.57
Tm	0.33	0.21	0.36	0.22	0.23	0.22	0.22
Yb	2.1	1.36	2.37	1.35	1.48	1.6	1.35
Lu	0.34	0.21	0.38	0.2	0.22	0.26	0.25
Mo	1.2	4.2	2.6	4.5	2.5	5	6.1
Cu	17.3	8.2	7.2	48.8	15.8	157.8	14
Pb	11	6.8	15.2	6.8	1.6	5.6	6.4
Sample	FG3	FG1	F2	F8	Y1	Y2	Y6
Major Oxides (wt %)							
SiO2	58.84	65.62	67.17	61.05	59.9	59.9	56.66
Al2O3	15.23	15.50	15.48	15.22	18.12	18.17	18.11
Fe2O3	7.17	5.66	3.59	5.33	5.67	5.58	6.22
MgO	3.32	0.86	0.60	1.44	1.78	1.83	3.29
CaO	5.02	4.61	4.46	4.70	4.88	4.82	6.67
Na2O	3.36	3.73	3.79	2.64	5.09	5.08	4.85
K2O	2.43	2.51	2.42	4.16	1.62	1.69	0.71
TiO2	0.46	0.49	0.51	0.53	0.62	0.63	0.92
P2O5	0.17	0.21	0.20	0.17	0.37	0.37	0.21
MnO	0.07	0.07	0.05	0.10	0.11	0.11	0.12
LOI	3.6	0.5	1.5	4.3	1.7	1.7	2.1
Total	99.77	99.81	99.82	99.67	99.89	99.91	99.9
Mg#	33.97	14.44	15.66	23.09	25.86	26.71	37.02
Trace Element (ppm)							
Ni	199.4	130.0	32.1	12.2	3.4	3.8	9.8
Sc	10	8	9	7	6	7	15
Ba	736	749	745	1145	620.4	589.6	587.2
Co	16.1	8.5	5.2	7.7	10.8	11.5	23.1
Cs	1.4	1.6	1.7	6.9	3.5	2.9	5.4
Ga	12.8	14.0	15.8	17.3	17.4	18.4	18.1
Hf	3.3	3.7	4.2	6.2	5	5	3.5
Nb	7.0	8.5	8.3	19.2	7.9	8.3	8.3
Rb	84.2	78.7	74.7	134.2	91.6	76.1	60.7
Sr	451.2	493.3	500.8	741.0	444	480.4	641.9

Ta	0.5	0.7	0.7	1.2	0.6	0.6	0.7
Th	12.6	12.3	12.8	29.4	10.5	11.5	8.4
U	4.3	4.7	6.0	7.9	3.4	3.2	3.4
V	65	63	66	49	60	59	130
Zr	143.5	161.4	162.3	245.9	209.2	220	158.7
Y	14.0	15.6	15.2	23.0	20.9	21.5	20.2
La	24.7	27.0	26.8	55.5	24.8	23.4	17.4
Ce	42.6	46.9	47.7	99.1	48.9	48.3	36.4
Pr	4.67	5.08	5.12	11.32	5.42	5.48	4.16
Nd	16.0	17.7	18.2	42.2	21.1	21.3	16.5
Sm	2.92	3.23	3.17	6.83	3.6	3.6	3.1
Eu	0.80	0.85	0.88	1.34	1.13	1.15	1.01
Gd	2.88	2.93	2.95	5.45	3.45	3.9	3.71
Tb	0.41	0.45	0.45	0.79	0.6	0.69	0.67
Dy	2.23	2.46	2.65	3.69	3.5	3.83	3.81
Ho	0.47	0.51	0.51	0.73	0.65	0.69	0.66
Er	1.37	1.46	1.44	1.94	2.22	2.37	2.28
Tm	0.23	0.24	0.24	0.33	0.33	0.32	0.31
Yb	1.45	1.58	1.43	2.01	2.12	2.31	2.02
Lu	0.22	0.24	0.23	0.34	0.31	0.37	0.35
Mo	39.0	35.5	8.1	3.1	3.8	4.1	3.8
Cu	35.8	26.6	13.3	3.9	6.8	7.3	18.6
Pb	6.4	5.4	3.9	16.6	1.4	1.6	3.9

Sample	Y5	F11	Y8	F15	P6	P9	P5
Major Oxides (wt %)							
SiO2	51.49	56.80	59.39	52.68	56.75	56.81	56.84
Al2O3	17.66	17.57	17.74	17.41	17.1	18.48	17.29
Fe2O3	6.44	6.70	6.48	8.10	6.34	4.7	6.17
MgO	3.45	3.48	1.80	2.38	2.29	2.23	2.05
CaO	4.34	6.42	4.94	6.79	5.04	5.57	5.12
Na2O	6.92	4.70	4.84	3.56	5.18	5.29	5.29
K2O	1.63	0.78	1.78	2.55	2.31	2.49	2.3
TiO2	1.04	0.90	0.63	1.00	1.63	1.39	1.71
P2O5	0.28	0.23	0.36	0.31	0.43	0.37	0.41
MnO	0.11	0.12	0.12	0.09	0.08	0.05	0.07
LOI	6.4	2.1	1.7	4.9	2.7	2.5	2.6
Total	99.77	99.77	99.80	99.76	99.87	99.89	99.87
Mg#	37.31	36.59	23.58	24.61	28.64	34.52	26.96
Trace Element (ppm)							
Ni	13.6	22.8	15.6	22.6	3.6	6.2	4.4
Sc	16	16	6	15	13	14	14

Ba	549.3	560	630	572	618.2	554	591.6
Co	21.6	20.9	10.0	13.6	12.9	13.8	14.5
Cs	4.9	4.6	2.5	2.1	1.8	0.3	2.1
Ga	13.4	16.1	16.9	14.9	18.9	18.5	18.7
Hf	3.4	3.2	4.9	4.0	6.2	5.2	6.7
Nb	5.8	7.9	8.5	9.0	18	14.8	17.8
Rb	36.8	51.3	56.9	75.7	58.9	69.5	69.4
Sr	445.5	556.2	483.8	569.8	455.8	490.2	456.1
Ta	0.4	0.6	0.6	0.4	1.2	1	1.3
Th	5.4	8.2	12.2	10.7	11.1	10.3	11.4
U	1	2.7	3.3	2.3	3.8	2.7	3.7
V	141	123	60	159	163	142	165
Zr	149.6	136.8	198.8	170.9	284.1	228.9	276.1
Y	21.2	21.9	21.6	22.5	32.1	26.8	32.5
La	15.4	17.7	26.1	25.1	33.8	27.8	34.3
Ce	32.2	33.4	48.1	48.1	68.6	56.3	68.6
Pr	3.96	3.96	5.80	5.76	7.63	6.42	7.66
Nd	16.9	15.7	23.2	23.3	29.6	24.8	29.7
Sm	3.4	3.33	4.22	4.32	5.9	5	5.6
Eu	1.11	1.08	1.21	1.25	1.58	1.38	1.53
Gd	3.46	3.47	3.84	4.35	5.33	4.49	5.48
Tb	0.62	0.61	0.63	0.69	0.99	0.83	0.95
Dy	3.52	3.49	3.37	3.49	5.4	4.4	5.45
Ho	0.64	0.73	0.73	0.72	1.01	0.81	1.01
Er	2.19	2.12	2.13	2.15	3.38	2.66	3.29
Tm	0.33	0.34	0.35	0.34	0.48	0.41	0.5
Yb	2.4	2.06	2.16	2.03	3.11	2.36	3.08
Lu	0.32	0.32	0.36	0.34	0.48	0.36	0.46
Mo	1.6	4.7	5.6	4.8	2.7	1.4	2.9
Cu	15.7	29.1	11.8	16.2	8.7	9.5	8.8
Pb	6.8	5.0	4.3	7.0	4.2	11.7	4.1

Sample	P8	FG26	PK1	KA1	KA2	LAV 1	FG27
Major Oxides (wt %)							
SiO2	55.41	52.51	52.78	60.07	51.74	53.15	52.46
Al2O3	17.66	18.38	18.8	17.34	16.14	15.95	18.52
Fe2O3	6.29	7.24	7.01	5.26	7.03	6.54	7.22
MgO	2.68	4.62	4.49	1.89	5.66	5.92	4.39
CaO	5.73	7.95	7.96	4.05	9.66	7.89	7.97
Na2O	4.94	3.57	3.61	5.6	2.92	3.28	3.73
K2O	2.24	0.81	0.88	2.07	1.08	1.51	0.92
TiO2	1.33	0.86	0.85	0.95	0.8	0.75	0.84

P2O5	0.33	0.18	0.18	0.39	0.22	0.23	0.17
MnO	0.07	0.10	0.1	0.13	0.11	0.1	0.10
LOI	3.1	3.5	3.1	2.1	4.5	4.4	3.4
Total	99.78	99.76	99.79	99.89	99.91	99.78	99.76
Mg#	32.13	41.49	41.58	28.53	47.22	50.14	40.32
Trace Element (ppm)							
Ni	21.1	33.7	26.2	3.5	24.4	76.5	53.7
Sc	15	18	17	9	24	20	17
Ba	508	425	451.5	732.8	500.3	830.7	435
Co	13.9	21.7	22.1	7	24.6	24.3	21.8
Cs	0.2	0.7	1	2.2	1.4	2.9	1.1
Ga	18.1	17.8	17.1	20	15.8	15.2	16.8
Hf	4.2	2.7	3.2	6.3	2.9	3.3	2.9
Nb	14.9	5.2	4.9	17.8	6.6	8.6	5.5
Rb	37.6	30.4	23.9	91.3	45.1	76.4	30.2
Sr	467.9	562.1	552.4	463.3	571.5	601.5	531.7
Ta	0.9	0.3	0.3	1.1	0.4	0.6	0.4
Th	10.0	6.5	4.4	12.6	5.5	7.3	5.5
U	3.1	1.7	1.7	4.8	1.6	2.6	1.7
V	135	182	180	76	198	164	172
Zr	202.5	105.5	104.1	278.3	107.6	113.8	107.4
Y	27.5	20.8	19.6	30.9	19.6	18.5	19.1
La	26.5	14.9	13.8	35.6	16.8	21	15.3
Ce	50.5	29.2	29.3	72.5	34.3	40.4	28.5
Pr	6.14	3.94	3.58	8.2	4.14	4.62	3.71
Nd	23.9	16.9	15.3	31.1	17.9	20	14.8
Sm	4.56	3.62	3.4	5.2	3.5	3.7	3.46
Eu	1.33	1.09	1.02	1.48	1.09	1.13	1.04
Gd	4.70	3.63	3.2	5.29	3.51	3.55	3.45
Tb	0.76	0.61	0.62	1.01	0.64	0.56	0.59
Dy	4.25	3.43	3.22	5.52	3.4	3.25	3.46
Ho	0.88	0.70	0.64	1	0.63	0.62	0.72
Er	2.54	2.03	2.04	3.52	1.93	1.98	2.07
Tm	0.41	0.33	0.31	0.49	0.27	0.27	0.34
Yb	2.62	1.99	1.95	3.16	1.83	1.73	1.95
Lu	0.43	0.34	0.28	0.53	0.28	0.29	0.31
Mo	4.7	3.1	3	4.3	2	2.4	9.1
Cu	13.2	39.7	36.9	2.5	35.8	38.5	40.2
Pb	14.6	3.7	3.5	2.3	5.5	4.9	4.1
Sample	A3	A5	A6	D6	F20	F18	F27
Major Oxides (wt %)							

SiO2	53.01	47.39	58.29	51.74	52.52	52.85	51.05
Al2O3	15.89	17.12	17.71	16.36	15.89	15.18	15.75
Fe2O3	6.94	8.89	5.04	6.49	6.73	6.50	7.13
MgO	6.01	5.5	2.62	6.39	6.57	6.40	7.31
CaO	6.98	7.71	5.22	8.11	7.90	7.54	8.62
Na2O	3.04	4.34	4.1	3.17	3.23	3.14	3.07
K2O	2.48	1.55	2.97	0.6	0.70	0.78	1.55
TiO2	0.64	0.77	0.5	0.72	0.70	0.69	0.75
P2O5	0.18	0.26	0.21	0.17	0.18	0.19	0.20
MnO	0.06	0.13	0.07	0.09	0.11	0.11	0.10
LOI	4.4	6.1	3.1	6	5.1	6.3	4.1
Total	99.71	99.78	99.84	99.92	99.71	99.72	99.70
Mg#	49.04	40.74	36.61	52.24	52.03	52.25	53.25
Trace Element (ppm)							
Ni	103.4	19.5	5.8	132	136.7	114.0	99.1
Sc	24	27	10	20	20	20	25
Ba	634	894.6	980	506.5	566	560	572
Co	24.1	29.8	14.1	28.5	29.9	28.5	25.2
Cs	0.6	2.3	1.2	1.5	2.0	3.2	0.3
Ga	15.8	17	16.1	15.2	15.5	15.4	14.0
Hf	2.6	2.3	3.2	3.2	2.7	3.1	2.7
Nb	6.1	4.3	7	6.4	6.8	6.7	5.4
Rb	54.1	34.2	91.8	34.3	30.6	43.9	33.3
Sr	588.7	1201	557	512.9	648.1	577.2	512.0
Ta	0.4	0.2	0.5	0.3	0.4	0.4	0.1
Th	7.3	5.4	10.1	4	4.6	7.0	5.1
U	1.9	1.7	2.9	1.3	1.4	2.0	1.4
V	155	267	111	144	147	140	180
Zr	103.6	80.5	115.8	109.4	105.5	118.7	88.3
Y	16.8	18.1	16.4	18.2	17.9	20.1	17.5
La	20.1	19.9	24	15	15.1	18.6	17.6
Ce	35.4	40.7	47.6	30.1	29.6	33.8	35.5
Pr	4.34	5	5.18	3.55	3.51	4.05	4.34
Nd	17.0	20.2	19.9	14.8	14.2	16.1	18.3
Sm	3.43	4.3	3.5	2.9	3.02	3.44	3.57
Eu	0.95	1.14	0.94	0.95	0.99	1.03	1.01
Gd	3.26	3.6	2.99	2.96	3.07	3.48	3.47
Tb	0.51	0.58	0.51	0.52	0.55	0.58	0.53
Dy	3.00	3.27	2.67	3.01	3.31	3.53	3.12
Ho	0.61	0.55	0.48	0.57	0.67	0.66	0.61
Er	1.61	1.81	1.59	2.02	1.97	1.92	1.74
Tm	0.26	0.25	0.25	0.3	0.29	0.31	0.28

Yb	1.67	1.55	1.71	1.83	1.92	1.92	1.73
Lu	0.25	0.23	0.25	0.27	0.28	0.30	0.27
Mo	1.0	1.4	2.1	1.5	1.5	1.6	4.3
Cu	29.8	103.1	36.2	30.9	37.1	31.9	54.9
Pb	4.0	7.8	4.8	4.4	5.5	5.7	3.9
Sample	F28	T1	F21	F23	F22	F24	F25
Major Oxides (wt %)							
SiO2	51.39	55.40	53.52	55.03	53.29	57.34	58.78
Al2O3	15.25	18.06	15.30	16.75	15.88	17.52	17.13
Fe2O3	7.58	6.70	7.07	6.16	6.72	6.85	6.17
MgO	2.74	2.74	5.45	4.30	5.36	3.45	2.70
CaO	9.36	6.05	8.24	5.89	8.64	6.38	5.71
Na2O	3.12	3.55	3.29	3.86	3.33	4.14	3.84
K2O	1.96	2.52	0.90	2.24	0.85	1.30	2.17
TiO2	0.72	0.57	0.66	0.66	0.69	0.76	0.62
P2O5	0.24	0.25	0.19	0.19	0.19	0.21	0.19
MnO	0.15	0.07	0.10	0.07	0.09	0.12	0.10
LOI	7.3	3.8	4.9	4.6	4.6	1.7	2.3
Total	99.79	99.70	99.70	99.76	99.71	99.74	99.74
Mg#	28.65	31.24	46.14	43.68	46.98	35.88	32.72
Trace Element (ppm)							
Ni	25.3	17.8	87.4	51.0	113.3	24.6	17.0
Sc	20	12	21	18	21	15	11
Ba	423	1042	633	632	645	612	621
Co	23.2	17.1	25.7	19.6	26.8	18.4	14.5
Cs	1.1	1.1	8.3	0.7	11.4	3.1	1.1
Ga	15.5	17.9	15.1	15.5	14.6	18.5	17.8
Hf	2.7	3.0	3.1	3.2	3.3	3.8	3.9
Nb	5.4	7.0	8.4	5.5	7.7	7.2	7.8
Rb	54.7	56.0	127.6	59.9	99.5	77.2	59.0
Sr	465.1	669.6	575.7	437.6	594.0	538.3	536.8
Ta	0.3	0.4	0.5	0.4	0.4	0.5	0.4
Th	4.5	12.6	8.8	6.6	9.0	7.3	7.8
U	1.8	3.1	2.5	1.8	2.4	2.4	2.8
V	169	143	154	145	151	154	123
Zr	102.8	113.5	109.9	113.1	108.7	140.5	141.6
Y	21.8	15.4	17.7	17.3	16.7	23.2	18.9
La	15.7	28.4	21.9	13.6	20.4	22.5	22.2
Ce	31.2	50.7	40.9	28.8	36.3	43.0	41.2
Pr	3.92	6.05	4.68	3.75	4.54	5.15	4.78
Nd	17.3	24.6	18.0	15.5	18.4	19.6	17.9

Sm	3.60	3.94	3.33	3.13	3.23	3.97	3.56
Eu	1.13	1.05	0.96	0.97	0.95	1.18	1.01
Gd	3.79	3.34	3.30	3.22	3.39	3.93	3.39
Tb	0.61	0.49	0.54	0.53	0.55	0.68	0.54
Dy	3.54	2.55	3.15	2.97	2.75	3.85	3.06
Ho	0.72	0.48	0.60	0.63	0.63	0.77	0.60
Er	2.04	1.42	1.75	1.71	1.59	2.31	1.76
Tm	0.34	0.24	0.29	0.27	0.30	0.37	0.30
Yb	2.10	1.41	1.75	1.66	1.77	2.28	1.78
Lu	0.33	0.23	0.27	0.26	0.28	0.38	0.29
Mo	4.1	4.6	7.8	0.4	8.5	4.5	3.6
Cu	30.0	33.6	37.4	40.2	46.6	27.2	22.9
Pb	3.9	7.4	5.4	3.5	4.9	2.3	6.2

Sample	F26	F34	F35	F32	F31	GE8	GE12
Major Oxides (wt %)							
SiO2	58.44	58.95	59.48	53.58	54.32	51.6	51.34
Al2O3	17.06	14.96	14.91	16.47	16.82	17.08	15.58
Fe2O3	6.91	4.98	5.25	9.29	9.61	6.74	7.82
MgO	2.66	1.15	1.46	4.25	3.98	5.76	6.96
CaO	5.93	5.27	4.75	7.71	7.65	10.26	9.57
Na2O	4.30	1.77	1.88	3.41	3.61	3.19	2.53
K2O	1.54	5.77	5.44	1.00	1.12	0.94	1.53
TiO2	0.65	0.72	0.51	0.78	0.77	0.9	0.75
P2O5	0.18	0.24	0.15	0.24	0.25	0.21	0.17
MnO	0.11	0.08	0.09	0.15	0.15	0.13	0.12
LOI	2.0	5.7	5.8	2.9	1.5	2.9	3.5
Total	99.78	99.56	99.69	99.74	99.75	99.78	99.92
Mg#	29.96	20.42	23.6	33.7	31.51	48.71	49.72
Trace Element (ppm)							
Ni	34.5	14.9	24.1	13.4	17.7	69.3	29.8
Sc	11	7	8	26	26	25	26
Ba	611	1495	1112	487	489	418.5	527.9
Co	14.4	7.1	9.1	24.9	24.6	30.6	29.1
Cs	2.4	9.6	9.5	1.1	1.0	1.2	1.1
Ga	16.9	17.7	17.1	16.6	16.2	15.3	15.6
Hf	4.0	7.3	6.2	2.9	2.8	3.1	2.5
Nb	7.6	19.5	18.1	3.2	3.3	9.3	4.2
Rb	62.2	171.8	217.0	69.7	50.5	25.8	20.2
Sr	501.9	1299.7	550.5	553.3	545.6	553.6	653.7
Ta	0.3	1.1	1.2	0.2	0.2	0.5	0.3
Th	9.0	26.6	30.2	3.8	3.4	3.5	5.8

U	2.9	7.3	4.7	1.2	1.0	1	2
V	116	140	75	238	235	184	223
Zr	137.9	300.1	226.4	86.0	86.1	118.2	86.6
Y	19.1	24.1	22.1	23.8	23.5	19.7	17.1
La	22.5	61.7	53.9	14.4	14.2	15.8	17.8
Ce	40.1	114.2	99.7	29.0	30.2	31.7	37.7
Pr	4.99	13.19	10.90	3.89	3.90	3.97	4.56
Nd	19.0	47.9	39.0	17.4	17.0	17.2	18.8
Sm	3.76	7.67	6.20	4.03	3.87	3.3	3.3
Eu	1.04	1.58	1.23	1.19	1.19	1	1.08
Gd	3.58	5.89	4.99	4.11	4.11	3.4	3.53
Tb	0.56	0.87	0.74	0.69	0.70	0.62	0.59
Dy	3.06	4.05	3.72	3.96	3.98	3.3	3.01
Ho	0.63	0.81	0.77	0.85	0.87	0.62	0.55
Er	1.91	2.29	2.05	2.36	2.34	1.88	1.87
Tm	0.31	0.37	0.35	0.38	0.38	0.29	0.27
Yb	1.96	2.23	2.12	2.28	2.26	1.74	1.76
Lu	0.30	0.36	0.34	0.35	0.35	0.27	0.26
Mo	10.0	3.8	5.8	3.1	5.6	2.4	2
Cu	26.3	9.2	8.1	23.2	19.3	30.7	43.7
Pb	2.5	19.9	26.8	3.3	2.0	2.6	5.7

Sample	YS5	YS4	YS10	YS7	YS6	YS2	YS3
Major Oxides (wt %)							
SiO2	51.46	51.63	53.84	51.58	51.46	52.37	52.66
Al2O3	15.98	16.19	18.34	15.83	15.89	15.53	15.89
Fe2O3	7.55	7.31	6.24	7.58	7.73	6.73	7.23
MgO	5.51	5.55	2.97	6.02	6.08	5.84	5.51
CaO	8.12	7.52	7.45	7.22	8.50	8.49	8.11
Na2O	3.12	3.12	4.42	3.00	2.92	3.02	3.18
K2O	2.39	2.56	1.01	2.94	2.19	1.36	2.35
TiO2	0.83	0.81	1.07	0.84	0.78	0.72	0.79
P2O5	0.25	0.24	0.25	0.25	0.22	0.22	0.24
MnO	0.12	0.08	0.11	0.12	0.11	0.10	0.11
LOI	4.3	4.7	4.1	4.3	3.8	5.2	3.6
Total	99.70	99.70	99.81	99.71	99.71	99.66	99.70
Mg#	44.78	45.76	34.59	46.88	46.64	49.09	45.85
Trace Element (ppm)							
Ni	38.2	34.1	33.6	53.9	38.1	82.5	35.4
Sc	24	22	17	23	24	21	23
Ba	704	726	330	668	630	829	743
Co	24.1	22.8	20.5	24.4	23.5	26.2	25.1

Cs	0.4	1.0	0.9	0.5	0.6	2.8	0.6
Ga	14.2	14.8	15.0	14.9	14.1	15.3	14.7
Hf	2.7	3.4	2.9	2.9	2.6	3.0	3.3
Nb	8.6	9.2	6.2	8.7	8.2	8.5	8.9
Rb	48.3	66.3	31.4	67.9	55.5	60.4	58.4
Sr	552.7	511.7	463.9	520.5	475.6	654.3	533.5
Ta	0.6	0.5	0.4	0.5	0.4	0.6	0.6
Th	5.9	7.2	6.5	6.5	5.0	8.6	6.1
U	1.9	1.7	1.6	1.6	1.7	2.9	1.8
V	174	170	135	180	175	165	174
Zr	109.5	117.0	144.9	119.8	97.2	109.1	112.9
Y	16.5	16.6	20.2	17.5	16.3	18.1	17.3
La	17.5	19.2	16.5	18.0	16.1	23.3	18.0
Ce	35.2	34.6	30.9	31.5	31.4	43.2	34.8
Pr	4.35	4.60	4.10	4.46	3.91	5.16	4.27
Nd	16.9	17.6	16.6	18.1	16.0	21.4	17.6
Sm	3.55	3.80	3.42	3.73	3.30	3.99	3.64
Eu	1.03	1.08	1.15	1.12	0.98	1.15	1.06
Gd	3.35	3.54	3.67	3.59	3.35	3.72	3.57
Tb	0.54	0.57	0.62	0.56	0.49	0.58	0.54
Dy	2.84	2.99	3.20	2.84	2.70	3.17	3.10
Ho	0.59	0.63	0.76	0.61	0.55	0.64	0.62
Er	1.62	1.60	2.02	1.63	1.57	1.73	1.69
Tm	0.25	0.26	0.36	0.28	0.25	0.28	0.27
Yb	1.61	1.66	2.11	1.67	1.54	1.76	1.59
Lu	0.25	0.25	0.31	0.27	0.24	0.26	0.25
Mo	3.0	2.0	4.9	7.5	3.5	7.5	1.8
Cu	54.0	66.3	36.5	43.7	68.1	52.2	48.6
Pb	3.5	4.7	2.5	2.3	3.3	9.2	5.6

Sample	YR9	YR16	YR3	YR5	YR10	YR7	YR8
Major Oxides (wt %)							
SiO2	54.47	54.74	52.51	52.73	53.73	52.58	52.74
Al2O3	15.88	16.16	15.5	15.55	16.47	15.33	16.04
Fe2O3	7.73	7.41	7.1	7.07	6.7	7.36	7.3
MgO	5.59	5.44	6.47	6.5	4.87	6.63	7.56
CaO	7.99	7.65	8.92	8.95	8.86	8.44	7.62
Na2O	3.50	3.70	2.85	3	3.38	2.94	3.38
K2O	1.36	1.56	1.4	1.48	1.51	1.34	1.66
TiO2	0.73	0.73	0.63	0.63	0.8	0.75	0.92
P2O5	0.22	0.24	0.2	0.2	0.23	0.22	0.23
MnO	0.13	0.13	0.11	0.1	0.12	0.11	0.12

LOI	2.1	1.9	4	3.6	3	4.1	2.1
Total	99.69	99.68	99.75	99.87	99.73	99.87	99.76
Mg#	44.55	44.93	50.31	50.53	44.68	50.02	53.5
Trace Element (ppm)							
Ni	162.9	8.9	19.3	56.8	95.7	41.8	46.8
Sc	23	20	24	23	23	23	20
Ba	765	827	758.1	763.4	816	741.3	722.3
Co	25.9	25.3	25.7	28.1	26	28.4	32.1
Cs	2.5	2.4	1.6	1.4	2.3	2.7	3.3
Ga	15.8	15.6	13.8	14.6	17.6	14	16.1
Hf	2.5	3.2	2.6	2.6	3.3	2.7	2.8
Nb	6.6	9.0	4	4.2	7.9	7	10.6
Rb	59.3	83.7	35.4	34.9	59.1	60.5	86.7
Sr	571.3	583.7	587.8	591.1	599.1	546.1	549
Ta	0.4	0.6	0.3	0.3	0.5	0.5	0.7
Th	8.5	8.9	6.1	6.5	6.8	5.9	6.3
U	2.7	2.7	2.2	2.2	2.8	2.1	1.8
V	168	155	184	190	181	167	178
Zr	106.9	115.0	92.4	96.5	115	104	122.9
Y	19.4	17.2	16	16.4	20.3	19.4	16.9
La	21.6	23.0	18	18.3	21	18.3	16.9
Ce	41.1	43.1	35.8	36.8	41.2	37.9	36.3
Pr	4.84	5.07	4.13	4.3	4.79	4.36	4.21
Nd	18.2	19.6	17	18.2	20.3	18.4	18
Sm	3.90	3.93	3.6	3.5	3.7	3.2	3.3
Eu	1.10	1.05	0.96	1	1.04	0.98	0.99
Gd	3.78	3.68	3.2	3.26	3.7	3.29	3.32
Tb	0.61	0.54	0.53	0.57	0.64	0.63	0.62
Dy	3.60	3.16	2.79	2.86	3.5	3.21	3.28
Ho	0.68	0.60	0.51	0.51	0.68	0.6	0.54
Er	1.94	1.79	1.67	1.68	2.17	1.87	1.83
Tm	0.31	0.28	0.24	0.28	0.31	0.31	0.23
Yb	1.91	1.61	1.44	1.71	2.12	1.85	1.48
Lu	0.29	0.26	0.23	0.24	0.31	0.3	0.27
Mo	3.6	12.9	2.7	2.3	3.1	2.6	3.6
Cu	40.8	36.6	47.1	60.2	41.8	48.7	35.3
Pb	3.7	2.4	7.6	7.6	3.1	5.1	1.9

Sample	YD1	YD2	FG28	FG29	FG20	YS1	YR1	YR4
Major Oxides (wt %)								
SiO2	52.86	53.95	54.97	52.87	47.13	53.82	53.91	54.30
Al2O3	16.44	16.38	16.07	15.33	16.88	16.45	15.86	15.40

Fe2O3	6.4	7.14	6.06	7.13	9.56	6.51	6.43	6.45
MgO	5.92	5.41	4.88	5.62	7.16	5.53	6.19	5.89
CaO	8.34	8.19	4.93	7.38	3.61	8.44	9.01	8.94
Na2O	3.17	3.22	4.19	3.82	3.39	3.25	3.14	3.67
K2O	1.67	1.89	2.97	2.19	2.73	2.47	1.31	1.45
TiO2	0.75	0.75	0.68	0.69	0.75	0.85	0.65	0.66
P2O5	0.23	0.21	0.20	0.20	0.10	0.25	0.20	0.27
MnO	0.09	0.1	0.09	0.13	0.08	0.09	0.12	0.14
LOI	3.9	2.6	4.7	4.3	8.3	2.7	2.9	2.1
Total	99.83	99.88	99.74	99.72	99.79	100.33	99.76	99.27
Mg#	50.69	45.71	47.22	46.69	45.42	48.56	51.68	50.36
Trace Element (ppm)								
Ni	40.7	62.6	134.5	64.5	33	67.1	42.5	108.6
Sc	20	22	17	22	40	24	26	22
Ba	973	778.2	765	700	122	748	732	756
Co	24	26.2	19.4	25.0	33.3	0.0	0.0	0.0
Cs	2.4	0.7	3.5	0.5	25.2	2.0	2.0	2.0
Ga	16.1	15.8	14.4	17.0	14.9	15.0	15.0	14.0
Hf	3.3	2.8	2.7	2.7	1.7	2.9	2.6	2.5
Nb	8.5	6.1	8.0	5.6	1.4	9.0	4.1	7.4
Rb	48.4	46.2	90.0	48.4	72.7	66.0	46.0	47.0
Sr	729.8	555.8	386.8	397.6	240.8	515.0	557.0	563.0
Ta	0.6	0.4	0.5	0.4	0.1	0.6	0.3	0.4
Th	8.8	6.4	7.3	6.7	1.3	6.3	6.9	6.2
U	2.7	2.3	2.4	1.9	0.4	1.8	2.2	1.3
V	178	180	128	165	202	173	181	173
Zr	120.6	105.4	114.9	98.3	56.2	123.0	98.0	128.0
Y	17.8	19.4	15.6	15.6	17.2	18.0	17.3	19.0
La	23.5	21	18.5	18.6	5.2	19.8	19.8	20.0
Ce	47.9	40.6	34.6	34.8	10.6	37.8	36.7	34.300
Pr	5.47	4.73	4.17	4.25	1.66	4.48	4.30	4.100
Nd	21.8	18.8	15.7	16.1	7.3	17.6	17.0	15.9
Sm	4	3.6	3.30	3.53	2.13	4.00	3.81	3.73
Eu	1.05	1.03	0.95	0.99	0.77	1.20	1.12	0.97
Gd	3.74	3.54	3.20	3.33	2.56	3.82	3.61	3.32
Tb	0.64	0.59	0.49	0.53	0.47	0.60	0.56	0.51
Dy	3.2	3.36	2.71	2.88	2.88	3.54	3.32	3.21
Ho	0.55	0.62	0.57	0.59	0.62	0.70	0.66	0.56
Er	1.84	2.02	1.56	1.54	1.78	1.93	1.82	1.72
Tm	0.27	0.31	0.27	0.25	0.30	0.28	0.26	0.24
Yb	1.63	1.93	1.50	1.50	1.72	1.71	1.66	1.63
Lu	0.25	0.3	0.24	0.24	0.25	0.27	0.26	0.27

Mo	2.2	2	4.3	1.2	1.1	2	3.5	4.1
Cu	49	63.6	36.9	53.9	15.3	70.0	67.0	56.0
Pb	7.4	6.2	3.0	6.6	1.7	11.0	16.7	3.9

APPENDIX B

Sr, Nd and Pb isotope compositions of Eocene volcanic rocks.

	$^{87}\text{Sr}/^{86}\text{Sr}$	$^{143}\text{Nd}/^{144}\text{Nd}$	ϵNd	$^{206}\text{Pb}/^{204}\text{Pb}$	$^{207}\text{Pb}/^{204}\text{Pb}$	$^{208}\text{Pb}/^{204}\text{Pb}$	$\Delta 7/4$	$\Delta 8/4$
F11	0.70404	0.51279	4.06	18.68	15.64	38.90	12.87	68.57
F23	0.70559	0.51268	1.93	18.58	15.63	38.81	12.92	72.53
F26	0.70531	0.51261	0.55	18.31	15.61	38.72	13.84	95.72
FG26	0.70479	0.51273	2.79	18.57	15.61	38.77	11.15	69.47
YR16	0.70520	0.51265	1.32	18.32	15.62	38.73	14.88	95.44
YD2	0.70524	0.51263	1.00	18.69	15.63	38.85	11.68	62.67
PK1	0.70477	0.51273	2.81	18.55	15.60	38.74	10.70	69.12
KA1	0.70469	0.51269	2.17	18.01	15.61	38.69	17.31	128.92
YS1	0.70516	0.51266	1.53	18.73	15.63	38.83	10.97	55.53
GE8	0.70489	0.51268	1.98	18.69	15.64	38.90	12.67	67.71
FG3	0.70524	0.51261	0.53	18.67	15.64	38.89	12.76	69.41
P6	0.70463	0.51266	1.60	18.49	15.65	38.87	15.55	88.50
F24	0.70524	0.51263	0.95	18.34	15.62	38.75	14.13	95.05
F31	0.70466	0.51277	3.61	18.41	15.57	38.58	8.41	70.20
FG1	0.70522	0.51263	0.83	18.58	15.63	38.86	13.27	76.77
F20	0.70547	0.51268	1.96	18.73	15.63	38.86	11.24	59.56
YR1	0.70535	0.51264	1.07	18.73	15.62	38.83	10.42	54.97

YR4	0.70534	0.51265	1.26	18.65	15.63	38.83	12.32	65.77
YS7	0.70526	0.51267	1.63	18.51	15.62	38.76	12.51	75.99
Y6	0.70409	0.51281	4.33	19.01	15.67	38.86	11.98	24.67
GE12	0.70523	0.51268	1.79	18.61	15.62	38.80	11.79	66.56
YR8	0.70515	0.51266	1.50	Nd	Nd	Nd	Nd	Nd
K14	0.70538	0.51262	0.59	18.77	15.67	38.85	14.40	52.34
D6	0.70502	0.51265	1.14	18.79	15.65	38.90	12.58	55.45

APPENDIX C

Normative compositions of Eocene volcanic rocks.

Samples	A3	A5	A6	D6	F11	F15	F18	F2	F20	F21	F22	F23	F24	F25	F26	F27	F28
Qz	4.78	0	9.36	7.03	9.37	6.59	9.18	26.84	7.41	9.23	8.25	6.94	11.08	13.4	12.64	1.87	8.82
or	15.43	9.82	18.2	3.79	4.73	15.95	4.95	14.6	4.39	5.63	5.3	13.95	7.86	13.2	9.33	9.62	12.57
ab	27.03	32.95	35.9	28.6	40.75	31.82	28.48	32.66	28.93	29.41	29.67	34.35	35.75	33.38	37.24	27.22	28.58
an	23.51	24.21	21.86	30.53	25.14	25.32	26.81	18.39	28.36	25.69	27.24	22.87	25.9	23.71	23.22	25.78	23.6
ne	0	3.42	0	0	0	0	0	0	0	0	0	0	0	0	0	0	0
C	0	0	0	0	0	0	0	0	0	0	0	0	0	0	0	0	0
Di wo	5.4	7	2.08	5.19	3.15	4.31	5.57	1.74	5.51	7.34	7.5	3.3	2.7	2.27	2.9	7.97	8.61
Di en	4.66	6.03	1.79	4.48	2.72	3.71	4.8	1.5	4.75	6.32	6.47	2.85	2.33	1.96	2.5	6.87	7.42
Hy en	11.15	0	4.99	12.58	6.21	2.58	12.37	0.03	12.66	8.09	7.66	8.47	6.49	4.98	4.32	12.3	0
Ol fo	0	6.08	0	0	0	0	0	0	0	0	0	0	0	0	0	0	0
mt	0.21	0.45	0.24	0.31	0.4	0.31	0.39	0.17	0.38	0.35	0.31	0.24	0.4	0.34	0.37	0.34	0.53
he	7.16	9.2	5.06	6.71	6.6	8.35	6.71	3.55	6.87	7.24	6.87	6.32	6.72	6.11	6.83	7.24	7.85
Samples	F31	F32	F34	F35	F8	Fg1	Fg20	Ys2	Ys3	Ys4	Ys5	Ys6	Ys7	Yr9	Ys10	Fg26	Fg27
Qz	9.4	9.9	17.42	18.11	19.81	24.45	0	6.82	3.62	2.59	2.49	2.89	1.69	7.09	6.29	6.65	5.68
or	6.76	6.12	36.44	34.34	25.85	14.99	17.69	8.54	14.5	15.98	14.87	13.54	18.28	8.26	6.26	4.99	5.66
ab	31.12	29.82	15.97	16.96	23.44	31.83	31.38	27.11	28.05	27.82	27.73	25.8	26.65	30.38	39.14	31.42	32.79
an	26.87	27.57	16.84	17.2	18.22	18.27	19.63	26.3	23.06	23.81	23.66	24.82	22.07	24.2	28.48	33	32.27
ne	0	0	0	0	0	0	0	0	0	0	0	0	0	0	0	0	0

C	0	0	0	0	0	0	1.93	0	0	0	0	0	0	0	0	0	0
Di wo	4.95	5.02	3.56	3.32	2.63	2.02	0	7.7	7.91	6.5	7.82	8.05	6.51	6.9	4.29	3.38	3.7
Di en	4.27	4.33	3.07	2.86	2.26	1.74	0	6.64	6.82	5.6	6.74	6.94	5.61	5.95	3.69	2.91	3.19
Hy en	5.88	6.66	0	1.03	1.52	0.43	14.19	8.86	7.56	9.04	7.75	8.95	10.21	8.4	4.08	9.11	8.22
Ol fo	0	0	0	0	0	0	3.8	0	0	0	0	0	0	0	0	0	0
mt	0.5	0.51	0.28	0.03	0.34	0.23	0.29	0.35	0.38	0.28	0.41	0.38	0.41	0.44	0.38	0.34	0.34
he	9.47	9.26	5.13	5.58	5.36	5.56	10.27	6.91	7.29	7.52	7.66	7.82	7.68	7.64	6.28	7.3	7.27
Samples	Fg28	Fg29	Fg3	Ge12	Ge8	K10	K11	K12	K14	K17	K19	K6	Ka1	Ka2	Lava1	P5	P6
Qz	3.33	2.15	16.17	4.53	3.61	27.61	27.96	30.02	34.34	11.19	23.6	15.69	9.24	6.13	6.04	5.34	5.6
or	18.52	13.61	14.99	9.41	5.76	14.09	14.24	13.62	13.41	5.66	18.2	8.8	12.58	6.71	9.39	14.05	14.13
ab	37.34	33.93	29.61	22.23	27.91	31.75	31.51	30.4	28.49	29.76	34.76	36.6	48.61	25.94	29.15	46.17	45.26
an	17.11	19.1	20.08	27.64	30.5	19.01	18.94	19.55	18.55	32.19	17.55	21.98	16.46	29.12	25.55	17.14	17.11
ne	0	0	0	0	0	0	0	0	0	0	0	0	0	0	0	0	0
C	0	0	0	0	0	0	0	0	0	0	0	0	0	0	0	0	0
Di wo	3.63	8.09	2.46	9.07	9.27	2.49	2.32	2.04	1.17	0.03	1.61	2.28	1.75	8.88	6.52	3.8	3.66
Di en	3.13	6.98	2.12	7.82	7.99	2.14	2	1.76	1.01	0.03	1.38	1.97	1.51	7.66	5.62	3.27	3.15
Hy en	9.74	7.79	6.53	10.27	6.91	0.2	0.08	0.13	0.5	15.08	0	8.19	3.35	7.22	9.94	2.02	2.77
Ol fo	0	0	0	0	0	0	0	0	0	0	0	0	0	0	0	0	0
mt	0.31	0.45	0.24	0.41	0.44	0.23	0.13	0.1	0.1	0.25	0.07	0.2	0.44	0.38	0.34	0.24	0.27
he	6.18	7.18	7.31	7.85	6.67	2.02	2.36	1.93	2	5.2	2.25	3.81	5.1	7.13	6.64	6.21	6.37
Samples	P8	P9	Pk1	T1	Y1	Y2	Y5	Y6	Y8	Yd1	Yd2	Yr10	Yr16	Yr3	Yr5	Yr7	Yr8
Qz	3.95	3.18	6.41	9.37	11.8	11.58	0	8.4	12.14	4.92	5.99	6.29	6.15	6.15	5.21	6.36	2.21
or	13.75	15.18	5.4	15.58	9.8	10.22	10.36	4.31	10.77	10.33	11.52	9.26	9.46	8.67	9.12	8.3	10.09

ab	43.33	46.09	31.62	31.36	43.99	43.9	49.18	42.02	41.86	28.01	28.05	29.62	32.07	25.22	26.41	26.02	29.35
an	20.09	19.88	33.63	27.02	22.26	22.23	13.2	26.15	21.88	26.82	25.37	26.2	23.42	26.52	25.57	25.8	24.3
ne	0	0	0	0	0	0	7.4	0	0	0	0	0	0	0	0	0	0
C	0	0	0	0	0	0	0	0	0	0	0	0	0	0	0	0	0
Di wo	3.94	3.6	3.06	1.82	1.05	0.93	4.15	3.25	1.34	6.87	6.9	8.1	6.48	8.28	8.64	7.54	6.08
Di en	3.39	3.1	2.63	1.57	0.9	0.8	3.58	2.8	1.16	5.92	5.95	6.98	5.58	7.14	7.45	6.5	5.24
Hy en	3.56	2.64	9	5.59	3.65	3.88	0	5.63	3.45	9.55	7.99	5.64	8.36	9.8	9.48	10.86	14.18
Ol fo	0	0	0	0	0	0	3.98	0	0	0	0	0	0	0	0	0	0
mt	0.24	0.17	0.34	0.24	0.37	0.37	0.39	0.4	0.4	0.31	0.34	0.41	0.44	0.38	0.34	0.38	0.4
he	6.36	4.73	7.03	6.84	5.54	5.45	6.65	6.1	6.35	6.48	7.13	6.67	7.3	7.18	7.13	7.45	7.22

APPENDIX D

Trace element ratios used in the text.

Samples	K17	K14	K19	K12	K6	K10	K11	FG3	FG1	F2	F8	Y1	Y2
Ba/La	28.38	27.64	24.97	31.05	30.27	31.06	29.35	29.80	27.74	27.80	20.63	25.02	25.20
Ba/Nb	88.53	110.57	77.21	119.26	111.12	111.35	100.90	105.14	88.12	89.76	59.64	78.53	71.04
La/Nb	3.12	4.00	3.09	3.84	3.67	3.59	3.44	3.53	3.18	3.23	2.89	3.14	2.82
Ba/Ta	1164	1548	1081	1372	1352	1522	1345	1472	1070	1064	954	1034	983
Th/La	0.45	0.44	0.36	0.48	0.48	0.48	0.56	0.51	0.46	0.48	0.53	0.42	0.49
Th/Nb	1.41	1.77	1.11	1.84	1.75	1.73	1.91	1.80	1.45	1.54	1.53	1.33	1.39
Nb/La	0.32	0.25	0.32	0.26	0.27	0.28	0.29	0.28	0.31	0.31	0.35	0.32	0.35
Ce/Pb	4.45	7.18	3.61	7.25	30.69	9.45	8.28	6.66	8.69	12.23	5.97	34.93	30.19
Nb/U	2.79	1.11	1.48	0.91	1.49	1.11	1.21	1.63	1.81	1.38	2.43	2.32	2.59
Ce/Yb	23.33	35.88	23.12	36.52	33.18	33.06	39.26	29.38	29.68	33.36	49.30	23.07	20.91
Zr/Ba	0.23	0.20	0.25	0.19	0.21	0.20	0.22	0.19	0.22	0.22	0.21	0.34	0.37
Ti/Eu	3231	3150	3300	3333	3481	3103	3293	3450	3459	3477	2373	3292	3287
Sr/Y	26.43	35.90	20.24	36.97	34.76	37.25	38.61	32.23	31.62	32.95	32.22	21.24	22.34
La/Yb	13.67	20.59	12.78	19.63	18.11	18.38	20.37	17.03	17.09	18.74	27.61	11.70	10.13
Zr/Hf	39.42	38.33	39.29	38.60	36.98	43.02	41.16	43.48	43.62	38.64	39.66	41.84	44.00
(Dy/Yb)_N	1.03	1.02	0.92	1.22	1.04	1.08	1.24	1.01	1.02	1.21	1.20	1.08	1.09
(La/Sm)_N	4.91	5.91	5.48	5.41	5.85	6.42	6.00	5.35	5.29	5.35	5.14	4.36	4.11

(La/Yb)_N	9.11	13.73	8.52	13.09	12.07	12.25	13.58	11.36	11.39	12.49	18.41	7.80	6.75
(Eu/Eu)*	0.89	0.87	0.87	0.85	0.88	0.91	0.85	0.83	0.83	0.87	0.65	0.97	0.93
(Ce/Ce)*	0.91	0.99	1.01	1.01	1.01	1.01	1.05	0.96	0.97	0.99	0.96	1.02	1.03
(Nb/Nb)*	0.16	0.13	0.19	0.13	0.14	0.14	0.13	0.14	0.16	0.15	0.16	0.17	0.17
(Ti/Ti)*	0.38	0.38	0.38	0.38	0.41	0.37	0.38	0.42	0.41	0.43	0.23	0.42	0.40
∑ REE	121.86	112.99	130.09	112.98	113.45	122.20	118.87	100.95	110.63	111.77	231.57	118.13	117.71

Samples	Y6	Y5	F11	Y8	F15	P6	P9	P5	P8	FG26	PK1	KA1	KA2
Ba/La	33.75	35.67	31.64	24.14	22.79	18.29	19.93	17.25	19.17	28.52	32.72	20.58	29.78
Ba/Nb	70.75	94.71	70.89	74.12	63.56	34.34	37.43	33.24	34.09	81.73	92.14	41.17	75.80
La/Nb	2.10	2.66	2.24	3.07	2.79	1.88	1.88	1.93	1.78	2.87	2.82	2.00	2.55
Ba/Ta	839	1373	933	1050	1430	515	554	455	564	1417	1505	666	1251
Th/La	0.48	0.35	0.46	0.47	0.43	0.33	0.37	0.33	0.38	0.44	0.32	0.35	0.33
Th/Nb	1.01	0.93	1.04	1.44	1.19	0.62	0.70	0.64	0.67	1.25	0.90	0.71	0.83
Nb/La	0.48	0.38	0.45	0.33	0.36	0.53	0.53	0.52	0.56	0.35	0.36	0.50	0.39
Ce/Pb	9.33	4.74	6.68	11.19	6.87	16.33	4.81	16.73	3.46	7.89	8.37	31.52	6.24
Nb/U	2.44	5.80	2.93	2.58	3.91	4.74	5.48	4.81	4.81	3.06	2.88	3.71	4.13
Ce/Yb	18.02	13.42	16.21	22.27	23.69	22.06	23.86	22.27	19.27	14.67	15.03	22.94	18.74
Zr/Ba	0.27	0.27	0.24	0.32	0.30	0.46	0.41	0.47	0.40	0.25	0.23	0.38	0.22
Ti/Eu	5465	5622	5000	3124	4800	6190	6043	6706	6000	4734	5000	3851	4404
Sr/Y	31.78	21.01	25.40	22.40	25.32	14.20	18.29	14.03	17.01	27.02	28.18	14.99	29.16
La/Yb	8.61	6.42	8.59	12.08	12.36	10.87	11.78	11.14	10.11	7.49	7.08	11.27	9.18
Zr/Hf	45.34	44.00	42.75	40.57	42.73	45.82	44.02	41.21	48.21	39.07	32.53	44.17	37.10

(Dy/Yb)_N	1.23	0.96	1.11	1.02	1.13	1.14	1.22	1.16	1.06	1.13	1.08	1.14	1.22
(La/Sm)_N	3.55	2.87	3.36	3.91	3.68	3.63	3.52	3.88	3.68	2.61	2.57	4.33	3.04
(La/Yb)_N	5.74	4.28	5.73	8.06	8.24	7.25	7.85	7.42	6.74	4.99	4.72	7.51	6.12
(Eu/Eu)*	0.91	0.98	0.96	0.90	0.87	0.85	0.87	0.83	0.87	0.91	0.93	0.85	0.94
(Ce/Ce)*	1.04	1.00	0.97	0.95	0.97	1.03	1.02	1.02	0.96	0.92	1.01	1.03	1.00
(Nb/Nb)*	0.24	0.22	0.23	0.16	0.19	0.32	0.30	0.31	0.32	0.18	0.22	0.29	0.24
(Ti/Ti)*	0.64	0.71	0.63	0.39	0.58	0.67	0.68	0.74	0.71	0.58	0.58	0.41	0.53
Σ REE	92.38	86.45	88.31	122.20	121.94	167.29	138.02	167.61	129.52	82.71	78.66	174.60	90.22

Samples	LAV 1	FG27	A3	A5	A6	D6	F20	F18	F27	F28	T1	F21	F23
Ba/La	39.56	28.43	31.54	44.95	40.83	33.77	37.48	30.11	32.50	26.94	36.69	28.90	46.47
Ba/Nb	96.59	79.09	103.93	208.05	140.00	79.14	83.24	83.58	105.93	78.33	148.86	75.36	114.91
La/Nb	2.44	2.78	3.30	4.63	3.43	2.34	2.22	2.78	3.26	2.91	4.06	2.61	2.47
Ba/Ta	1385	1088	1585	4473	1960	1688	1415	1400	5720	1410	2605	1266	1580
Th/La	0.35	0.36	0.36	0.27	0.42	0.27	0.30	0.38	0.29	0.29	0.44	0.40	0.49
Th/Nb	0.85	1.00	1.20	1.26	1.44	0.63	0.68	1.04	0.94	0.83	1.80	1.05	1.20
Nb/La	0.41	0.36	0.30	0.22	0.29	0.43	0.45	0.36	0.31	0.34	0.25	0.38	0.40
Ce/Pb	8.24	6.95	8.85	5.22	9.92	6.84	5.38	5.93	9.10	8.00	6.85	7.57	8.23
Nb/U	3.31	3.24	3.21	2.53	2.41	4.92	4.86	3.35	3.86	3.00	2.26	3.36	3.06
Ce/Yb	23.35	14.62	21.20	26.26	27.84	16.45	15.42	17.60	20.52	14.86	35.96	23.37	17.35
Zr/Ba	0.14	0.25	0.16	0.09	0.12	0.22	0.19	0.21	0.15	0.24	0.11	0.17	0.18
Ti/Eu	3982	4846	4042	4053	3191	4547	4242	4019	4455	3823	3257	4125	4082
Sr/Y	32.51	27.84	35.04	66.35	33.96	28.18	36.21	28.72	29.26	21.33	43.48	32.53	25.29

La/Yb	12.14	7.85	12.04	12.84	14.04	8.20	7.86	9.69	10.17	7.48	20.14	12.51	8.19
Zr/Hf	34.48	37.03	39.85	35.00	36.19	34.19	39.07	38.29	32.70	38.07	37.83	35.45	35.34
(Dy/Yb)_N	1.23	1.16	1.18	1.38	1.02	1.08	1.13	1.20	1.18	1.10	1.18	1.18	1.17
(La/Sm)_N	3.59	2.80	3.71	2.93	4.34	3.27	3.16	3.42	3.12	2.76	4.56	4.16	2.75
(La/Yb)_N	8.09	5.23	8.02	8.56	9.36	5.46	5.24	6.46	6.78	4.98	13.43	8.34	5.46
(Eu/Eu)*	0.94	0.91	0.86	0.86	0.87	0.98	0.98	0.90	0.87	0.93	0.86	0.88	0.93
(Ce/Ce)*	0.99	0.92	0.92	0.99	1.03	1.00	0.98	0.94	0.98	0.96	0.94	0.98	0.98
(Nb/Nb)*	0.24	0.21	0.17	0.14	0.16	0.29	0.28	0.20	0.20	0.22	0.13	0.21	0.20
(Ti/Ti)*	0.52	0.59	0.48	0.49	0.37	0.58	0.54	0.49	0.54	0.48	0.41	0.49	0.51
∑ REE	103.10	79.70	92.39	103.08	111.57	78.78	78.48	89.72	92.07	86.32	124.90	101.42	77.00

Samples	F22	F24	F25	F26	F34	F35	F32	F31	GE8	GE12	YS5	YS4	YS10
Ba/La	31.62	27.20	27.97	27.16	24.23	20.63	33.82	34.44	26.49	29.66	40.23	37.81	20.00
Ba/Nb	83.77	85.00	79.62	80.39	76.67	61.44	152.19	148.18	45.00	125.69	81.86	78.91	53.23
La/Nb	2.65	3.13	2.85	2.96	3.16	2.98	4.50	4.30	1.70	4.24	2.03	2.09	2.66
Ba/Ta	1613	1224	1553	2037	1359	927	2435	2445	837	1760	1173	1452	825
Th/La	0.44	0.32	0.35	0.40	0.43	0.56	0.26	0.24	0.22	0.33	0.34	0.38	0.39
Th/Nb	1.17	1.01	1.00	1.18	1.36	1.67	1.19	1.03	0.38	1.38	0.69	0.78	1.05
Nb/La	0.38	0.32	0.35	0.34	0.32	0.34	0.22	0.23	0.59	0.24	0.49	0.48	0.38
Ce/Pb	7.41	18.70	6.65	16.04	5.74	3.72	8.79	15.10	12.19	6.61	10.06	7.36	12.36
Nb/U	3.21	3.00	2.79	2.62	2.67	3.85	2.67	3.30	9.30	2.10	4.53	5.41	3.88
Ce/Yb	20.51	18.86	23.15	20.46	51.21	47.03	12.72	13.36	18.22	21.42	21.86	20.84	14.64
Zr/Ba	0.17	0.23	0.23	0.23	0.20	0.20	0.18	0.18	0.28	0.16	0.16	0.16	0.44

Ti/Eu	4358	3864	3683	3750	2734	2488	3933	3882	5400	4167	4835	4500	5583
Sr/Y	35.57	23.20	28.40	26.28	53.93	24.91	23.25	23.22	28.10	38.23	33.50	30.83	22.97
La/Yb	11.53	9.87	12.47	11.48	27.67	25.42	6.32	6.28	9.08	10.11	10.87	11.57	7.82
Zr/Hf	32.94	36.97	36.31	34.48	41.11	36.52	29.66	30.75	38.13	34.64	40.56	34.41	49.97
(Dy/Yb)_N	1.02	1.11	1.13	1.02	1.19	1.15	1.14	1.15	1.24	1.12	1.15	1.18	0.99
(La/Sm)_N	4.00	3.59	3.95	3.79	5.09	5.50	2.26	2.32	3.03	3.41	3.12	3.20	3.05
(La/Yb)_N	7.68	6.58	8.31	7.65	18.45	16.95	4.21	4.19	6.05	6.74	7.25	7.71	5.21
(Eu/Eu)*	0.87	0.90	0.88	0.85	0.69	0.66	0.89	0.91	0.91	0.96	0.90	0.89	0.99
(Ce/Ce)*	0.91	0.97	0.97	0.92	0.97	1.00	0.94	0.98	0.97	1.01	0.98	0.89	0.91
(Nb/Nb)*	0.20	0.19	0.20	0.18	0.17	0.15	0.15	0.16	0.43	0.14	0.29	0.27	0.21
(Ti/Ti)*	0.52	0.46	0.45	0.45	0.28	0.24	0.47	0.47	0.63	0.54	0.60	0.55	0.73
∑ REE	95.08	109.97	102.37	103.70	263.11	226.01	84.89	85.35	85.09	95.08	89.58	92.38	85.72

Samples	YS7	YS6	YS2	YS3	YR9	YR16	YR3	YR5	YR10	YR7	YR8	YD1	YD2
Ba/La	37.11	39.13	35.58	41.28	35.42	35.96	42.12	41.72	38.86	40.51	42.74	41.40	37.06
Ba/Nb	76.78	76.83	97.53	83.48	115.91	91.89	189.53	181.76	103.29	105.90	68.14	114.47	127.57
La/Nb	2.07	1.96	2.74	2.02	3.27	2.56	4.50	4.36	2.66	2.61	1.59	2.76	3.44
Ba/Ta	1336	1575	1382	1238	1913	1378	2527	2545	1632	1483	1032	1622	1946
Th/La	0.36	0.31	0.37	0.34	0.39	0.39	0.34	0.36	0.32	0.32	0.37	0.37	0.30
Th/Nb	0.75	0.61	1.01	0.69	1.29	0.99	1.53	1.55	0.86	0.84	0.59	1.04	1.05
Nb/La	0.48	0.51	0.36	0.49	0.31	0.39	0.22	0.23	0.38	0.38	0.63	0.36	0.29
Ce/Pb	13.70	9.52	4.70	6.21	11.11	17.96	4.71	4.84	13.29	7.43	19.11	6.47	6.55
Nb/U	5.44	4.82	2.93	4.94	2.44	3.33	1.82	1.91	2.82	3.33	5.89	3.15	2.65

Ce/Yb	18.86	20.39	24.55	21.89	21.52	26.77	24.86	21.52	19.43	20.49	24.53	29.39	21.04
Zr/Ba	0.18	0.15	0.13	0.15	0.14	0.14	0.12	0.13	0.14	0.14	0.17	0.12	0.14
Ti/Eu	4500	4776	3757	4472	3982	4171	3938	3780	4615	4592	5576	4286	4369
Sr/Y	29.74	29.18	36.15	30.84	29.45	33.94	36.74	36.04	29.51	28.15	32.49	41.00	28.65
La/Yb	10.78	10.45	13.24	11.32	11.31	14.29	12.50	10.70	9.91	9.89	11.42	14.42	10.88
Zr/Hf	41.31	37.38	36.37	34.21	42.76	35.94	35.54	37.12	34.85	38.52	43.89	36.55	37.64
(Dy/Yb)_N	1.11	1.15	1.18	1.28	1.23	1.28	1.27	1.09	1.08	1.14	1.45	1.28	1.14
(La/Sm)_N	3.05	3.09	3.70	3.13	3.51	3.70	3.16	3.31	3.59	3.62	3.24	3.72	3.69
(La/Yb)_N	7.19	6.97	8.83	7.55	7.54	9.52	8.33	7.13	6.60	6.59	7.61	9.61	7.25
(Eu/Eu)*	0.92	0.89	0.90	0.89	0.86	0.83	0.85	0.89	0.85	0.92	0.91	0.82	0.87
(Ce/Ce)*	0.85	0.96	0.95	0.96	0.97	0.97	1.00	1.00	0.99	1.03	1.04	1.02	0.99
(Nb/Nb)*	0.28	0.32	0.21	0.29	0.17	0.22	0.13	0.13	0.23	0.23	0.35	0.20	0.18
(Ti/Ti)*	0.58	0.61	0.47	0.56	0.47	0.50	0.45	0.44	0.52	0.53	0.64	0.47	0.51
∑ REE	88.36	82.38	110.34	91.00	103.86	107.67	90.10	93.21	105.46	95.20	91.27	115.84	102.43
Samples	FG28	FG29	FG20	YS1	YR1	YR4	Samples	FG28	FG29	FG20	YS1	YR1	YR4
Ba/La	41.35	37.63	23.46	37.72	37.03	37.80	La/Yb	12.33	12.40	3.02	11.60	11.91	12.27
Ba/Nb	95.63	125.00	87.14	82.93	176.81	102.16	Zr/Hf	42.56	36.41	33.06	42.41	38.43	51.20
La/Nb	2.31	3.32	3.71	2.20	4.78	2.70	(Dy/Yb)_N	1.18	1.26	1.10	1.35	1.31	1.29
Ba/Ta	1530	1750	1220	1247	2614	1890	(La/Sm)_N	3.55	3.33	1.55	3.14	3.28	3.39
Th/La	0.39	0.36	0.25	0.32	0.35	0.31	(La/Yb)_N	8.22	8.27	2.02	7.73	7.94	8.18
Th/Nb	0.91	1.20	0.93	0.70	1.68	0.84	(Eu/Eu)*	0.88	0.87	1.01	0.93	0.91	0.83
Nb/La	0.43	0.30	0.27	0.45	0.21	0.37	(Ce/Ce)*	0.95	0.95	0.87	0.97	0.96	0.92
Ce/Pb	11.53	5.27	6.24	3.43	2.19	8.79	(Nb/Nb)*	0.24	0.17	0.19	0.28	0.12	0.23

Nb/U	3.33	2.95	3.50	5.07	1.91	5.69	(Ti/Ti)*	0.53	0.50	0.75	0.48	0.51	0.54
Ce/Yb	23.07	23.20	6.16	22.08	22.11	21.04	Σ REE	87.76	89.13	38.24	97.68	94.82	90.46
Zr/Ba	0.15	0.14	0.46	0.16	0.13	0.17	Sr/Y	24.79	25.49	14.00	28.61	32.22	29.63
Ti/Eu	4295	4182	5844	4250	3482	4082							

APPENDIX E

Major and trace element compositions of Late Cretaceous granitic rocks.

Major Oxides								
(wt %)	C1	C3	C8	C14	C15	116	119	23-21
SiO₂	64.82	74.78	65.08	76.33	52.87	73.68	59.21	75.68
TiO₂	0.360	0.085	0.492	0.049	0.510	0.175	0.696	0.056
Al₂O₃	16.57	12.76	16.06	12.61	19.77	12.95	16.41	13.06
FeO*	2.63	0.98	3.68	0.85	3.91	1.71	4.82	0.46
MnO	0.073	0.037	0.086	0.009	0.110	0.031	0.111	0.079
MgO	0.77	0.07	1.31	0.06	1.59	0.52	1.70	0.03
CaO	3.56	0.86	4.14	0.40	4.17	1.41	7.25	0.38
Na₂O	3.53	2.99	3.22	3.45	4.70	2.78	2.75	3.35
K₂O	4.67	5.27	4.57	4.77	7.36	4.43	5.07	5.17
P₂O₅	0.107	0.010	0.156	0.010	0.234	0.041	0.214	0.007
LOI (%)	1.82	1.19	0.70	0.68	4.48	1.02	0.91	0.46
Sum	98.90	99.03	99.48	99.21	99.71	98.75	99.15	98.72
Trace Elements								
(ppm)								
Ni	1	0	1	0	4	0	3	0
Cr	7	0	10	2	8	1	15	1
Sc	4	1	7	1	6	3	7	3
V	38	2	57	1	94	21	49	2
Ba	1016	93	965	59	1433	410	1206	63
Rb	173	286	181	156	269	225	207	457
Sr	706	90	616	32	1101	95	1009	67
Zr	218	90	250	86	378	104	280	81
Y	16	16	23	25	24	26	28	22
Nb	14.6	20.0	20.6	18.5	41.6	12.8	22.4	55.2
Ga	18	14	19	14	17	13	19	13
Cu	4	5	5	74	30	8	8	3
Zn	46	30	64	9	78	16	87	18
Pb	36	72	62	22	59	29	43	91
Th	32	52	32	38	55	27	30	36
U	8	14	7	8	19	9	6	22
Hf	5.66	3.71	6.49	4.26	7.51	3.72	7.11	3.34
Ta	1.10	2.50	1.61	2.03	2.48	2.17	1.52	7.45
Cs	5.89	5.43	8.85	2.01	45.82	5.49	9.07	26.50

La	59.36	29.18	66.78	19.46	105.48	29.82	71.73	15.80
Ce	98.30	52.67	120.44	40.55	187.38	51.18	126.17	38.92
Pr	9.75	5.32	12.66	4.94	19.90	5.48	13.52	4.36
Nd	31.52	16.80	42.65	17.47	67.47	17.88	47.02	15.68
Sm	5.13	3.03	7.41	4.50	11.47	3.66	8.55	3.87
Eu	1.22	0.29	1.45	0.19	2.66	0.44	1.73	0.45
Gd	3.85	2.37	5.62	4.07	8.00	3.36	6.88	3.49
Tb	0.55	0.39	0.80	0.70	1.03	0.62	1.00	0.74
Dy	3.06	2.38	4.42	4.38	5.08	4.00	5.64	4.83
Ho	0.60	0.50	0.85	0.90	0.88	0.87	1.09	1.00
Er	1.65	1.58	2.28	2.59	2.22	2.58	2.88	3.01
Tm	0.25	0.26	0.34	0.41	0.31	0.44	0.43	0.51
Yb	1.61	1.88	2.17	2.64	1.89	3.07	2.67	3.56
Lu	0.26	0.31	0.34	0.42	0.28	0.51	0.41	0.55

APPENDIX F

Sr, Nd and Pb isotope compositions of Late Cretaceous granitic rocks.

Samples	$^{206}\text{Pb}/^{204}\text{Pb}$	$^{207}\text{Pb}/^{204}\text{Pb}$	$^{208}\text{Pb}/^{204}\text{Pb}$	$^{87}\text{Sr}/^{86}\text{Sr}$	ϵNd	$^{143}\text{Nd}/^{144}\text{Nd}$
C3	18.86	15.70	39.06	0.70940	-7.32	0.51216
C8	18.85	15.75	39.23	0.70955	-7.91	0.51213
C14	18.85	15.69	39.19	0.70992	-7.85	0.51213
MCG 23-21	18.95	15.75	39.13	0.70954	-7.43	0.51216
MCG116	18.72	15.67	38.98	0.71002	-6.51	0.51220
MCG 119	18.86	15.73	39.17	0.70869	-7.53	0.51215

CURRICULUM VITAE

PERSONAL INFORMATION

Surname, Name: Geneli, Fatma

Nationality: Turkish (TC)

Date and Place of Birth: 15 April 1978, Aksaray

Phone: +903122105740

Fax: +903122105750

e- mail: fgeneli@metu.edu.tr, fgeneli@gmail.com

EDUCATION

Degree	Institution	Year of Graduation
MS	Nigde University	
	Geological Engineering	2003
BS	Nigde University	
	Geological Engineering	1999
High School	Aksaray High School	1994

WORK EXPERIENCE

Year	Place	Enrollment
2008-2009	University of Texas at Austin	Research Scholar
2003-present	METU Geological Engineering	Teaching Assistant
1999-2003	Nigde University	Teaching Assistant

MEMBERSHIPS

National Commission of Turkey on Volcanology and Chemistry of the Earth's Interior (TUVAK)

The European Association for Geochemistry, EAG

FOREIGN LANGUAGES

Fluent English

PUBLICATIONS

Refereed Journals

Gençaliolu Kuşcu, G., Geneli, F., 2010. Review of post-collisional volcanism in the Central Anatolian Volcanic Province (Turkey), with special reference to the Tepekoy Volcanic Complex. *International Journal of Earth Science* 99, 593–621

National and International Conference Presentations

Geneli, F., Göncüoğlu, M., Lassiter, J., and Toksoy-Köksal, F., 2010 Eocene post-collisional volcanism in the Central Anatolian Crystalline Complex, Turkey: Petrology and geodynamic significance. XIX Congress of the Carpathian- Balkan Geological Association, 23- 26 September 2010, Greece.

Geneli, F., and Gençaliolu-Kuşcu, G., 2009. Post collisional volcanism in the Central Anatolian Volcanic Province, with special reference to the Tepeköy Volcanic Complex (Niğde), 62. Türkiye Jeoloji Kurultayı, Ankara, Abstracts, 620-621.

Geneli, F., and Gençaliolu-Kuşcu, G., 2008, Mio-Pliocene Post-Collisional Calc-Alkaline Volcanism in Central Anatolia: Tepekoy Volcanic Complex (Niğde), Goldschmidt 2008 conference, from sea to ski, July 13-18 Vancouver, Canada

Göncüoğlu, M., and Geneli, F., 2008, Eocene Volcanism in the Central Anatolian Crystalline Complex: Geochemical indications for a change from post-collision to extension, Goldschmidt 2008 conference, from sea to ski, July 13-18 Vancouver, Canada

Geneli, F., ve Gençaliolu-Kuşcu, G., 2004. “Tepeköy (Niğde) Volkaniklerinin Jeokimyası” I. Ulusal Jeokimya Sempozyumu, Bildiri Özleri Kitabı, 31

Geneli, F., ve Gençalioglu-Kuşcu, G., 2003. "Tepeköy (Niğde) Volkaniklerinin Jeolojik ve Petrolojik Özellikleri" Mersin Üniversitesi Mühendislik Fakültesi Jeoloji Mühendisliği Bölümü 10. Yıl Sempozyumu, Mersin, Bildiri Özleri Kitabı, 44.

COURSES and SUMMER SCHOOLS ATTENDED

- 1) Magmatic Petrogenesis Summer School (7-12 July 2001), TÜBİTAK-MTA-JMO, Akçakoca.
- 2) "Volcanic Processes, Products and Successions: Modern and Ancient Systems (6-10 August 2001), TÜBİTAK-UNDP-ODTÜ, ODTÜ, Ankara"Short Course in Isotope Geochemistry"(6-8 July 2005) Cumhuriyet University, Sivas-University of Nevada, Reno-TUBİTAK-BAYG.
- 3) Physics of Volcanic Systems and their Eruptions. (26-29 September 2005, İTÜ, İstanbul) Prof. Dr. Claude Jaupart (Geophysical Institute of Paris, France).
- 4) An international summer school on isotope geochemistry and geochronology of tectonic processes (17-22 September 2007, Marmaris) organized by Cumhuriyet University.
- 5) Short Course, minerals, inclusions and volcanic processes" (13-15 December 2008) Geological Society of America, Sanfransisco, USA.